NASA Contractor Report 174880

Shock Tube Study of the Fuel Structure Effects on the Chemical Kinetic Mechanisms Responsible for Soot Formation Part II

M. Frenklach, D.W. Clary, and M.K. Ramachandra

Louisiana State University
Baton Rouge, Louisiana

May 1985

Prepared for
Lewis Research Center
Under Grant NAG 3-477

NASA
National Aeronautics and
Space Administration

TABLE OF CONTENTS

	Page
INTRODUCTION	1
APPARATUS AND PROCEDURES	2
TEST RESULTS	3
DISCUSSION OF TEST RESULTS	60
1. Effect of Oxygen	60
2. Effect of Fuel Structure	61
a) Pyrolysis of individual hydrocarbons	61
b) Pyrolysis of hydrocarbon mixtures	64
DETAILED KINETIC MODELING	67
1. Introduction	67
2. Computer Model	68
3. Results and Discussion	127
a) Formation of the first aromatic ring	127
b) Formation of two-ring aromatics	131
c) Further growth of the fused polycyclic aromatics	135
d) Species concentration profiles	137
e) Formation of soot	137
MAIN CONCLUSIONS	161
FUTURE RESEARCH DIRECTIONS	162
REFERENCES	163
APPENDIX A - PUBLICATIONS AND PRESENTATIONS	166
APPENDIX B - PROFESSIONAL PERSONNEL	168

INTRODUCTION

This report covers our research activities from October 25, 1983 to October 24, 1984 under the auspices of NASA Grant No. NAG 3-477; the report is actually a continuation of our previous report[1], NASA CR-174661, for NASA Contract NAS 3-23542. In the previous work, soot formation in toluene-, benzene-, and acetylene-oxygen-argon mixtures was investigated. We have continued the study of the influence of oxygen on soot formation from hydrocarbons; this report presents the results obtained in oxidation of allene, 1,3-butadiene, vinylacetylene, and chlorobenzene.

We have suggested[1,2] that the soot formation mechanism is probably the same for both pyrolysis and oxidation of hydrocarbons. Therefore, in continuation of our efforts to investigate the effects of fuel structure on the chemical kinetic mechanisms responsible for soot formation, we have concentrated on the pyrolysis studies. We report here our new results obtained in shock-tube pyrolysis of ethylene, vinylacetylene, 1-butene and chlorobenzene. We have initiated a study of soot formation in mixtures of hydrocarbons. The report presents the results obtained in pyrolysis of acetylene-hydrogen, benzene-acetylene, benzene-butadiene, and chlorobenzene-acetylene argon-diluted mixtures.

The report is organized in three main parts: experimental results, discussion of the experimental results, and computer modeling of soot formation in shock-tube pyrolysis of acetylene. The latter is the first attempt of a detailed chemical kinetic modeling of soot formation. The modeling work was performed in collaboration[3] with Professor William C. Gardiner, Jr. of the University of Texas and Dr. Stephen E. Stein of the National Bureau of Standards.

APPARATUS AND PROCEDURES

The experimental apparatus and procedures used in this study were similar to those described in our previous report[1]. Briefly, the experiments were conducted behind reflected shock waves in a 7.62 cm i.d. shock tube. The test gas mixtures were prepared manometrically. The stated purities of the gases were: argon-99.998%, acetylene-99.6%, oxygen-99.8%, allene-93%, 1,3-butadiene-99%, ethylene-99.5%, 1-butene-99.9% and hydrogen-99.99%. These gases were used without further purificatior The vinylacetylene used was of technical grade with up to 2% impurities. It was supplied by Wiley Organics as a 50% solution by weight in xylene, to which 0.1% by weight of P-tertiary-butylcatechol had been added. From this solution vinylacetylene vapor was distilled at 0°C and was found by gas chromatographic analysis to contain less than 0.5% xylene. The toluene (Reagent, Baker), benzene (Spectranalyzed, Fisher) and chlorobenzene (Reagent, Baker) were purified by repeated freezing and evacuation. The shock tube was cleaned after every run.

The soot conversion was determined by measuring the attenuation of a He-Ne 632.8 nm laser beam. As in our previous studies, the soot yields were calculated according to Graham's model[4] but leaving out the quantity $E(m) = -\mathrm{Im}[(m^2-1)/(m^2+2)]$, where m is the complex refractive index of soot particles. This arbitrary form of reporting the results was chosen to emphasize the ambiguity in the value of m and in the laser-extinction model itself[5,6]. An additional source of uncertainty is possible absorption of the laser beam by molecular species rather than soot particles; light at 632.8 nm is already absorbed by compounds with as few as six aromatic rings[7]. However, Rawlins and co-workers[8,9]

concluded from their recent optical studies that light extinction at 632.8 nm is primarily caused by soot particles.

TEST RESULTS

Table I summarizes the experimental conditions of the mixtures covered in this report. Mixtures A to K were used to study and compare soot formation from aliphatic hydrocarbons: acetylene, ethylene, vinylacetylene and 1-butene. The remaining mixtures (L to W) were utilized to study soot formation from individual aromatic hydrocarbons (benzene and chlorobenzene) and their mixtures with aliphatic hydrocarbons (acetylene, allene, vinylacetylene and 1,3-butadiene). The measured soot yield, induction times for soot appearance and rates of soot formation are reported in Figs. 1 through 51.

TABLE I. EXPERIMENTAL CONDITIONS.

Mixture	Composition (% vol. in argon) Fuel	O_2	T_5 (K)	P_5 (bar)	$C_5 \times 10^6$ (mol/cm^3)	$[C]_5 \times 10^{-17}$ (carbon atoms/cm^3)
A*	1.09, C_2H_2		1665-3040	2.14-3.87	15.31-15.69	2.01-2.06
B	2.72, C_2H_2		1674-2413	2.11-3.05	15.16-15.42	4.97-5.05
C*	4.65, C_2H_2		1687-3122	1.25-2.33	8.70- 9.22	4.87-5.16
D	4.65, C_2H_4		2024-2874	1.50-2.11	8.68- 8.98	4.86-5.03
E*	0.726, C_3H_4		526-2294	1.93-2.91	15.06-15.39	1.98-2.02
F	0.726, C_3H_4	0.726	1497-2041	1.93-2.56	15.10-15.72	1.98-2.06
G*	0.54, C_4H_6		1664-2415	2.10-3.01	14.94-15.32	94-1.99
H	0.54, C_4H_6	0.54	1560-2082	2.02-2.68	15.09-15.65	1.96-2.04
I	0.54, C_4H_4		1670-2424	2.18-3.09	15.31-15.73	1.99-2.05
J	0.54, C_4H_4	0.54	1599-2020	2.08-2.60	15.40-15.71	2.00-2.04
K	0.54, C_4H_8		1630-2299	2.08-2.96	15.34-15.66	2.00-2.04
L$^+$	0.311, C_7H_8		15252349	1.98-3.00	14.52-15.74	1.90-2.06
M$^+$	0.311, C_6H_6		1561-2272	1.93-2.87	14.90-15.59	1.67-1.75
N$^+$	0.311, C_6H_6	0.311	1515-2242	1.98-2.83	15.16-15.68	1.70-1.76
P	0.311, C_6H_5Cl		1446-2201	1.89-2.81	15.11-15.86	1.70-1.78
Q	0.311, C_6H_5Cl	0.311	1433-2184	1.81-2.77	14.74-15.74	1.66-1.77
R	4.65, C_2H_2 + 4.65, H_2		1744-2427	1.30-1.80	8.84- 9.08	4.75-5.09
S	0.311, C_6H_5Cl + 1.09, C_2H_2		1475-2237	1.92-2.82	15.02-15.75	3.66-3.84
T	0.311, C_6H_6 + 0.54, C_2H_2		1571-2300	2.03-2.91	14.53-15.58	2.58-2.76

Table I. (continued)

Mixture	Composition (% vol. in argon) Fuel	O_2	T_5 (K)	P_5 (bar)	$C_5 \times 10^6$ (mol/cm^3)	$[C]_5 \times 10^{-17}$ (carbon atoms/cm^3)
U	0.311, C_6H_6 + 1.09, C_2H_2		1506-2279	1.94-2.86	15.10-15.52	3.68-3.78
V	0.311, C_6H_6 + 2.72, C_2H_2		1593-2427	2.04-3.06	14.97-15.55	6.58-6.84
W	0.311, C_6H_6 + 0.54, C_4H_6		1537-2433	1.98-3.07	15.14-15.51	3.67-3.76

* These experiments were performed with the partial support of the Office of Fossil Energy, U.S. Department of Energy, under the auspices of Grant Number DE-FG 22-80 PC30247.

+ These experiments were reported in NASA CR-174661 and are reproduced here for purposes of comparison.

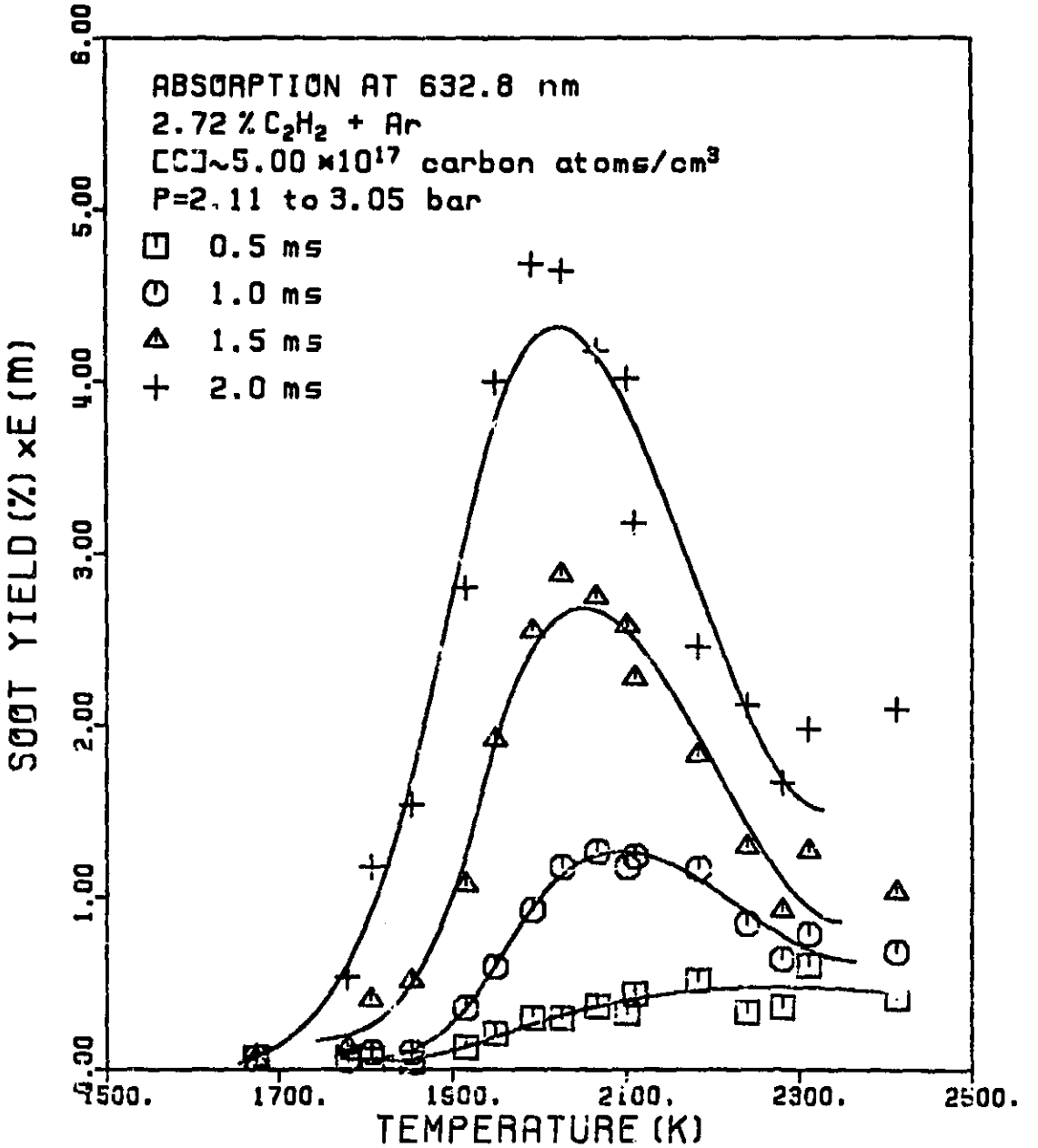

Figure 1. Soot yields vs. temperature at different reaction times for the mixture of 2.72% acetylene-argon.

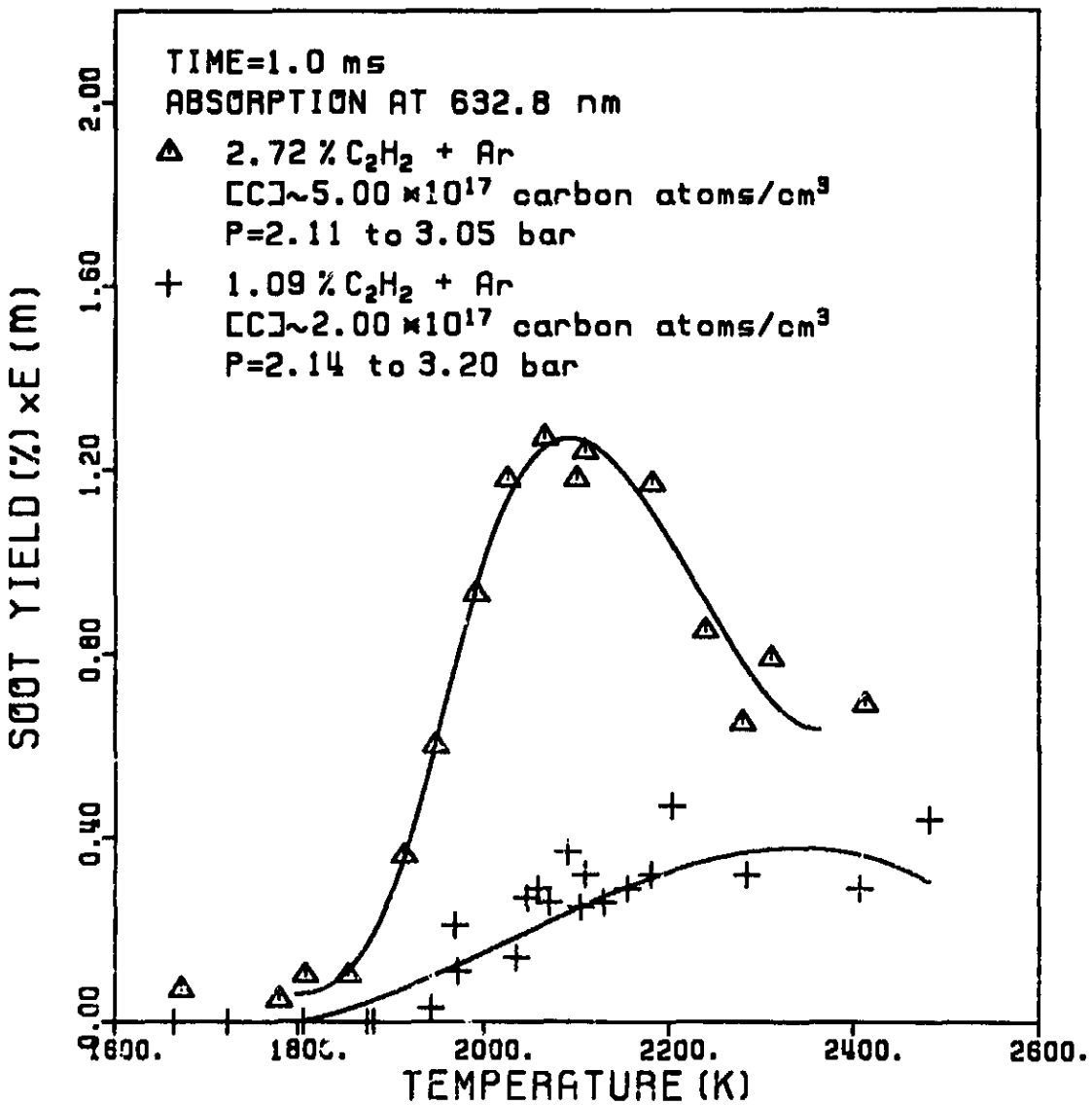

Figure 2. Comparison of soot yield at 1.0 ms for the mixtures 2.72% acetylene-argon and 1.09% acetylene-argon.

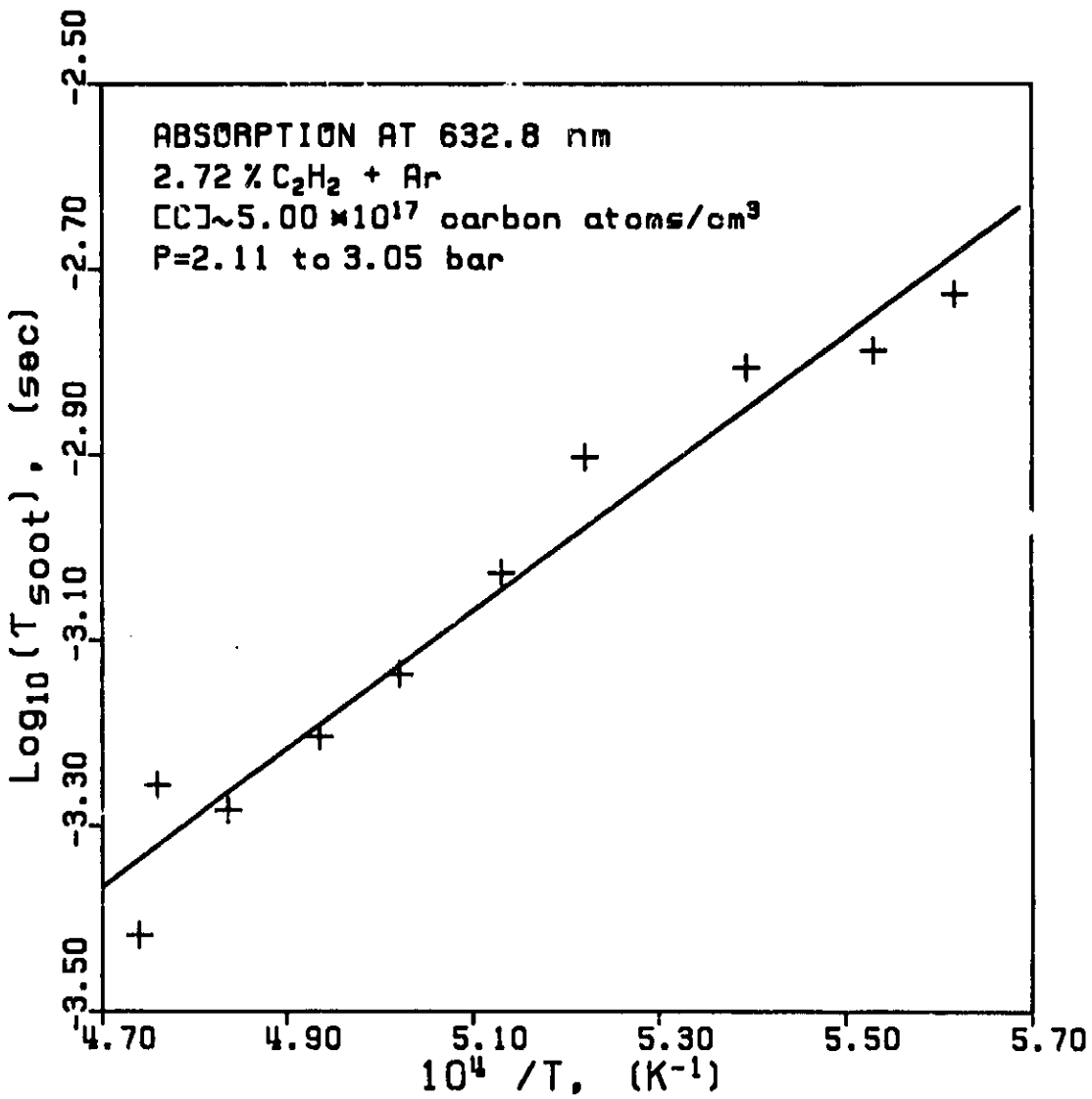

Figure 3. Soot induction times for the mixture of 2.72% acetylene-argon.

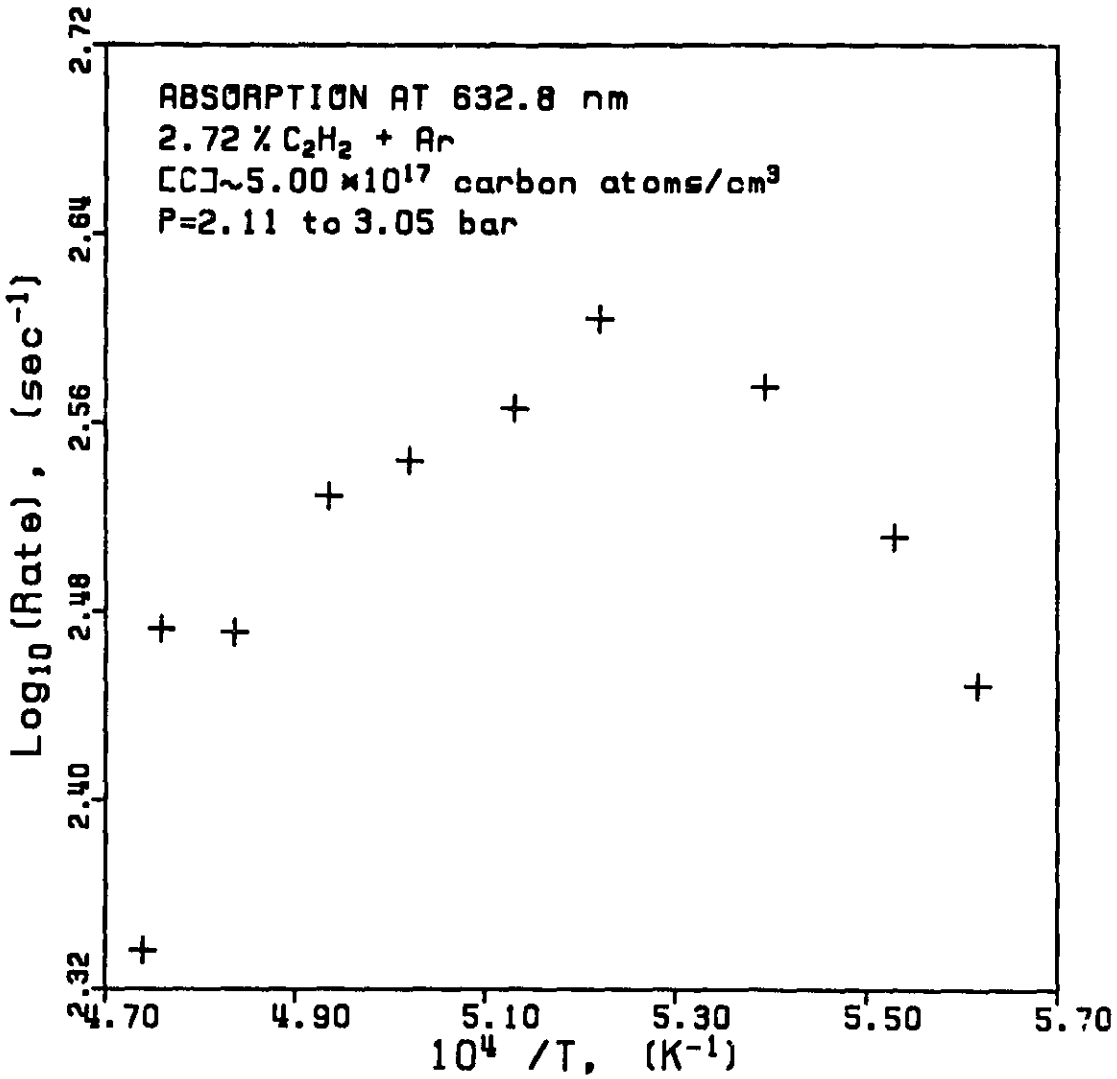

Figure 4. Soot formation rates for the mixture 2.72% acetylene-argon.

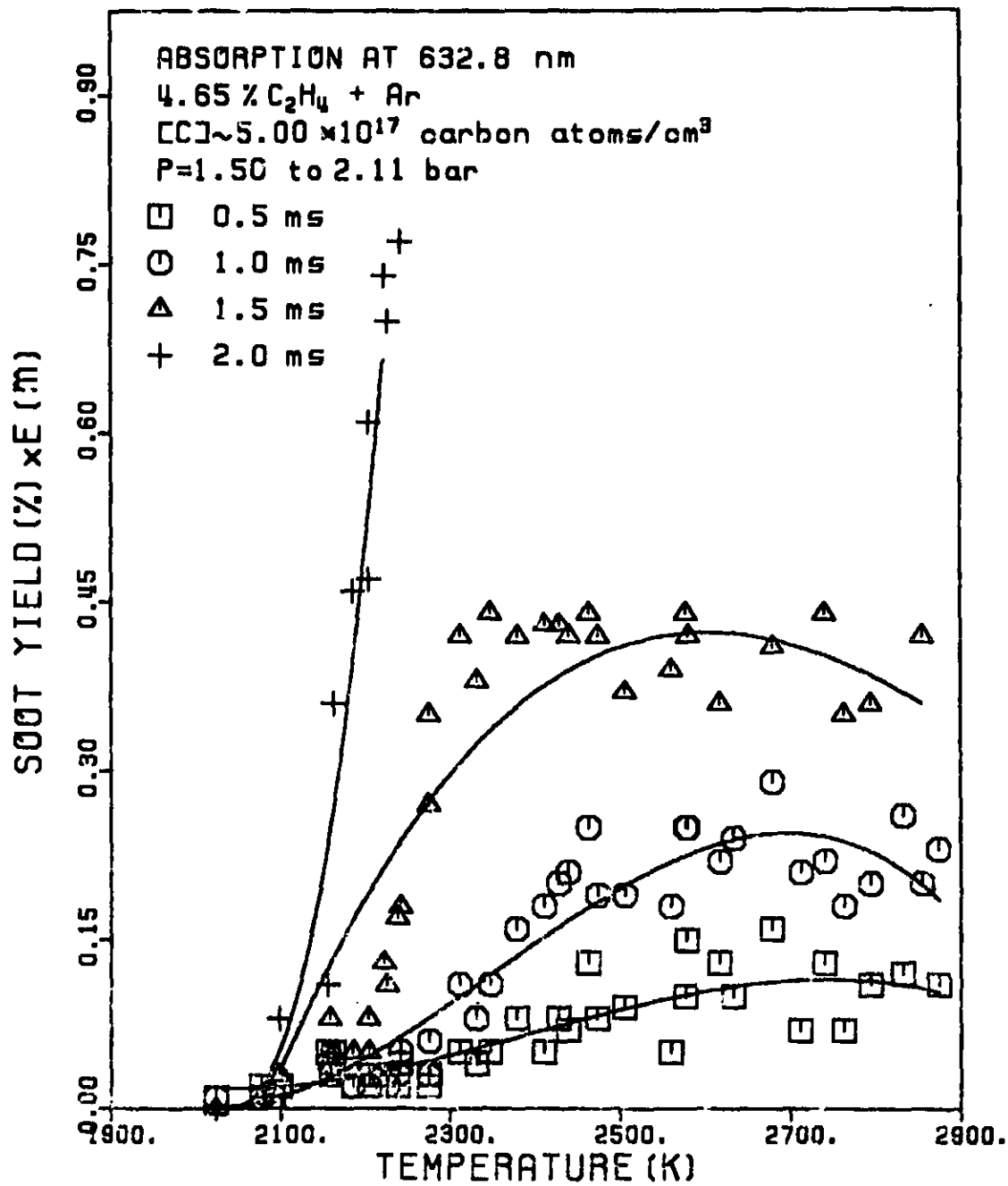

Figure 5. Soot yields vs. temperature at different reaction times for the mixture 4.65% ethylene-argon.

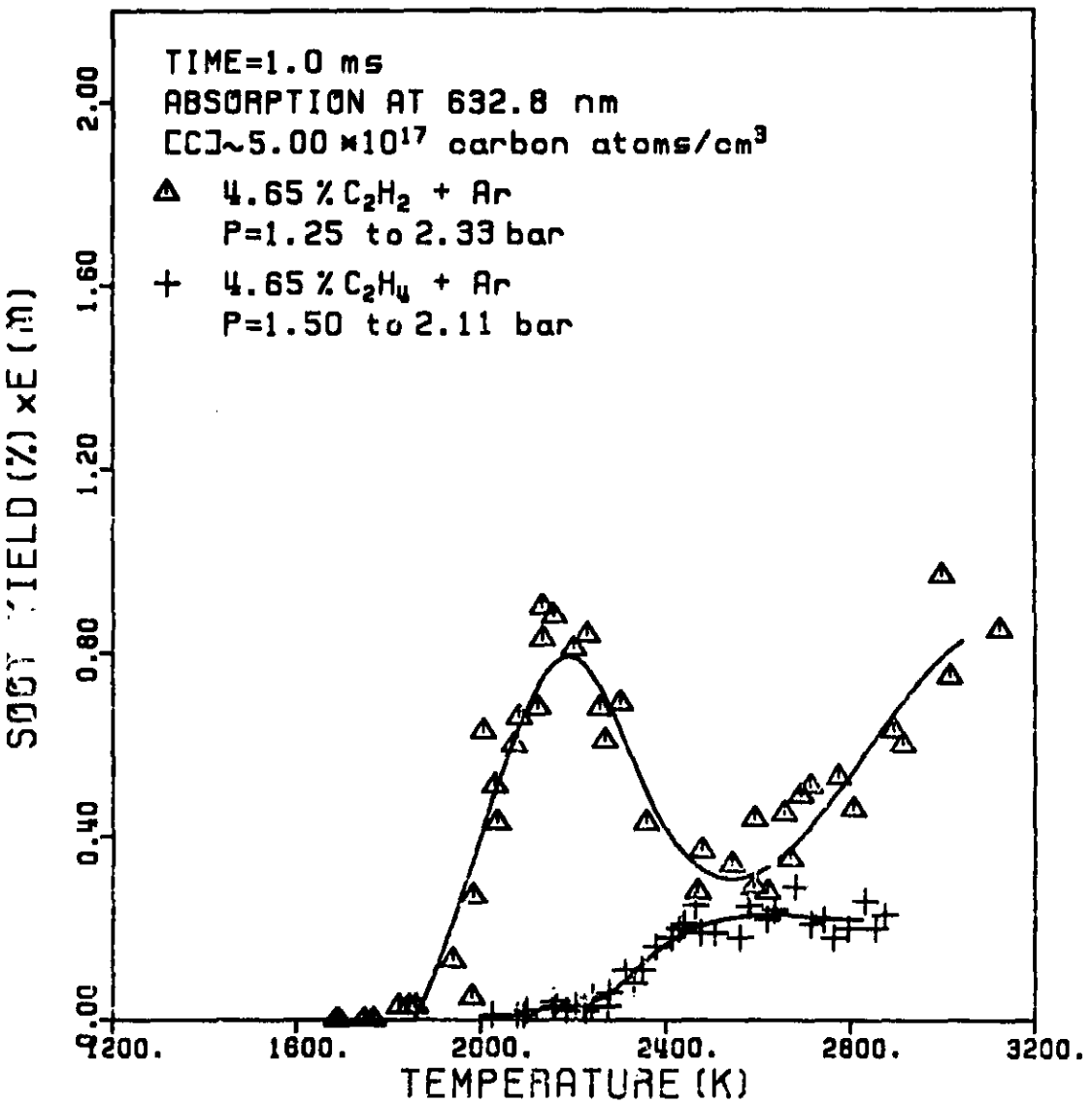

Figure 6. Comparison of soot yield at 1.0 ms for the mixtures 4.65% acetylene-argon and 4.65% ethylene-argon.

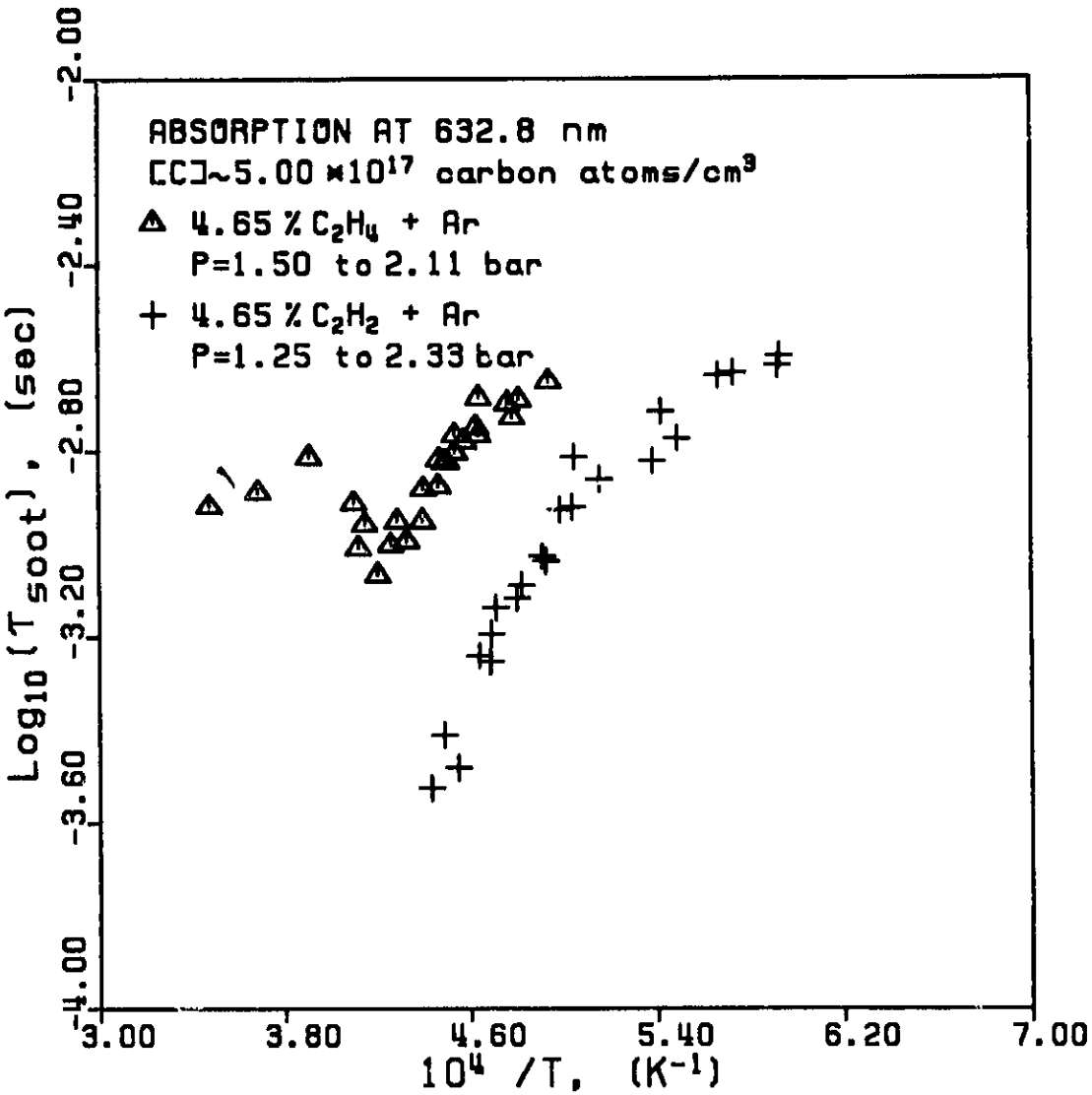

Figure 7. Soot induction times for the mixtures 4.65% ethylene-argon and 4.65% acetylene-argon.

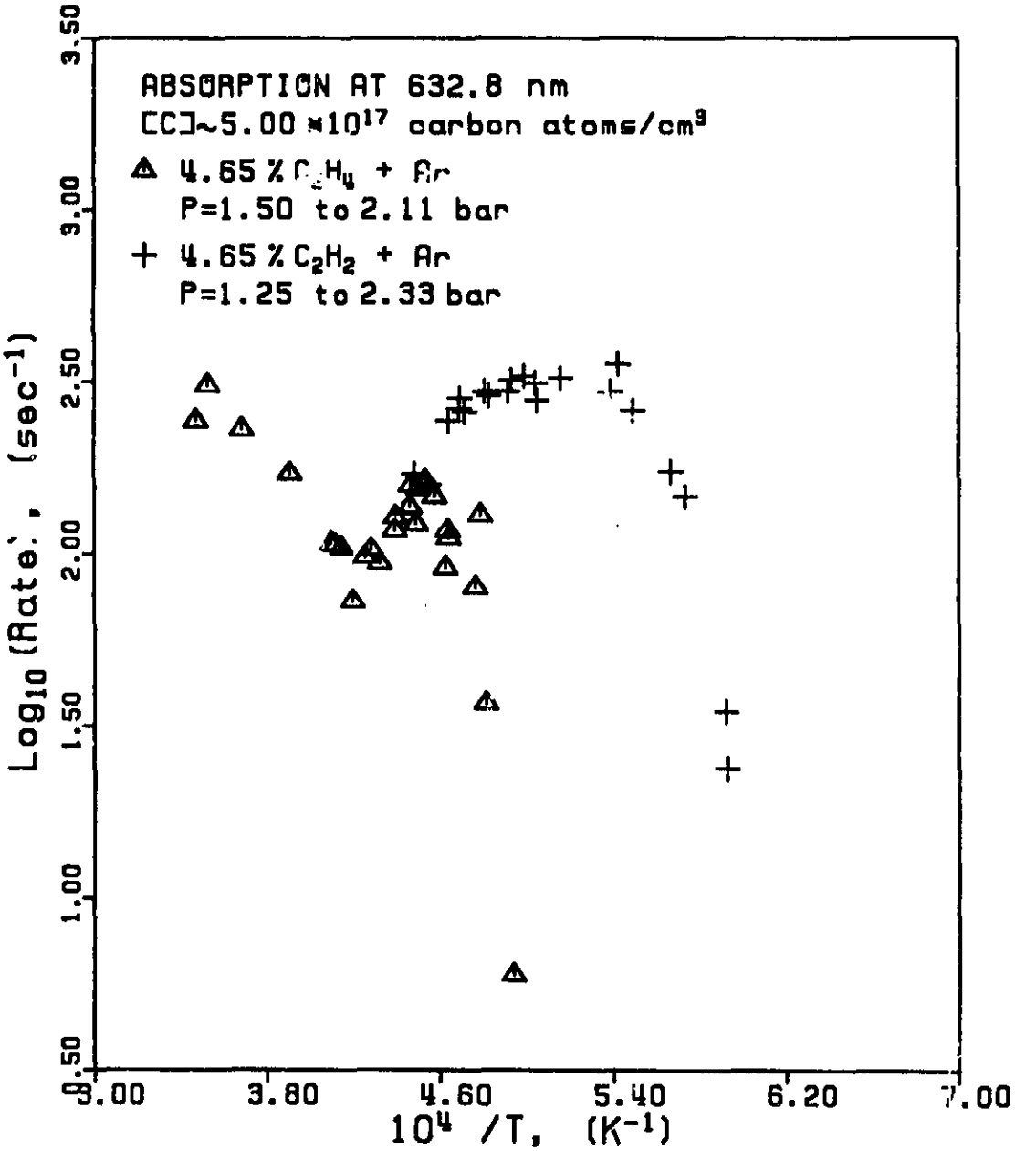

Figure 8. Soot formation rates for the mixtures 4.65% ethylene-argon and 4.65% acetylene-argon.

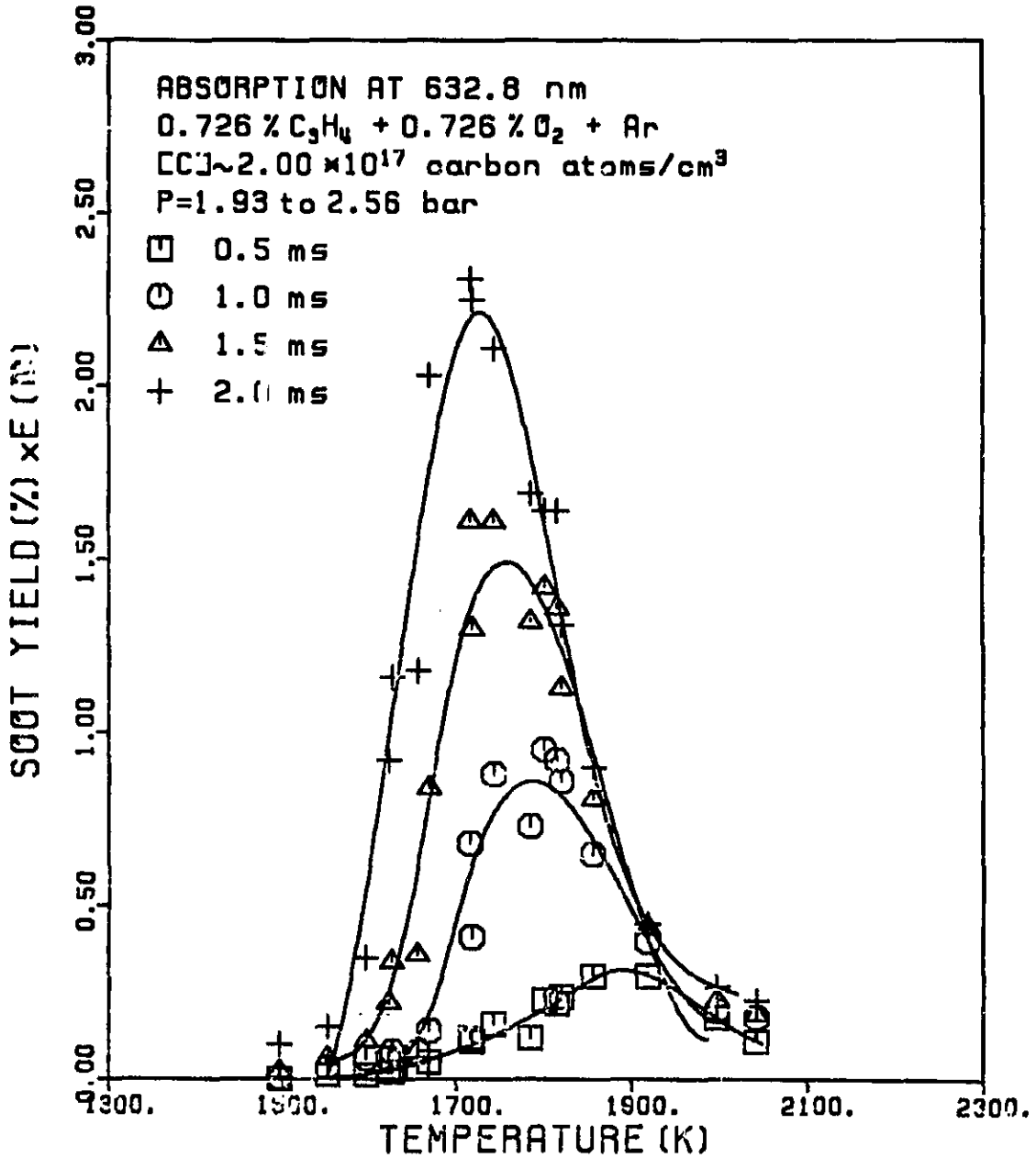

Figure 9. Soot yields vs. temperature at different reaction times for the mixture 0.726% allene-0.726% oxygen-argon.

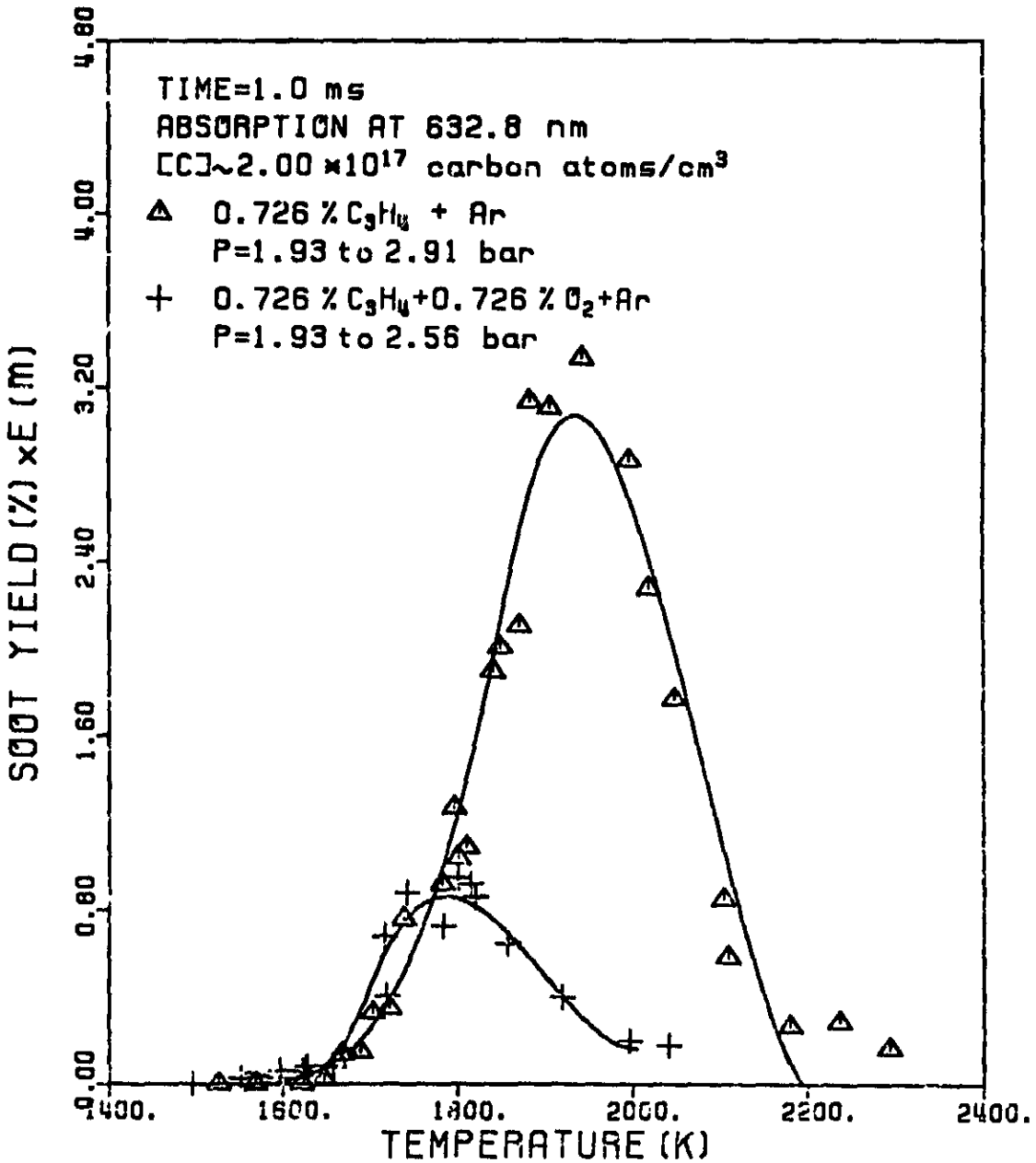

Figure 10. Comparison of soot yield at 1.0 ms for the mixtures 0.726% allene-argon and 0.726% allene-0.726% oxygen-argon.

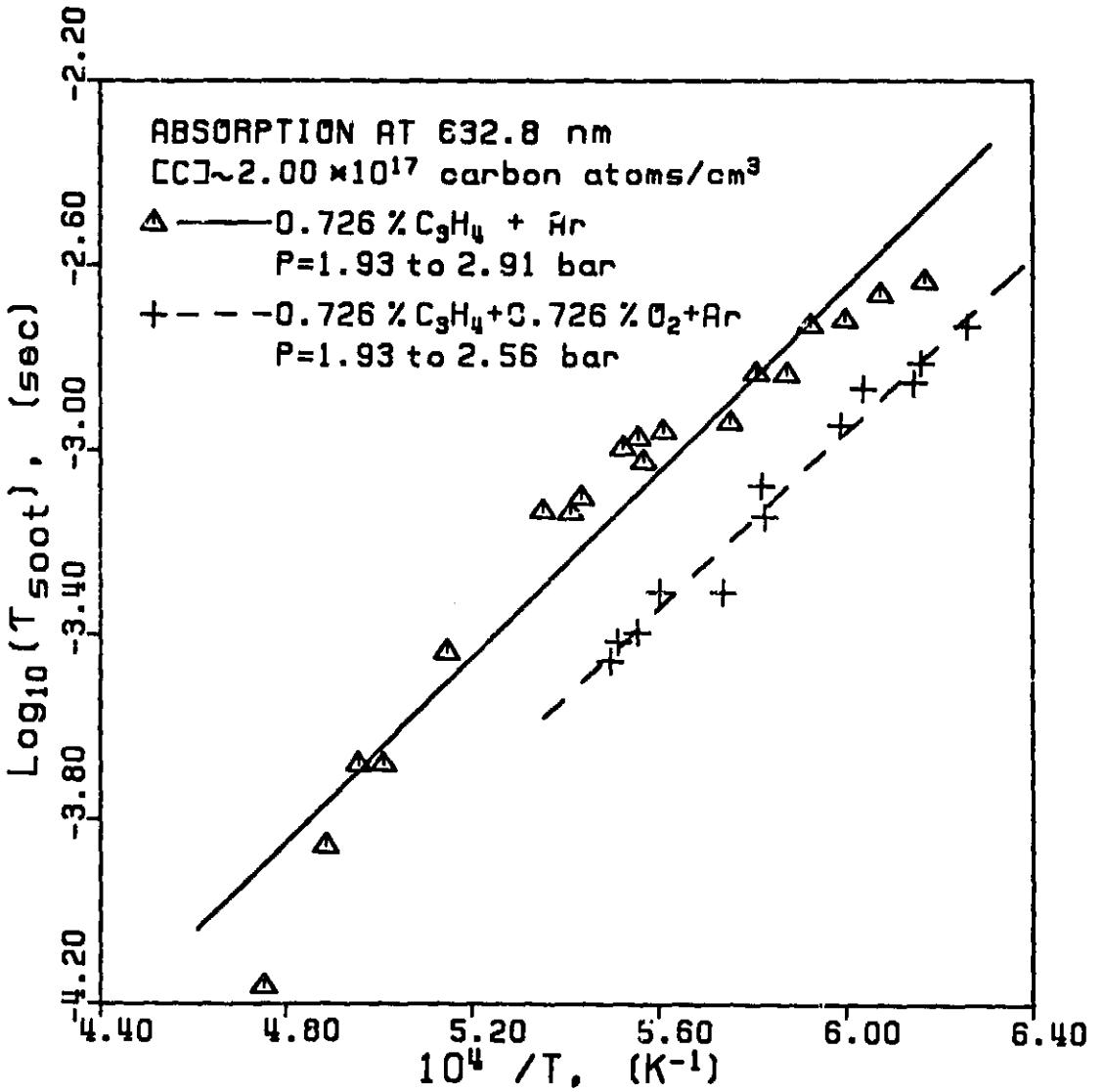

Figure 11. Soot induction times for the mixtures of 0.726% allene-argon and 0.726% allene-0.726% oxygen-argon.

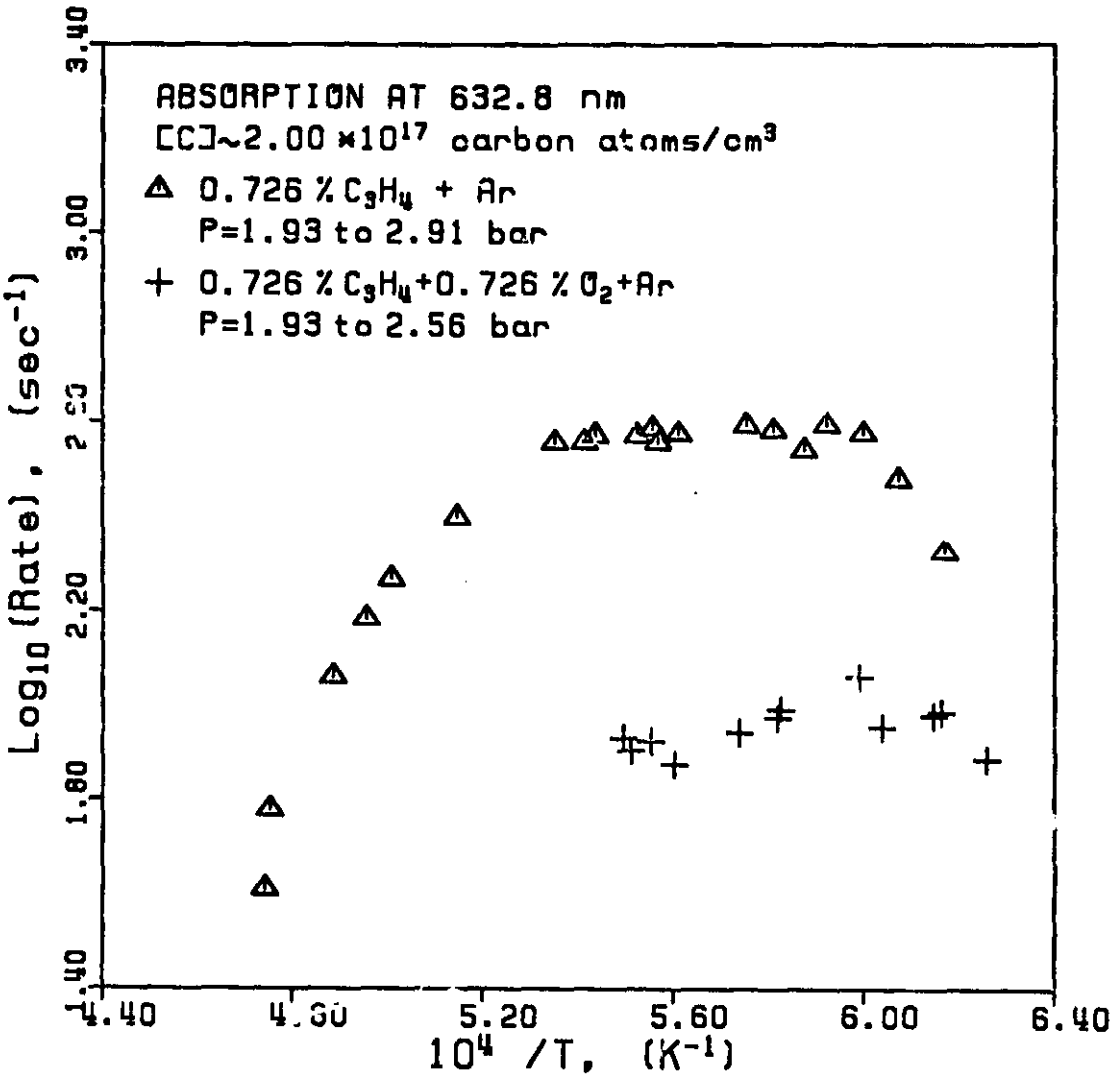

Figure 12. Soot formation rates for the mixtures 0.726% allene-argon and 0.726% allene-0.726% oxygen-argon.

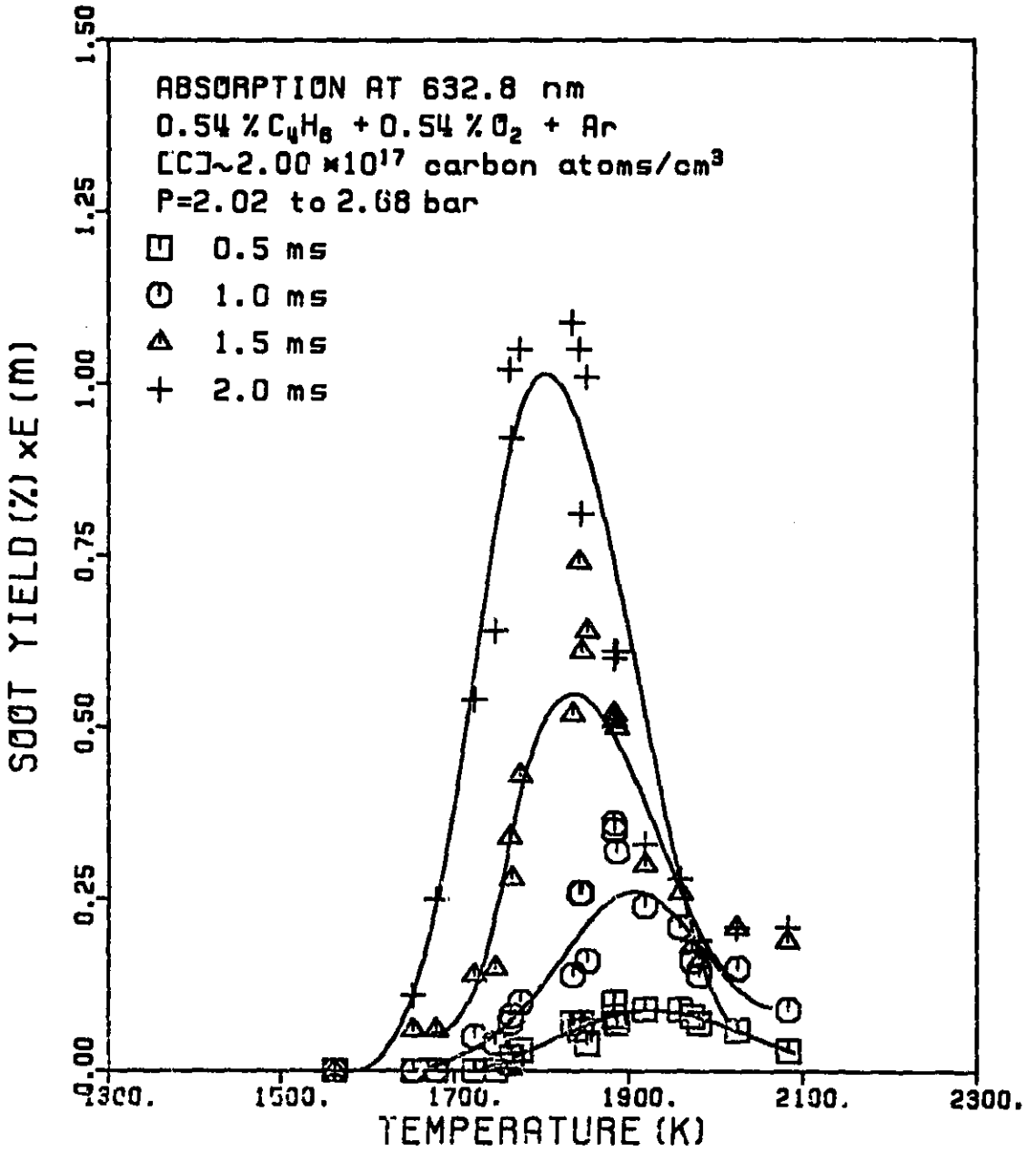

Figure 13. Soot yields vs. temperature at different reaction times for the mixture 0.54% 1,3-butadiene-0.54% oxygen-argon.

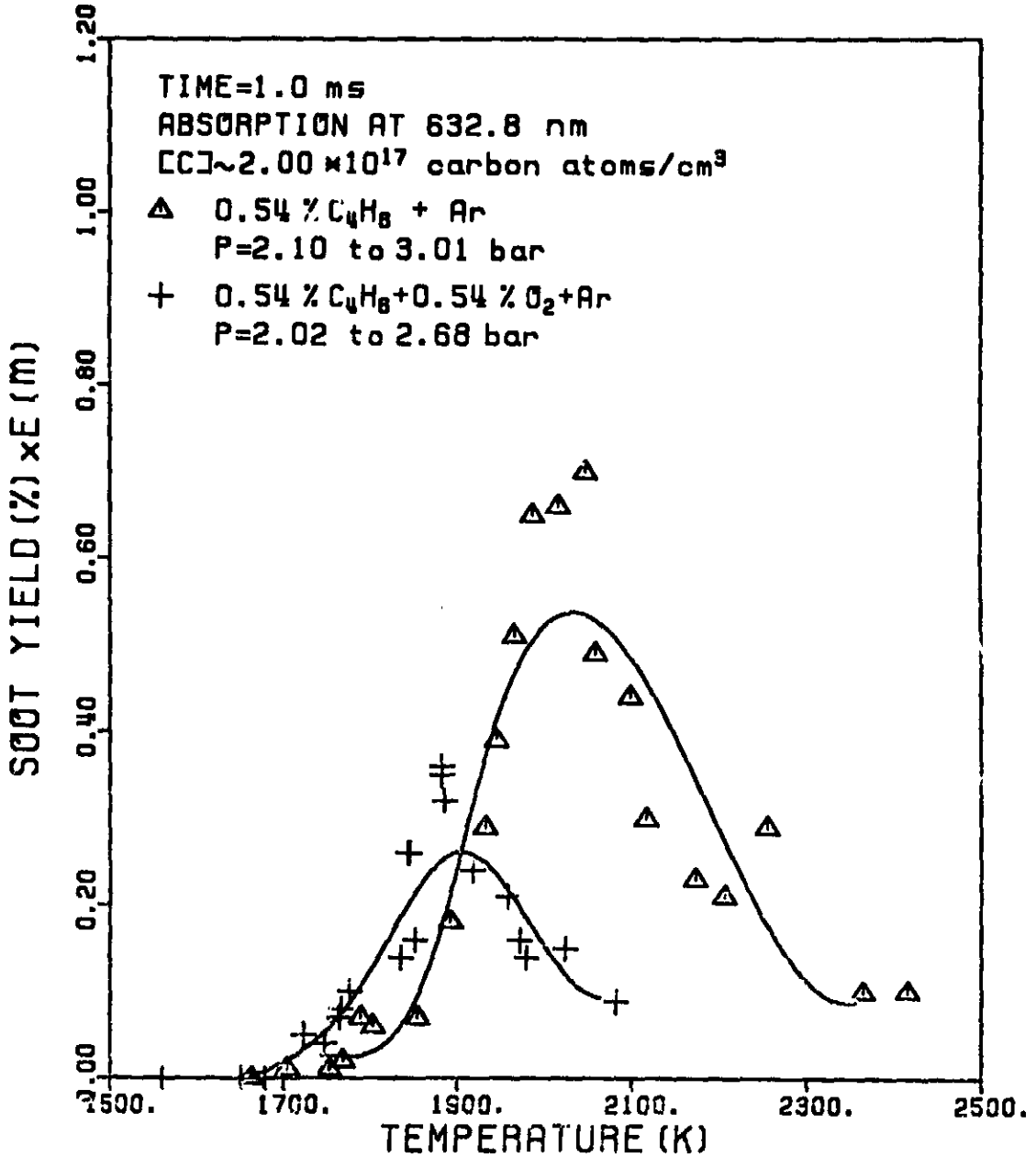

Figure 14. Comparison of soot yield at 1.0 ms for the mixtures 0.54% 1,3-butadiene-argon and 0.54% 1,3-butadiene-0.54% oxygen-argon.

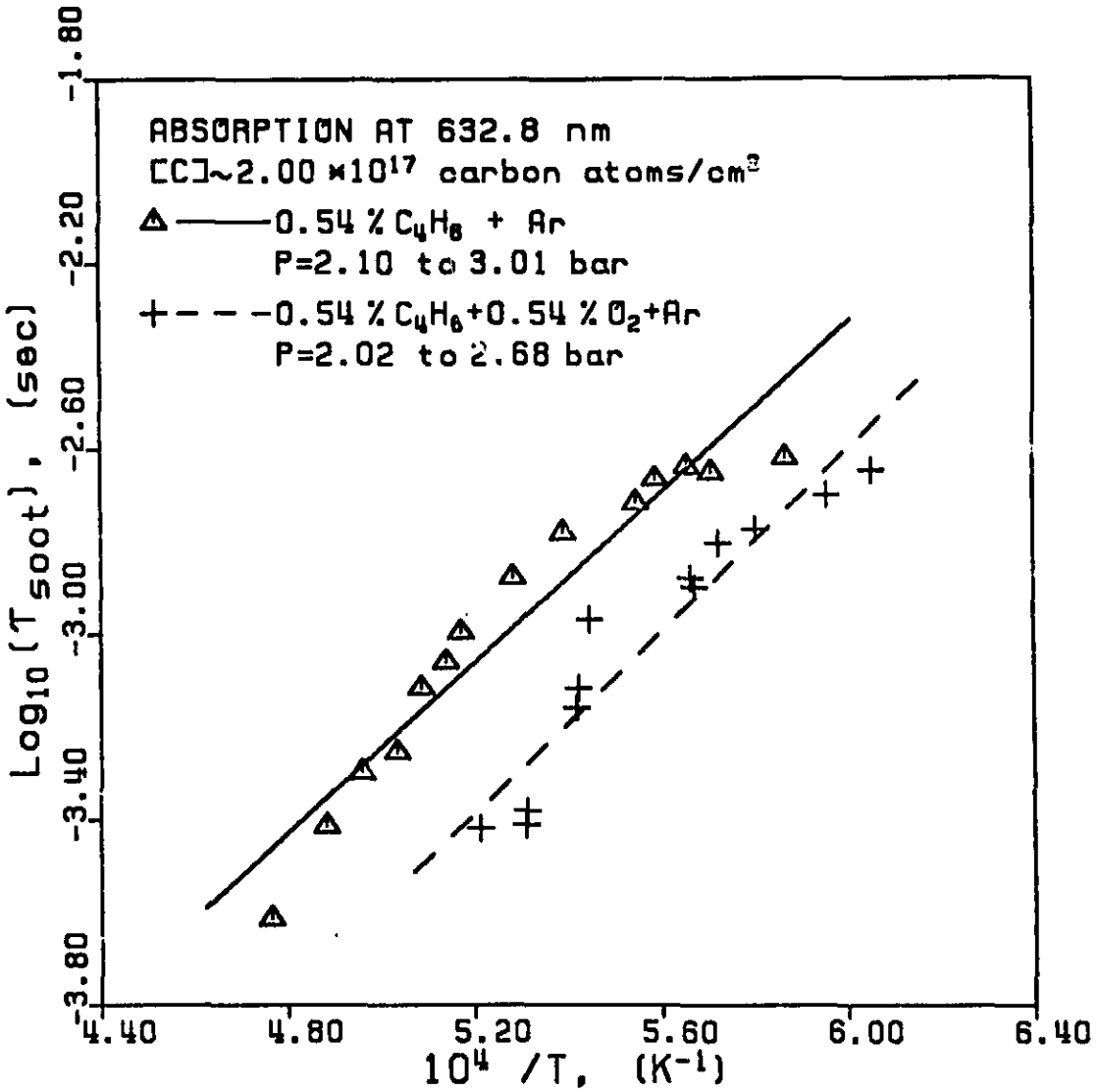

Figure 15. Soot induction times for the mixtures 0.54% 1,3-butadiene-argon and 0.54% 1,3-butadiene-0.54% oxygen-argon.

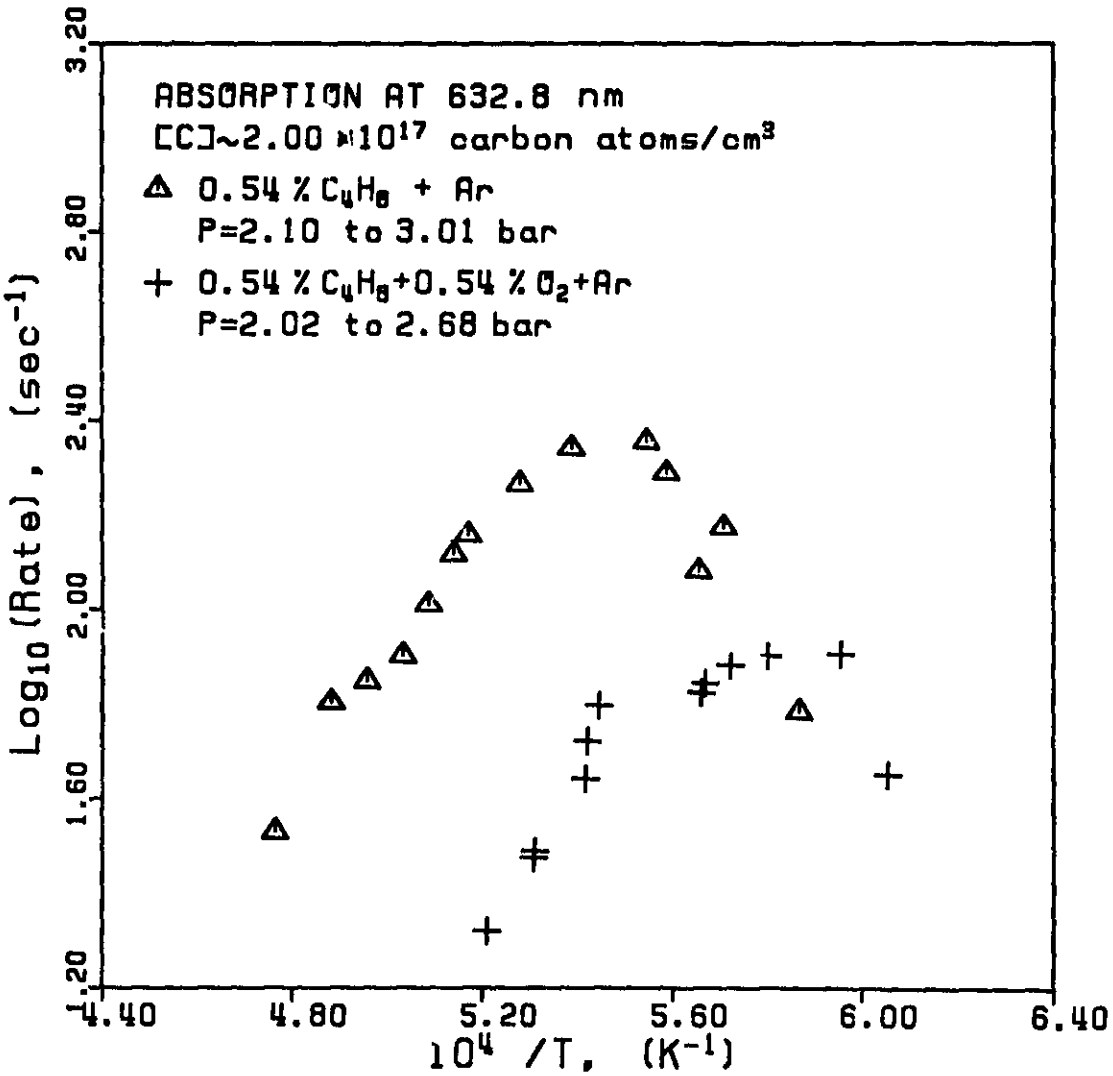

Figure 16. Soot formation rates for the mixtures 0.54% 1,3-butadiene-argon and 0.54% 1,3-butadiene-0.54% oxygen-argon.

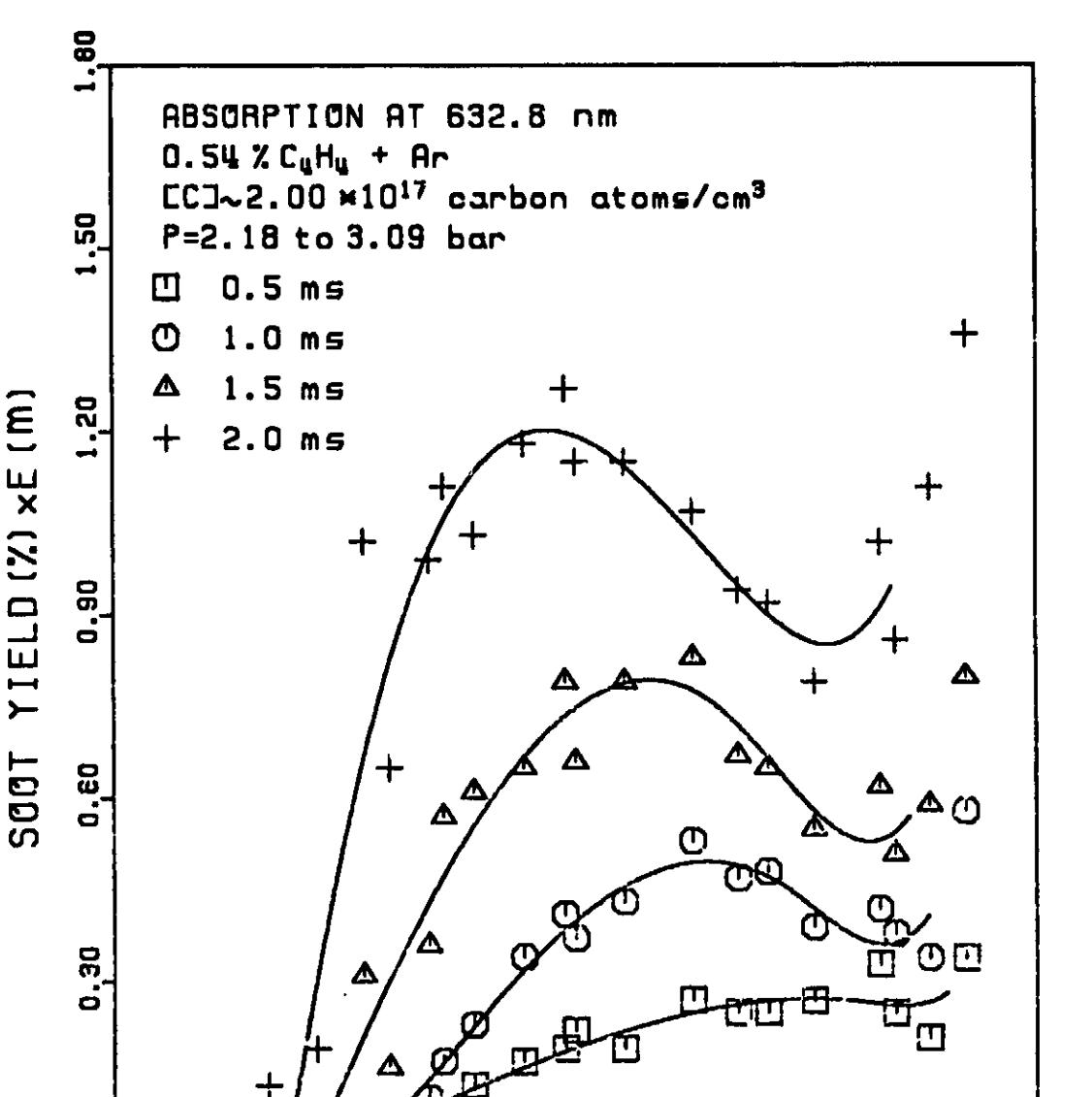

Figure 17. Soot yields vs. temperature at different reaction times for the mixture 0.54% vinylacetylene-argon.

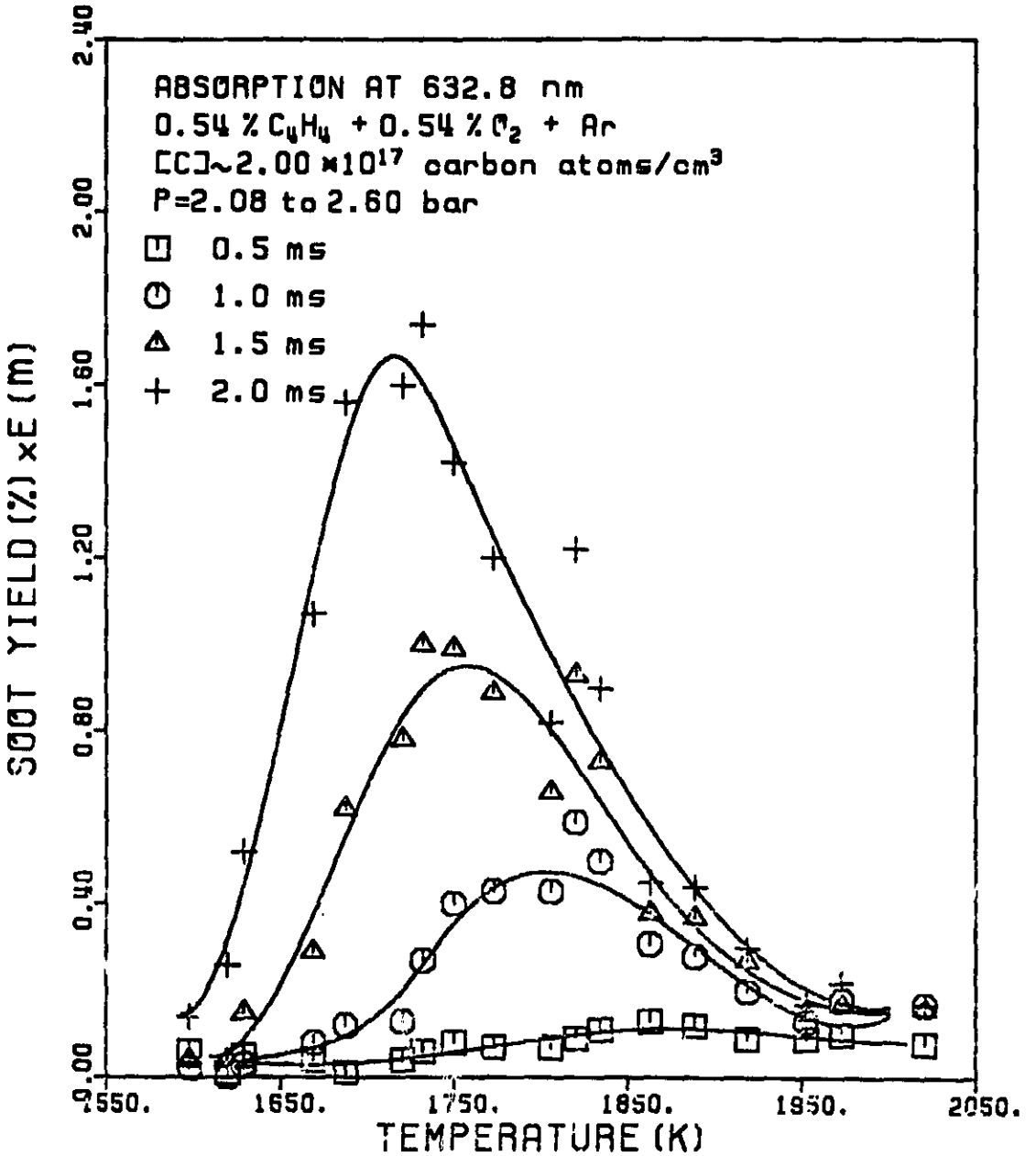

Figure 18. Soot yields vs. temperature at different reaction times for the mixture 0.54% vinylacetylene-0.54% oxygen-argon.

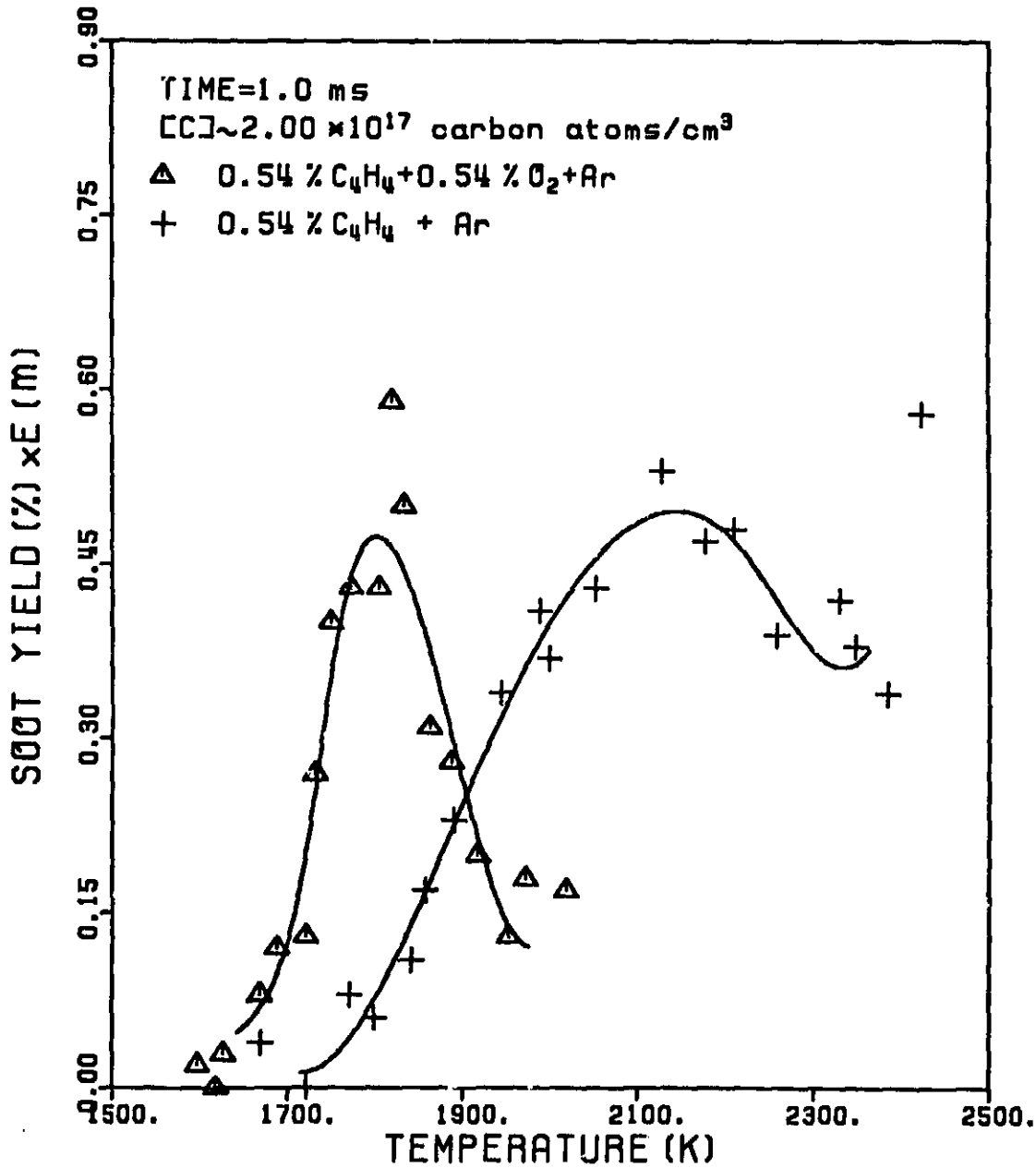

Figure 19. Comparison of soot yield at 1.0 ms for the mixtures 0.54% vinylacetylene-argon and 0.54% vinylacetylene-0.54% oxygen-argon.

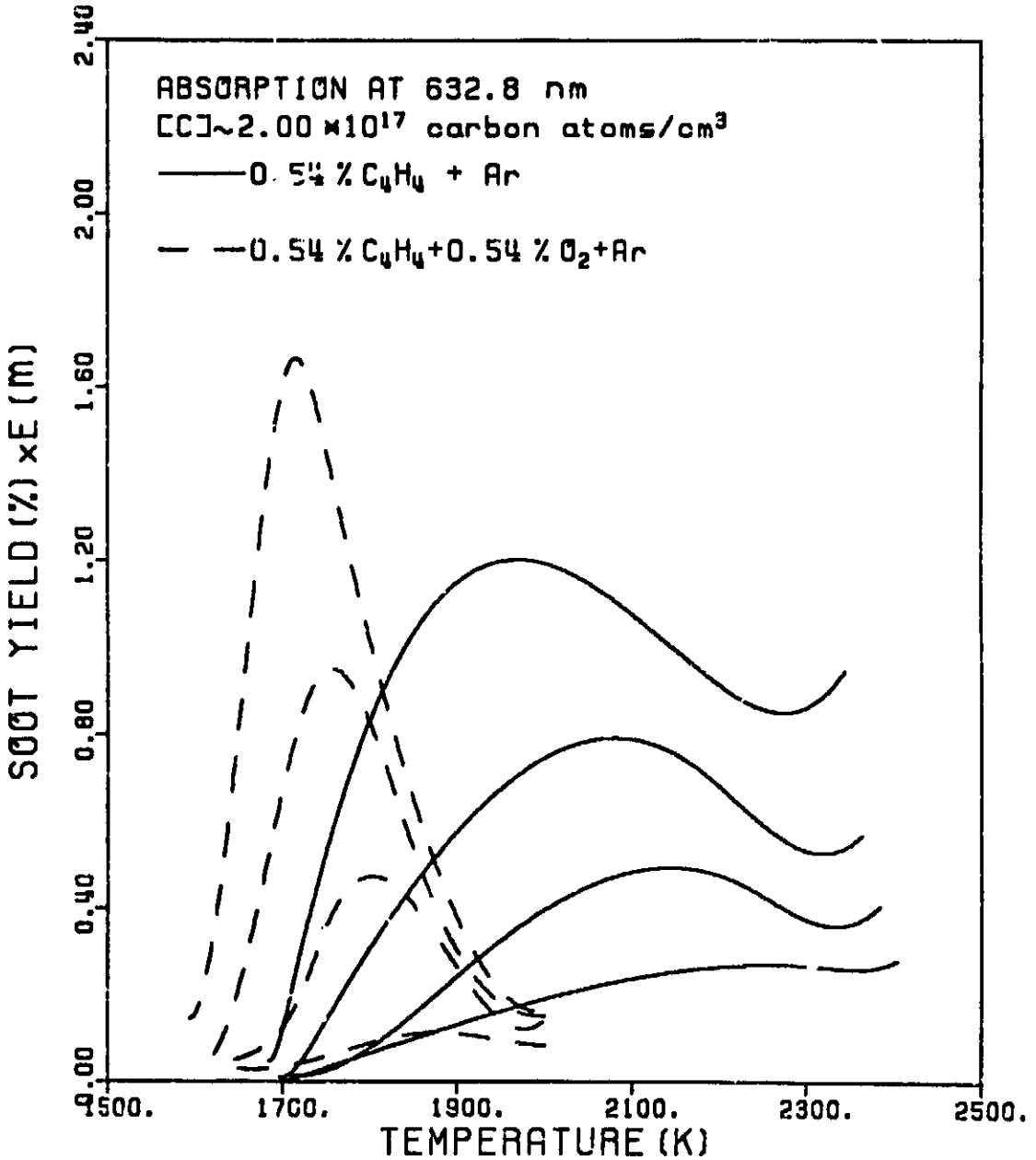

Figure 20. Comparison of soot yield at reaction times of 0.5, 1.0, 1.5 and 2.0 ms for the mixtures 0.54% vinylacetylene-argon and 0.54% vinylacetylene-0.54% oxygen-argon.

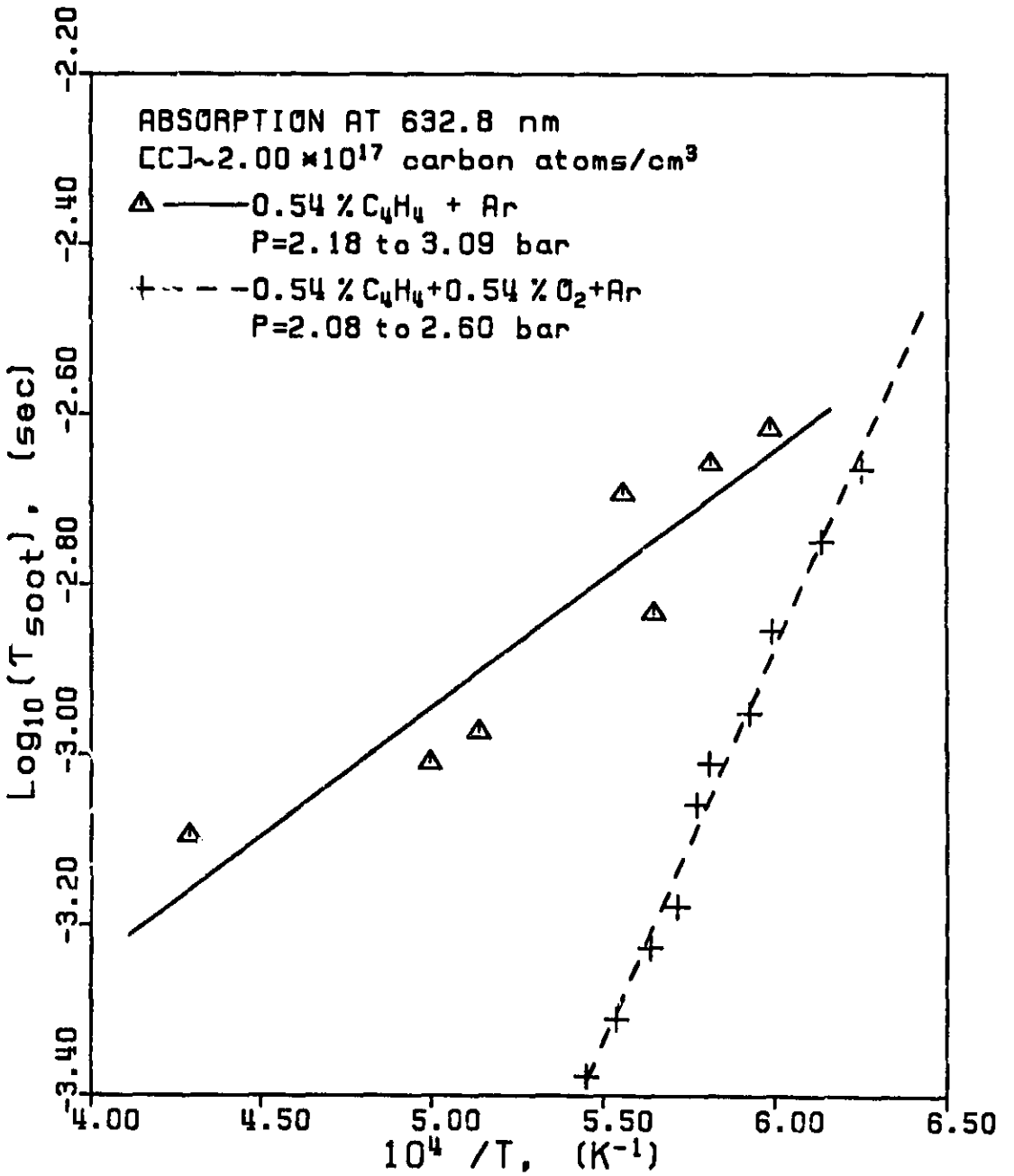

Figure 21. Soot induction times for the mixtures 0.54% vinylacetylene-argon and 0.54% vinylacetylene-0.54% oxygen-argon.

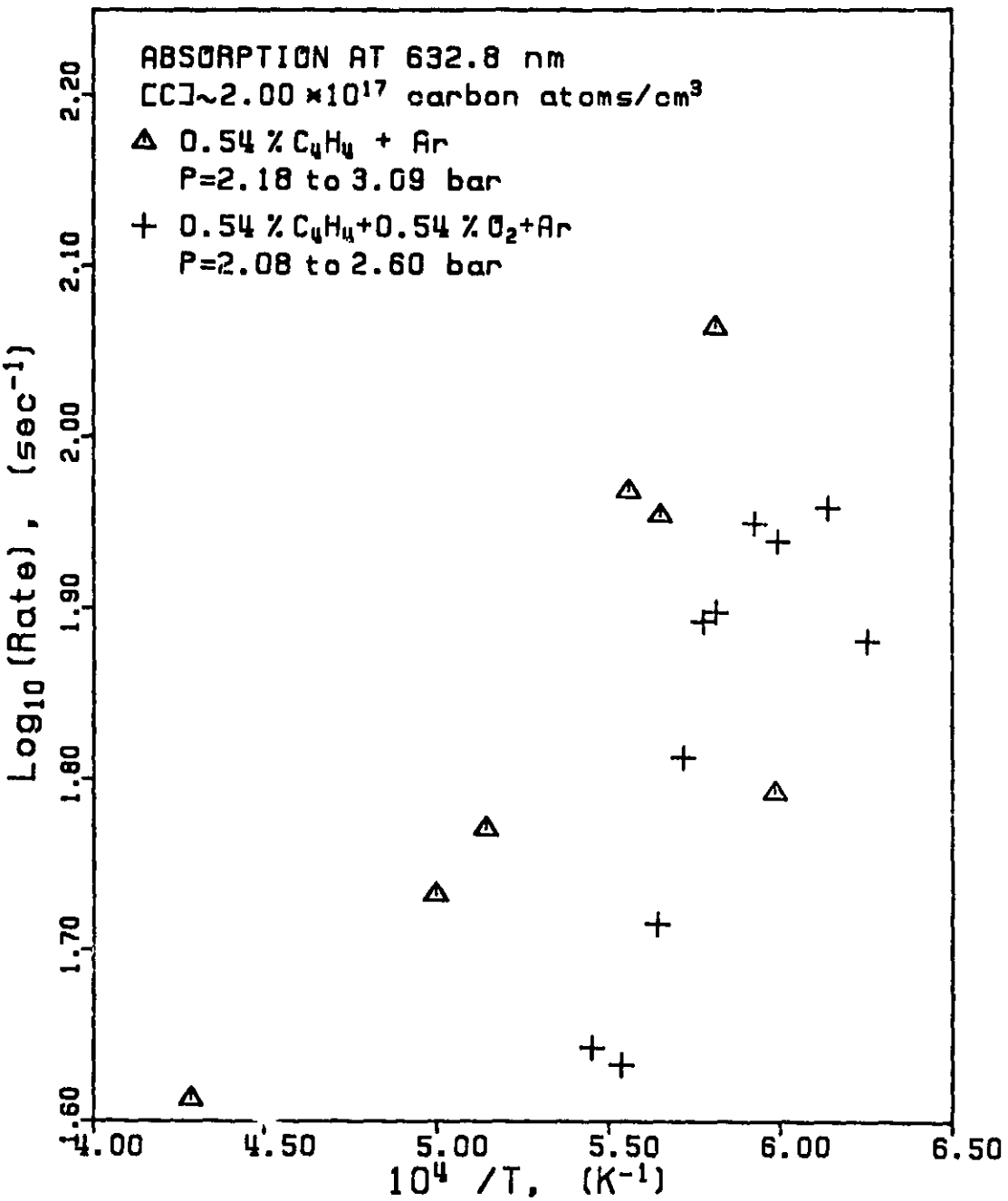

Figure 22. Soot formation rates for the mixtures 0.54% vinylacetylene-argon and 0.54% vinylacetylene-0.54% oxygen-argon.

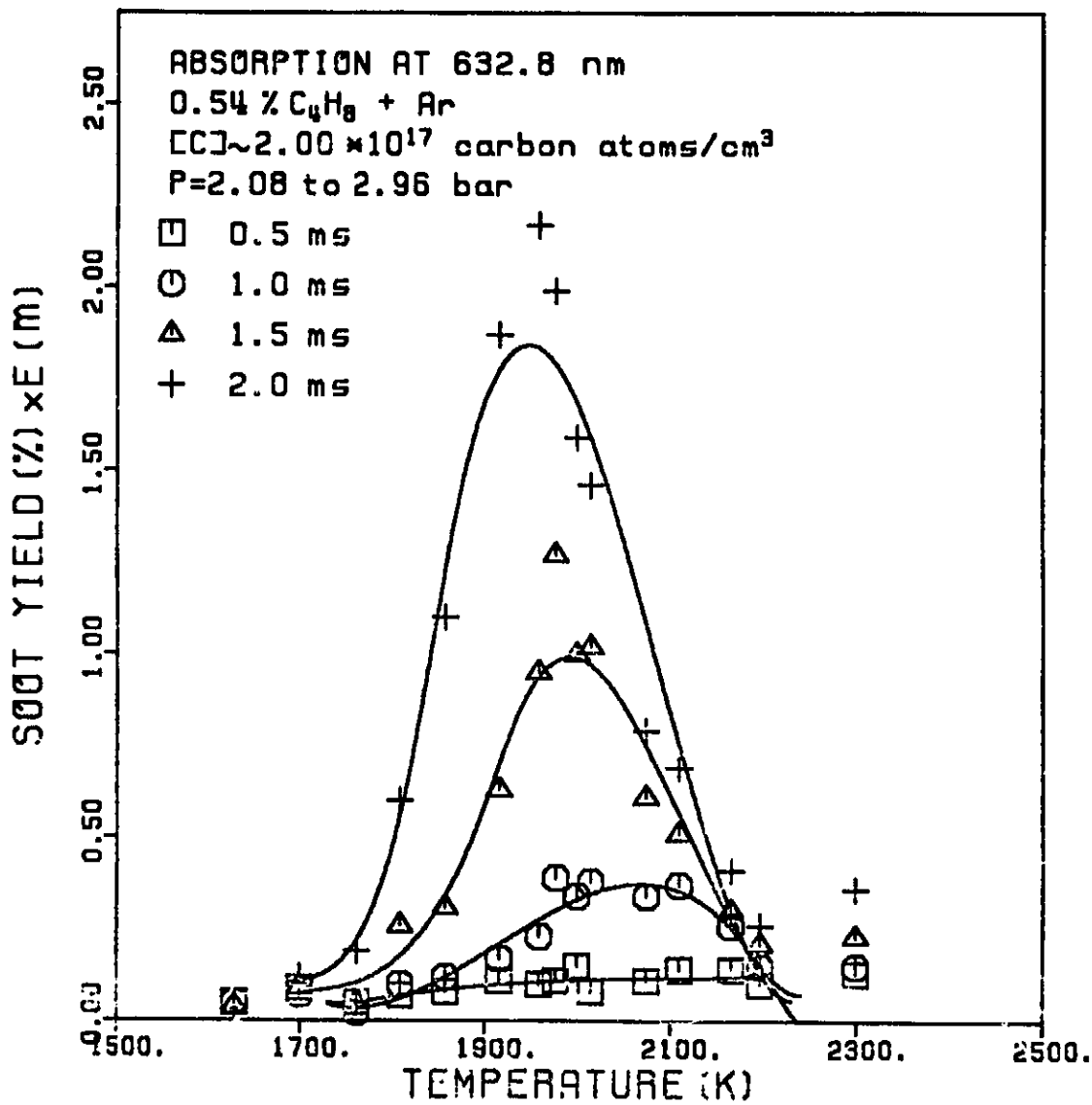

Figure 23. Soot yields vs. temperature at different reaction times for the mixture 0.54% 1-butene-argon.

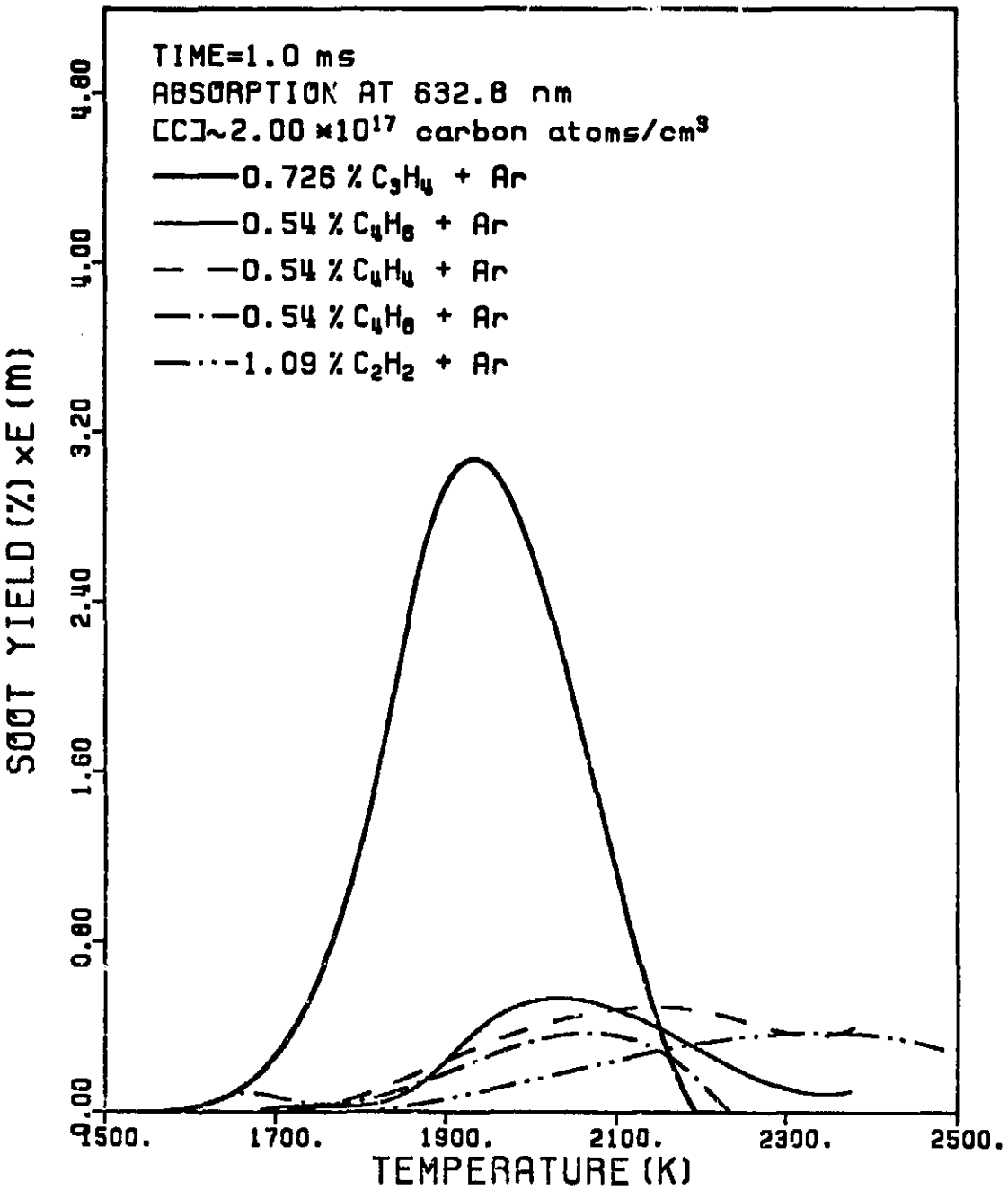

Figure 24. Comparison of soot yield at a reaction time of 1.0 ms for the mixtures 0.726% allene-argon, 0.54% 1,3-butadiene-argon, 0.54% vinylacetylene-argon, 0.54% 1-butene-argon and 1.09% acetylene-argon.

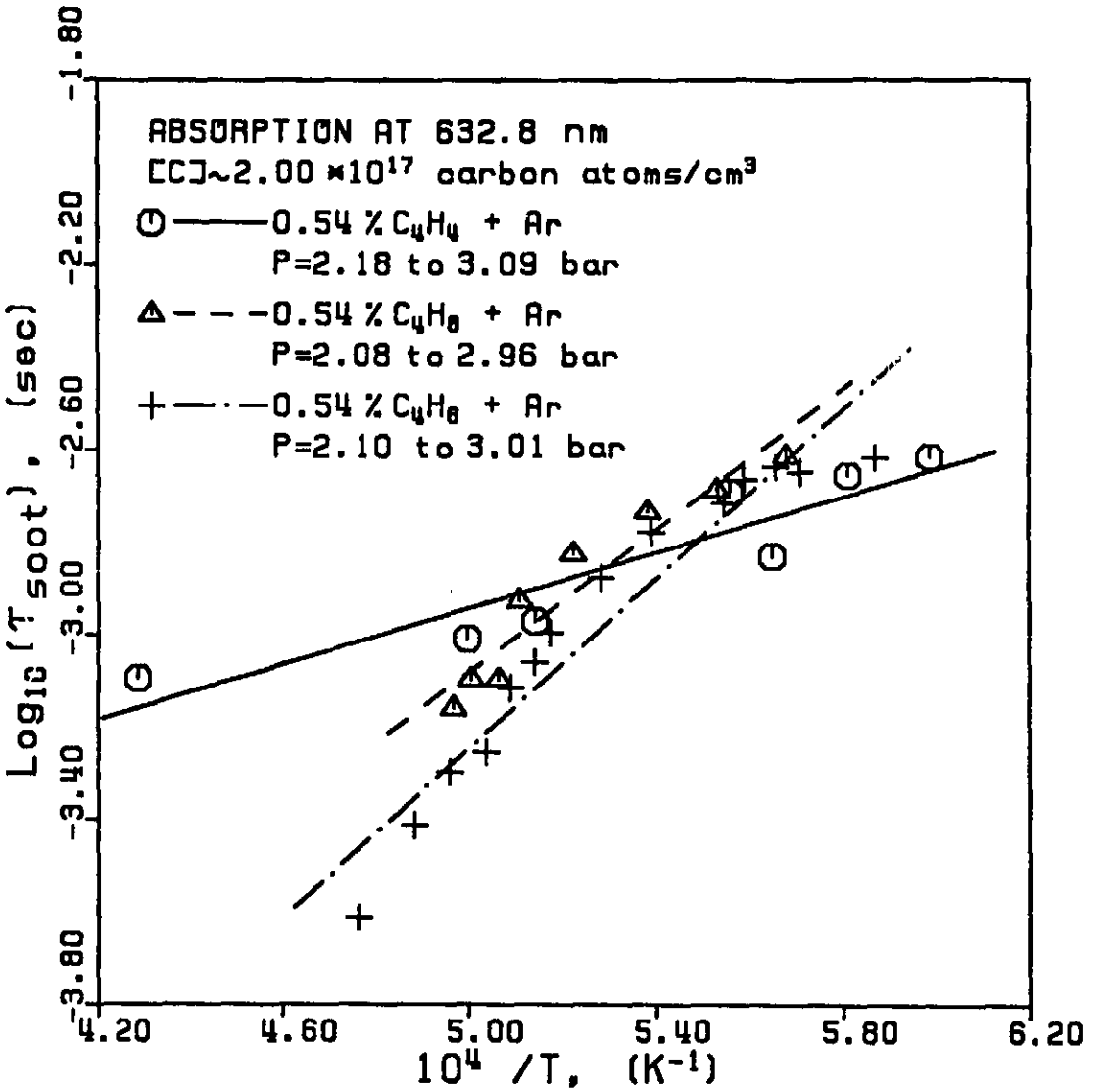

Figure 25. Soot induction times for the mixtures 0.54% vinylacetylene-argon, 0.54% 1-butene-argon and 0.54% 1,3-butadiene-argon.

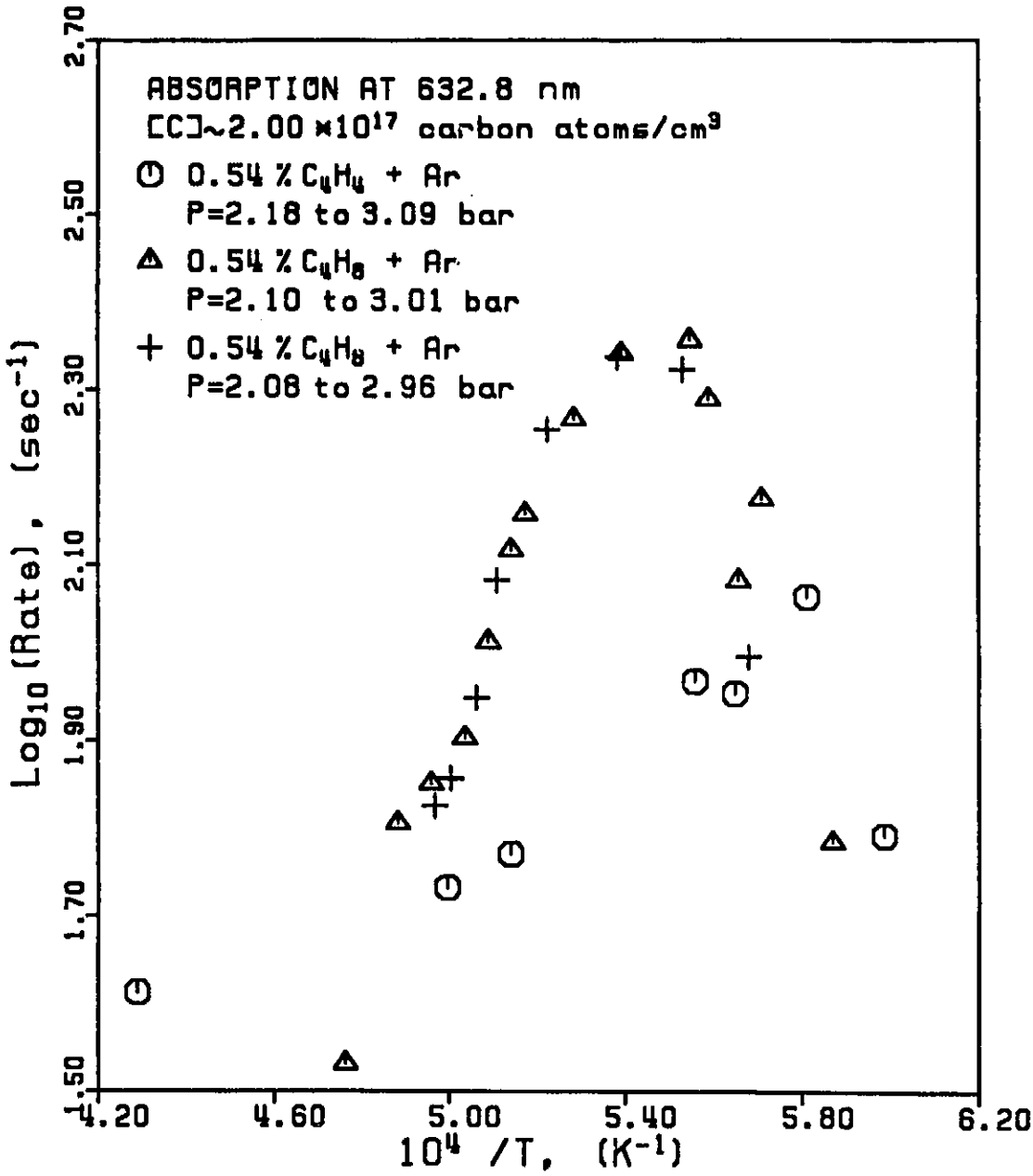

Figure 26. Soot formation rates for the mixtures 0.54% vinylacetylene-argon, 0.54% 1-butene-argon and 0.54% 1,3-butadiene-argon.

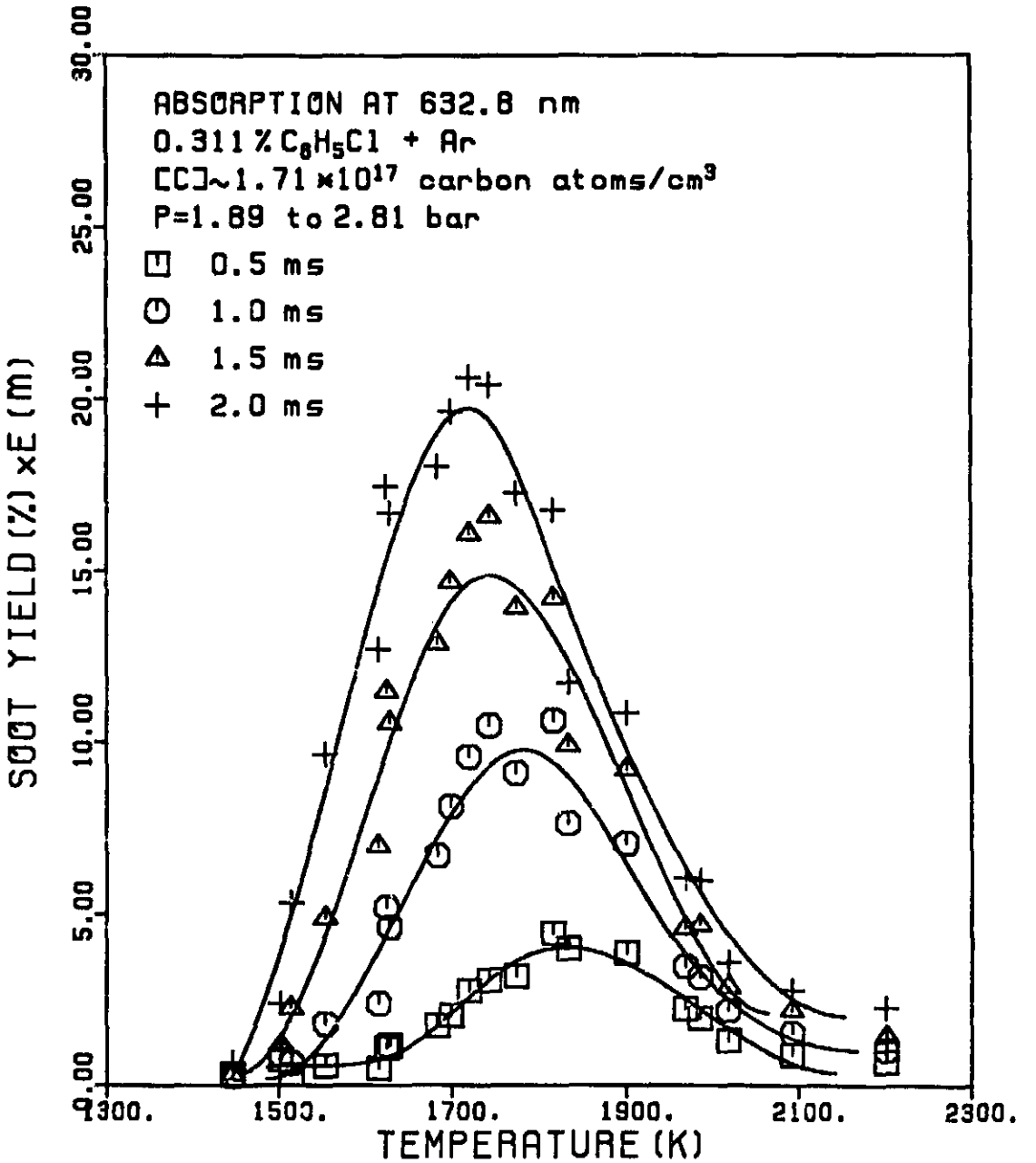

Figure 27. Soot yields vs. temperature at different reaction times for the mixture 0.311% chlorobenzene-argon.

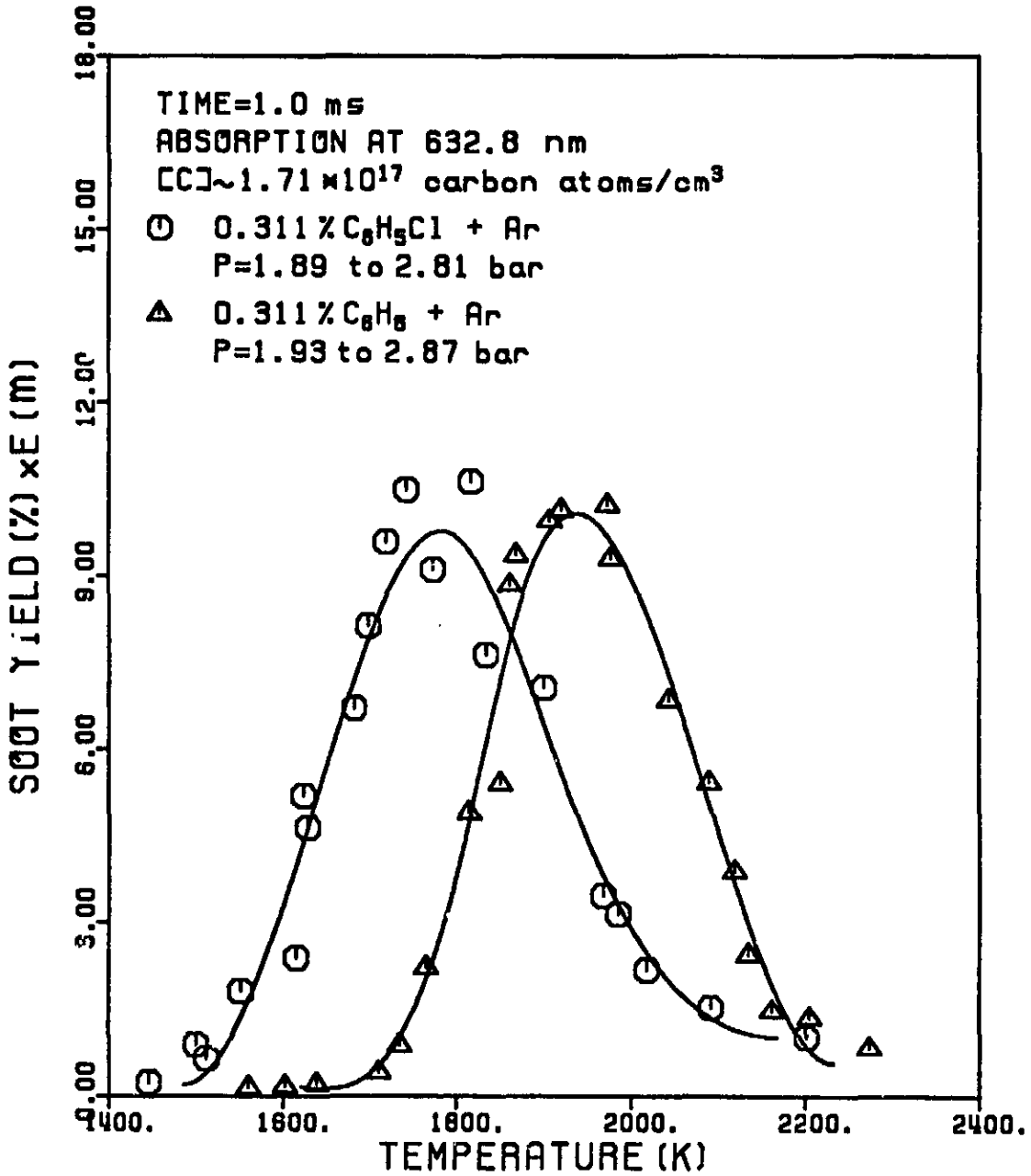

Figure 28. Comparison of soot yield at a reaction time of 1.0 ms for the mixtures 0.311% chlorobenzene-argon and 0.311% benzene-argon.

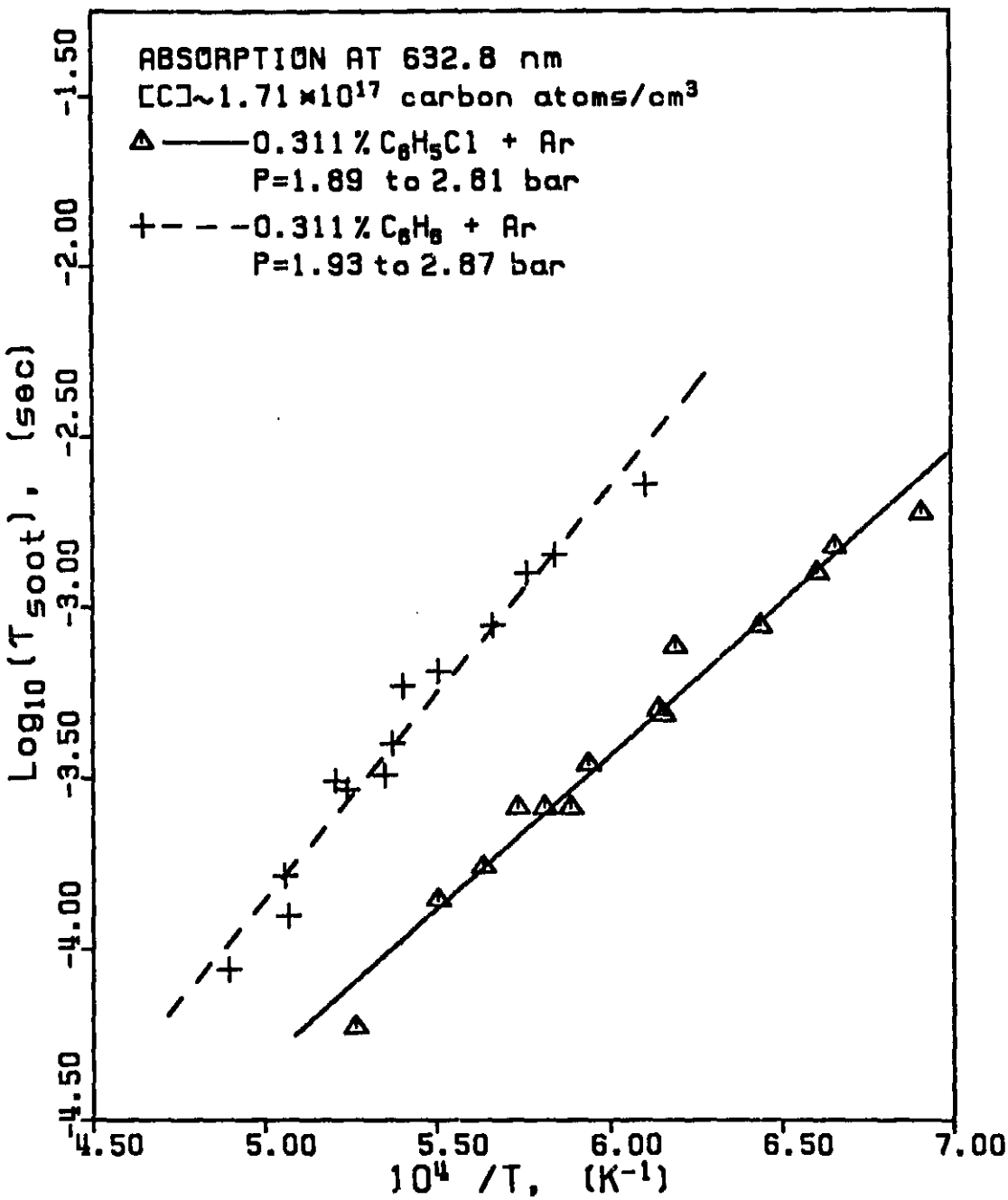

Figure 29. Soot induction times for the mixtures 0.311% benzene-argon and 0.311% chlorobenzene-argon.

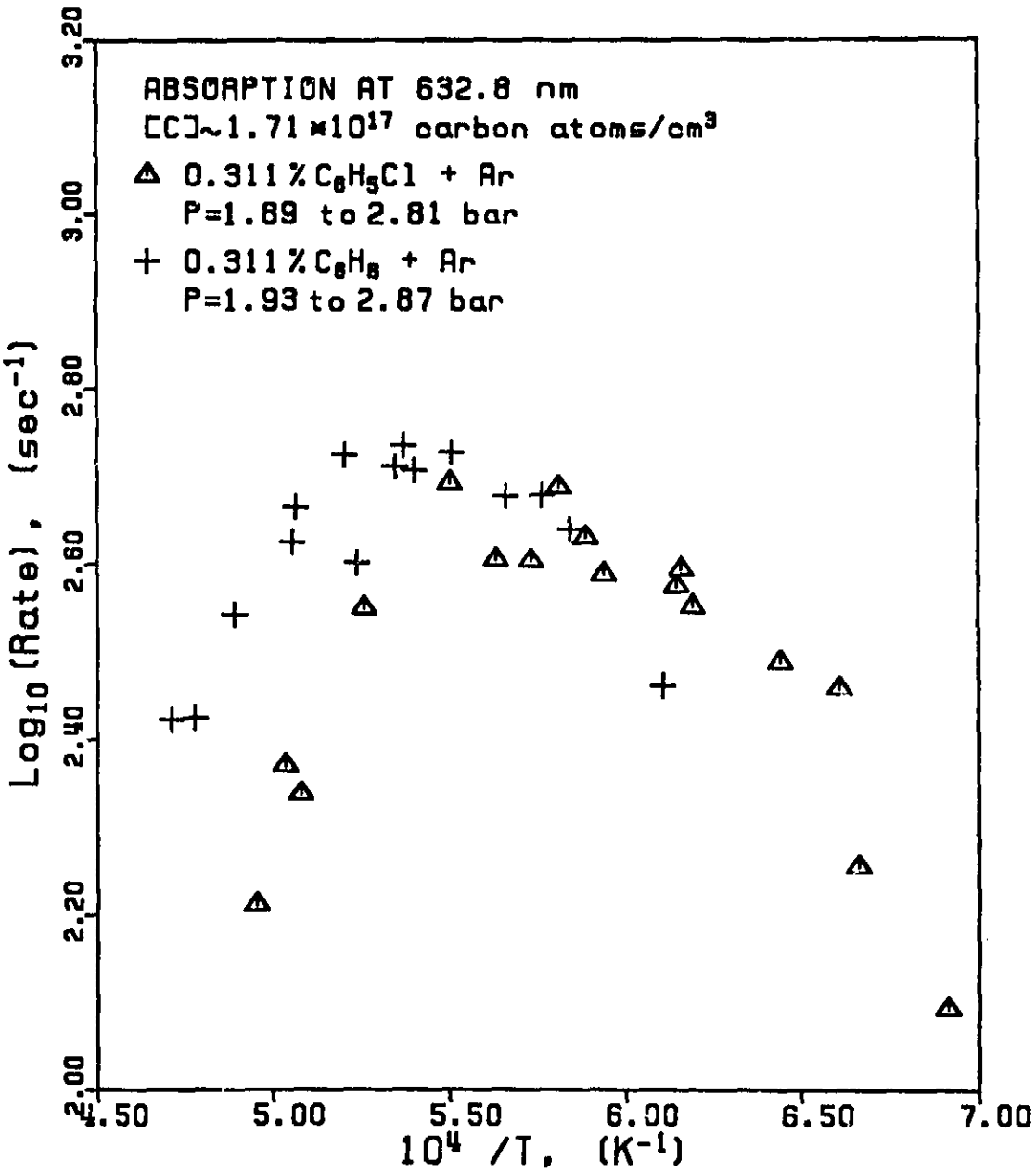

Figure 30. Soot formation rates for the mixtures 0.311% benzene-argon and 0.311% chlorobenzene-argon.

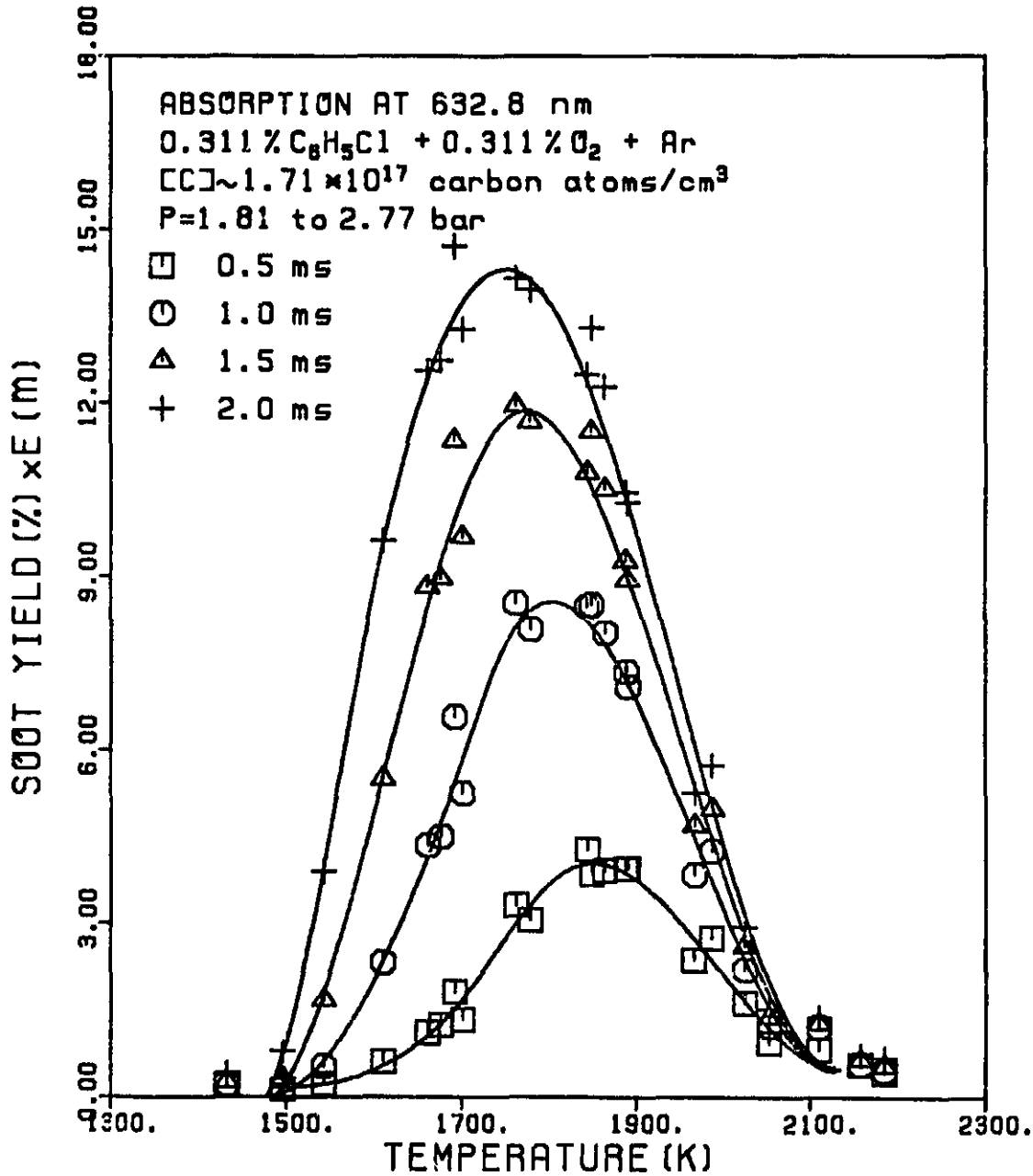

Figure 31. Soot yields vs. temperature at different reaction times for the mixture 0.311% chlorobenzene-0.311% oxygen-argon.

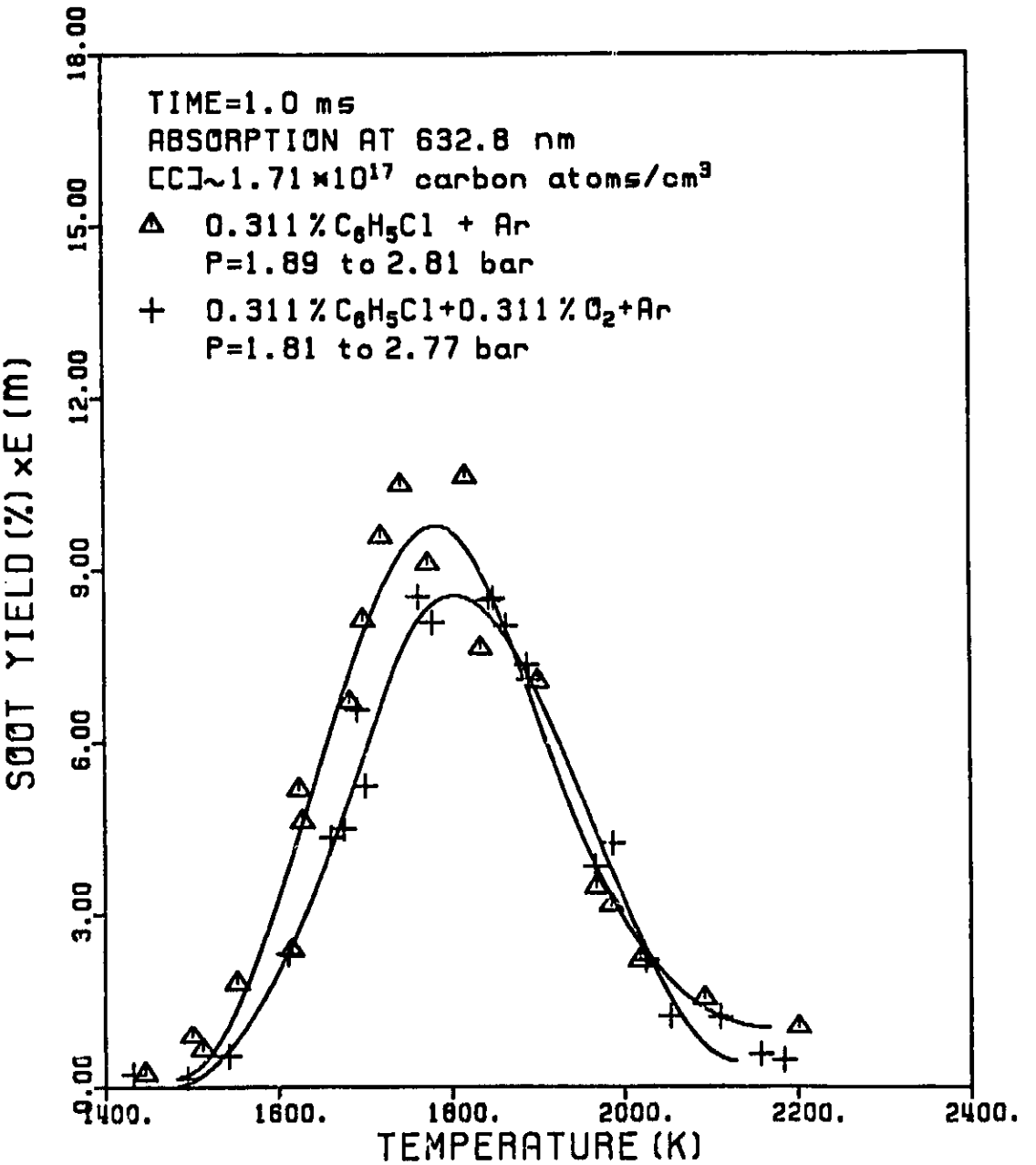

Figure 32. Comparison of soot yield at a reaction time of 1.0 ms for the mixtures 0.311% chlorobenzene-argon and 0.311% chlorobenzene-0.311% oxygen-argon.

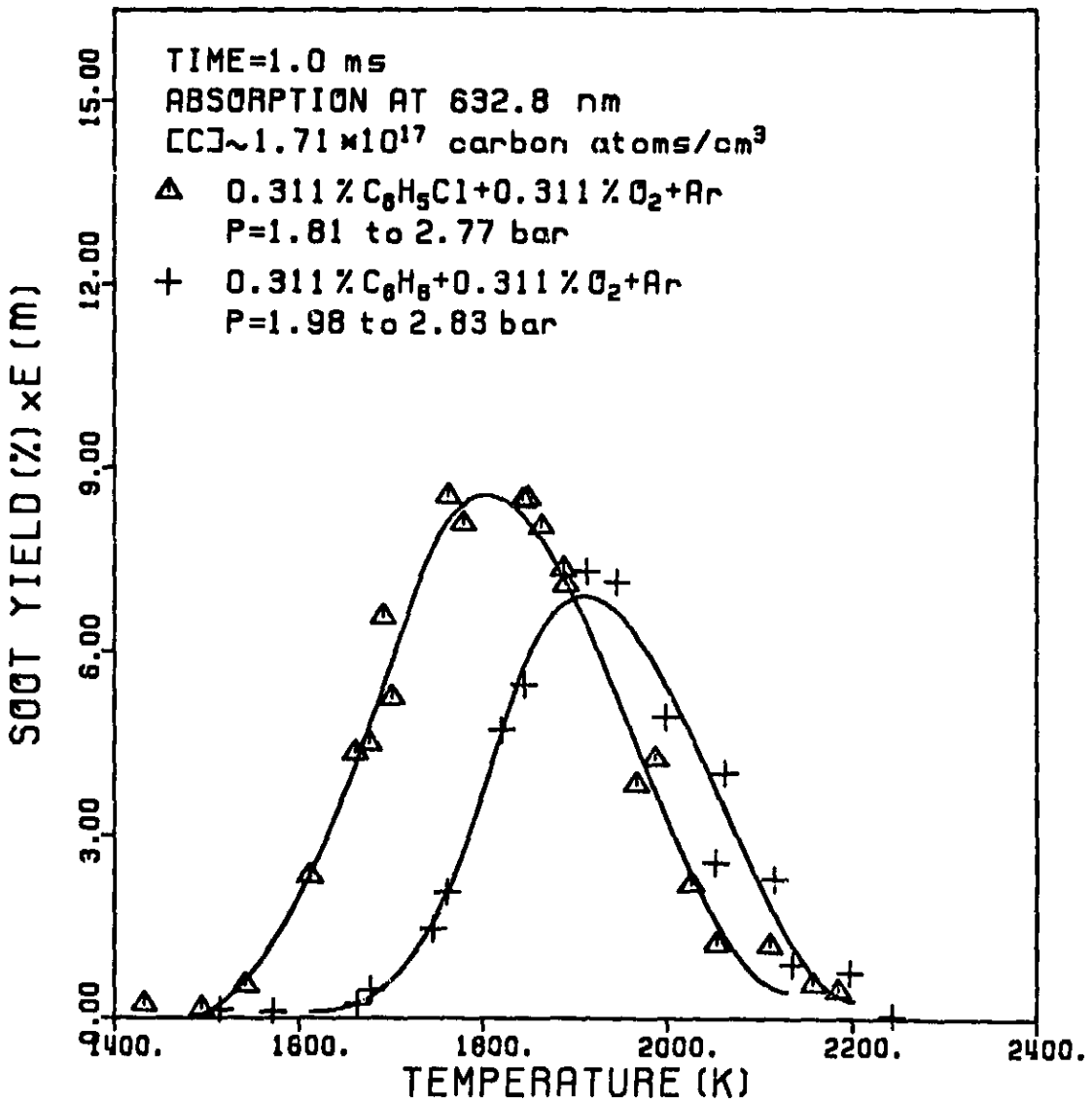

Figure 33. Comparison of soot yield at a reaction time of 1.0 ms for the mixtures 0.311% chlorobenzene-0.311% oxygen-argon and 0.311% benzene-0.311% oxygen-argon.

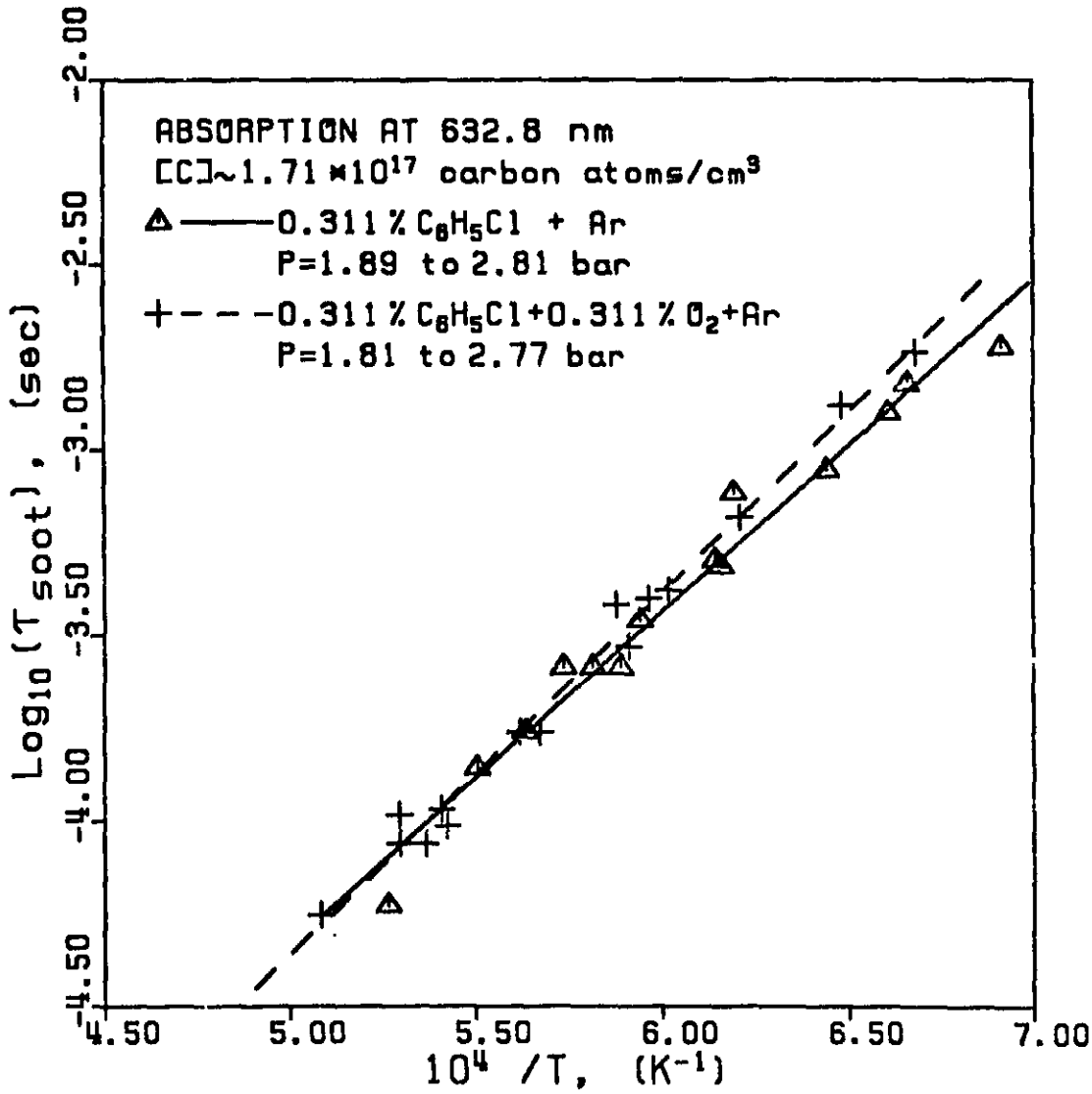

Figure 34. Soot induction times for the mixtures 0.311% chlorobenzene-argon and 0.311% chlorobenzene-0.311% oxygen-argon.

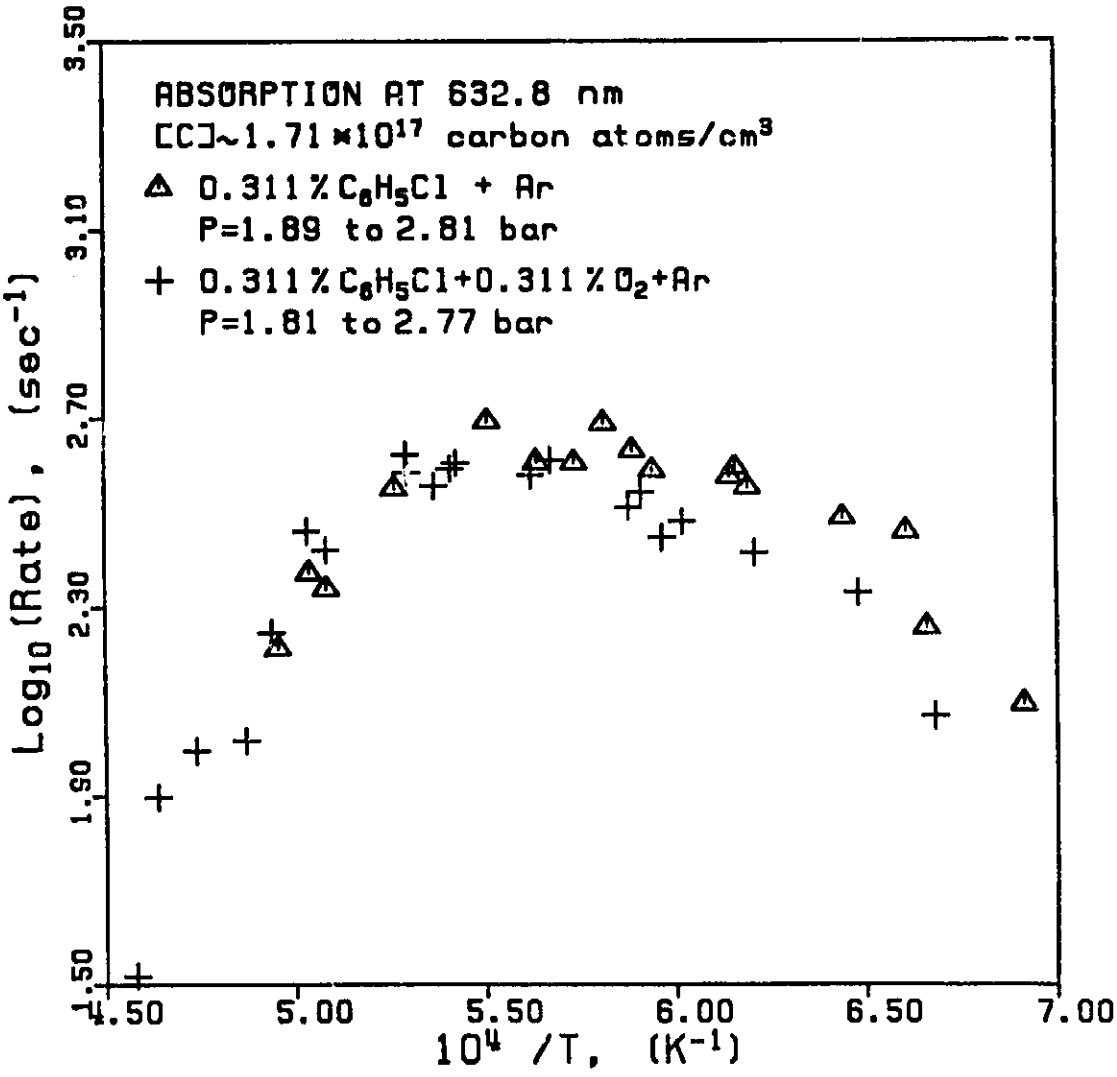

Figure 35. Soot formation rates for the mixtures 0.311% chlorobenzene-argon and 0.311% chlorobenzene-0.311% oxygen-argon.

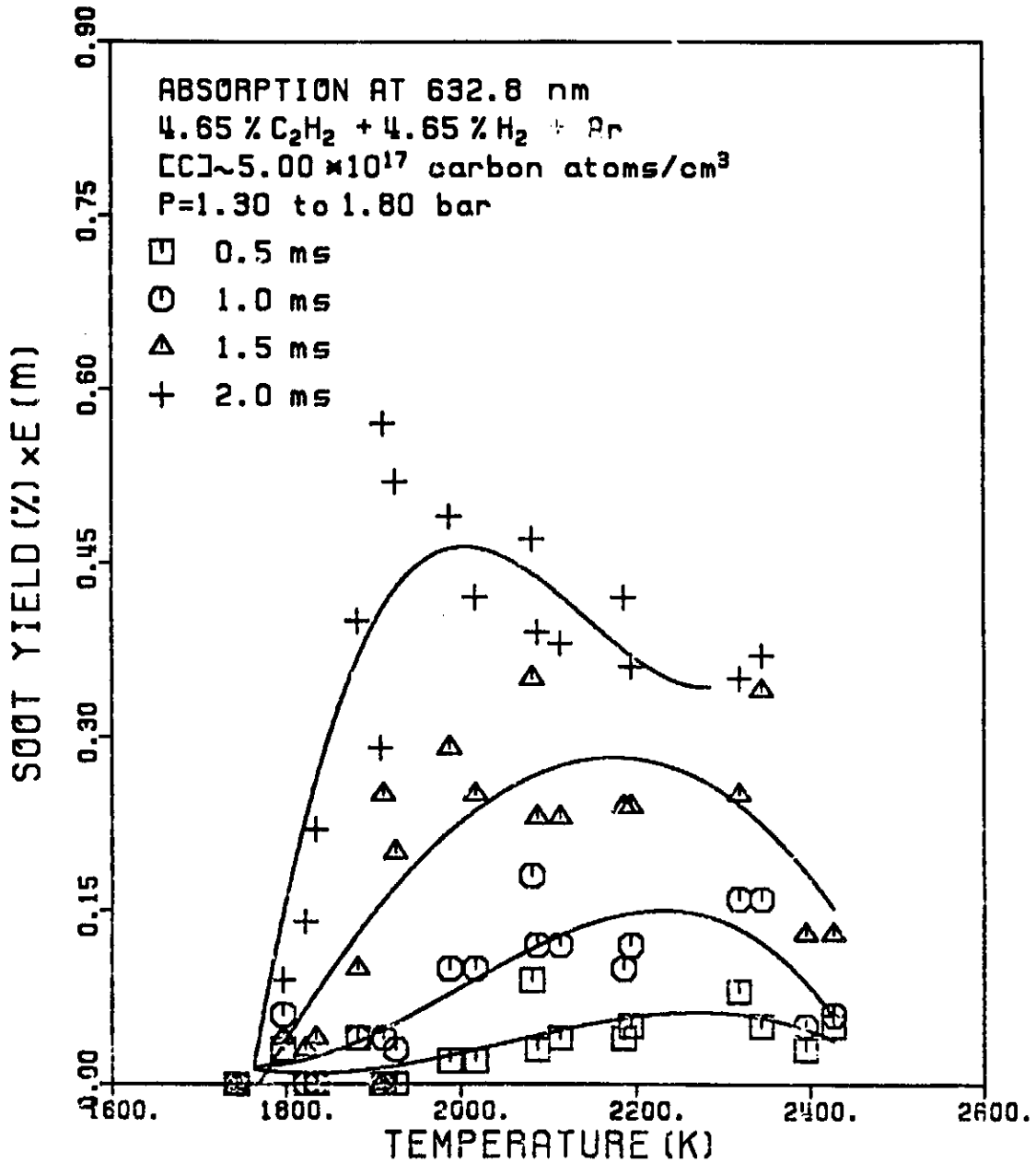

Figure 36. Soot yields vs. temperature at different reaction times for the mixture 4.65% acetylene-4.65% hydrogen-argon.

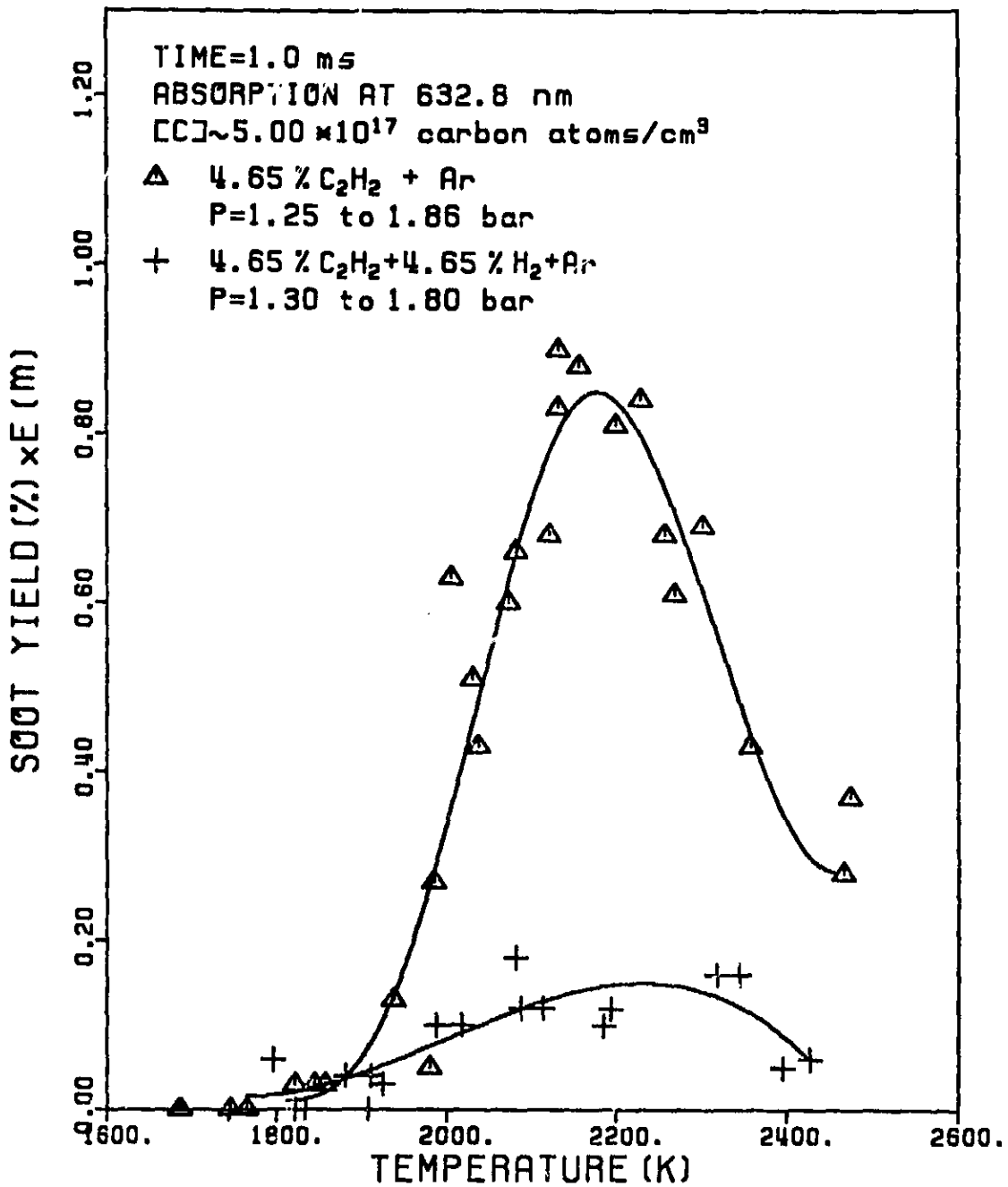

Figure 37. Comparison of soot yield at a reaction time of 1.0 ms for the mixtures 4.65% acetylene-argon and 4.65% acetylene-4.65% hydrogen-argon.

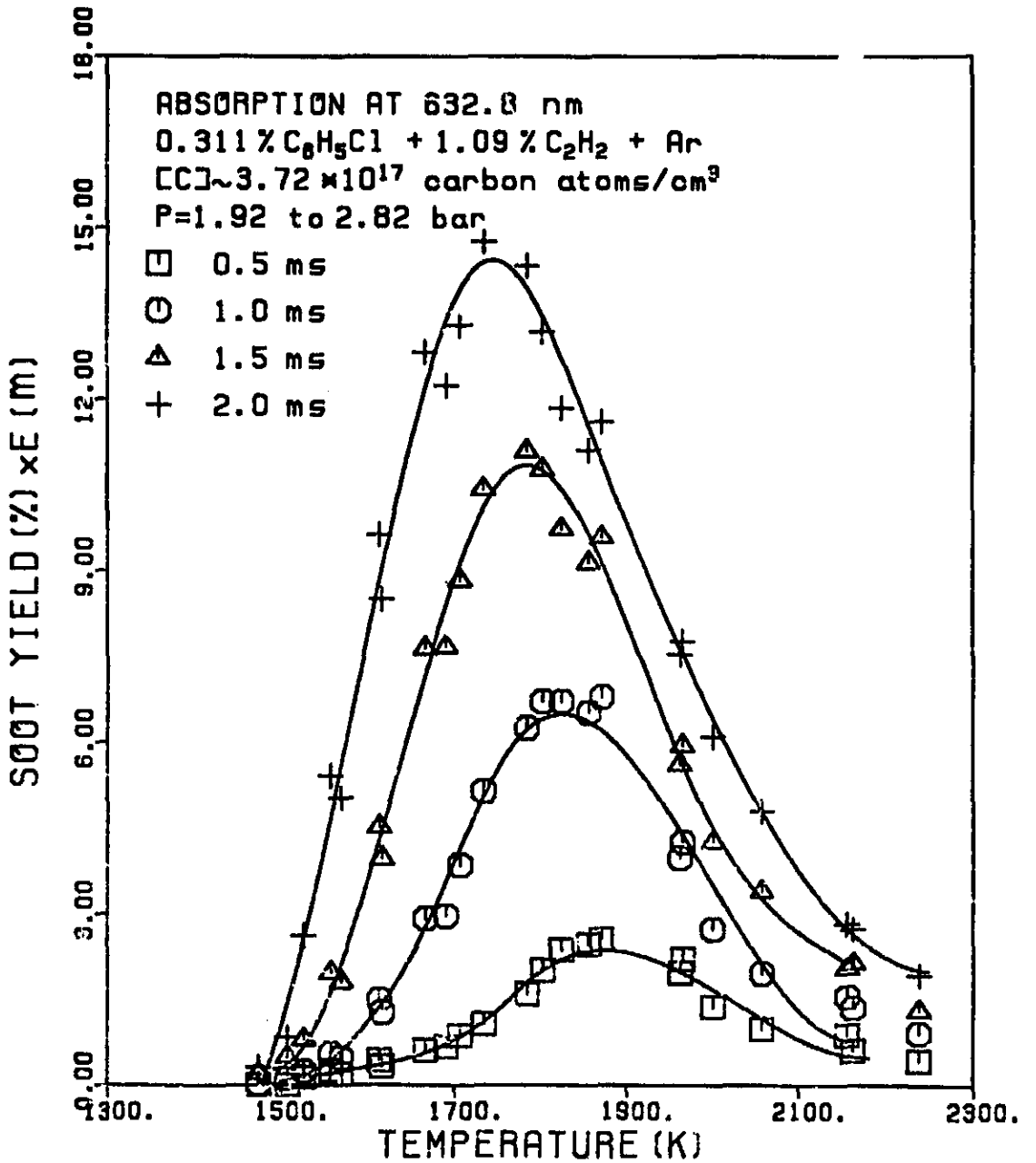

Figure 38. Soot yields vs. temperature at different reaction times for the mixture 0.311% chlorobenzene-1.09% acetylene-argon.

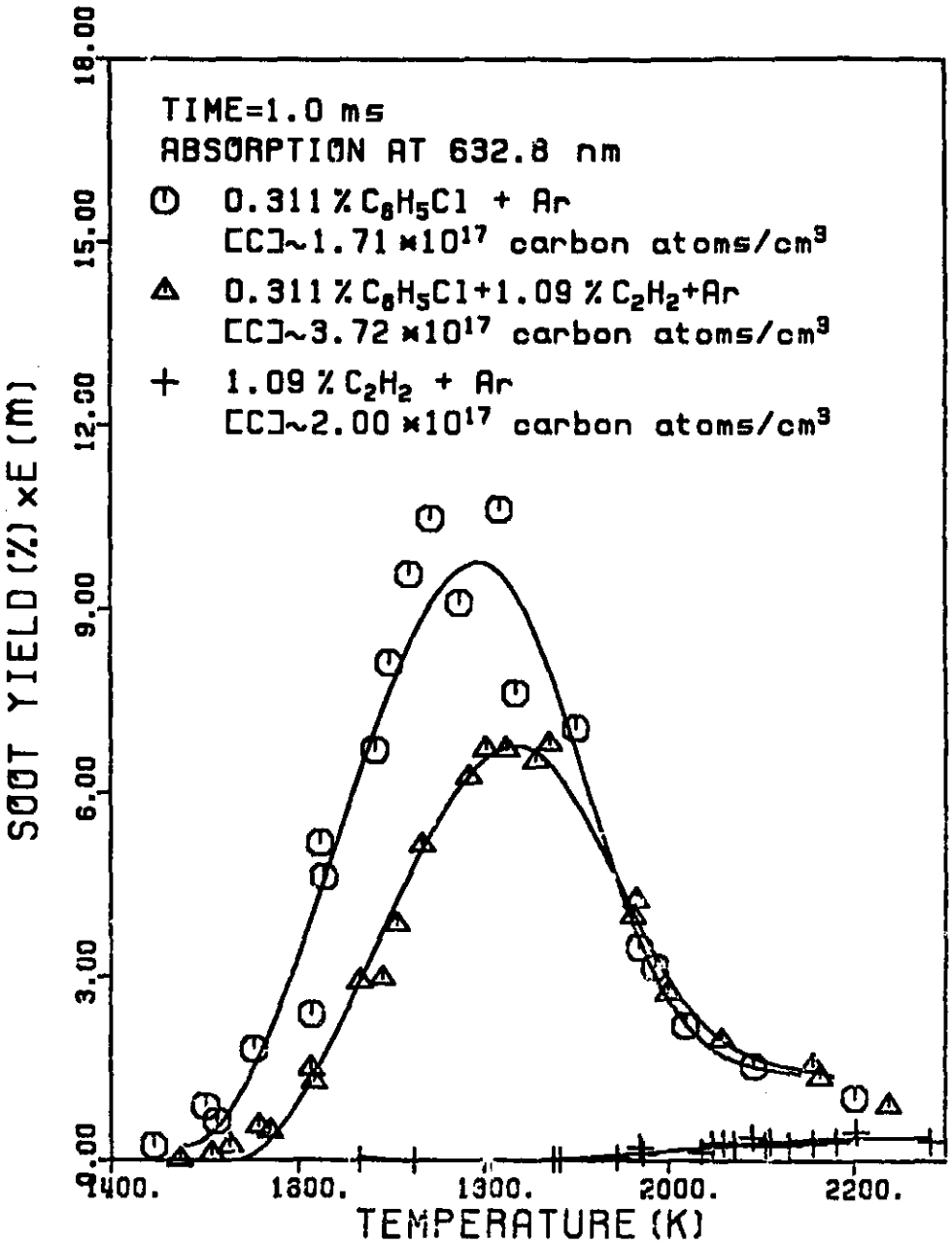

Figure 39. Comparison of soot yield at a reaction time of 1.0 ms for the mixtures 0.311% chlorobenzene-argon, 0.311% chlorobenzene-1.09% acetylene-argon and 1.09% acetylene-argon.

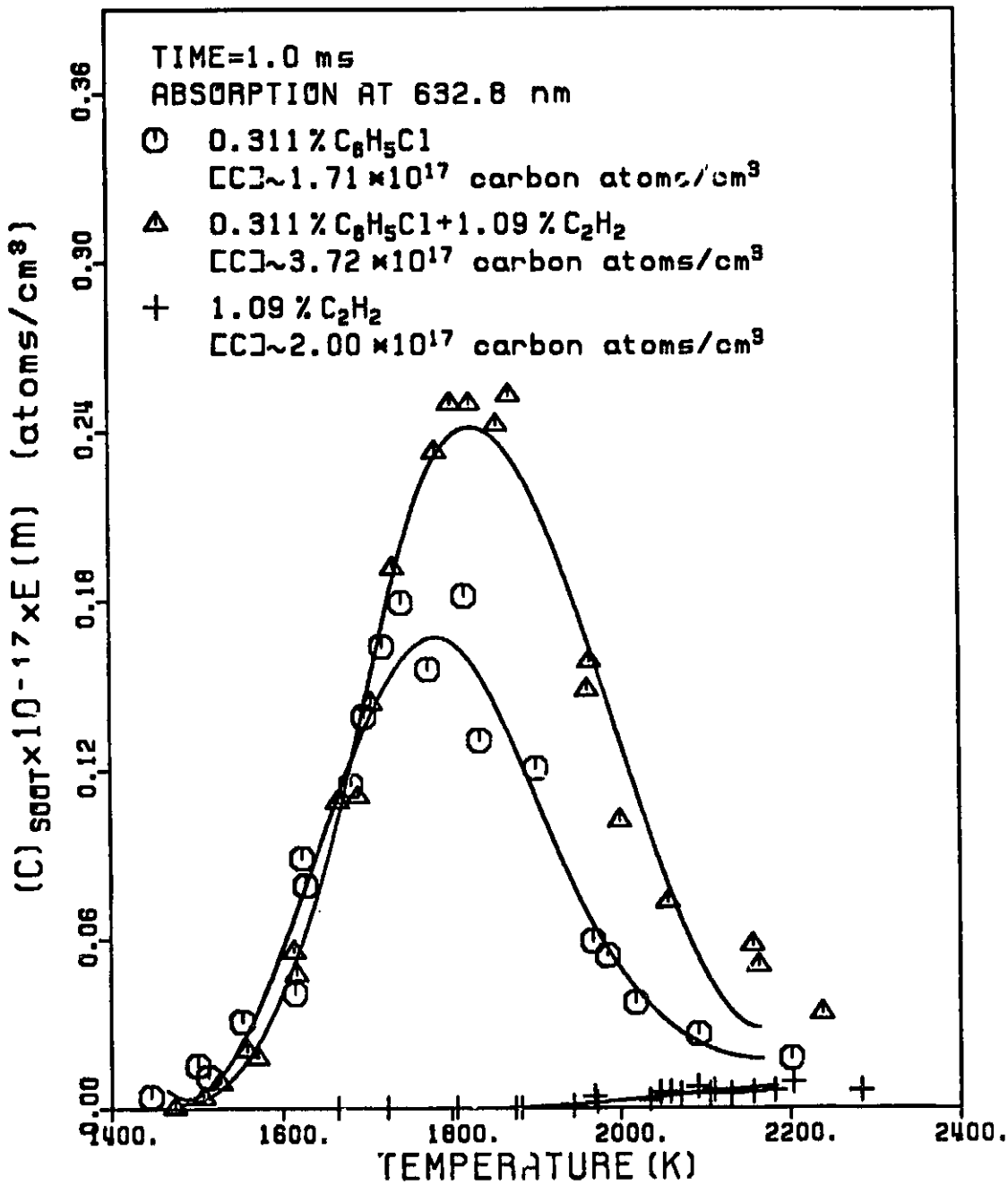

Figure 39a. Comparison of the amount of soot formed at a reaction time of 1.0 ms for the mixtures 0.311% chlorobenzene-argon, 0.311% chlorobenzene-1.09% acetylene-argon and 1.09% acetylene-argon.

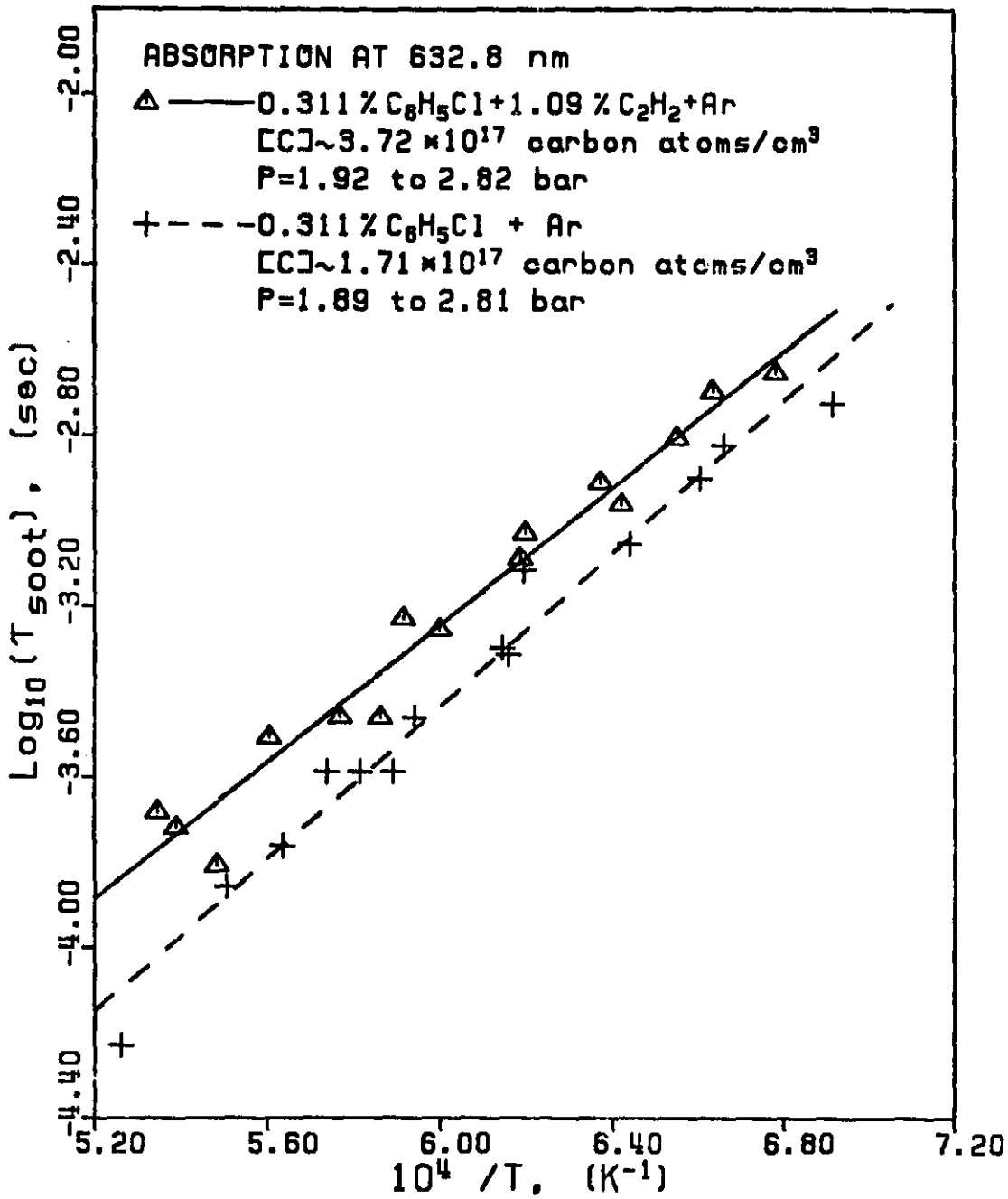

Figure 40. Soot induction times for the mixtures 0.311% chlorobenzene-1.09% acetylene-argon and 0.311% chlorobenzene-argon.

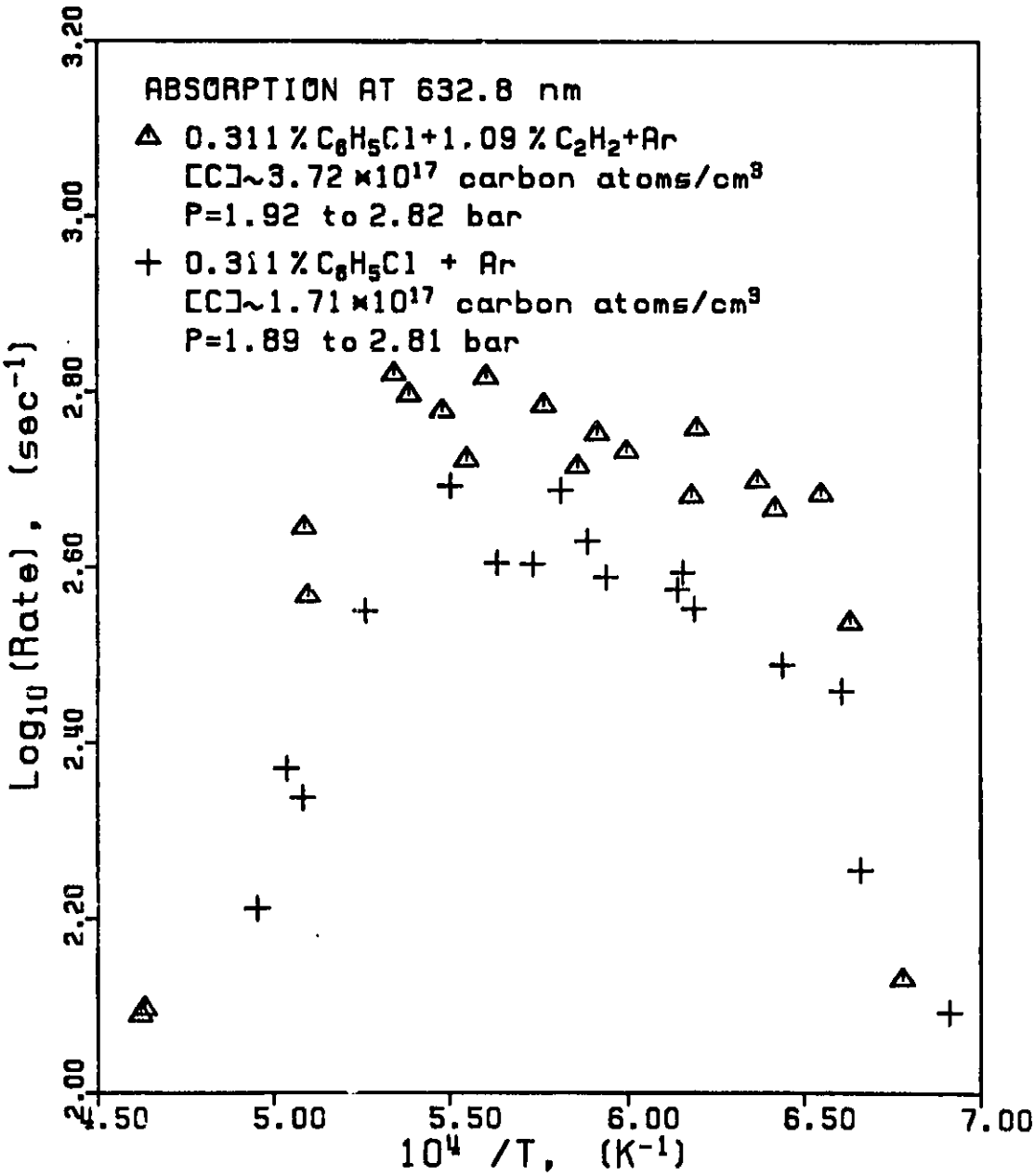

Figure 41. Soot formation rates for the mixtures 0.311% chlorobenzene-1.09% acetylene-argon and 0.311% chlorobenzene-argon.

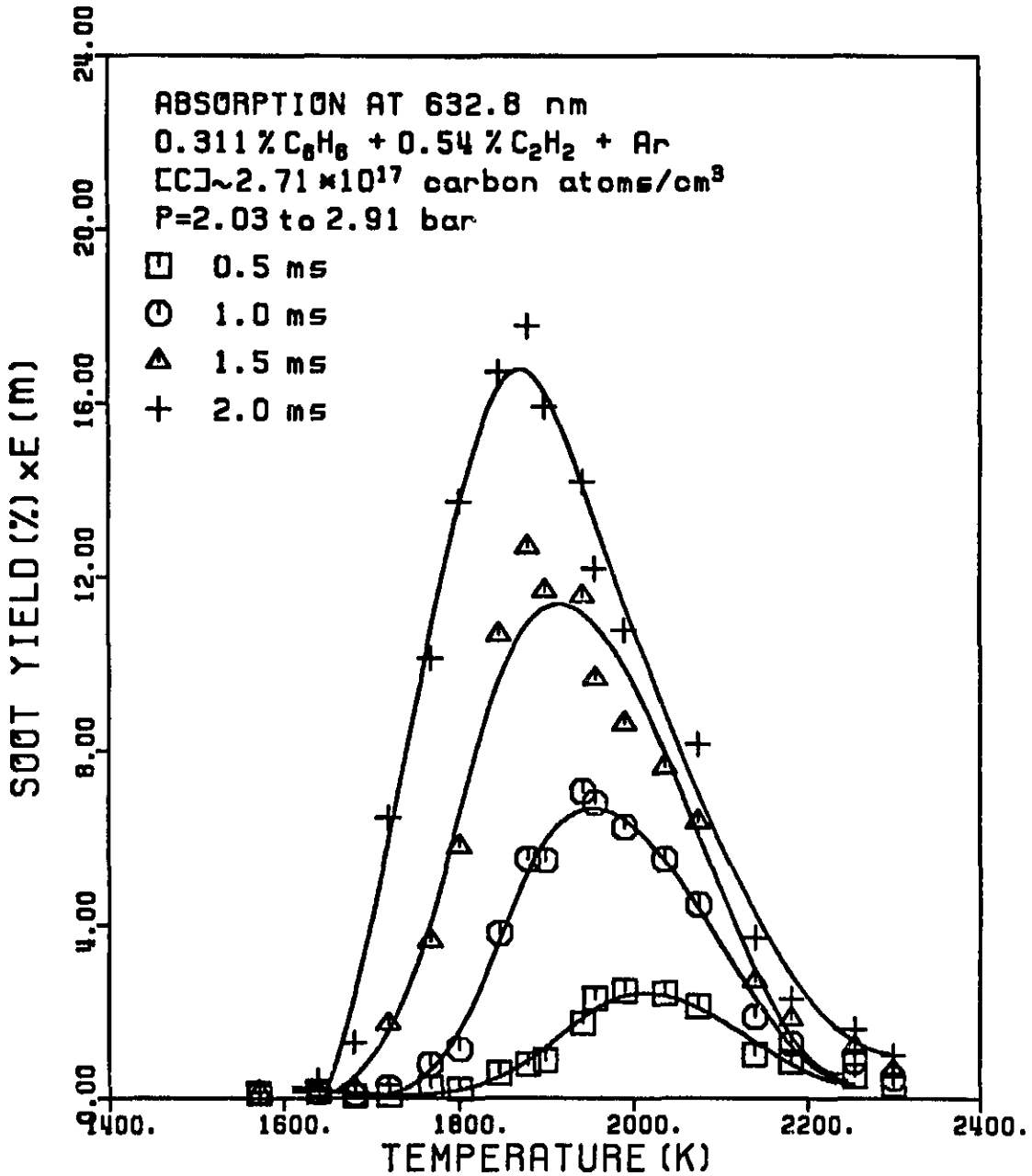

Figure 42. Soot yields vs. temperature at different reaction times for the mixture 0.311% benzene-0.54% acetylene-argon.

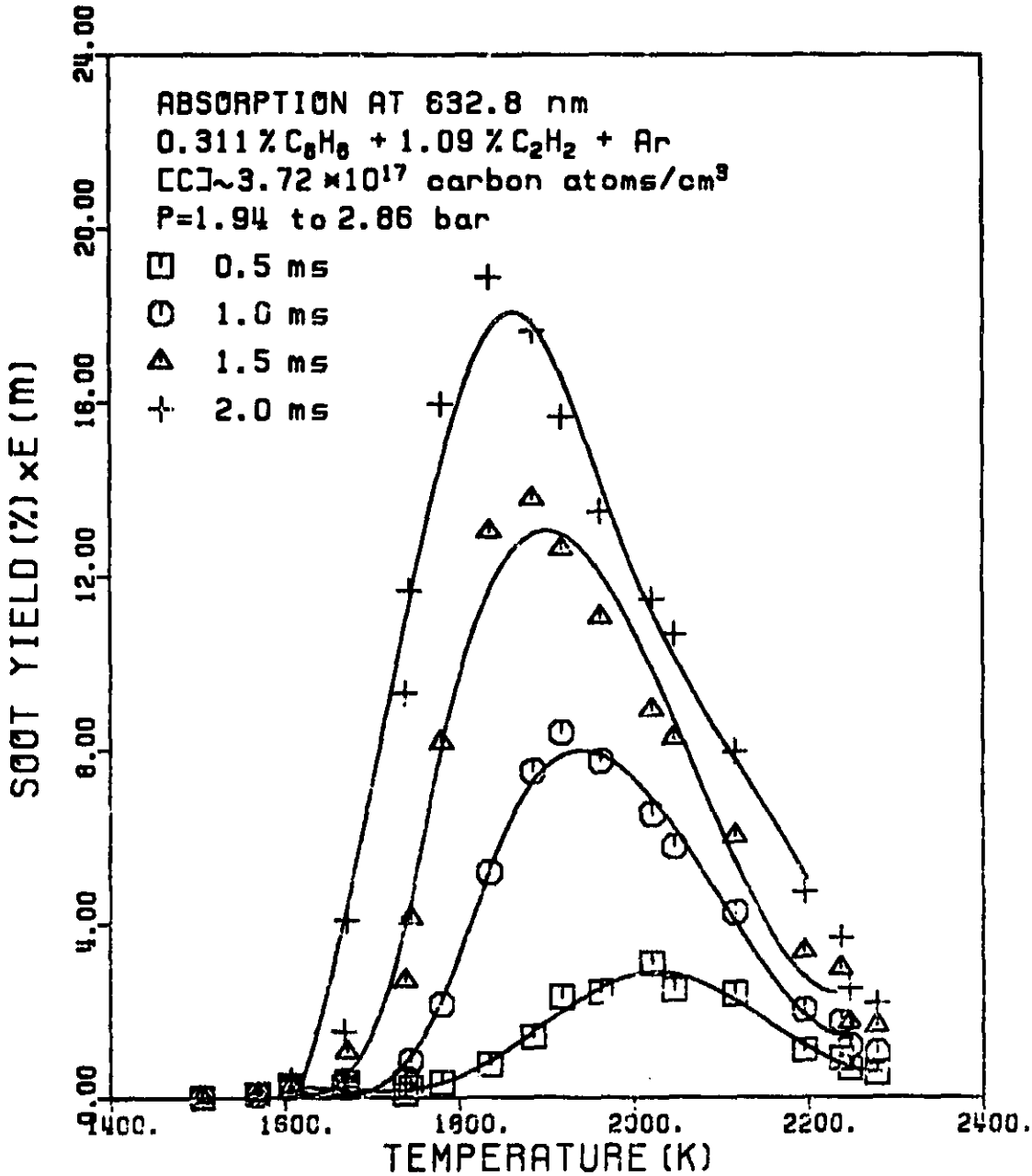

Figure 43. Soot yields vs. temperature at different reaction times for the mixture 0.311% benzene-1.09% acetylene-argon.

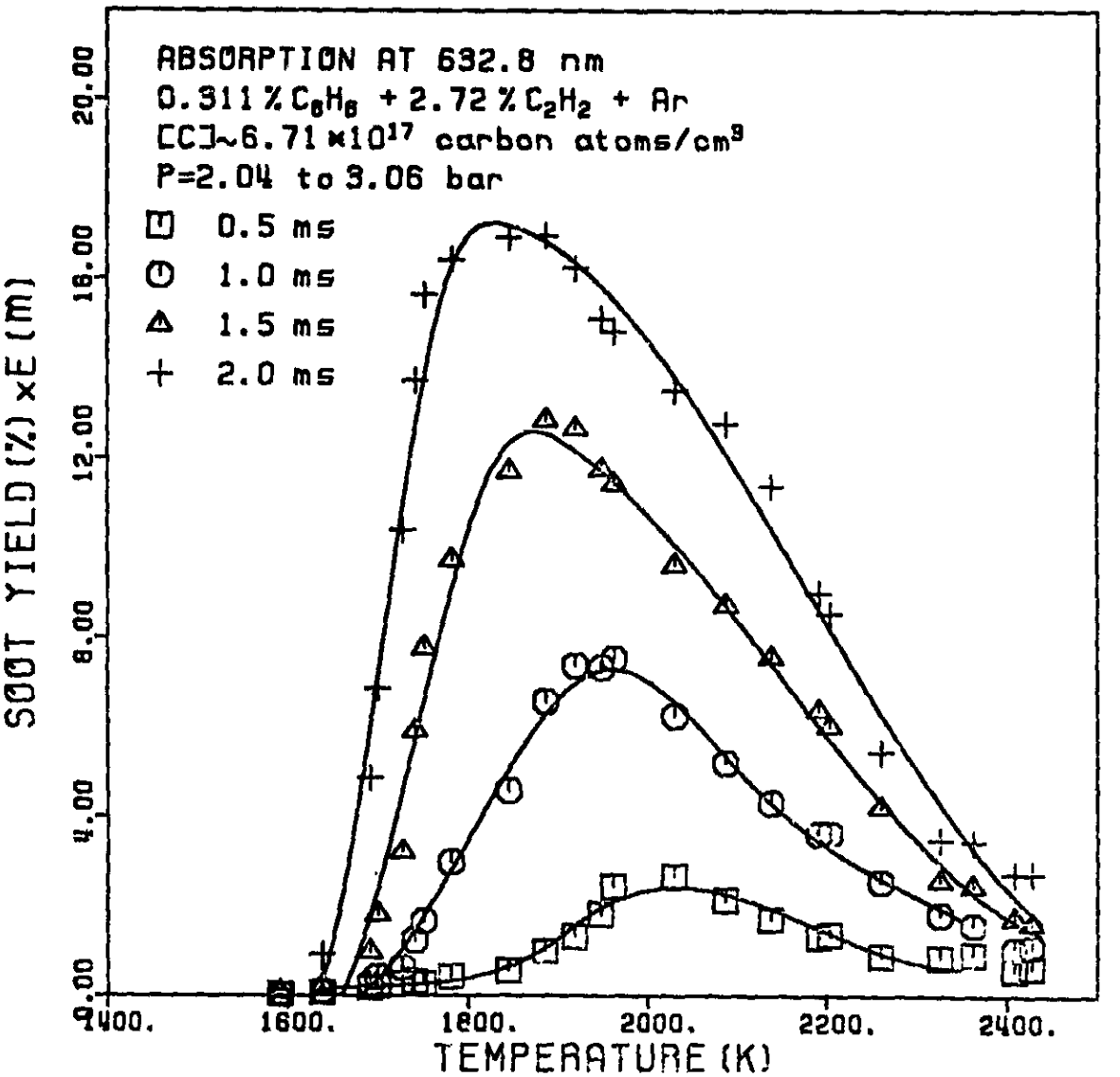

Figure 44. Soot yields vs. temperature at different reaction times for the mixture 0.311% benzene-2.72% acetylene-argon.

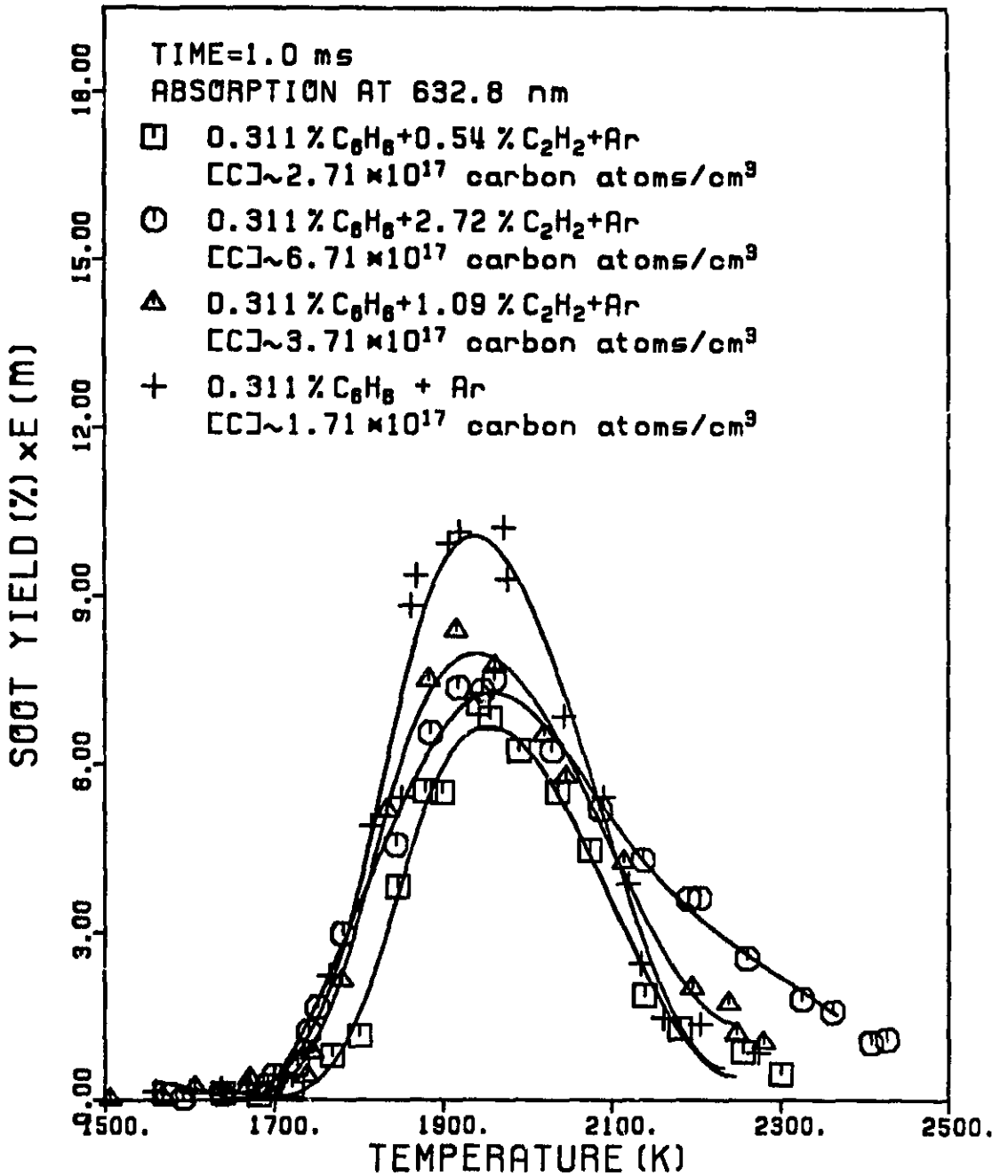

Figure 45. Comparison of soot yield at a reaction time of 1.0 ms for the mixtures 0.311% benzene-0.54% acetylene-argon, 0.311% benzene-2.72% acetylene-argon, 0.311% benzene-1.09% acetylene-argon and 0.311% benzene-argon.

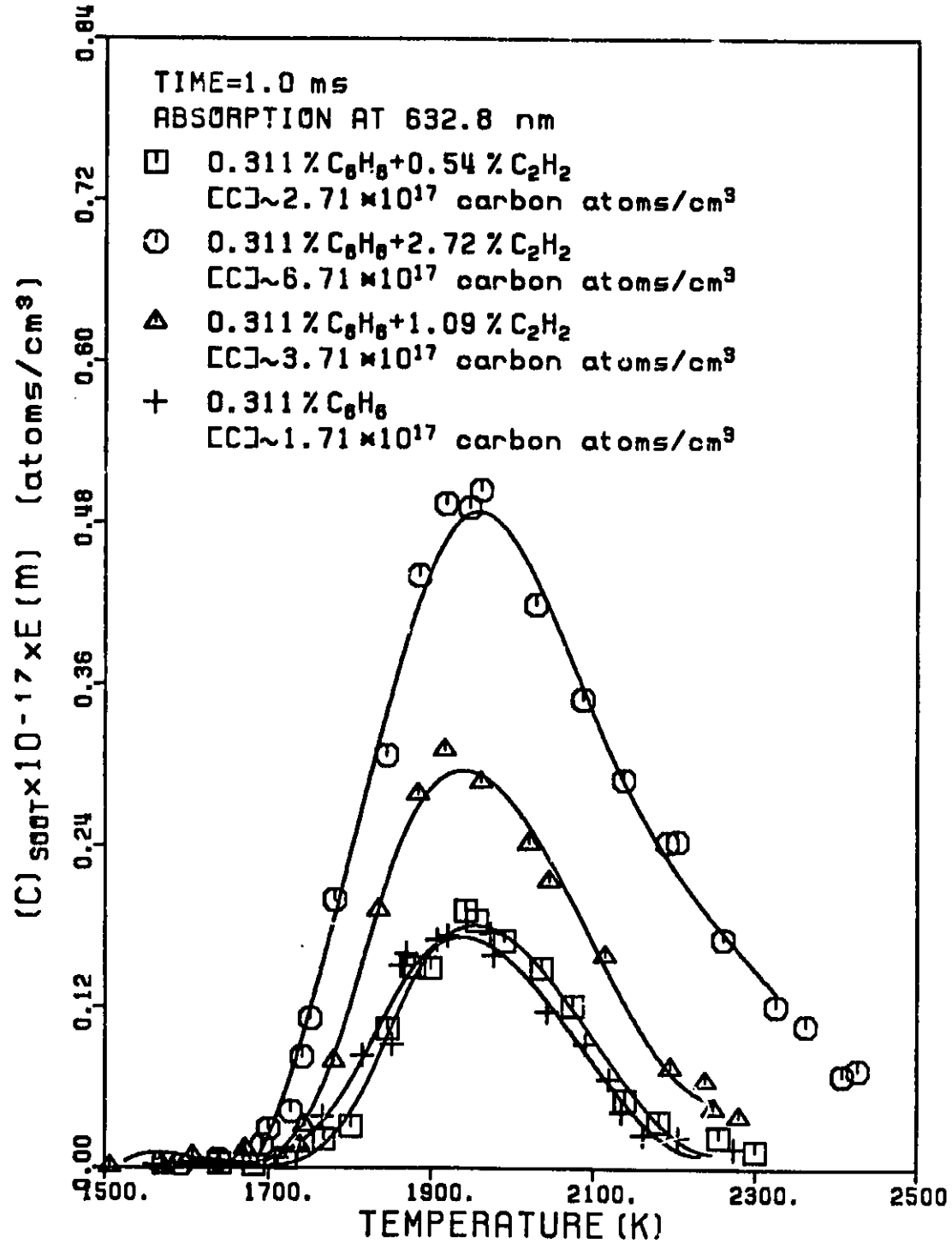

Figure 45a. Comparison of the amount of soot formed at a reaction time of 1.0 ms for the mixtures 0.311% benzene-0.54% acetylene-argon, 0.311% benzene-2.72% acetylene-argon, 0.311% benzene-1.09% acetylene argon and 0.311% benzene-argon.

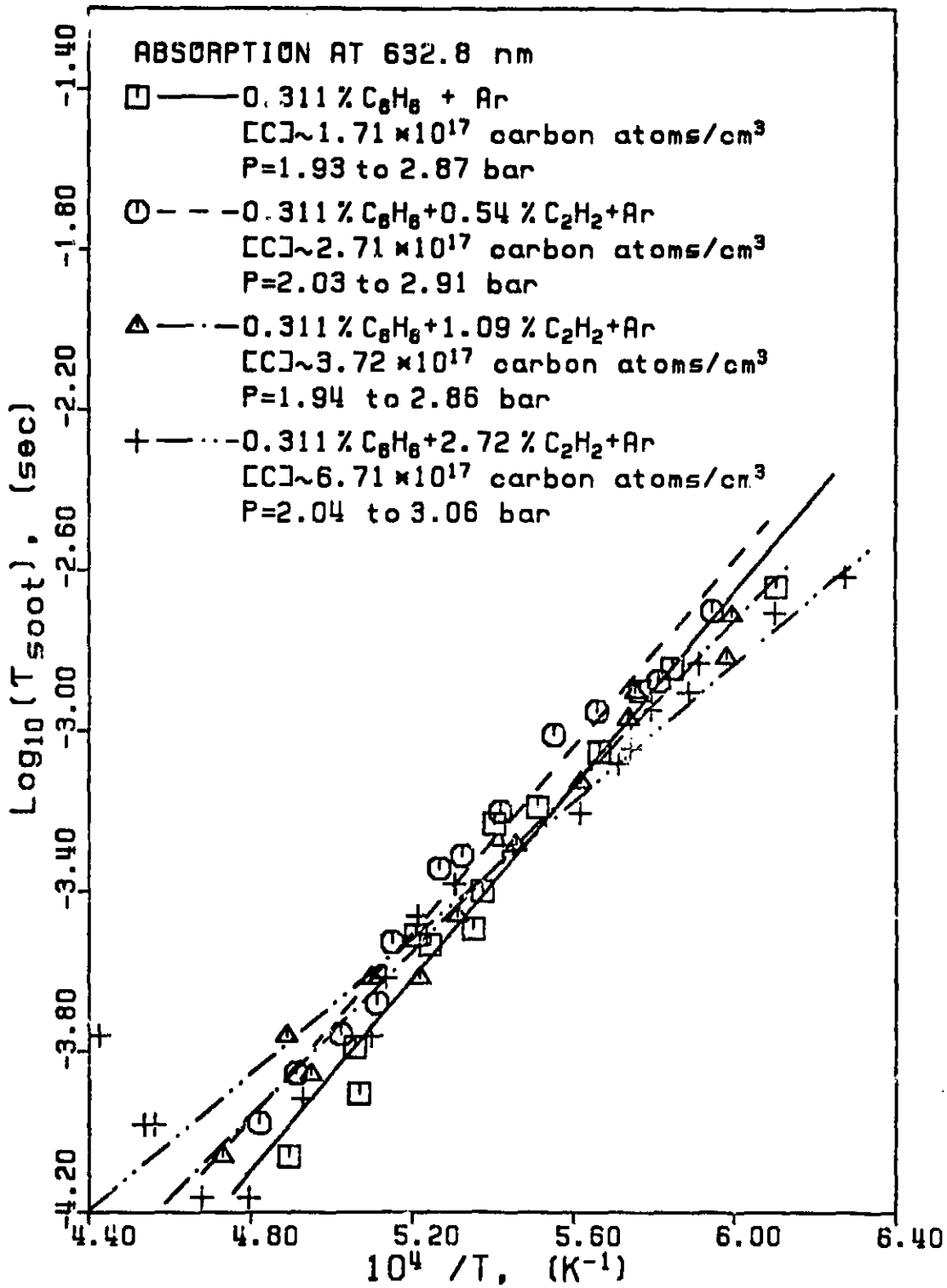

Figure 46. Soot induction times for the mixtures 0.311% benzene-argon, 0.311% benzene-0.54% acetylene-argon, 0.311% benzene-1.09% acetylene-argon and 0.311% benzene-2.72% acetylene-argon.

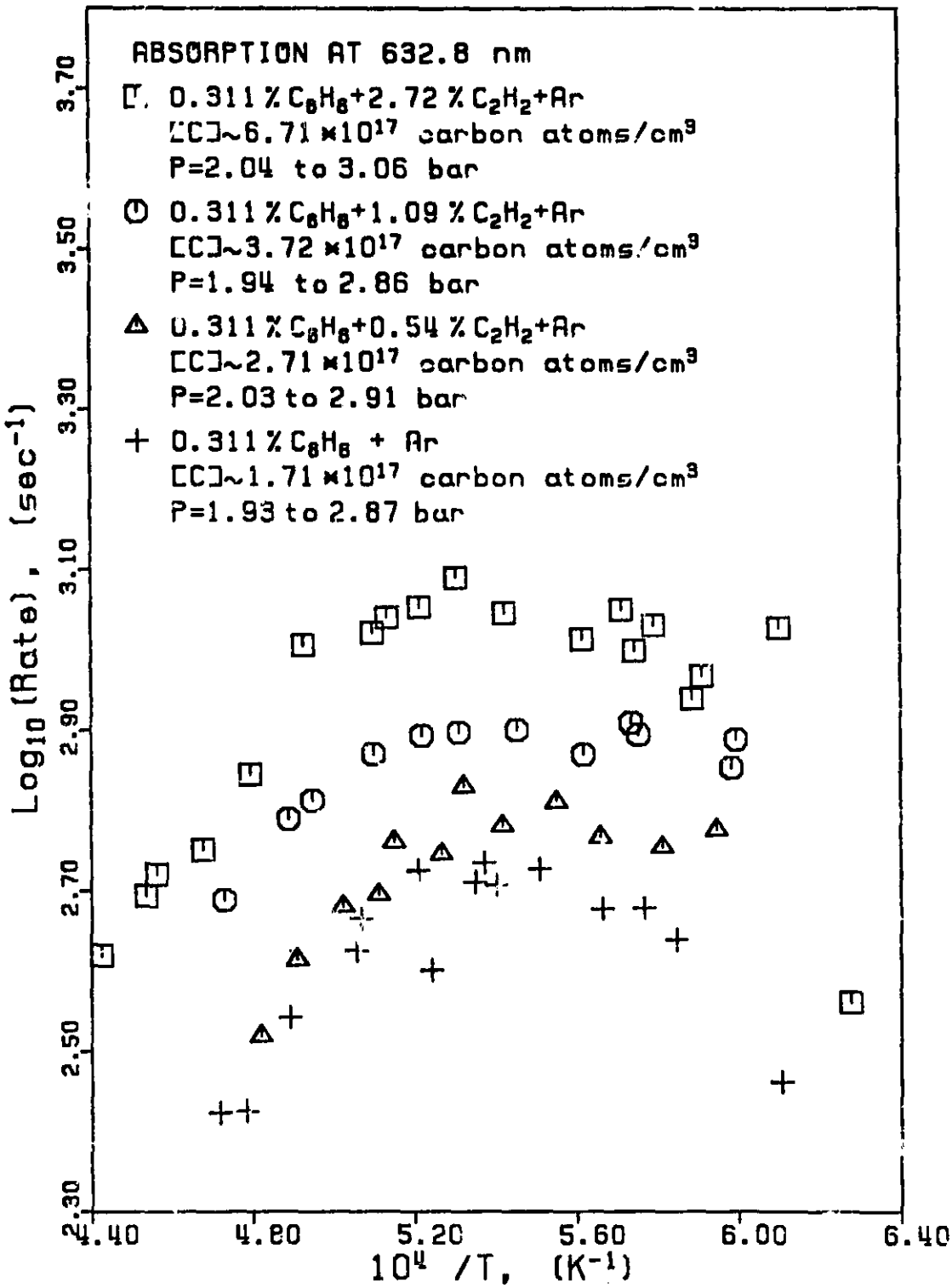

Figure 47. Soot formation rates for the mixtures 0.311% benzene-argon, 0.311% benzene-0.54% acetylene-argon, 0.311% benzene-1.09% acetylene-argon and 0.311% benzene-2.72% acetylene-argon.

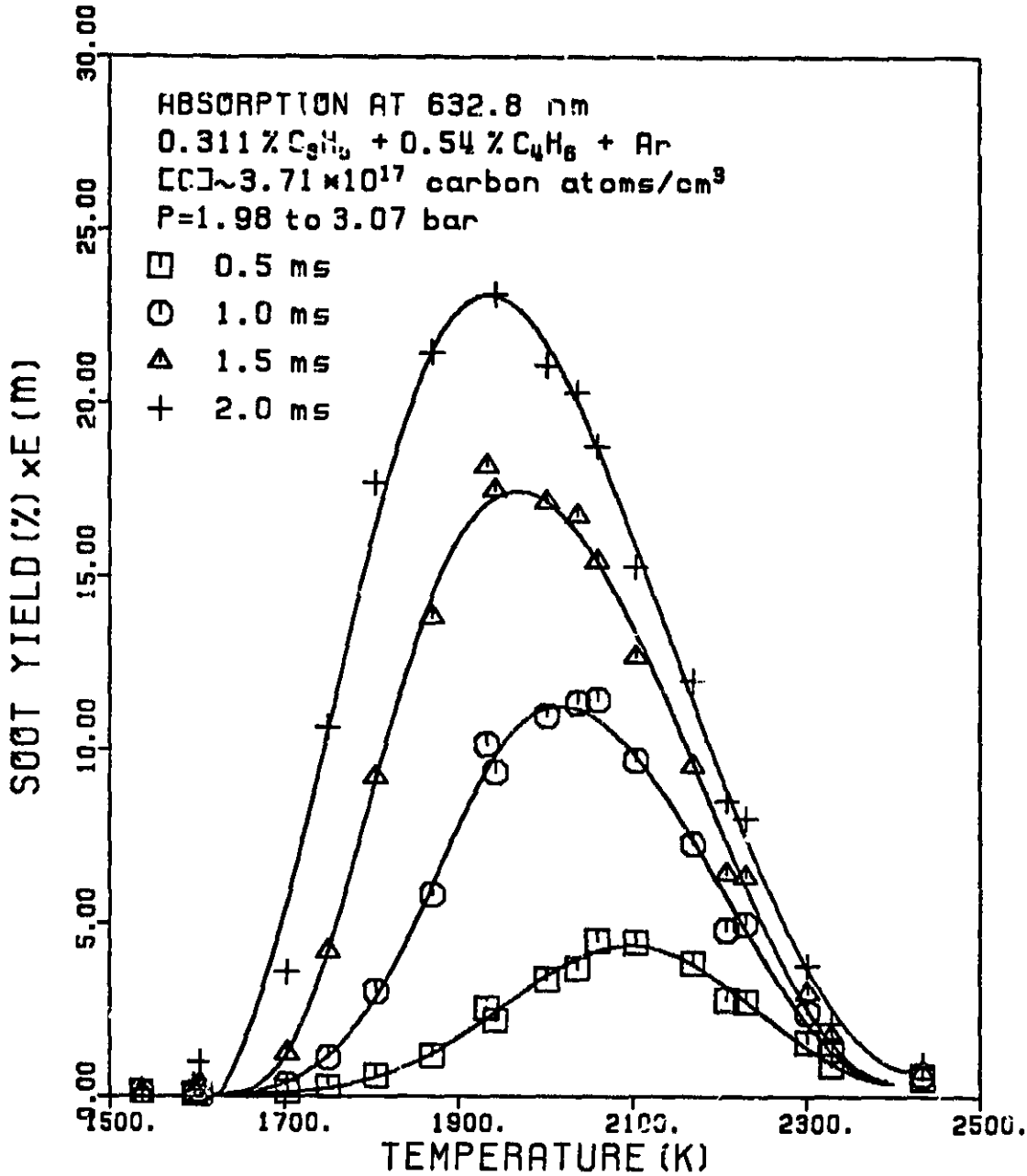

Figure 48. Soot yields vs. temperature at different reactions times for the mixture 0.311% benzene-0.54% 1,3-butadiene-argon.

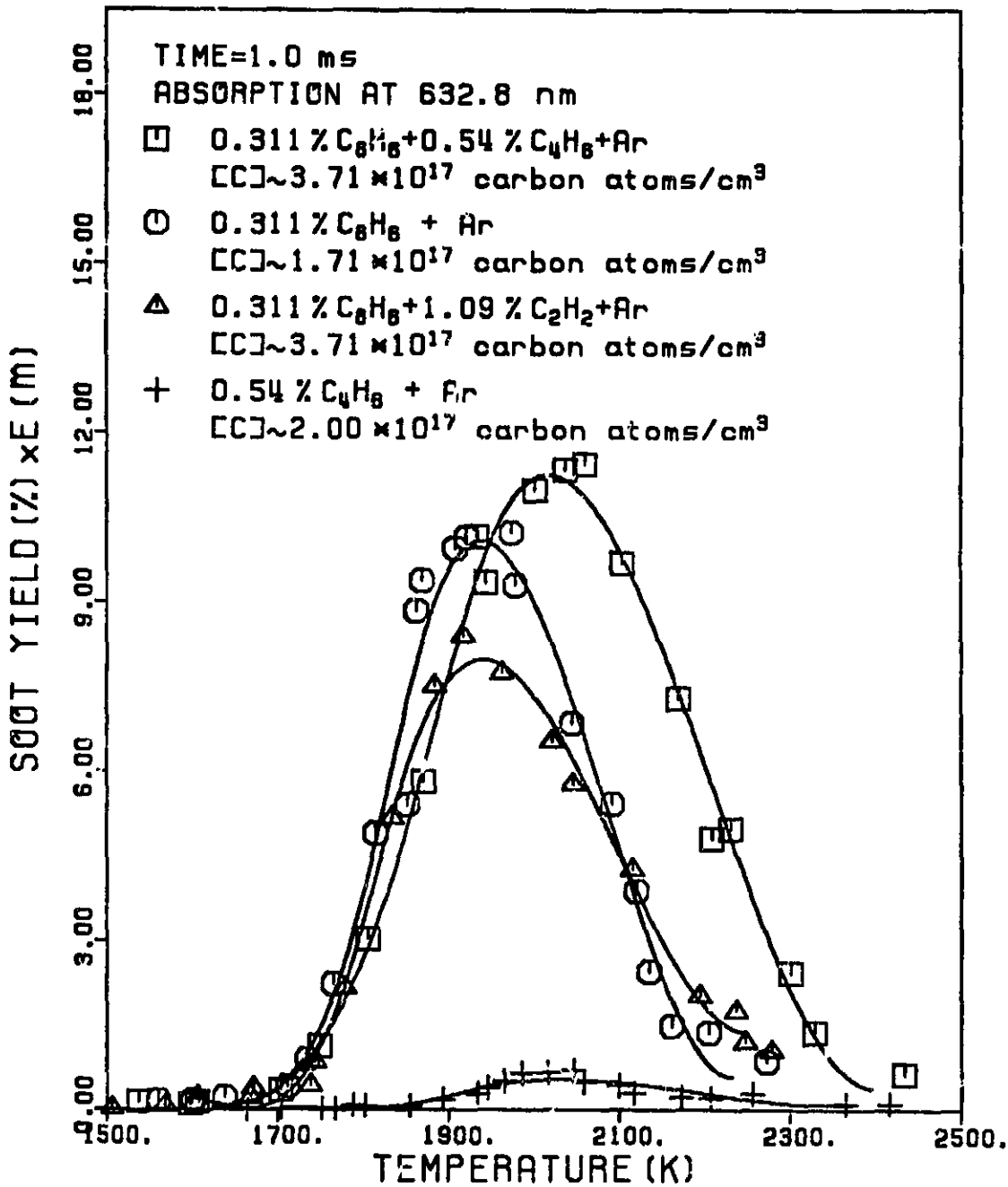

Figure 49. Comparison of soot yield at a reaction time of 1.0 ms for the mixtures 0.311% benzene-0.54% 1,3-butadiene-argon, 0.311% benzene-argon, 0.311% benzene-1.09% acetylene-argon and 0.54% 1,3-butadiene-argon.

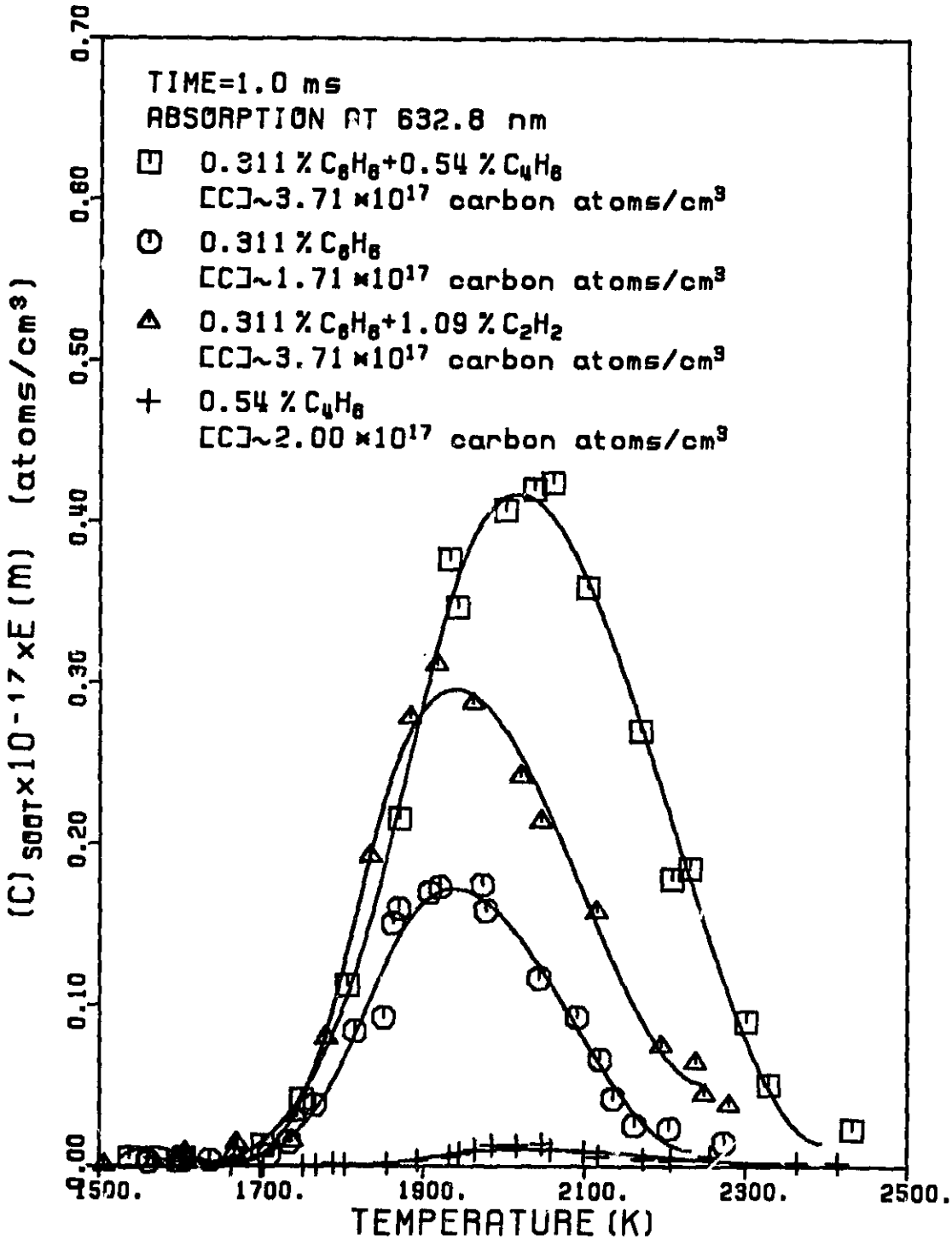

Figure 49a. Comparison of the amount of soot formed at a reaction time of 1.0 ms for the mixtures 0.311% benzene-0.54% 1,3-butadiene-argon, 0.311% benzene-argon, 0.311% benzene-1.09% acetylene-argon, and 0.54% 1,3-butadiene-argon.

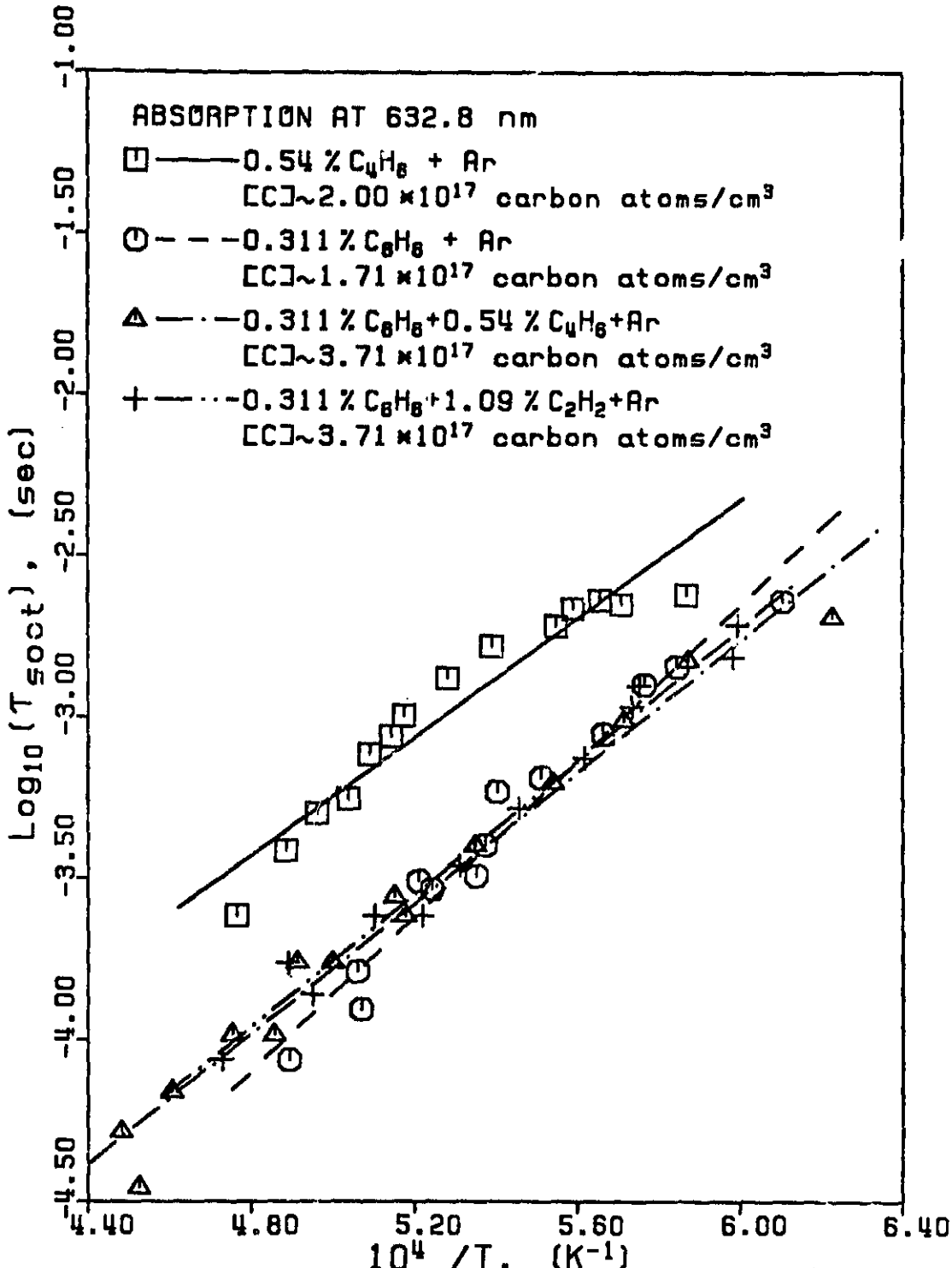

Figure 50. Soot induction times for the mixtures 0.54% 1,3-butadiene-argon, 0.311% benzene-argon, 0.311% benzene-0.54% 1,3-butadiene-argon and 0.311% benzene-1.09% acetylene-argon.

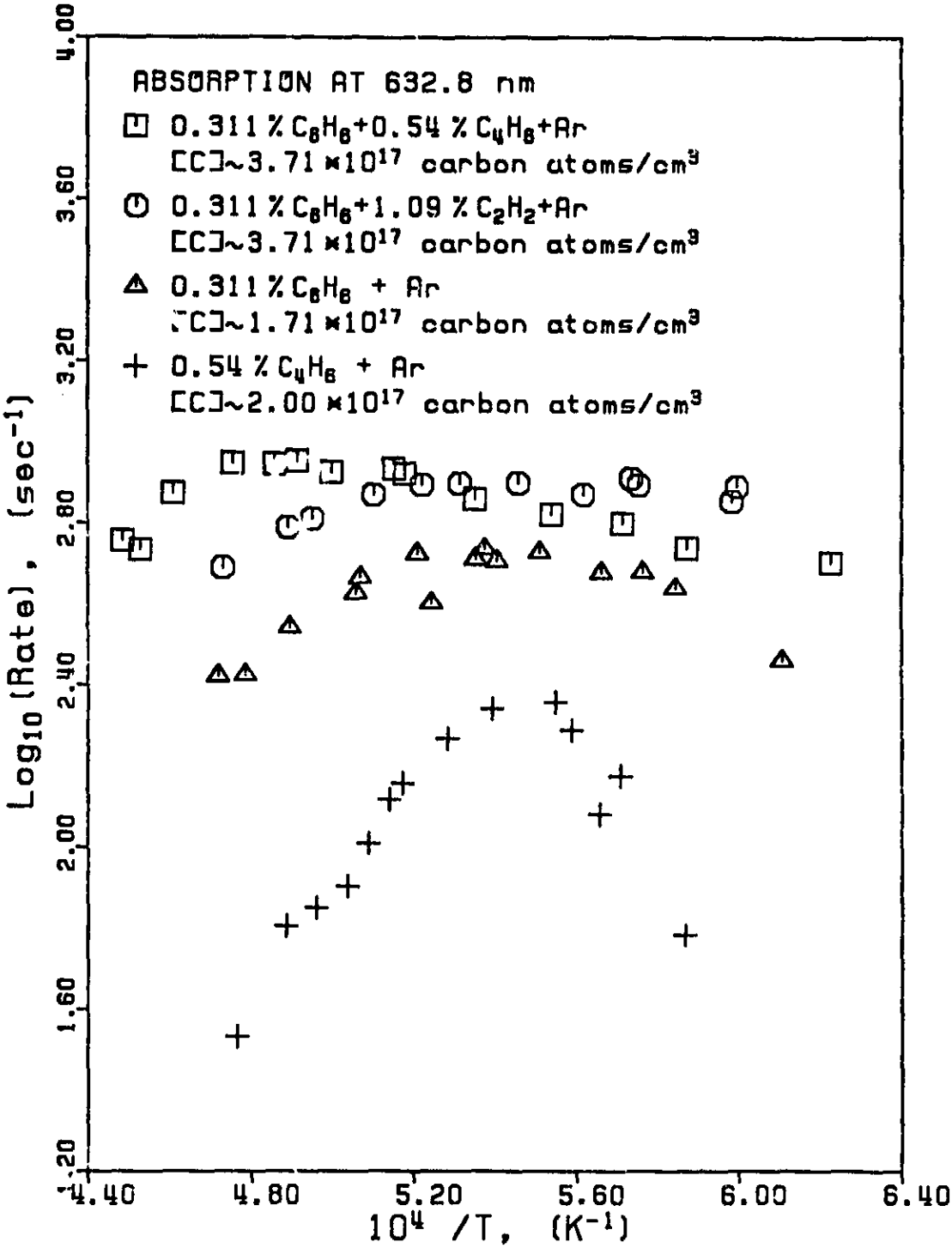

Figure 51: Soot formation rates for the mixtures 0.54% 1,3-butadiene-argon, 0.311% benzene-argon, 0.311% benzene-0.54% 1,3-butadiene-argon and 0.311% benzene-1.09% acetylene-argon.

DISCUSSION OF TEST RESULTS

1. Effect of Oxygen

The effects produced by the addition of relatively small amounts of molecular oxygen on soot formation from allene (Figs. 9-12), 1,3-butadiene (Figs. 13-16), vinylacetylene (Figs. 18-22) and chlorobenzene (Figs. 31-35) have been investigated. Analysis of these results indicates that the effect of oxygen is principally similar to the effect observed for acetylene and toluene[1,2]. Soot promotion at lower temperatures and its suppression at higher ones can be explained as previously by interaction between oxidizing agents and active intermediates: at lower temperatures the addition of oxygen enhances the rate of fuel pyrolysis while at higher temperatures soot precursors are destroyed by oxidation.

There are, however, a number of distinct features. First, in the case of vinylacetylene, the addition of oxygen results in an increase of the maximum amount of soot formed, which is particularly noticeable at longer observation times (Fig. 20). For all other hydrocarbons studied, the addition of oxygen always reduced the peak amount of soot at a given reaction time. It is also interesting to note that the induction time for soot appearance has a significantly different temperature dependence in the case of vinylacetylene oxidation compared to that of its pyrolysis (Fig. 21). These dependences for other studied hydrocarbons are usually very similar (see e.g Figs. 11, 15 and 34).

A second distinct feature is the much smaller effect of oxygen on soot formation from chlorobenzene compared to that from benzene (Figs. 28,32,33). It can be explained, as will be discussed in more detail

later, by the faster pyrolysis initiation reaction of chlorobenzene compared to benzene. For a faster pyrolysis the influence of competitive reactions, in this case various oxidation reactions, should be smaller.

2. Effect of Fuel Structure

a) Pyrolysis of individual hydrocarbons

Figures 5-8, 17, and 23-30 present the results and their intercomparisons for additional hydrocarbons studied during the reported period. Figure 5 depicts the soot yields obtained in pyrolysis of ethylene and Figs. 6-8 compare these results with those of acetylene. The lower sooting tendency of ethylene compared to acetylene is in accord with the results of Fussey and co-workers[10,11]. Fussey et al.[10] explained the difference "by the variation in the time required to produce polyacetylenes from the reactant", assuming polyacetylenes to be the major soot precursors in that "the various hydrocarbons are likely to have a similar route to carbon from these species onwards". Polyacetylenes were not found to be important intermediates for soot formation in our modeling study, which will be discussed later in the report. Nevertheless, the route to soot identified by the model would be initiated faster in the pyrolysis of acetylene than in the pyrolysis of ethylene, which explains our and Fussey et al.'s experimental results.

Following similar arguments, the results obtained with 1-butene (Figs. 23-26), which are very close to those with 1,3-butadiene, can be rationalized. What is surprising, however, is the relatively low sooting tendency of vinylacetylene compared to allene (Figs. 17, 24).

Various theoretical considerations[12-17] indicate vinylacetylene to be as effective a soot precursor as allene. Our results, however, clearly show that soot formation from vinylacetylene is comparable to that from 1,3-butadiene and 1-butene rather than to that from allene.

Figures 27-30 present the results obtained in pyrolysis of a chlorobenzene mixture, where they are compared to the results obtained at similar conditions in the benzene mixture. Examining Fig. 28, one observes that the soot-yield bell is shifted to lower temperatures by about 150 K compared to benzene. The shift and its value can be explained by the difference between the cleavage of C-H and C-Cl bonds in benzene and chlorobenzene molecules, respectively.

The position of the soot-yield maximum in pyrolysis of aromatic hydrocarbons is determined[5,18] by the ratio

$$r = k_f/k_p[A]_0, \tag{1}$$

where k_f is the rate constant of ring fragmentation, $[A]_0$ is the initial hydrocarbon concentration, and k_p is the rate constant of the polymerization process forming soot. Assuming the maximum appears at the same value of r, one can write

$$k_f/k_p[A]_0 = k_f'/k_p'[A']_0, \tag{2}$$

where the left-hand side of Eq. (2) is ratio (1) for benzene and the right-hand side is that for chlorobenzene. For the conditions used in this study $[A]_0 = [A']_0$ (see Table I) and assuming $k_p = k_p'$, Eq. (2) can be rewritten as

$$k_f = k_f'. \tag{3}$$

Considering the energetics[3,19] of the elementary reactions which may constitute the fragmentation path for benzene molecule, the following sequence

$$\text{ØH} \rightarrow \text{Ø} + \text{H} \qquad \Delta H^0_{1800}=464 \text{ kJ/mol}; \ \Delta S^0_{1800}=153 \text{ J/mol·K}, \quad \text{(R1)}$$

$$\text{Ø} \rightarrow \text{HC}\equiv\text{C-CH=CH-CH=}\dot{\text{C}}\text{H} \qquad \Delta H^0_{1800}=247 \text{ kJ/mol}; \ \Delta S^0_{1800}= 65 \text{ J/mol·K}, \quad \text{(R2)}$$

where Ø denotes phenyl radical, is suggested for the experimental conditions used in this study. The rate limiting step of this sequence, particularly during the initial phase of pyrolysis, is reaction (R1). Hence, the rate constant of this reaction, k_1, should be considered for the left-hand side of Eq. (3). By analogy, the right-hand side of Eq. (3) is set equal to the rate constant of the following reaction

$$\text{ØCl} \rightarrow \text{Ø} + \text{Cl} \qquad \Delta H^0_{1800}=365 \text{ kJ/mol}; \ \Delta S^0_{1800}=123 \text{ J/mol·K}^{20,21}. \quad \text{(R3)}$$

Assuming the Arrhenius form for the rate coefficient expressions and assuming the ratio of the rate constants for the reverse directions of reactions (R1) and (R3) $k_-/k'_- = (\mu'/\mu)^{1/2}$, where μ and μ' are the reduced masses for the corresponding recombinations, Eq. (3) can be rewritten as

$$R\ell n(\mu'/\mu) + (\Delta S-\Delta S') = \Delta H/T_m - \Delta H'/T'_m \qquad (4)$$

where T_m and T'_m are the temperatures of soot yield maxima in mixtures M and P, respectively. For a reaction time of 1 ms, T_m is approximately equal to 1900 K (Fig. 28). Using the above thermodynamic data for 1800 K, the approximate midpoint of the temperature interval of interest, we obtain from Eq. (4) T'_m = 1772 K, so that the temperature shift, $T_m-T'_m$, equals approximately 130 K. This is in good agreement with the corresponding experimental value.

The above discussion is in disagreement with the conclusion of Singh and Kern[22] that "the phenyl radical is not the primary product of

benzene decomposition... [and] ... fragmentation of benzene [presumably by an elementary reaction] is the dominant pathway of the decomposition in the temperature range of 1400-2200 K". Their conclusion is based on the observation, previously noted by Smith and Johnson[23], that a larger concentration of phenyl radicals is observed in the pyrolysis of chlorobenzene than in the pyrolysis of benzene at similar conditions. This result can be explained, however, by a simple kinetic argument of consecutive reactions. Indeed, in a two-step sequence

$$\text{ØH} \xrightarrow{k_1} \text{Ø} \xrightarrow{k_2} \text{products},$$

the concentration of the intermediate, Ø, increases with the ratio k_1/k_2. Based on the previous discussion, for chlorobenzene this ratio at 1800 K is approximately 8 times larger than a similar ratio for benzene, which should result in a higher concentration of phenyl radicals for the former case.

b) Pyrolysis of hydrocarbon mixtures

Figures 36-51 present the results obtained in pyrolysis of binary hydrocarbon mixtures. Figure 36 presents soot yields obtained in a acetylene-hydrogen mixture and Fig. 37 depicts the comparison of these results with those obtained at similar conditions in the acetylene mixture. As can be seen in this figure, hydrogen strongly suppresses soot formation from acetylene. Our chemical kinetic model, which will be discussed later, predicts such behavior. The reason for the soot suppression, as follows from the model, is the increased rate of reverse reactions of hydrogen atom.

The effect of addition of acetylene on soot formation from benzene and chlorobenzene is examined in Figs. 38-47. It is instructive to

examine the effect of a hydrocarbon additive not only by analyzing fractional soot yields, as has been the usual practice in our works[1,2,5,24] as well as others[4,8,9], but also by considering the actual amounts of soot formed. For this purpose, we kept the molecular concentration of the main reactant, e.g., benzene, constant in Mixtures M, P, S, T, U, V and W (see Table I) rather than the total concentration of carbon atoms. While both approaches provide the same information for individual fuels, the information is complementary for fuel mixtures (cf. Figs. 39 and 39a, Figs. 45 and 45a, Figs. 49 and 49a). Thus, in the case of chlorobenzene, analysis of Fig. 39a indicates that the addition of acetylene practically does not affect the amount of soot formed at low temperatures, while Fig. 39 shows that the fractional conversion to soot is not changed at high temperatures. The l tter result is easily understood: at high temperatures the aromatic rings are entirely fragmented with acetylene being the main product. The only thing that matters is the total amount of carbon atoms (or acetylene concentration) present.

The low-temperature observation in Fig. 39a is not as simple as it may first appear - no influence of acetylene addition on soot formation from chlorobenzene. Indeed, our computational results, which are discussed later in the report, indicate that acetylene addition to aromatic radicals is one of the most important reactions in the polymerization growth of aromatic hydrocarbons. Why then does the addition of acetylene have no effect? While the answer to that question is presently under investigation in our laboratory, a preliminary explanation can follow from analysis of the rest of the experimental data.

Inspection of Figs. 40 and 41 indicates the addition of acetylene to chlorobenzene increases induction times for soot appearance (Fig.

40) and also increases the rates of soot production (Fig. 41). In other words, acetylene inhibits soot formation during the induction period and enhances it after that. The inhibition can be explained by the reaction between phenyl radical and acetylene: being fast and producing a relatively stable species (e.g. phenylacetylene), this reaction competes with phenyl fragmentation. Since the radical HC≡C-CH=CH-CH=$\dot{C}$H, formed in the fragmentation, and immediate products of its decomposition, C_4H_x species, are presumably more efficient "building blocks" than acetylene[24], the removal of phenyl radical from the fragmentation route may explain the observed phenomenon.

That the acetylene reactions are in a fine, competing balance is demonstrated by the results of acetylene addition to benzene (Figs. 42-47). At low acetylene concentration, there is no significant change in the amount of soot formed (Fig. 45a). However, as the concentration of acetylene is increased, the enhancement of soot production is well-pronounced. The results obtained with a benzene-1,3-butadiene mixture (Figs. 48-51) further support the hypothesis that C_4H_x species may be more efficient building blocks than acetylene: the addition of 1,3-butadiene increases both the fractional soot yields (Fig. 49) and the absolute amounts of soot (Fig. 49a) formed from benzene at high temperatures, indicating a synergistic effect.

It is interesting to note that the increase in induction time with the addition of acetylene is more pronounced in the case of chlorobenzene (Fig. 40) than in the comparable case of benzene (Fig. 46). The reason for this is the larger rate of production of phenyl radicals in the former case.

DETAILED KINETIC MODELING

1. Introduction

Soot formation is an important and persistently investigated aspect of combustion[15,16,25-27]. Nonetheless, the elementary chemical reactions leading to soot formation are still unknown. There is growing evidence that the reactions leading to soot formation involve only carbon- and hydrogen-containing species, as oxygen is bound in rich flames as CO and H_2O. For this reason a large number of studies of soot formation in hydrocarbon pyrolysis have been undertaken using flow reactors and shock tubes. While these experiments have not provided detailed composition profiles, they cover wide ranges of conditions and are more easily subjected to interpretive modeling studies at this time.

The objective of the present modeling was to discover the main chemical reaction pathways to soot by experimenting with detailed kinetic models of soot formation under the conditions used in shock-tube pyrolysis of acetylene[24]. The approach taken was to develop a mechanism composed of conventional elementary reactions and to compare the predicted time scale of soot formation and absolute values of soot yields with their experimental counterparts. Nearly all of the equilibrium constants and rate coefficients had to be estimated. A method to account for the infinite growth of soot mass also had to be developed.

After the reaction paths implied by our assumed thermochemistry and rate constants had been identified by study of the simulations, we became aware of a paper by Bockhorn et al.[28] in which astonishingly similar conclusions had been drawn from consideration of experimental composition profiles in sooting flames.

This part of our work was performed in collaboration[3] with Professor William C. Gardiner, Jr., of the University of Texas and Dr. Stephen E. Stein of the National Bureau of Standards.

2. Computer Model

The reaction mechanism has three logical components: a set of reactions describing acetylene pyrolysis, a set of reactions describing the formation of larger molecules and radicals and eventually small aromatic molecules and radicals, and a description of the further growth of aromatic rings. A total of approximately 600 elementary reversible reactions of 180 species were considered during the course of this modeling study.

The chemical species used in the mechanism are listed in Table II with both their structures and assigned computer names. Atomic hydrogen and molecular hydrogen, whose computer names (H and H2) are identical with those used conventionally, are not listed in Table II. The names were chosen for two principal reasons: first, complete IUPAC names were too long and unwieldy; and second, each name was required to provide a reasonable description of the species' structure. Our nomenclature system is not an attempt to design a universal method; it was developed to address the needs of our specific modeling work on soot formation. The task of developing a completely general nomenclature system is nontrivial[29].

The chemical species are described using 12 characters or less. The following terms are used to specify the basic structure of a compound:

TABLE II. REACTION SPECIES.

C_2H	$\bullet C\equiv C-H$
C_2H_2	$H-C\equiv C-H$
C_2H_3	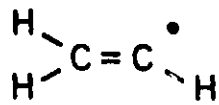
C_2H_4	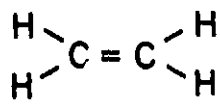
C_4H	$\bullet C\equiv C-C\equiv C-H$
C_4H_2	$H-C\equiv C-C\equiv C-H$
C_4H_3S	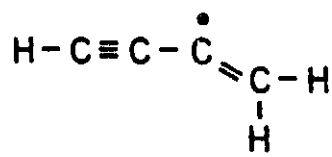
C_4H_3U	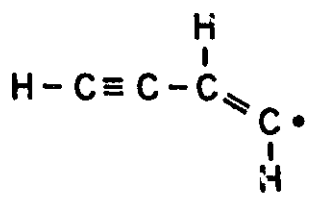

C_4H_4

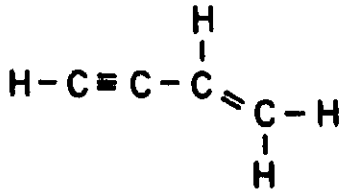

C_4H_5S

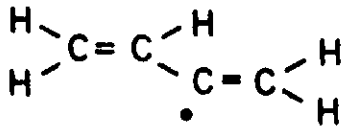

C_4H_5U

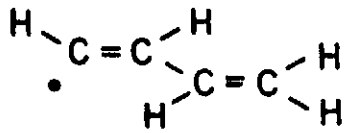

C_4H_6

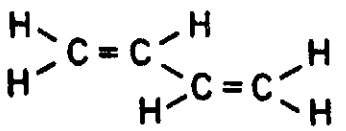

C_6H

C_6H_2

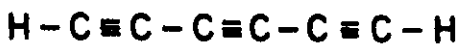

C_6H_3S

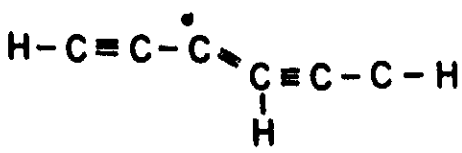

C_6H_3U

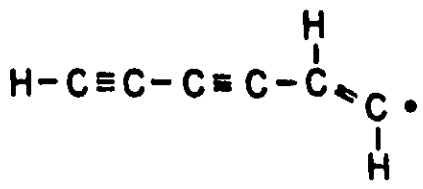

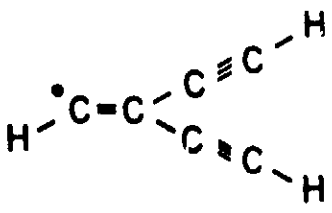

C_6H_4

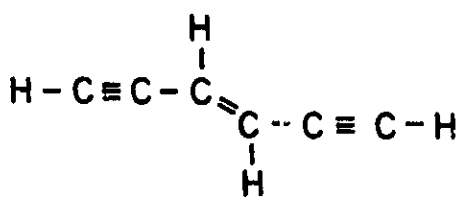

C_6H_4X

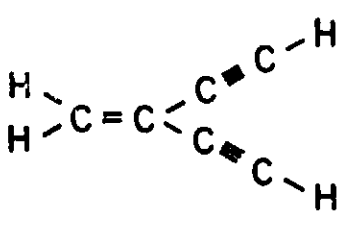

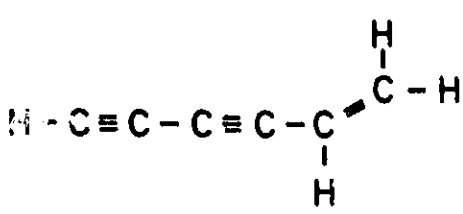

C_6H_5S

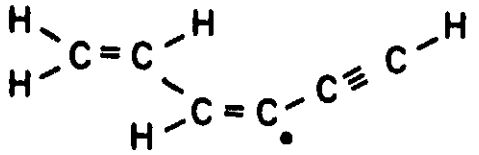

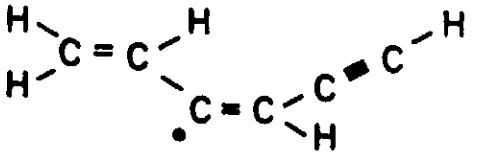

C_6H_5U

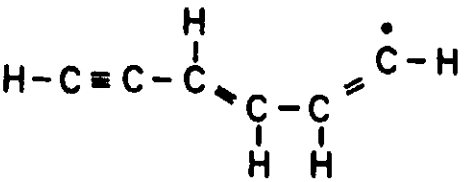

C_6H_6

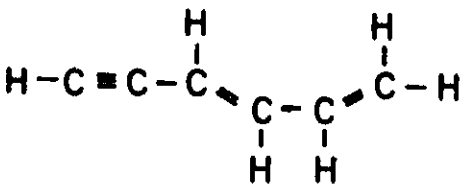

C_6H_7S

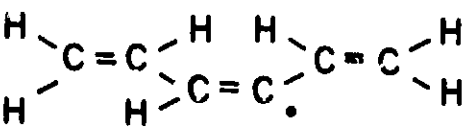

C_6H_7U

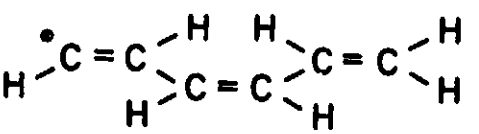

R 6 %

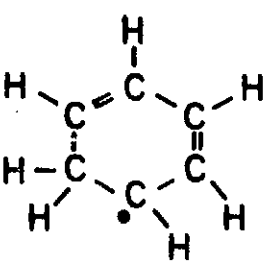

C_6H_8

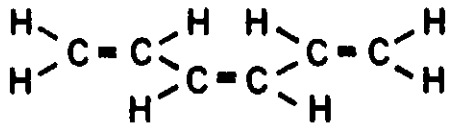

C_8H

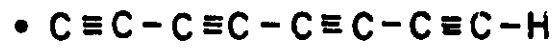

C_8H_2

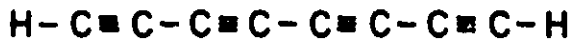

C_8H_3S

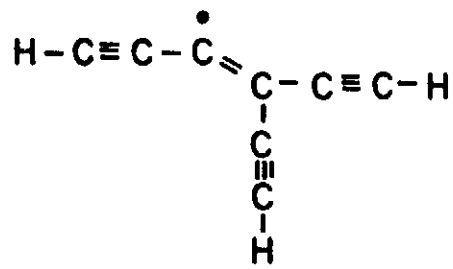

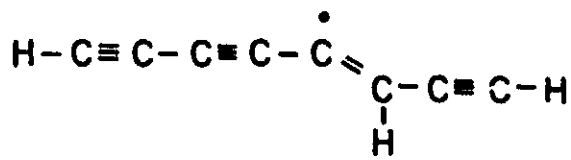

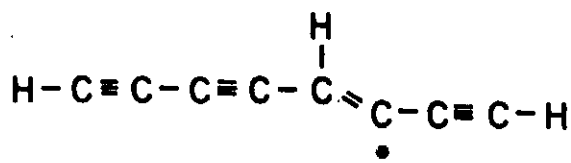

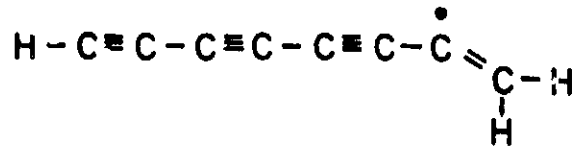

C_8H_4

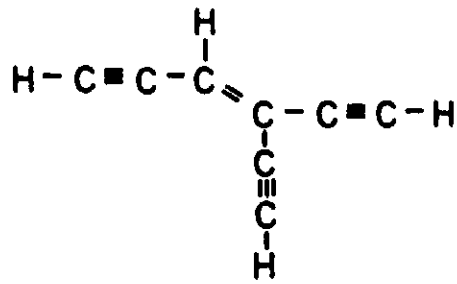

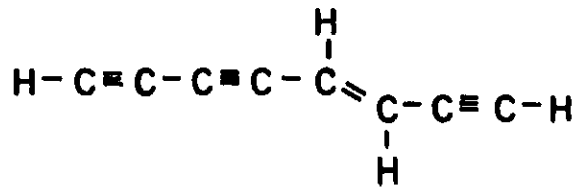

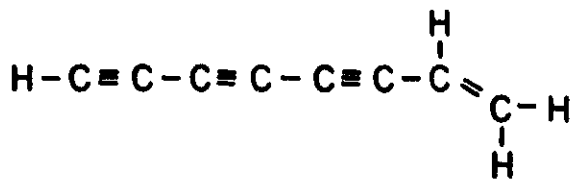

C_8H_5S

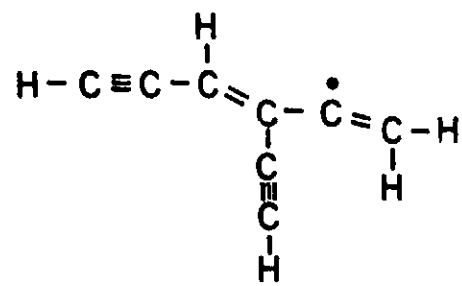

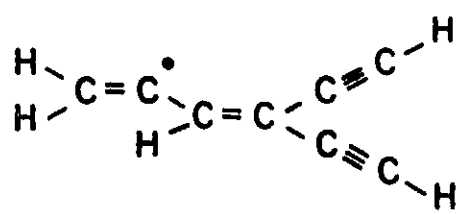

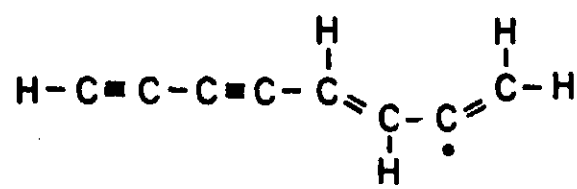

etc.

C_8H_5SX

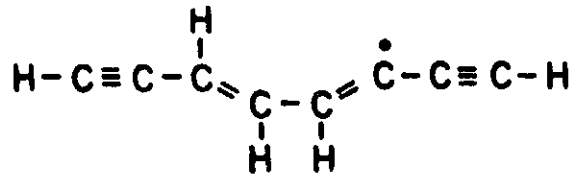

C_8H_5SY

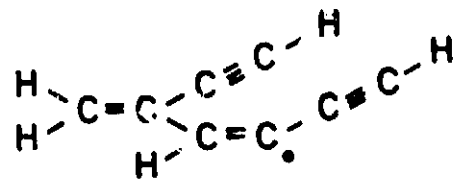

C_8H_5SZ

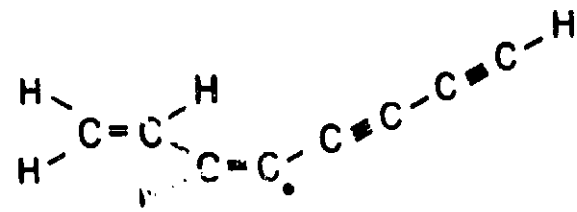

C_8H_5U

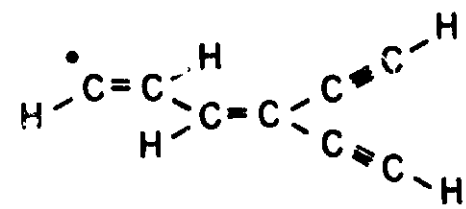

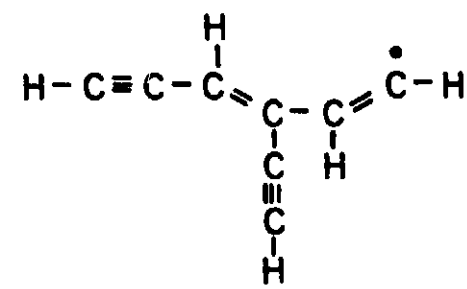

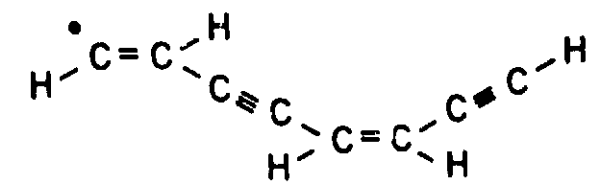

etc.

C_8H_6

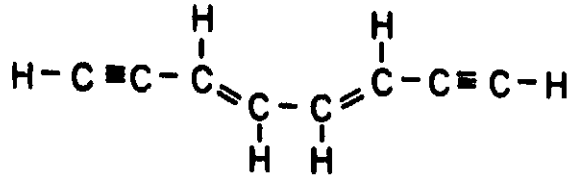

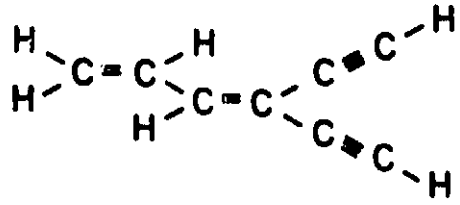

etc.

C_8H_7S

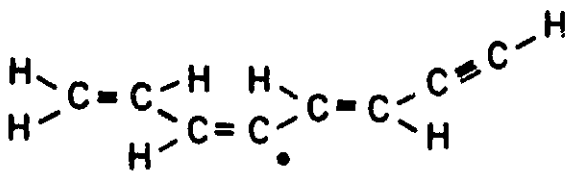

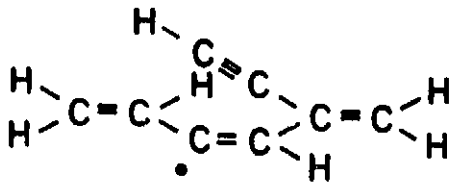

C_8H_7SX

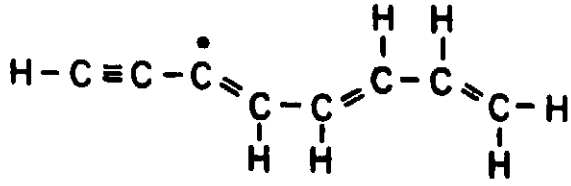

C_8H_8

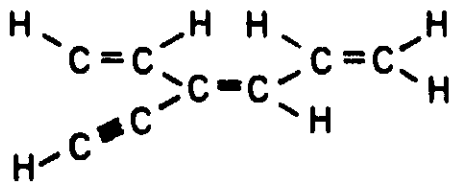

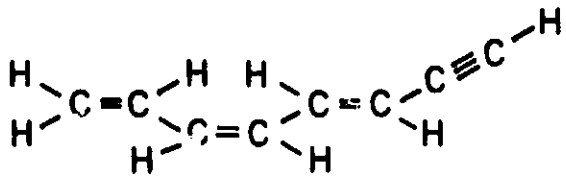

$C_{10}H_2$

$C_{10}H_3S$

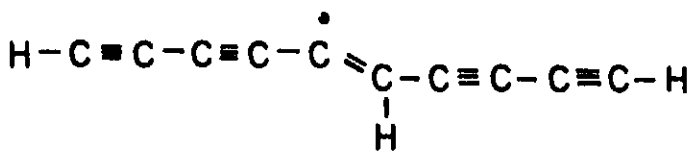

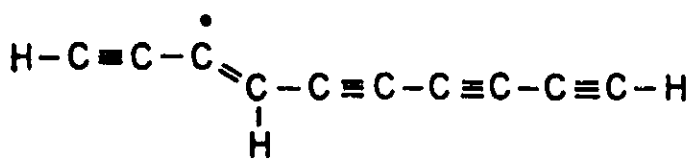

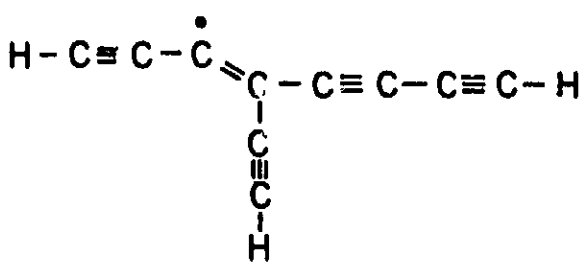

etc.

$C_{10}H_4$

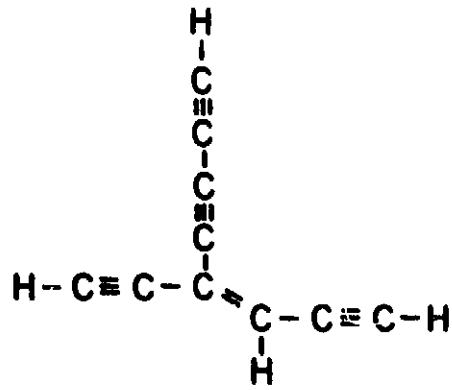

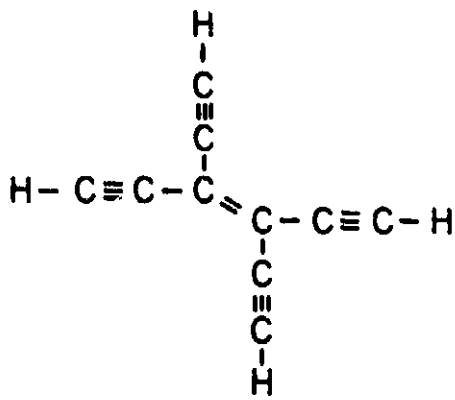

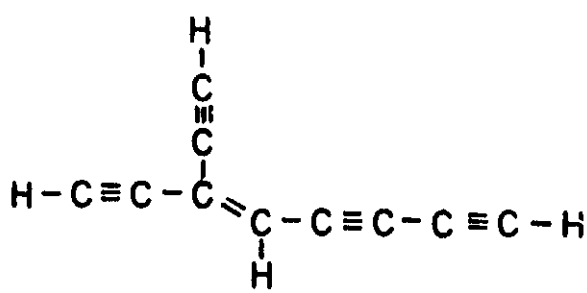

etc.

$C_{10}H_5S$

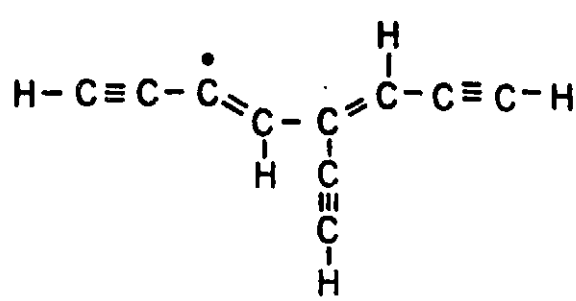

$C_{10}H_6$

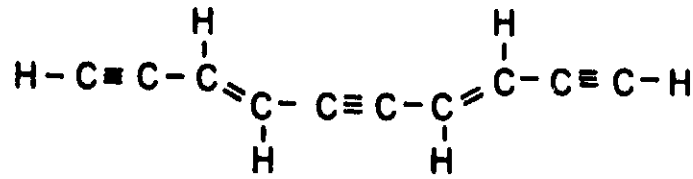

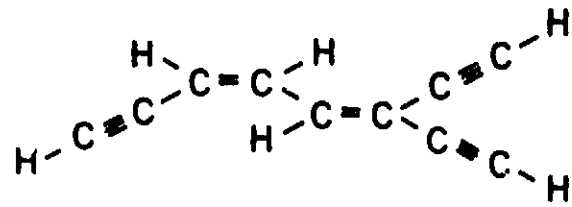

etc.

$C_{10}H_7S$

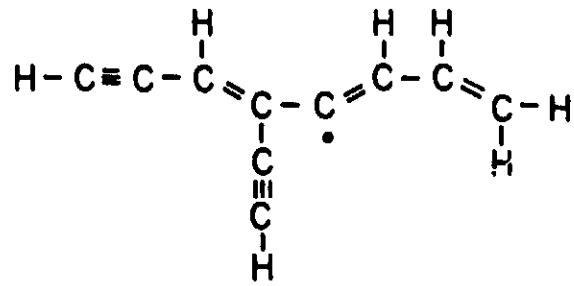

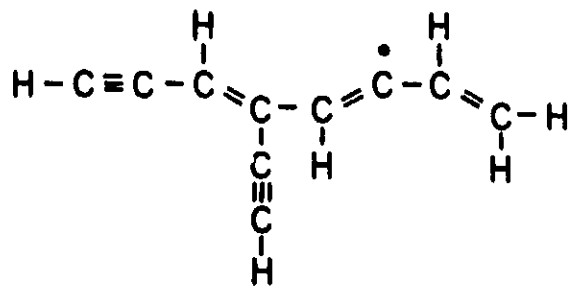

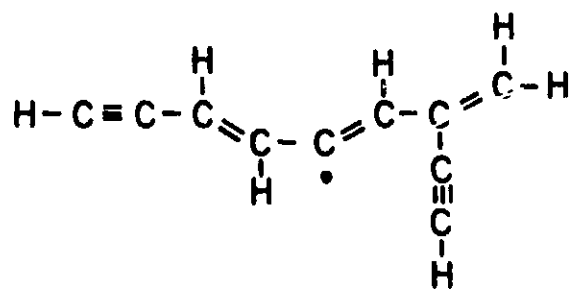

etc.

$C_{10}H_7SX$

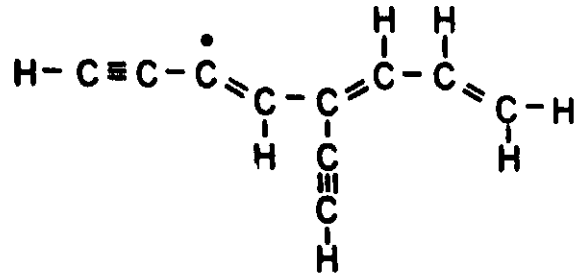

$C_{10}H_7U$

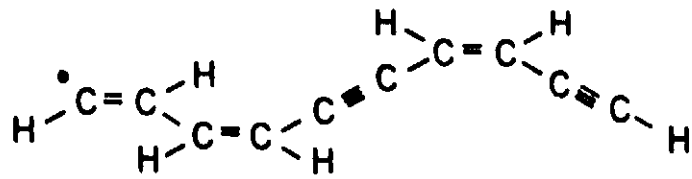

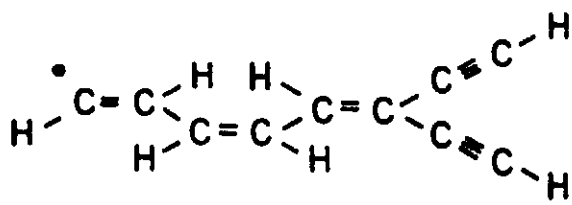

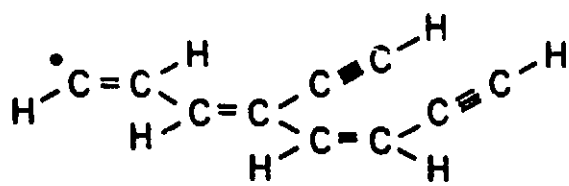

etc.

$C_{10}H_8$

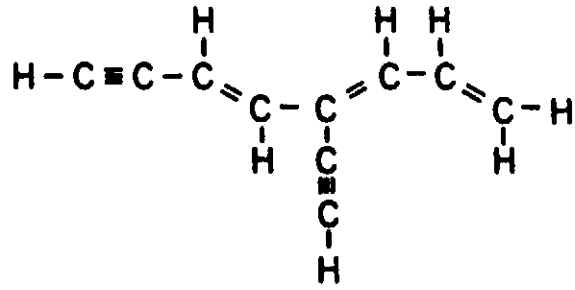

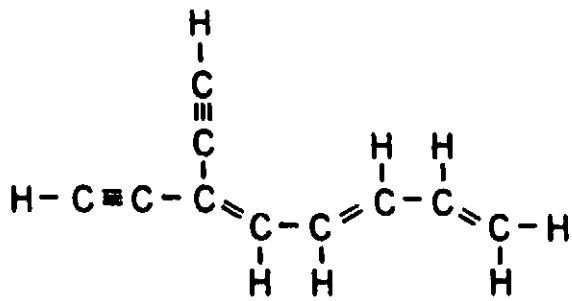

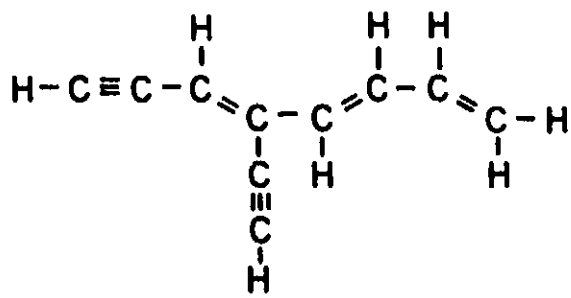

etc.

$C_{10}H_9S$

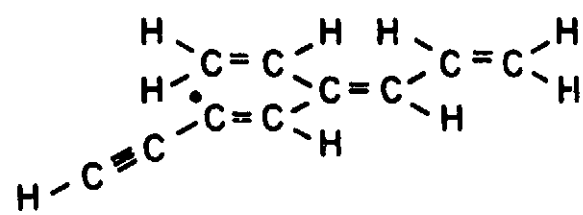

$C_{12}H_2$

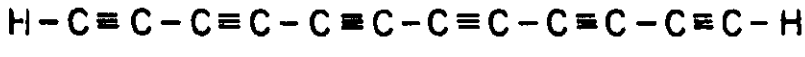

$C_{12}H_3S$

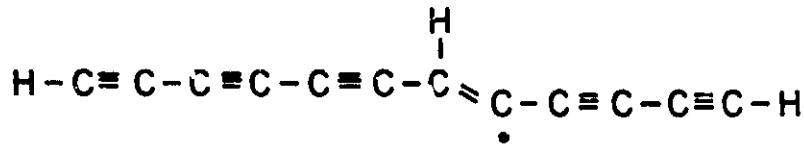

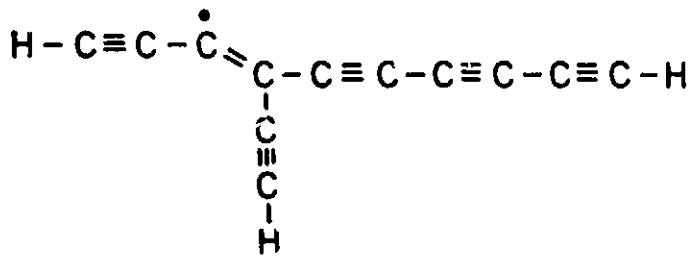

$C_{12}H_4$

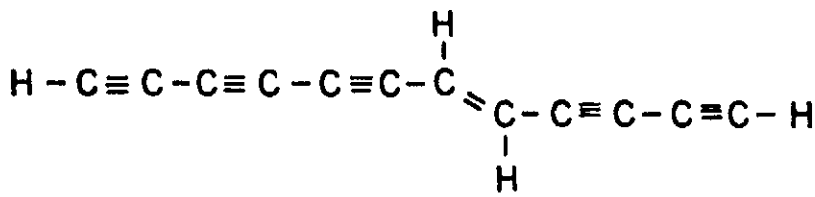

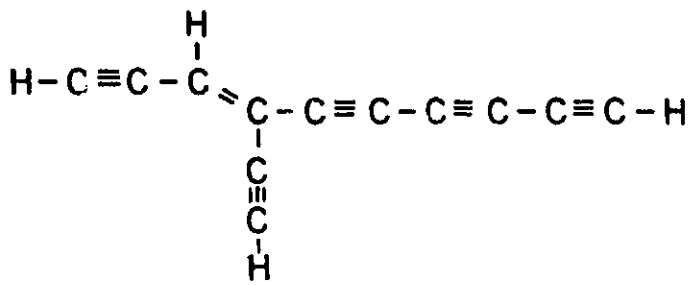

etc.

$C_{12}H_5S$

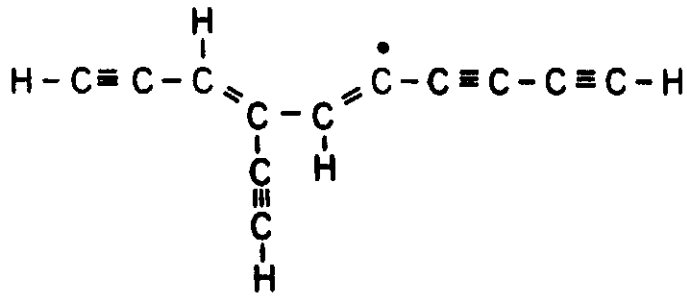

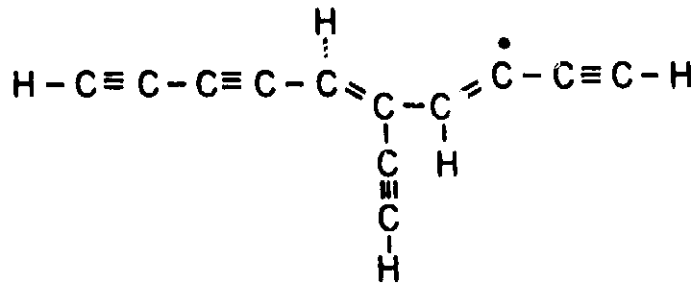

etc.

$C_{12}H_6$

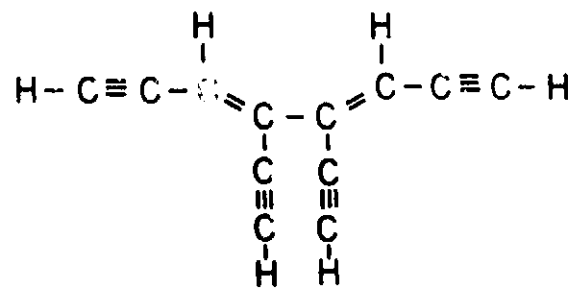

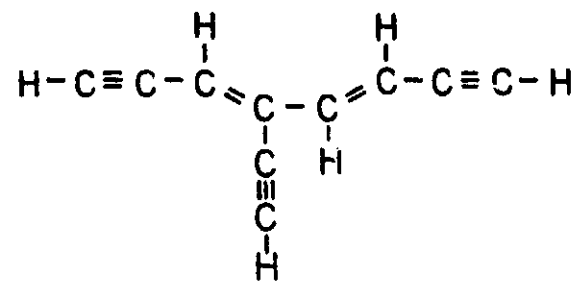

etc.

$C_{12}H_7S$

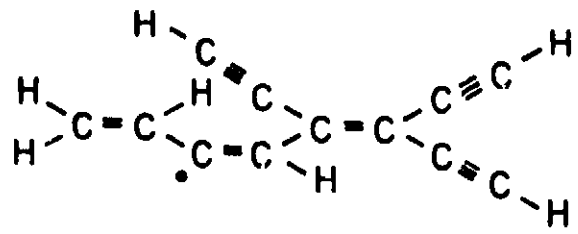

$C_{12}H_7SX$

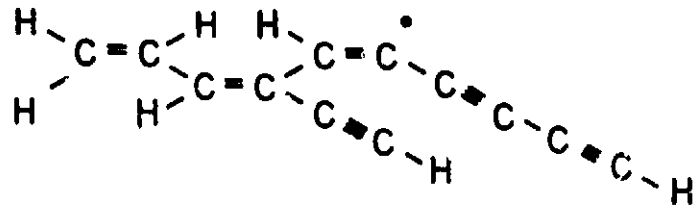

$C_{12}H_7SY$

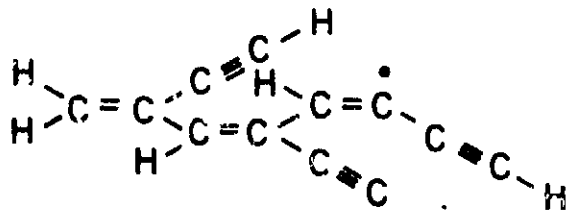

$C_{12}H_7SZ$

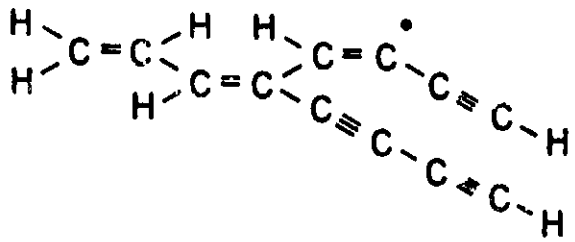

$C_{12}H_8$

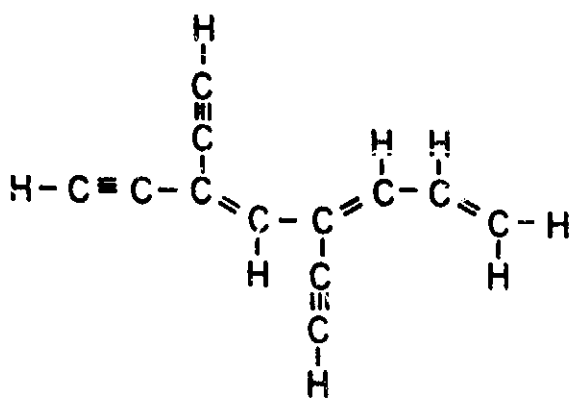

$C_{12}H_8X$

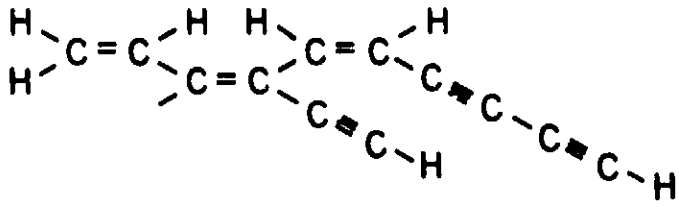

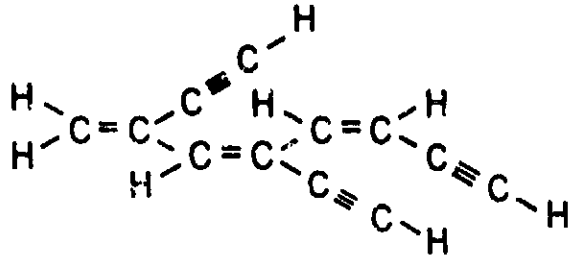

etc.

$C_{12}H_9S$

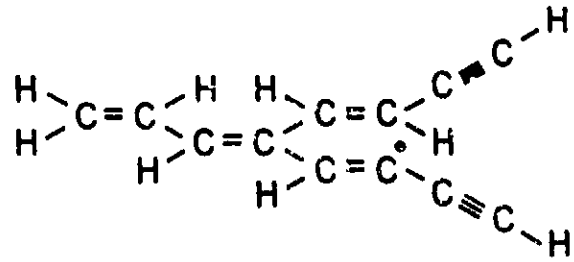

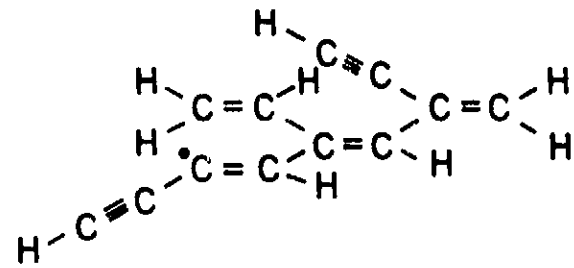

etc.

$C_{12}H_{10}$

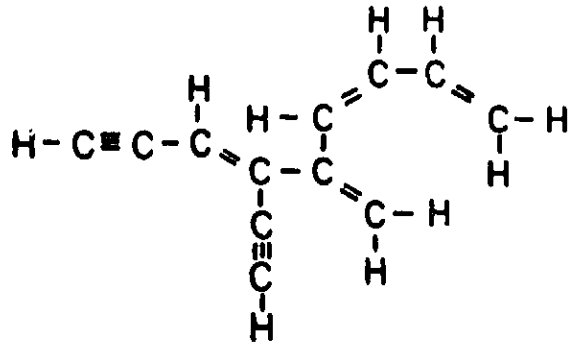

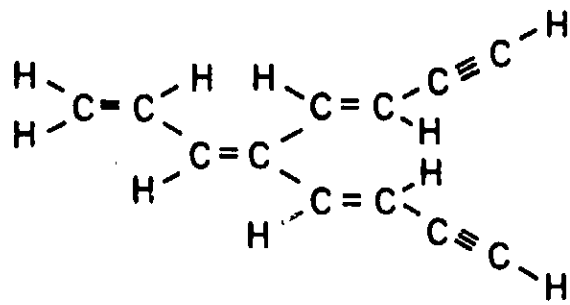

etc.

$C_{14}H_4$

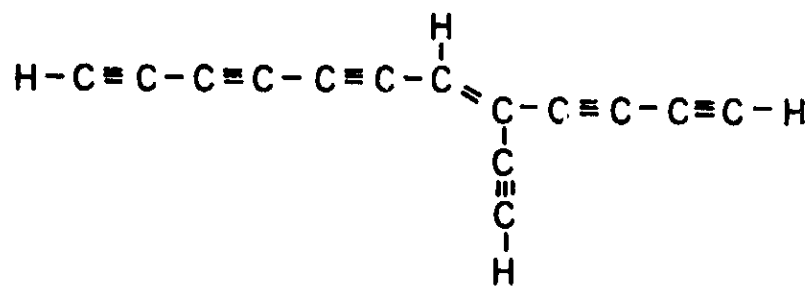

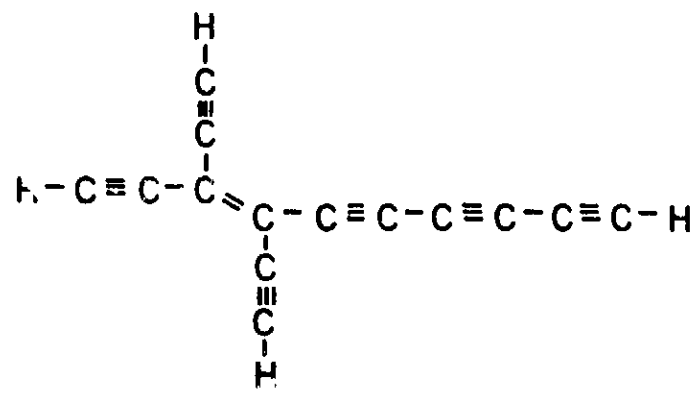

$C_{14}H_5S$

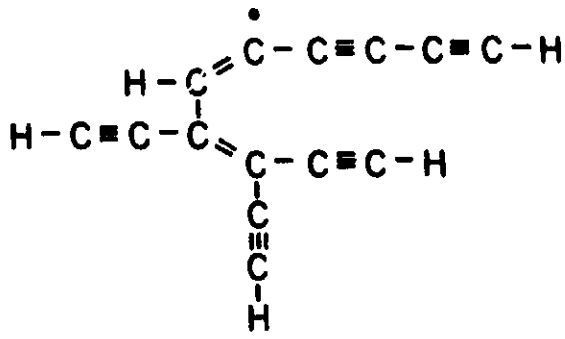

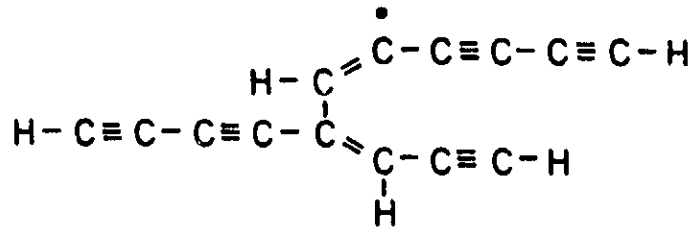

etc.

$C_{14}H_6$

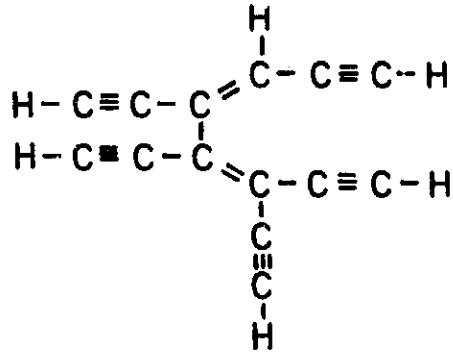

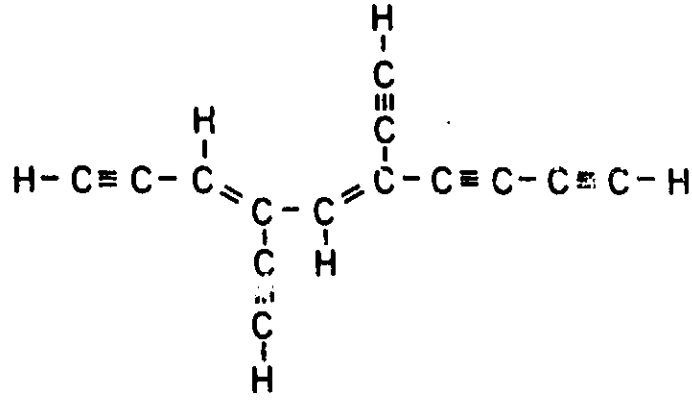

etc.

$C_{14}H_7S$

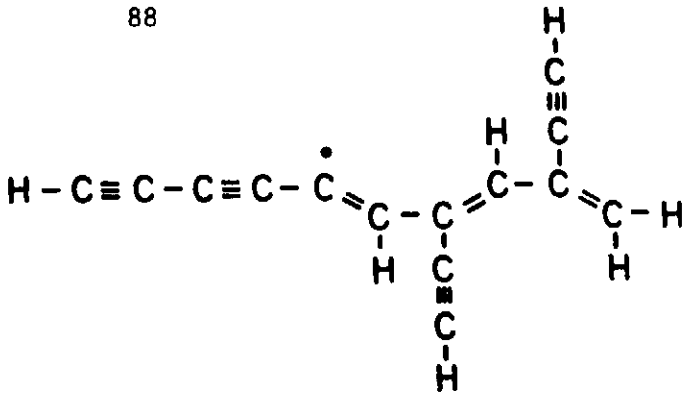

$C_{14}H_7SX$

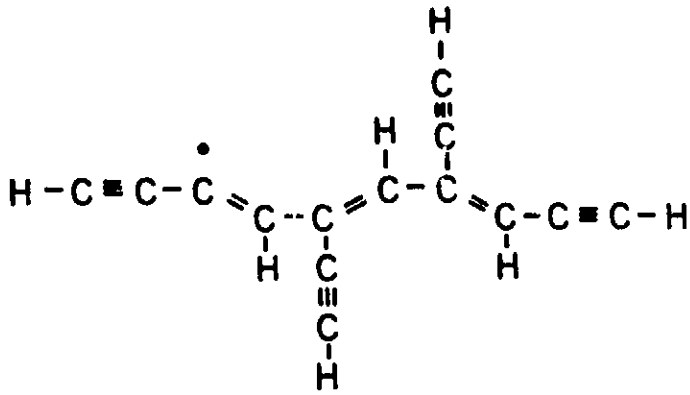

$C_{14}H_8$

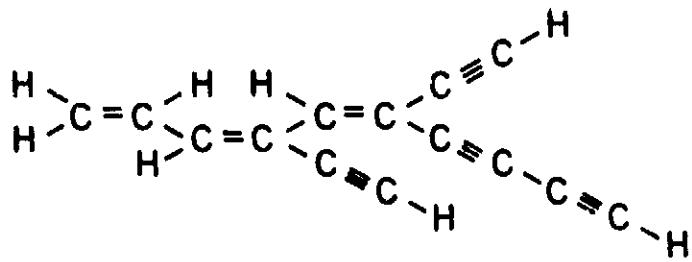

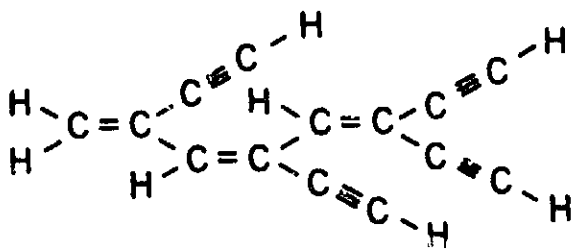

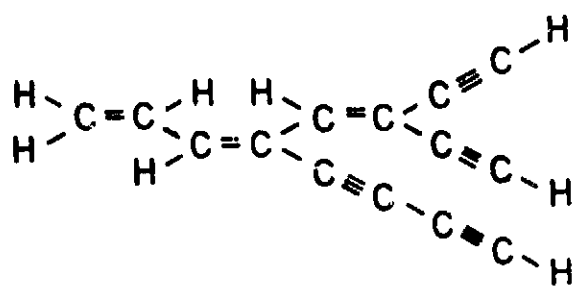

$C_{14}H_8X$

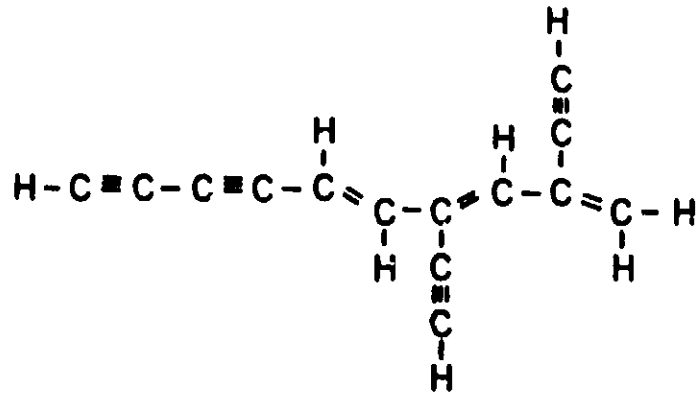

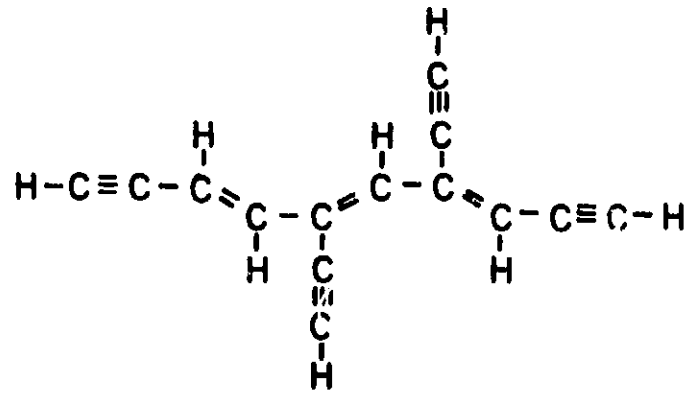

$C_{14}H_9S$

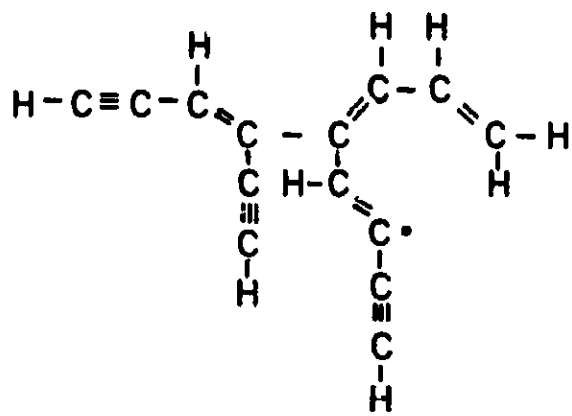

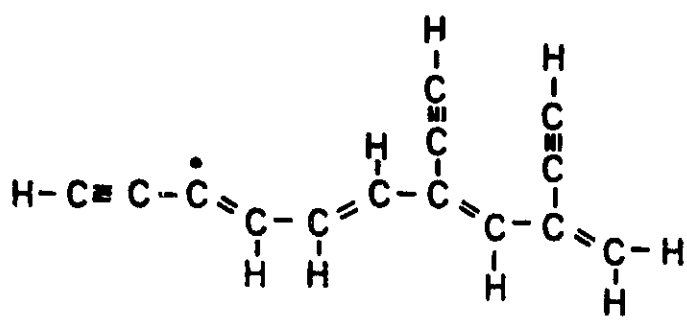

etc.

$C_{14}H_{10}$

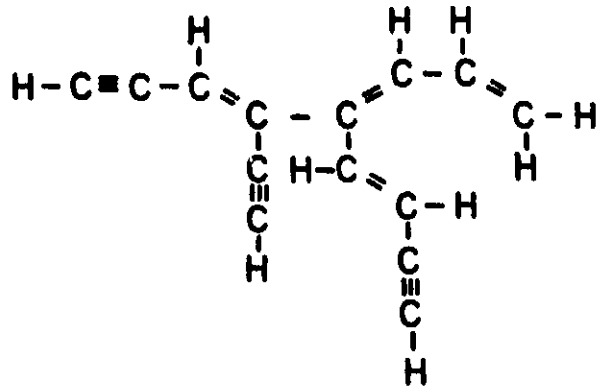

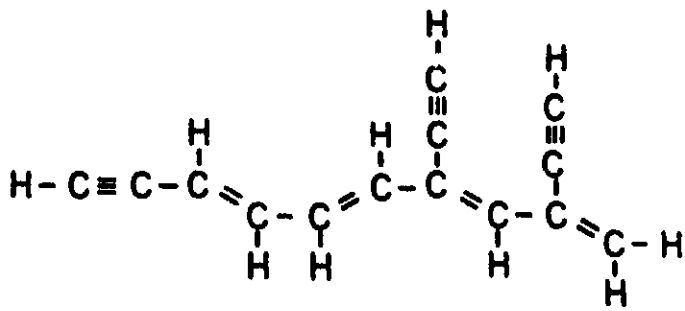

etc.

$C_{16}H_8$

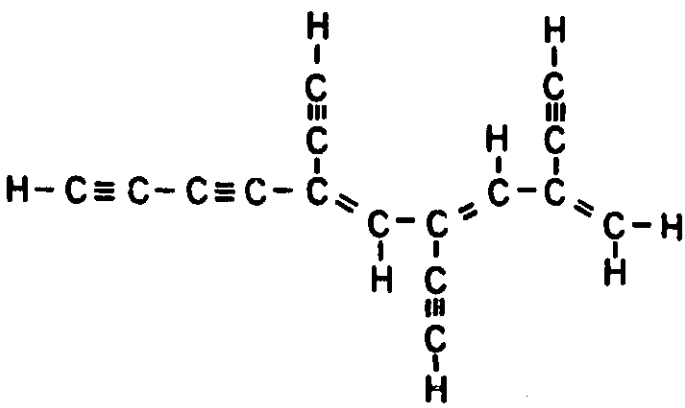

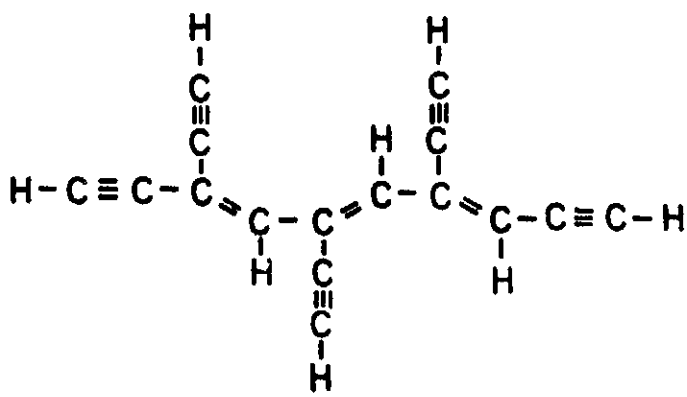

A_1- 

A_1 

A_1C_2H- 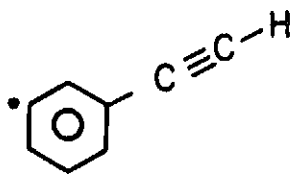

A_1C_2H* 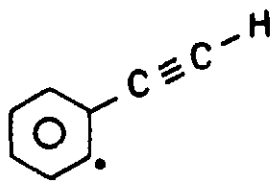

A_1C_2H 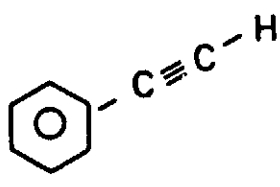

$A_1C_2H_2U$ 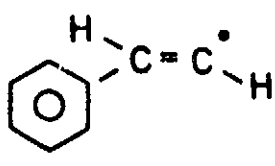

$A_1C_2H_3$ 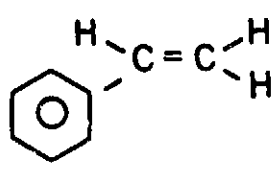

$A_1C_4H_2S$

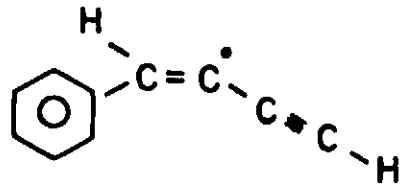

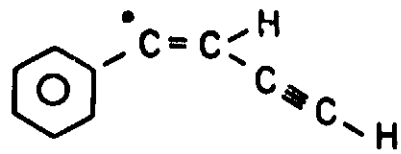

$A_1C_4H_3-$

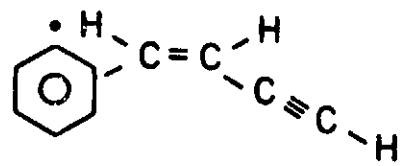

$A_1C_4H_3$

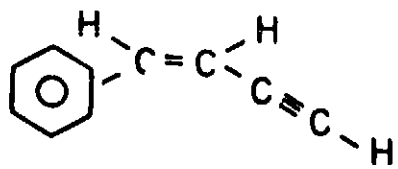

$A_1C_4H_4S$

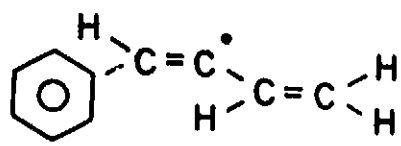

$A_1C_4H_4U$

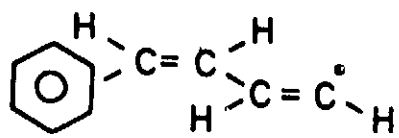

$A_1C_4H_5$

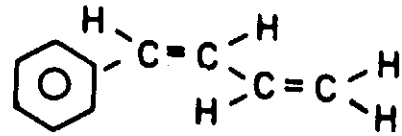

$A_1C_6H_2S$

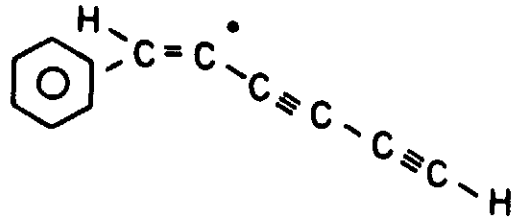

$A_1C_6H_3$

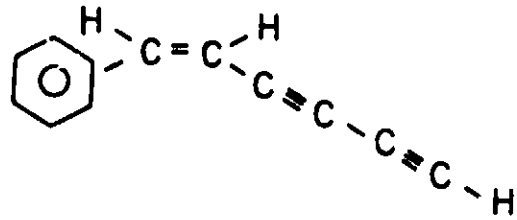

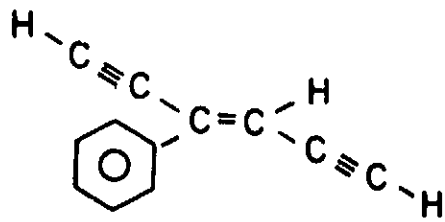

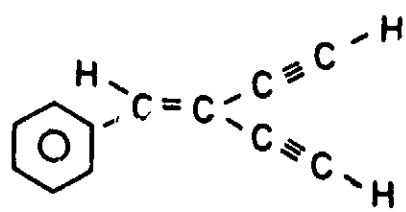

$A_1C_6H_4S$

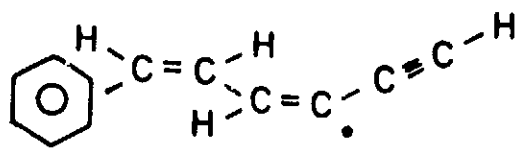

$A_1C_6H_4SX$

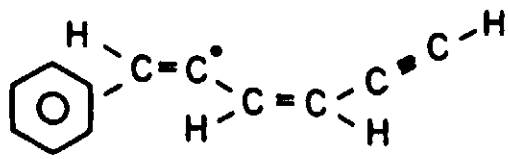

$A_1C_6H_4U$

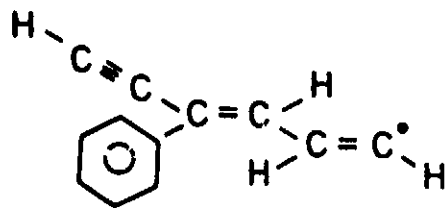

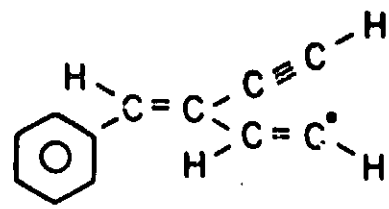

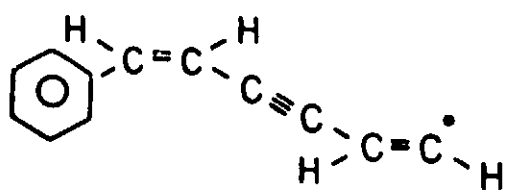

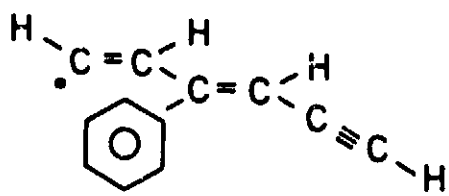

$A_1C_6H_5$

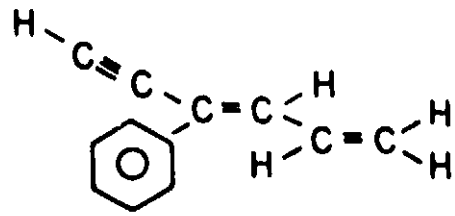

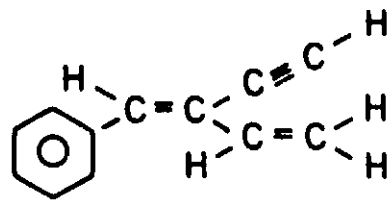

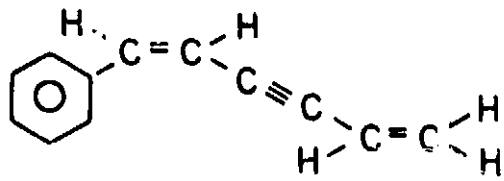

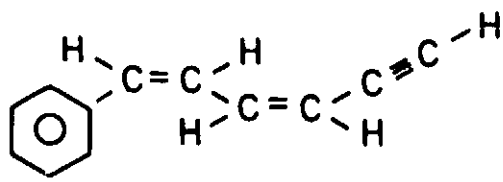

$A_1C_8H_4S$

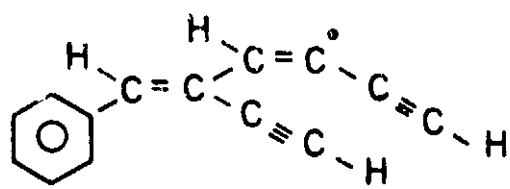

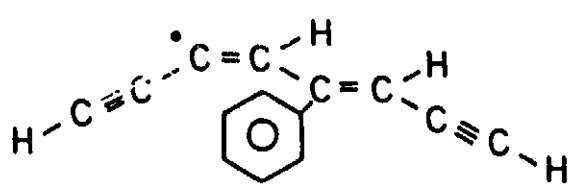

$A_1\ C_8H_5$

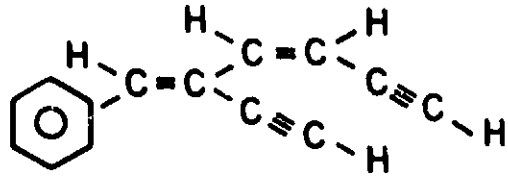

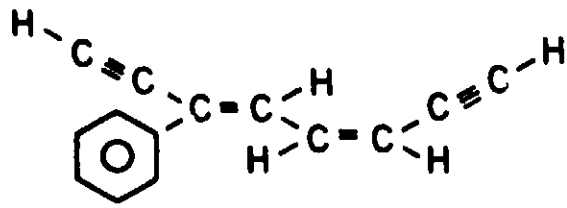

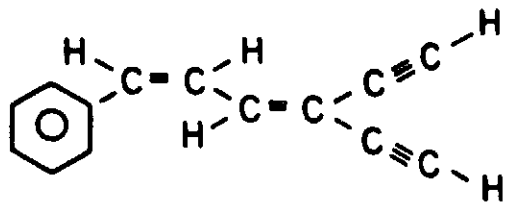

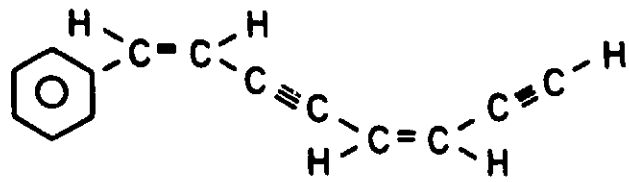

$A_1\ C_8H_6S$

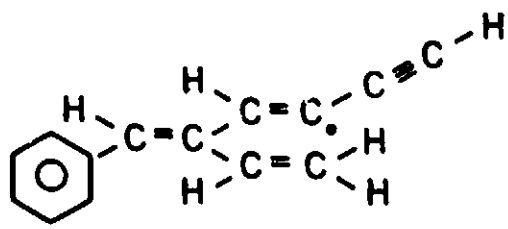

$A_1\ C_{10}H_4S$

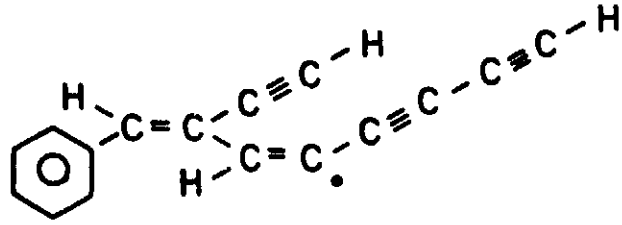

C - 2

$A_1\ C_{10}H_5$

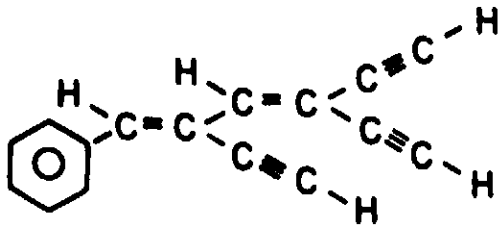

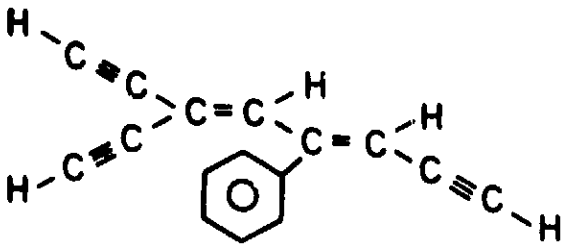

etc.

$A_1\ C_{10}H_6S$

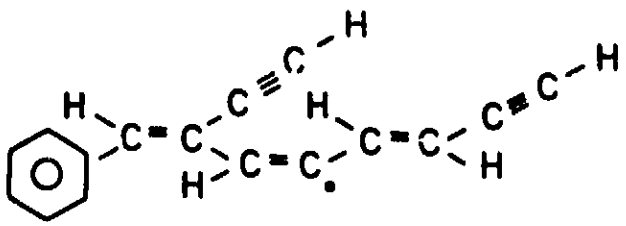

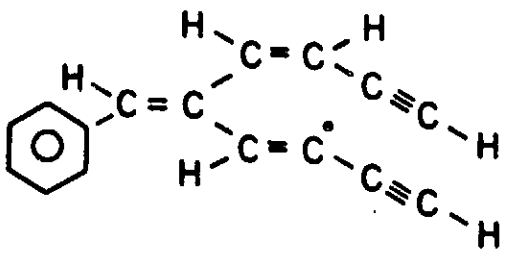

$A_1\ C_{10}H_8S$

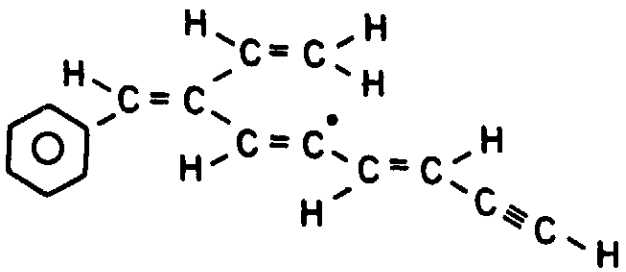

$A_1C_{12}H_6S$

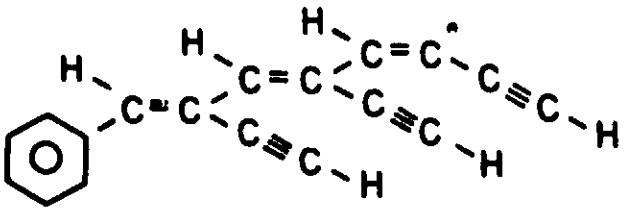

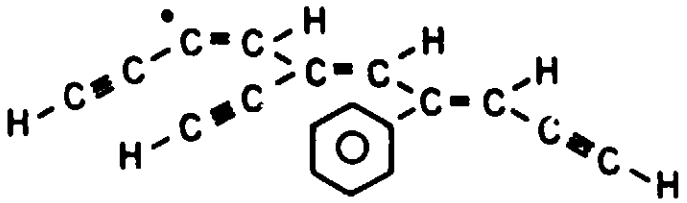

$A_1C_{12}H_8S$

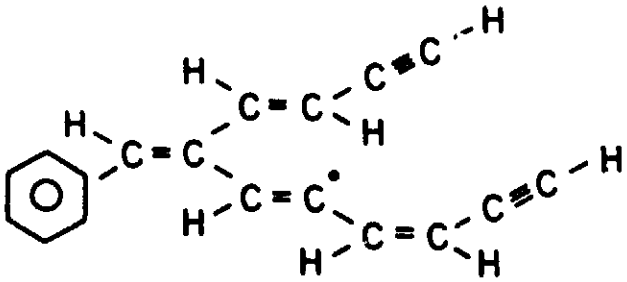

$A_1C_{14}H_6S$

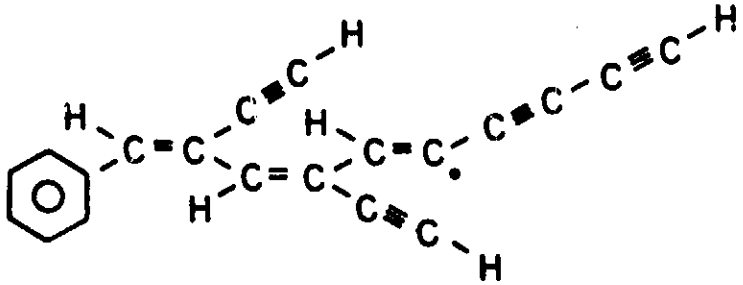

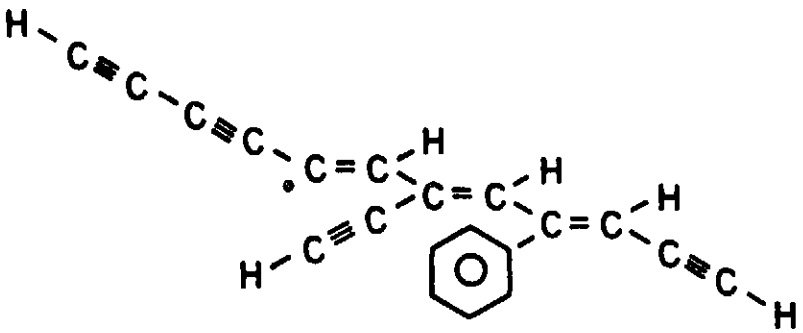

$A_1C_2H)_2-$

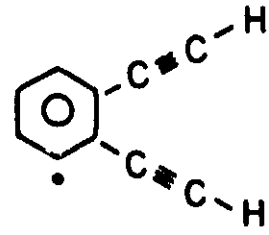

$A_1C_2H)_2$

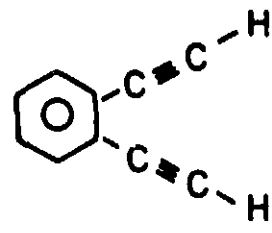

$A_1C_2H)_2X$

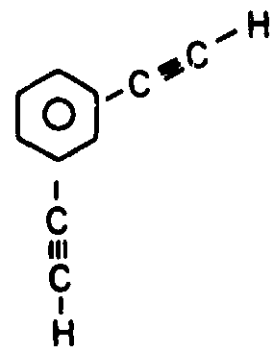

$A_1C_2HC_2H_2U$

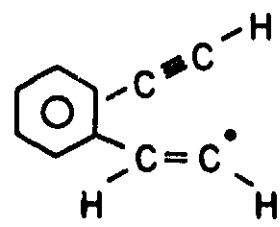

$A_1C_2HC_2H_3$

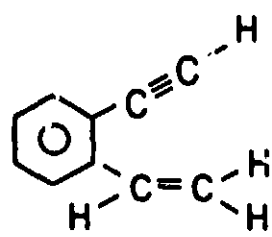

$A_1C_2HC_2H_3X$

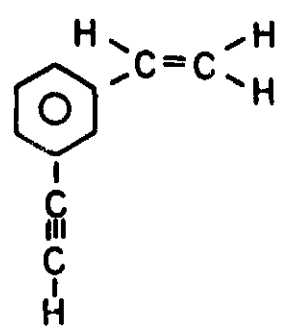

$A_1C_2HC_4H$

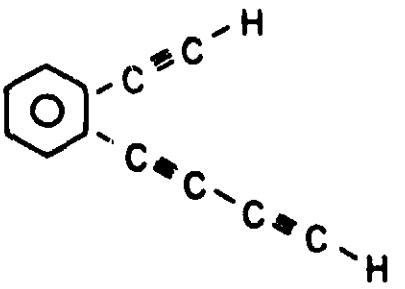

$A_1C_2HC_4HX$

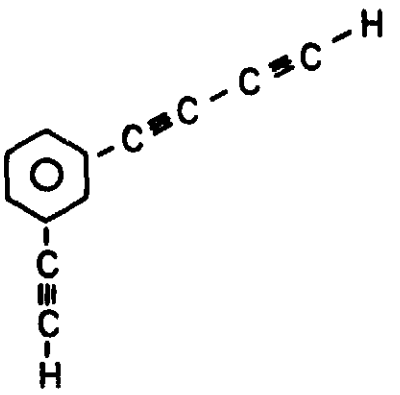

$A_1C_2HC_4H_2S$

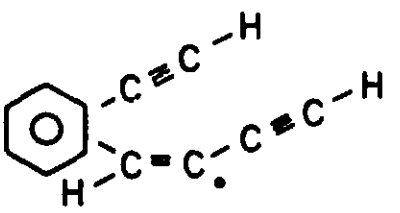

$A_1C_2HC_4H_3$

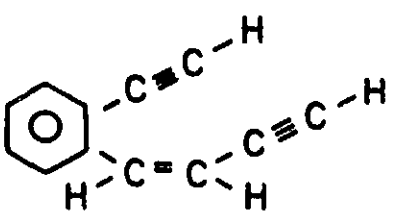

$A_1C_2HC_4H_3X$

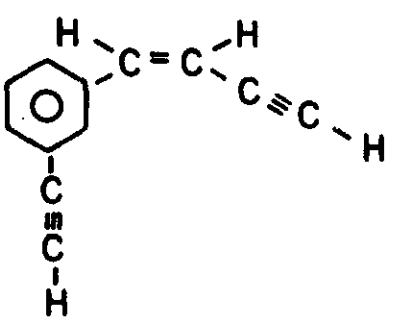

$Al(C_2H)_3$

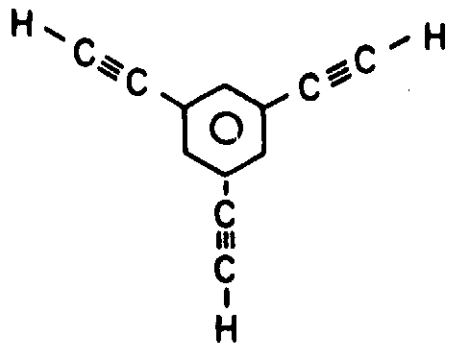

etc.

$Al(C_2H)_2C_4H$

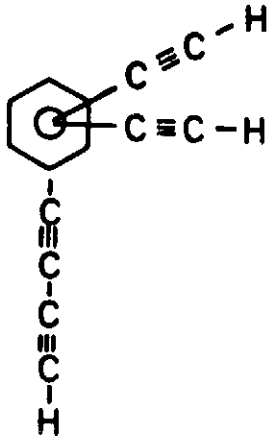

$Al(C_2H)_2C_4H_3$

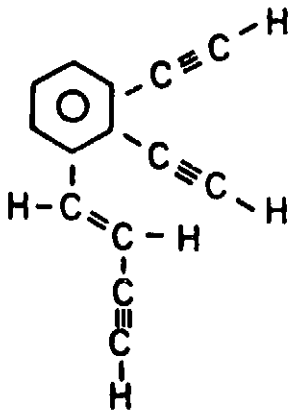

$Al(C_2H)_4$

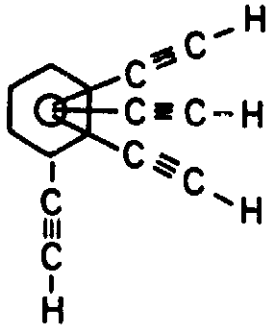

A_2- 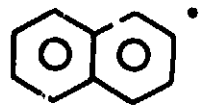

A_2-X 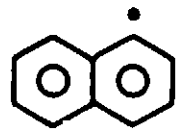

A_2 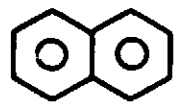

A_2C_2H* 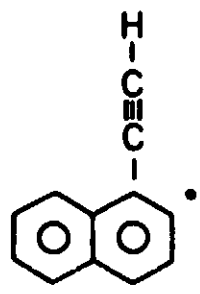

A_2C_2H*X 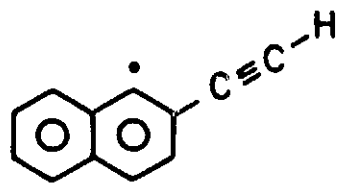

A_2C_2H- 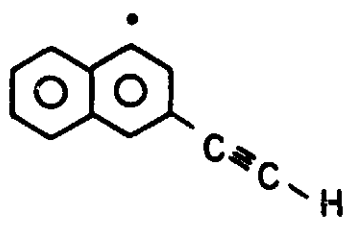

A_2C_2H 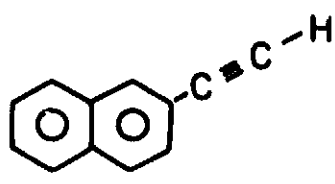

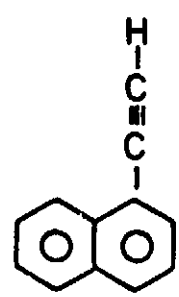

$A_2C_2H)_2$

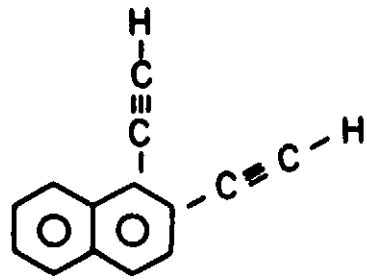

$A_2C_2H)_2X$

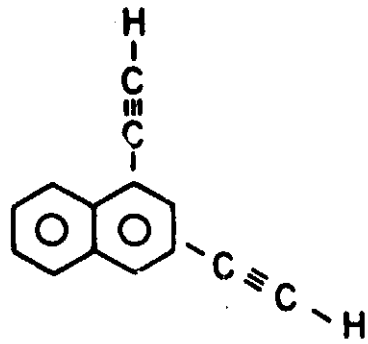

$A_2C_2HC_2H_2U$

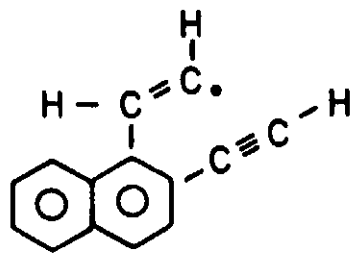

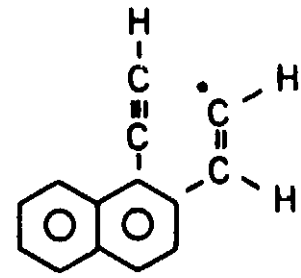

A_2R5-

A_2R5

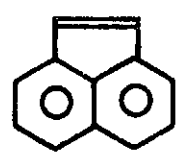

A_2R5C_2H*

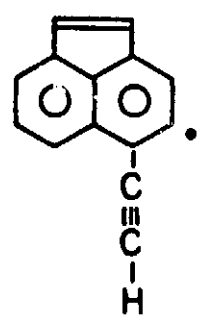

A_2R5C_2H

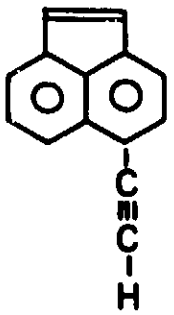

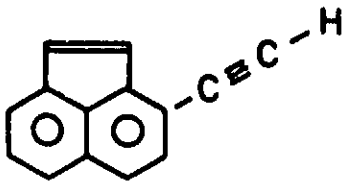

$A_2R5C_2H)_2$

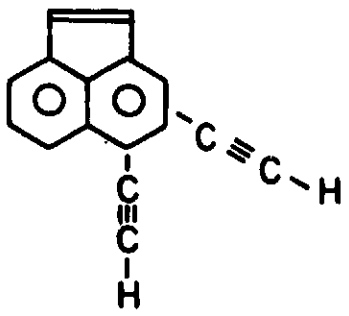

$A_2R5C_2HC_2H_2U$

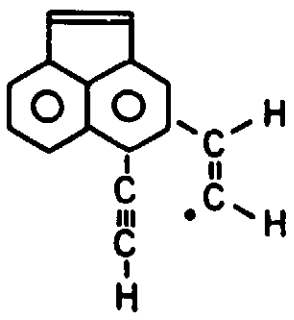

A_3-

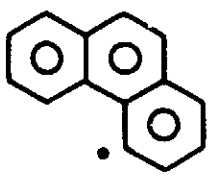

A_3

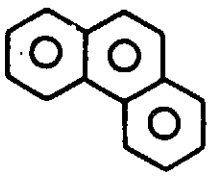

$A_3C_2H^*$

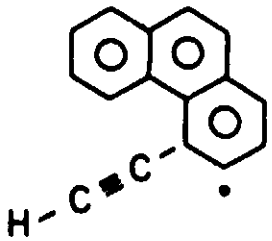

A_3C_2H

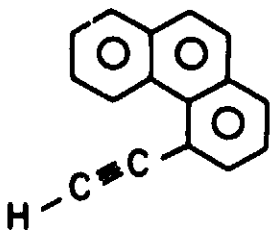

$A_3C_2H_2U$

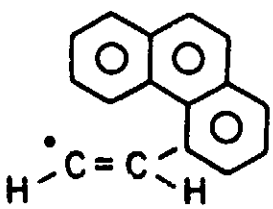

$A_3C_2H)_2$

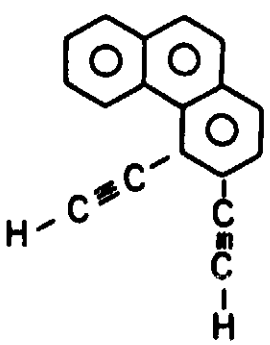

$A_3C_2HC_2H_2U$

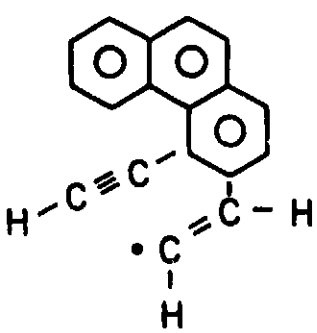

A_3R5-

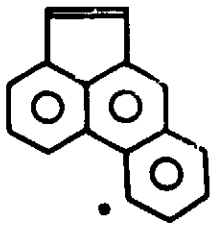

A_3R5

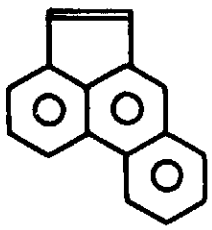

A_3R5C_2H

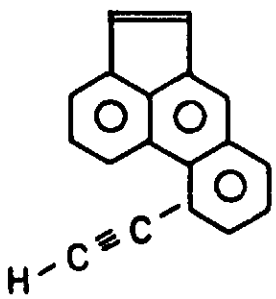

$A_3R5C_2H_2U$

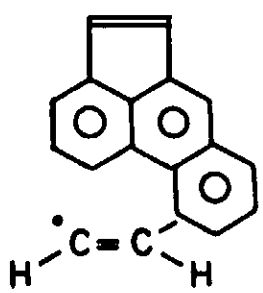

A_4-

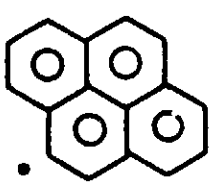

A_4

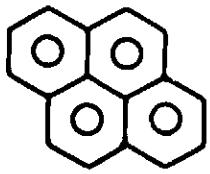

A_4C_2H *

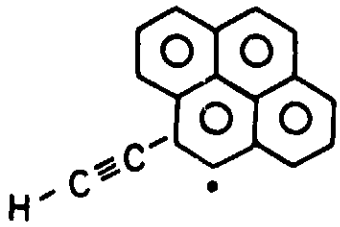

A_4C_2H

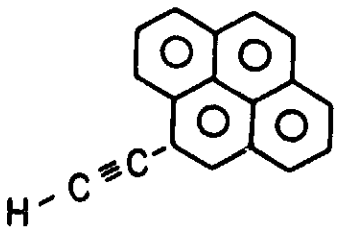

$A_4C_2H)_2$

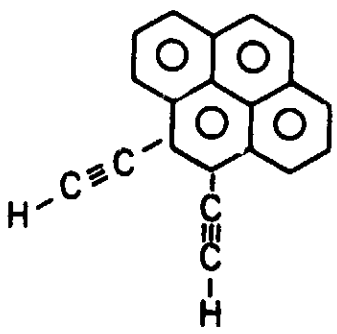

$A_4C_2HC_2H_2U$

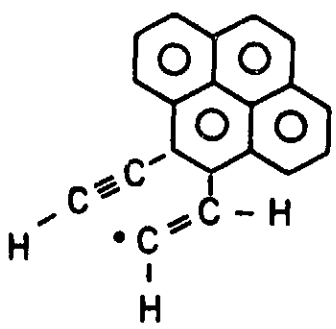

B_4 –

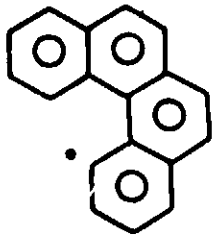

B_4

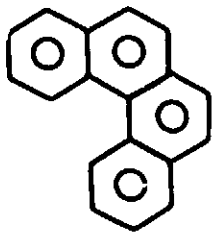

B_4C_2H *

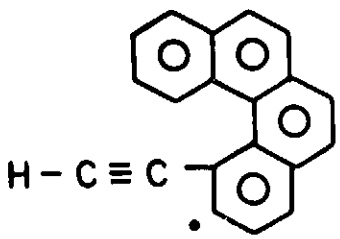

B_4C_2H

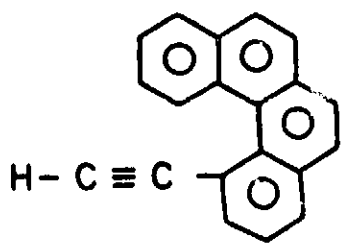

$B_4C_2H)_2$

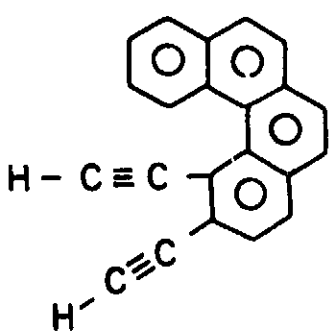

$B_4C_2HC_2H_2U$

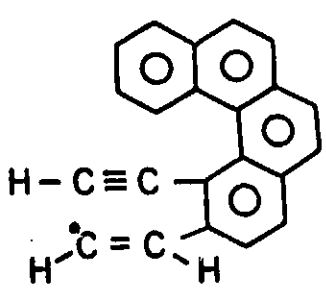

A_5- 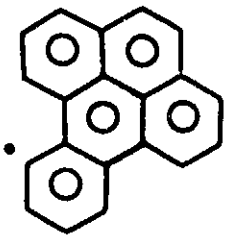

A_5 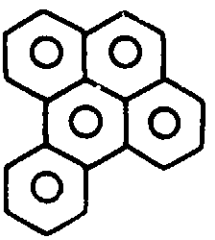

A_5C_2H 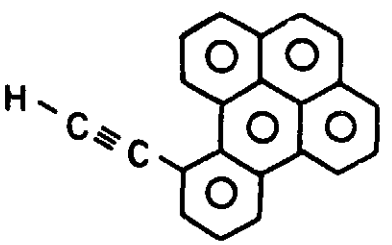

B_5- 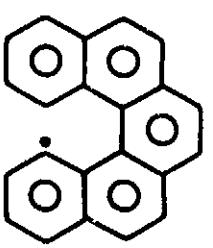

B_5 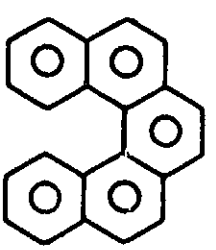

A_6- 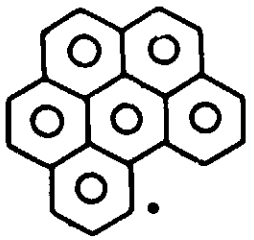

A_6 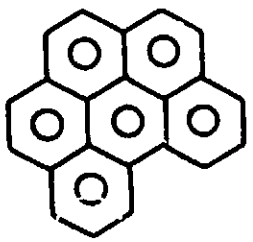

A_6C_2H 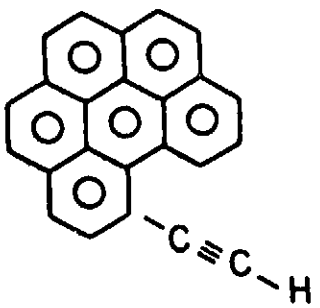

A_7- 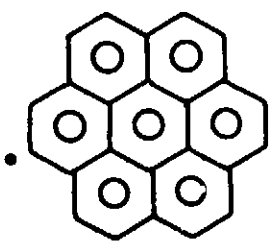

A_7 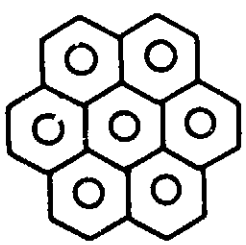

A_7C_2H* 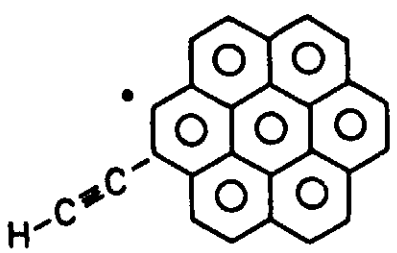

A_7C_2H

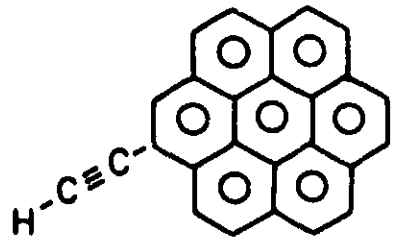

$A_7C_2H)_2$

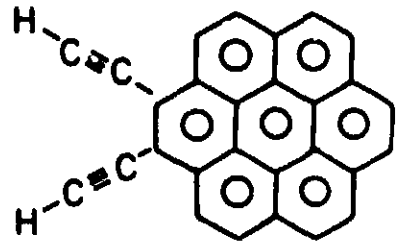

$A_7C_2HC_2H_2U$

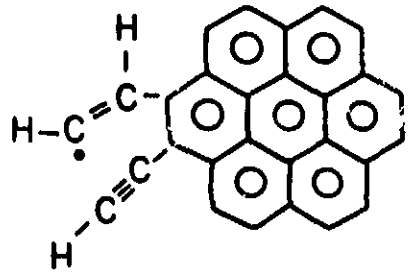

A_8-

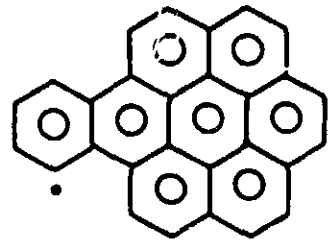

A_8

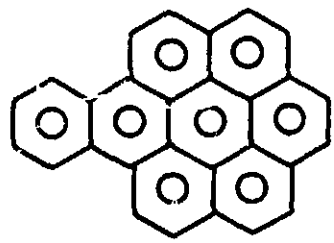

A_8C_2H

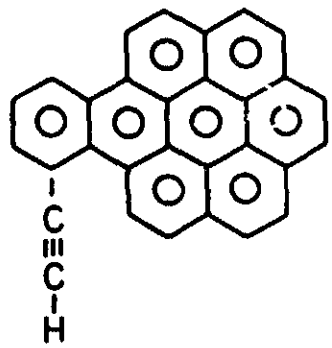

A_9^-

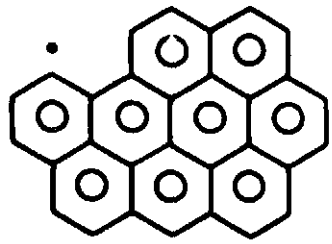

A_9

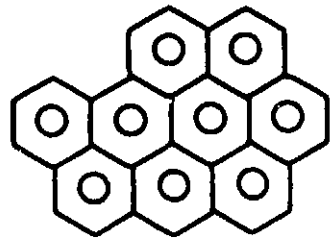

A_9C_2H

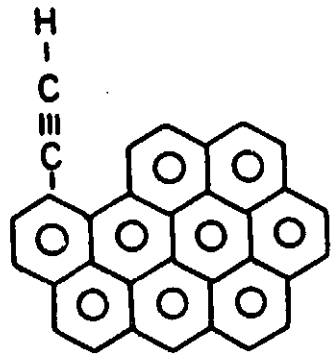

An: species of type A containing n fused aromatic rings. Species with these names include highly condensed polyaromatics such as pyrene, A4, and coronone, A7, (see Table II) and the intermediates (of Route 1 in Fig. 53) leading to their formation, such as phenanthrene, A3, and benzo[a] pyrene, A5. Species of type A with four or more rings are both ortho- and peri-fused; that is, the aromatic rings share i common faces but less than 2i common carbon atoms.

Bn: species of type B containing n fused aromatic rings. These species are involved in the external cyclization route (Route 2 of Fig. 53). Examples of species with these names are benzo[c]phenanthrene, B5, and dibenzo[c,d]phenanthrene, B6 (see Table II). Species of type B with fewer than seven rings are ortho-fused; i.e., the aromatic rings share i common sides and 2i common carbon atoms.

Rn: non-aromatic ring containing n carbon atoms.

CnHm: non-ring structure containing n carbon atoms and m hydrogen atoms; neither n nor m is printed if it equals one.

If a structure contains both aromatic and nonaromatic rings, the aromatic rings are specified first. For example, acenaphthalene is named as A2R5 (see Table II).

Ring substituents are listed as suffixes. They are listed in order of increasing number of carbon atoms; free-radical substituents come last. If two groups have an equal number of carbon atoms, they are listed in order of increasing number of hydrogen atoms. Multiple identical substituents are denoted by placing a right parenthesis and the number of such groups after the substituent name.

The names of all free radicals, other than ethynyl radicals, contain a special symbol indicating the type of radical. The symbol is placed after the structure description. These symbols are:

U: a vinyl radical with the unpaired electron located on a terminal carbon atom. Example: C4H3U (see Table II). The only exception to this naming rule is for C_2H_3, which was named C2H3 in accordance with convention.

S: a vinyl radical with the unpaired electron located on an internal carbon atom. Example: C4H3S (see Table II).

: a radical with the unpaired electron located on an aromatic ring and adjacent to a C2H substituent. Example: A1C2H (see Table II).

-: a radical which has the unpaired electron located on an aromatic ring and which is not described by "*". Example: A1- (see Table II).

%: a radical with the unpaired electron located on a non-aromatic ring. Example: R6% (see Table II).

If more than one structure would be assigned the same name using these rules, the structures are distinguished by letters placed at the ends of the names; e.g. the second species name would end with X, the third would end with Y and so on. When our initial computer experimentation established that distinctions between particular isomers were not important, the isomers were lumped under one name.

The reaction set is presented in Table III. The core of the acetylene pyrolysis model is based on the mechanism of Tanzawa and Gardiner[30] whose development entailed comparison with all of the available data. It was thus calibrated overall against the measured

TABLE III. REACTION MECHANISM.

	REACTIONS					REACTION CLASS	$\Delta H^{\circ}_{1700,kJ}$
(1)	C2H2	+ M	= H	+ C2H	+ M	0	505.9
(2)	C2H2	+ C2H2	= H	+ C4H3U		0	289.7
(3)	C2H2	+ H	= C2H3			0	-174.6
(4)	C2H2	+ C2H3	= H	+ C4H4		0	4.0
(5)	H	+ C4H3S	+ M	= C4H4	+ M	0	-426.8
(6)	H2	+ C2H	= C2H2	+ H		0	-57.2
(7)	C2H2	+ C2H	= H	+ C4H2		0	-63.5
(8)	C2H	+ C4H4	= C2H2	+ C4H3S		0	-79.1
(9)	C4H3S	+ M	= H	+ C4H2	+ M	0	186.3
(10)	C4H2	+ M	= H	+ C4H	+ M	0	508.0
(11)	C2H	+ C4H2	= H	+ C6H2		0	-61.4
(12)	C2H2	+ C4H	= H	+ C6H2		0	-63.5
(13)	C2H2	+ C6H	= H	+ C8H2		0	-63.5
(14)	C2H	+ C6H2	= H	+ C8H2		0	-61.4
(15)	C4H	+ C4H2	= H	+ C8H2		0	-61.4
(16)	C6H2	+ M	= H	+ C6H	+ M	0	508.0
(17)	C8H2	+ M	= H	+ C8H	+ M	0	508.0
(18)	H2	+ M	= H	+ H	+ M	0	448.7
(19)	H	+ C4H3U	+ M	= C4H4	+ M	0	-460.3
(20)	C4H3U	+ M	= H	+ C4H2	+ M	0	152.8
(21)	C2H	+ C4H4	= C2H2	+ C4H3U		0	-45.6
(22)	C2H2	+ C2H	= C4H3U			8	-216.2
(23)	H2	+ C4H3U	= H	+ C4H4		-2	-11.6
(24)	C2H2	+ C4H3U	= C6H5U			13	-221.1
(25)	C6H5U	= A1-				30	-202.3
(26)	C6H5U	= H	+ C6H4			-5	205.3
(27)	H	+ C6H5U	= C6H6			29	-460.3
(28)	H2	+ C6H5U	= H	+ C6H6		-2	-11.6
(29)	C2H	+ C6H5U	= C8H6			7	-521.7
(30)	C2H2	+ C6H5U	= C2H	+ C6H6		-4	45.6
(31)	C4H2	+ C4H3U	= C4H	+ C4H4		-4	47.7
(32)	C4H2	+ C4H3U	= C8H5SX			13	-252.5
(33)	C8H5SX	= A1C2H-				30	-149.1
(34)	C8H5SX	= H	+ C8H4			-5	238.8
(35)	H	+ C8H5SX	= C8H6			29	-426.8
(36)	H2	+ C8H5SX	= H	+ C8H6		-2	21.8
(37)	C2H2	+ C8H5SX	= C2H	+ C8H6		-4	79.1
(38)	H	+ C4H2	= H2	+ C4H		-1	59.3
(39)	H	+ C6H2	= H2	+ C6H		-1	59.3
(40)	H	+ C6H2	= C6H3S			5	-186.3
(41)	H	+ C8H2	= H2	+ C8H		-1	59.3
(42)	H	+ C8H2	= C8H3S			5	-186.3
(43)	C2H	+ C4H2	= C2H2	+ C4H		3	2.1
(44)	C2H	+ C6H2	= C2H2	+ C6H		3	2.1
(45)	C2H	+ C4H2	= C6H3S			8	-247.6
(46)	C2H	+ C6H2	= C8H3S			8	-247.6
(47)	C4H	+ C4H2	= C2H	+ C6H2		-10	-0.0
(48)	C4H	+ C6H2	= H	+ C10H2		9	-61.4
(49)	C4H	+ C4H2	= C8H3S			8	-247.6
(50)	C4H	+ C6H2	= C10H3S			8	-247.6
(51)	C4H2	+ C6H	= C2H	+ C8H2		-10	-0.0
(52)	C4H2	+ C6H	= H	+ C10H2		9	-61.4
(53)	C4H2	+ C6H	= C10H3S			8	-247.6
(54)	C6H	+ C6H2	= C4H	+ C8H2		-10	0.0
(55)	C6H	+ C6H2	= H	+ C12H2		9	-61.4
(56)	H	+ C6H3S	= C6H4			29	-426.8
(57)	H2	+ C6H3S	= H	+ C6H4		-2	21.8
(58)	C2H2	+ C6H3S	= C2H	+ C6H4		-4	79.1
(59)	C2H2	+ C6H3S	= H	+ C8H4		11	17.7
(60)	C4H2	+ C6H3S	= C4H	+ C6H4		-4	81.2
(61)	H	+ C8H3S	= C8H4			29	-426.8
(62)	H2	+ C8H3S	= H	+ C8H4		-2	21.8
(63)	C2H2	+ C8H3S	= C2H	+ C8H4		-4	79.1
(64)	H	+ C10H2	= C10H3S			5	-186.3

(65)	H2	+ C2H3	= H	+ C2H4	-2	-11.6
(66)	C2H2	+ C2H3	= C2H	+ C2H4	-4	45.6
(67)	H	+ C2H3	= C2H4		29	-460.3
(68)	C4H5U	= C2H2	+ C2H3		-13	221.1
(69)	C2H3	+ C4H2	= C6H5S		13	-232.7
(70)	C2H3	+ C4H2	= C2H	+ C4H4	12	67.5
(71)	C2H3	+ C4H2	= C2H4	+ C4H	-4	47.7
(72)	H2	+ C4H3S	= H	+ C4H4	-2	21.8
(73)	C2H2	+ C4H3S	= H	+ C6H4X	11	17.7
(74)	C4H2	+ C4H3S	= C4H	+ C4H4	-4	81.2
(75)	H	+ C4H4	= C4H5U		5	-225.1
(76)	C2H	+ C4H4	= C6H5S		8	-300.2
(77)	C6H6	= C2H3	+ C4H3U		-7	506.8
(78)	C6H5S	= ½	+ C6H4X		-5	238.8
(79)	H	+ C6H5S	= C6H6		29	-426.8
(80)	C2H	+ C6H5S	= C8H6		7	-488.2
(81)	H2	+ C6H5S	= H	+ C6H6	-2	21.8
(82)	C2H2	+ C6H5S	= C2H	+ C6H6	-4	79.1
(83)	C2H2	+ C6H5S	= H	+ C8H6	11	17.7
(84)	C8H5S	= H	+ C8H4		-5	238.8
(85)	H	+ C8H5S	= C8H6		29	-426.8
(86)	H2	+ C8H5S	= H	+ C8H6	-2	21.8
(87)	C2H2	+ C8H5S	= C2H	+ C8H6	-4	79.1
(88)	H	+ A1-	= A1		21	-470.8
(89)	A1	= H	+ C6H5U		22	673.0
(90)	C2H	+ A1-	= A1C2H		7	-512.4
(91)	A1C2H	= H	+ C8H5SX		22	619.8
(92)	H	+ A1C2H-	= A1C2H		21	-470.8
(93)	H2	+ A1C2H-	= H	+ A1C2H	-23	-22.1
(94)	C2H2	+ A1C2H-	= C2H	+ A1C2H	-24	35.2
(95)	C2H2	+ A1C2H-	= H	+ A1C2H)2X	-25	-6.5
(96)	H2	+ A1-	= H	+ A1	-23	-22.1
(97)	C2H2	+ A1-	= C2H	+ A1	-24	35.2
(98)	C2H2	+ A1-	= H	+ A1C2H	-25	-6.5
(99)	C4H2	+ A1-	= C4H	+ A1	-24	37.2
(100)	C4H2	+ A1-	= C2H	+ A1C2H	26	57.0
(101)	C4H2	+ A1-	= A1C4H2S		27	-181.6
(102)	H	+ A1C4H2S	= A1C4H3		29	-426.8
(103)	A1C4H3	= C4H3U	+ A1-		-7	455.7
(104)	H2	+ A1C4H2S	= H	+ A1C4H3	-2	21.8
(105)	C2H2	+ A1C4H2S	= C2H	+ A1C4H3	-4	79.1
(106)	C2H2	+ A1C4H2S	= H	+ A1C6H3	11	17.7
(107)	C4H2	+ A1C4H2S	= A1C8H4S		3	-219.0
(108)	A1C8H4S	= H	+ A2C2H)2X		20	44.2
(109)	H	+ A1C8H4S	= A1C8H5		29	-426.8
(110)	H2	+ A1C8H4S	= H	+ A1C8H5	-2	21.8
(111)	C2H2	+ A1C8H4S	= C2H	+ A1C8H5	-4	79.1
(112)	C2H2	+ A1C8H4S	= H	+ A1C10H5	11	17.7
(113)	C2H2	+ A1-	= A1C2H2U		27	-170.0
(114)	A1C2H2U	= H	+ A1C2H		-5	163.5
(115)	H	+ A1C2H2U	= A1C2H3		29	-460.3
(116)	H2	+ A1C2H2U	= H	+ A1C2H3	-2	-11.6
(117)	C2H	+ A1C2H2U	= A1C4H3		7	-501.9
(118)	C2H2	+ A1C2H2U	= A1C4H4U		13	-221.1
(119)	C4H2	+ A1C2H2U	= A1C6H4S		13	-232.7
(120)	A1C4H4U	= H	+ A2		20	-8.9
(121)	A1C4H4U	= H	+ A1C4H3		-5	225.1
(122)	H	+ A1C4H4U	= A1C4H5		29	-460.3
(123)	H2	+ A1C4H4U	= H	+ A1C4H5	-2	-11.6
(124)	C2H2	+ A1C4H4U	= C2H	+ A1C4H5	-4	45.6
(125)	C2H2	+ A1C4H4U	= H	+ A1C6H5	11	4.0
(126)	A1C6H4S	= H	+ A2C2H		20	24.5
(127)	A1C6H4S	= H	+ A1C6H3		-5	238.8
(128)	H	+ A1C6H4S	= A1C6H5		29	-426.8
(129)	H2	+ A1C6H4S	= H	+ A1C6H5	-2	21.8

(130)	C2H2	+ A1C6H4S	= C2H	+ A1C6H5		-4	79.1
(131)	C2H2	+ A1C6H4S	= H	+ A1C8H5		11	17.7
(132)	C2H2	+ A1C4H2S	= A1C6H4U			13	-135.1
(133)	A1C6H4U	= H	+ A2C2H			20	-61.5
(134)	A1C6H4U	= H	+ A1C6H3			-5	152.8
(135)	H	+ A1C6H4U	= A1C6H5			29	-512.8
(136)	H2	+ A1C6H4U	= H	+ A1C6H5		-2	-64.2
(137)	C2H2	+ A1C6H4U	= C2H	+ A1C6H5		-4	-6.9
(138)	C2H2	+ A1C6H4U	= H	+ A1C8H5		11	-68.3
(139)	H	+ A2-	= A2			21	-470.8
(140)	H2	+ A2-	= H	+ A2		-23	-22.1
(141)	C2H	+ A2-	= A2C2H			7	-512.4
(142)	C2H2	+ A2-	= C2H	+ A2		-24	35.2
(143)	A1C2H	= H	+ A1C2H*			-21	470.8
(144)	H	+ A1C2H	= H2	+ A1C2H*		23	22.1
(145)	C2H	+ A1C2H	= C2H2	+ A1C2H*		24	-35.2
(146)	A1C2H*	= C8H5U				-30	182.5
(147)	H	+ C8H5U	= C8H6			29	-460.3
(148)	H2	+ C8H5U	= H	+ C8H6		-2	-11.6
(149)	C2H2	+ C8H5U	= C2H	+ C8H6		-4	45.6
(150)	C2H2	+ C8H5U	= H	+ C10H6		11	-15.8
(151)	C8H5U	= H	+ C8H4			-5	205.3
(152)	C8H5U	= C2H2	+ C6H3U			-13	221.1
(153)	H	+ C6H3U	= C6H4			29	-460.3
(154)	H2	+ C6H3U	= H	+ C6H4		-2	-11.6
(155)	C2H2	+ C6H3U	= C2H	+ C6H4		-4	45.6
(156)	C2H2	+ C6H3U	= H	+ C8H4		11	-15.8
(157)	C6H3U	= C2H	+ C4H2			-8	214.2
(158)	C2H2	+ A1C2H*	= A1C2HC2H2U			27	-170.0
(159)	C2H2	+ A1C2H*	= H	+ A1C2H)2		-25	-6.5
(160)	A1C2HC2H2U	= H	+ A1C2H)2			-5	163.5
(161)	A1C2HC2H2U	= A2-X				30	-223.5
(162)	H	+ A1C2HC2H2U	= A1C2HC2H3			29	-460.3
(163)	H2	+ A1C2HC2H2U	= H	+ A1C2HC2H3		-2	-11.6
(164)	C2H2	+ A1C2HC2H2U	= C2H	+ A1C2HC2H3		-4	45.6
(165)	H	+ A2-X	= A2			21	-470.8
(166)	H2	+ A2-X	= H	+ A2		-23	-22.1
(167)	C2H2	+ A2-X	= C2H	+ A2		-24	35.2
(168)	C2H	+ A2-X	= A2C2H			7	-512.4
(169)	C4H2	+ A1C2H*	= A1C2HC4H2S			27	-181.6
(170)	A1C2HC4H2S	= H	+ A1C2HC4H			-5	177.2
(171)	A1C2HC4H2S	= A2C2H-				30	-190.1
(172)	H	+ A1C2HC4H2S	= A1C2HC4H3			29	-426.8
(173)	H2	+ A1C2HC4H2S	= H	+ A1C2HC4H3		-2	21.8
(174)	C2H2	+ A1C2HC4H2S	= C2H	+ A1C2HC4H3		-4	79.1
(175)	H	+ A2C2H*X	= A2C2H			21	-470.8
(176)	H2	+ A2C2H*X	= H	+ A2C2H		-23	-22.1
(177)	C2H2	+ A2C2H*X	= C2H	+ A2C2H		-24	35.2
(178)	C2H2	+ A2C2H*X	= H	+ A2R5C2H		27	-134.2
(179)	H	+ A1	= R6%			19	-90.7
(180)	R6%	= C6H7U				-20	78.4
(181)	C2H2	+ A2-X	= H	+ A2C2H		-25	-6.5
(182)	C2H2	+ A2-	= H	+ A2C2H		-25	-6.5
(183)	C2H2	+ A2C2H*	= C2H	+ A2C2H		-24	35.2
(184)	H	+ A2C2H*	= A2C2H			21	-470.8
(185)	H2	+ A2C2H*	= H	+ A2C2H		-23	-22.1
(186)	C2H2	+ A2C2H*	= H	+ A2C2H)2		-25	-6.5
(187)	C2H2	+ A2C2H*	= A2C2HC2H2U			27	-170.0
(188)	A2C2HC2H2U	= H	+ A2C2H)2			-5	163.5
(189)	A2C2HC2H2U	= A3-				30	-232.7
(190)	H	+ A3-	= A3			21	-470.8
(191)	H2	+ A3-	= H	+ A3		-23	-22.1
(192)	C2H2	+ A3-	= C2H	+ A3		-24	35.2
(193)	C2H2	+ A3-	= H	+ A3C2H		-25	-6.5
(194)	C2H2	+ A3-	= A3C2H2U			27	-170.0

(195) A3C2H2U	= H	+ A4			20	-50.6
(196) A2-	= A1C4H3-				-30	229.1
(197) H	+ A1C4H3-	= A1C4H3			21	-465.8
(198) H2	+ A1C4H3-	= H	+ A1C4H3		-23	-17.2
(199) C2H2	+ A1C4H3-	= C2H	+ A1C4H3		-24	40.1
(200) C2H2	+ A1C4H3-	= H	+ A1C2HC4H3		-25	-1.6
(201) A1C4H3-	= C10H7U				-30	125.9
(202) C10H7U	= H	+ C10H6			-5	205.3
(203) C10H7U	= C2H2	+ C8H5U			-13	221.1
(204) H	+ A4-	= A4			21	-470.8
(205) H2	+ A4-	= H	+ A4		-23	-22.1
(206) C2H2	+ A4-	= C2H	+ A4		-24	35.2
(207) C2H2	+ A4-	= H	+ A4C2H		-25	-6.5
(208) H	+ A4C2H*	= A4C2H			21	-470.8
(209) H2	+ A4C2H*	= H	+ A4C2H		-23	-22.1
(210) C2H2	+ A4C2H*	= C2H	+ A4C2H		-24	35.2
(211) C2H2	+ A4C2H*	= H	+ A4C2H)2		-25	-6.5
(212) C2H2	+ A4C2H*	= A4C2HC2H2U			27	-170.0
(213) A4C2HC2H2U	= H	+ A4C2H)2			-5	163.5
(214) A4C2HC2H2U	= A5-				30	-241.9
(215) H	+ A5-	= A5			21	-470.8
(216) H2	+ A5-	= H	+ A5		-23	-22.1
(217) C2H2	+ A5-	= C2H	+ A5		-24	35.2
(218) C2H2	+ A5-	= H	+ A5C2H		-25	-6.5
(219) C2H2	+ A5-	= H	+ A6		27	-220.6
(220) H	+ A6-	= A6			21	-470.8
(221) H2	+ A6-	= H	+ A6		-23	-22.1
(222) C2H2	+ A6-	= H	+ A6C2H		-25	-6.5
(223) C2H2	+ A6-	= C2H	+ A6		-24	35.2
(224) C2H2	+ A6-	= H	+ A7		27	-220.6
(225) H2	+ A3C2H*	= H	+ A3C2H		-23	-22.1
(226) H	+ A3C2H*	= A3C2H			21	-470.8
(227) C2H2	+ A3C2H*	= C2H	+ A3C2H		-24	35.2
(228) C2H2	+ A3C2H*	= H	+ A3C2H)2		-25	-6.5
(229) C2H2	+ A3C2H*	= A3C2HC2H2U			27	-170.0
(230) A3C2HC2H2U	= H	+ A3C2H)2			-5	163.5
(231) A3C2HC2H2U	= B4-				30	-203.4
(232) H2	+ B4-	= H	+ B4		-23	-22.1
(233) H	+ B4-	= B4			21	-470.8
(234) C2H2	+ B4-	= C2H	+ B4		-24	35.2
(235) C2H2	+ B4-	= H	+ B4C2H		-25	-6.5
(236) H2	+ B4C2H*	= H	+ B4C2H		-23	-22.1
(237) H	+ B4C2H*	= B4C2H			21	-470.8
(238) C2H2	+ B4C2H*	= C2H	+ B4C2H		-24	35.2
(239) C2H2	+ B4C2H*	= H	+ B4C2H)2		-25	47.9
(240) C2H2	+ B4C2H*	= B4C2HC2H2U			27	-115.6
(241) B4C2HC2H2U	= H	+ B4C2H)2			-5	163.5
(242) B4C2HC2H2U	= B5-				30	-274.5
(243) B5-	= H	+ A6			27	-83.0
(244) H	+ B5-	= B5			21	-428.9
(245) H2	+ B5-	= H	+ B5		-23	19.7
(246) C2H2	+ B5-	= C2H	+ B5		-24	77.0
(247) A2C2H*	= A1C2H*				31	
(248) A4C2H*	= A3-				31	
(249) H	+ A7-	= A7			21	-470.8
(250) H2	+ A7-	= H	+ A7		-23	-22.1
(251) C2H2	+ A7-	= C2H	+ A7		-24	35.2
(252) C2H2	+ A7-	= H	+ A7C2H		-25	-6.5
(253) H	+ A7C2H*	= A7C2H			21	-470.8
(254) H2	+ A7C2H*	= H	+ A7C2H		-23	-22.1
(255) C2H2	+ A7C2H*	= C2H	+ A7C2H		-24	35.2
(256) C2H2	+ A7C2H*	= H	+ A7C2H)2		-25	-6.5
(257) C2H2	+ A7C2H*	= A7C2HC2H2U			27	-170.0
(258) A7C2HC2H2U	= H	+ A7C2H)2			-5	163.5
(259) A7C2HC2H2U	= A8-				30	-241.9

(260)	H	+ A8-	= A8		21	-470.8
(261)	H2	+ A8-	= H	+ A8	-23	-22.1
(262)	C2H2	+ A8-	= C2H	+ A8	-24	35.2
(263)	C2H2	+ A8-	= H	+ A8C2H	-25	-6.5
(264)	C2H2	+ A8-	= H	+ A9	27	-220.6
(265)	H	+ A9-	= A9		21	-470.8
(266)	H2	+ A9-	= H	+ A9	-23	-22.1
(267)	C2H2	+ A9-	= H	+ A9C2H	-25	-6.5
(268)	C2H2	+ A9-	= C2H	+ A9	-24	35.2
(269)	C2H2	+ A9-	= H	+ A7	27	-220.6
(270)	C2H2	+ A2-X	= H	+ A2R5	27	-134.2
(271)	H	+ A2R5-	= A2R5		21	-470.8
(272)	C2H2	+ A2R5-	= C2H	+ A2R5	-24	35.2
(273)	H2	+ A2R5-	= H	+ A2R5	-23	-22.1
(274)	C2H2	+ A2R5-	= H	+ A2R5C2H	-25	-6.5
(275)	H	+ A2R5C2H	= H2	+ A2R5C2H*	23	22.1
(276)	H	+ A2R5C2H*	= A2R5C2H		21	-470.8
(277)	C2H2	+ A2R5C2H*	= C2H	+ A2R5C2H	-24	35.2
(278)	C2H2	+ A2R5C2H*	= H	+ A2R5C2H)2	-25	-6.5
(279)	C2H2	+ A2R5C2H*	= A2R5C2HC2H2U		27	-170.0
(280)	A2R5C2HC2H2U	= H	+ A2R5C2H)2		-5	163.5
(281)	A2R5C2HC2H2U	= A3R5-			30	-232.7
(282)	H	+ A3R5-	= A3R5		21	-470.8
(283)	H2	+ A3R5-	= H	+ A3R5	-23	-22.1
(284)	C2H2	+ A3R5-	= C2H	+ A3R5	-24	35.2
(285)	C2H2	+ A3R5-	= A3R5C2H2U		27	-170.0
(286)	A3R5C2H2U	= H	+ A3R5C2H		-5	163.5
(287)	A3R5C2H2U	= H	+ A4		20	
(288)	C2H2	+ C6H5U	= H	+ C8H6	11	-15.8
(289)	C2H	+ C8H5SX	= C10H6		7	-488.2
(290)	C2H2	+ C8H5SX	= H	+ C10H6	11	17.7
(291)	C4H	+ C6H	= C10H2		7	-569.4
(292)	C6H	+ C6H	= C12H2		7	-569.4
(293)	C6H	+ C6H2	= C12H3S		8	-247.6
(294)	C4H	+ C6H3S	= C10H4		7	-488.2
(295)	C2H3	+ C6H3S	= C8H6		7	-473.3
(296)	C4H3S	+ C6H3S	= C10H6		7	-459.6
(297)	C6H3S	+ C6H3S	= C12H6		7	-459.6
(298)	C6H2	+ C6H3S	= C2H	+ C10H4	12	81.2
(299)	C6H2	+ C6H3S	= C12H5S		8	-219.0
(300)	C2H	+ C8H3S	= C10H4		7	-488.2
(301)	C2H3	+ C8H3S	= C10H6		7	-473.3
(302)	C4H3S	+ C8H3S	= C12H6		7	-459.6
(303)	C6H3S	+ C8H3S	= C14H6		7	-459.6
(304)	C2H2	+ C8H3S	= H	+ C10H4	11	17.7
(305)	C4H2	+ C8H3S	= C2H	+ C10H4	12	81.2
(306)	C4H2	+ C8H3S	= C12H5S		13	-219.0
(307)	C6H2	+ C8H3S	= C4H	+ C10H4	12	81.2
(308)	C6H2	+ C8H3S	= C2H	+ C12H4	12	81.2
(309)	C6H2	+ C8H3S	= C14H5S		13	-219.0
(310)	H	+ C10H3S	= C10H4		29	-426.8
(311)	H2	+ C10H3S	= H	+ C10H4	-2	21.8
(312)	C2H	+ C10H3S	= C12H4		7	-488.2
(313)	C2H2	+ C10H3S	= C2H	+ C10H4	-4	79.1
(314)	C2H2	+ C10H3S	= H	+ C12H4	11	17.7
(315)	H	+ C12H2	= C12H3S		5	-186.3
(316)	C2H	+ C12H3S	= C14H4		7	-488.2
(317)	H	+ C12H3S	= C12H4		29	-426.8
(318)	H2	+ C12H3S	= H	+ C12H4	-2	21.8
(319)	C2H2	+ C12H3S	= C2H	+ C12H4	-4	79.1
(320)	C2H2	+ C12H3S	= H	+ C14H4	11	17.7
(321)	C10H5S	= H	+ C10H4		-5	238.8
(322)	H	+ C10H5S	= C10H6		29	-426.8
(323)	C2H	+ C10H5S	= C12H6		7	-488.2
(324)	H2	+ C10H5S	= H	+ C10H6	-2	21.8

(325)	C2H2	+ C10H5S	= C2H	+ C10H6		-4	79.1
(326)	C2H2	+ C10H5S	= H	+ C12H6		11	17.7
(327)	C12H5S	= H	+ C12H4			-5	238.8
(328)	H	+ C12H5S	= C12H6			29	-426.8
(329)	C2H	+ C12H5S	= C14H6			7	-488.2
(330)	H2	+ C12H5S	= H	+ C12H6		-2	21.8
(331)	C2H2	+ C12H5S	= C2H	+ C12H6		-4	79.1
(332)	C6H7U	= H	+ A1			20	12.3
(333)	C2H	+ C8H7SX	= C10H8			7	-488.2
(334)	C2H2	+ C8H7SX	= H	+ C10H8		11	17.7
(335)	C2H3	+ C8H4	= C10H7S			13	-285.2
(336)	C4H3S	+ C6H	= C10H4			7	-488.2
(337)	C4H3S	+ C6H2	= H	+ C10H4		11	19.8
(338)	C4H3S	+ C6H2	= C10H5S			13	-219.0
(339)	C4H3S	+ C6H4	= C10H7S			13	-271.5
(340)	C4H3S	+ C6H4X	= C10H7S			13	-271.5
(341)	C4H3S	+ C8H4	= C12H7S			13	-271.5
(342)	C4H4	+ C6H3S	= C10H7S			13	-271.5
(343)	C4H4	+ C8H3S	= C12H7S			13	-271.5
(344)	C4H4	+ C8H3S	= C2H3	+ C10H4		12	13.7
(345)	C6H7S	= H	+ H	+ A1-		18	516.6
(346)	C8H8	= H	+ H	+ A1C2H		18	472.6
(347)	C4H2	+ C6H7S	= C10H9S			13	-199.2
(348)	C10H9S	= H	+ C10H8			-5	238.8
(349)	C8H7S	= H	+ H	+ A1C2H-		18	516.5
(350)	C4H2	+ C8H7S	= C12H9S			13	-219.0
(351)	C12H9S	= H	+ C12H8X			-5	238.8
(352)	H	+ C12H9S	= C12H10			29	-426.8
(353)	H2	+ C12H9S	= H	+ C12H10		-2	21.8
(354)	C2H2	+ C12H9S	= C2H	+ C12H10		-4	79.1
(355)	C12H10	= C4H5U	+ C8H5S			-7	473.3
(356)	C10H7S	= H	+ C10H6			-5	238.8
(357)	H	+ C10H7S	= C10H8			29	-426.8
(358)	C10H8	= C4H5U	+ C6H3S			-7	473.3
(359)	H2	+ C10H7S	= H	+ C10H8		-2	21.8
(360)	C2H2	+ C10H7S	= C2H	+ C10H8		-4	79.1
(361)	C4H2	+ C10H7S	= C4H	+ C10H8		-4	81.2
(362)	C4H2	+ C10H7S	= C14H9S			13	-219.0
(363)	C14H9S	= H	+ C14H8X			-5	238.8
(364)	H	+ C14H9S	= C14H10			29	-426.8
(365)	H2	+ C14H9S	= H	+ C14H10		-2	21.8
(366)	C2H2	+ C14H9S	= C2H	+ C14H10		-4	79.1
(367)	C4H2	+ C6H5S	= C10H7SX			13	-219.0
(368)	C10H7SX	= H	+ C10H6			-5	238.8
(369)	H	+ C10H7SX	= C10H8			29	-426.8
(370)	H2	+ C10H7SX	= H	+ C10H8		-2	21.8
(371)	C2H2	+ C10H7SX	= C2H	+ C10H8		-4	79.1
(372)	C2H2	+ C10H7SX	= H	+ C12H8		11	17.7
(373)	C6H2	+ C6H5S	= C12H7SX			13	-219.0
(374)	C12H7SX	= H	+ C12H6			-5	238.8
(375)	H	+ C12H7SX	= C12H8X			29	-426.8
(376)	H2	+ C12H7SX	= H	+ C12H8X		-2	21.8
(377)	C2H2	+ C12H7SX	= C2H	+ C12H8X		-4	79.1
(378)	C2H2	+ C12H8X	= H	+ C14H8		11	203.6
(379)	C2H2	+ C8H5S	= H	+ C10H6		11	17.7
(380)	C2H2	+ C8H5SY	= H	+ C10H6		11	17.7
(381)	C2H2	+ C8H5SZ	= H	+ C10H6		11	17.7
(382)	C4H2	+ C8H5S	= C2H	+ C10H6		12	81.2
(383)	C4H2	+ C8H5SY	= C2H	+ C10H6		12	81.2
(384)	C4H2	+ C8H5SZ	= C2H	+ C10H6		12	81.2
(385)	C4H2	+ C8H5SY	= C12H7SY			13	-219.0
(386)	C4H2	+ C8H5SZ	= C12H7SZ			13	-219.0
(387)	C12H7SY	= C4H2	+ C8H5S			-13	219.0
(388)	C12H7SZ	= C4H2	+ C8H5S			-13	219.0
(389)	C12H7SY	= H	+ C12H6			-5	238.8

(390)	C12H7SZ	= H	+ C12H6		-5	238.8
(391)	H	+ C12H7SY	= C12H8X		29	-426.8
(392)	H	+ C12H7SZ	= C12H8X		29	-426.8
(393)	C12H8	= C6H3U	+ C6H5S		-7	493.1
(394)	C12H8X	= C4H3U	+ C8H5SY		-7	493.1
(395)	H2	+ C12H7SY	= H	+ C12H8X	-2	21.8
(396)	H2	+ C12H7SZ	= H	+ C12H8X	-2	21.8
(397)	C2H2	+ C12H7SY	= C2H	+ C12H8X	-4	79.1
(398)	C2H2	+ C12H7SZ	= C2H	+ C12H8X	-4	79.1
(399)	C2H2	+ C12H7SY	= H	+ C14H8	11	17.7
(400)	C2H2	+ C12H7SZ	= H	+ C14H8	11	17.7
(401)	C6H2	+ C8H5S	= C4H	+ C10H6	12	81.2
(402)	C6H2	+ C8H5SY	= C4H	+ C10H6	12	81.2
(403)	C6H2	+ C8H5SY	= C14H7S		13	-219.0
(404)	C14H7S	= H	+ C14H6		-5	238.8
(405)	C14H7S	= C6H2	+ C8H5S		-13	219.0
(406)	H	+ C14H7S	= C14H8X		29	-426.8
(407)	C14H8	= C4H3S	+ C10H5S		-7	459.6
(408)	C2H	+ C14H7S	= C16H8		7	-488.2
(409)	H2	+ C14H7S	= H	+ C14H8X	-2	21.8
(410)	C2H2	+ C14H7S	= C2H	+ C14H8X	-4	79.1
(411)	C2H2	+ C14H7S	= H	+ C16H8	11	17.7
(412)	C4H2	+ C10H5S	= C4H	+ C10H6	-4	81.2
(413)	C4H2	+ C10H5S	= C2H	+ C12H6	12	81.2
(414)	C4H2	+ C10H5S	= C14H7SX		13	-219.0
(415)	C14H7SX	= H	+ C14H6		-5	238.8
(416)	C14H7SX	= C6H2	+ C8H5S		-13	219.0
(417)	H	+ C14H7SX	= C14H8X		29	-426.8
(418)	C2H	+ C14H7SX	= C16H8		7	-488.2
(419)	H2	+ C14H7SX	= H	+ C14H8X	-2	21.8
(420)	C2H2	+ C14H7SX	= C2H	+ C14H8X	-4	79.1
(421)	C2H2	+ C14H7SX	= H	+ C16H8	11	17.7
(422)	C14H8X	= C6H3S	+ C8H5S		-7	459.6
(423)	A1C8H5	= H	+ H	+ A2C2H)2	18	471.1
(424)	H	+ C2H3	= C2H2	+ H2	32	-274.0
(425)	C2H2	+ C4H5U	= C6H7U		13	-221.1
(426)	C2H	+ C6H7U	= C2H2	+ C6H6	32	-280.8
(427)	H	+ C6H7U	= H2	+ C6H6	32	-223.6
(428)	H	+ C6H6	= C6H7U		5	-225.1
(429)	H	+ C4H3U	= H2	+ C4H2	32	-295.9
(430)	H	+ C4H3S	= H2	+ C4H2	32	-262.4
(431)	H	+ C6H3U	= H2	+ C6H2	32	-295.9
(432)	H	+ C6H5U	= H2	+ C6H4	32	-243.4
(433)	H	+ C4H5U	= H2	+ C4H4	32	-223.6
(434)	H	+ C6H7U	= C6H8		32	-460.3
(435)	H2	+ C6H7U	= H	+ C6H8	-2	-11.6
(436)	C2H2	+ C6H7U	= C2H	+ C6H8	-4	45.6
(437)	C2H	+ C4H5U	= C6H6		7	-501.9
(438)	H	+ C8H5U	= H2	+ C8H4	32	-243.4
(439)	C4H3U	+ C6H3U	= C4H2	+ C6H4X	32	-307.5
(440)	C2H	+ C2H	= C4H2		7	-569.4
(441)	C2H	+ C4H	= C6H2		7	-569.4
(442)	C2H	+ C6H	= C8H2		7	-569.4
(443)	C4H	+ C4H	= C8H2		7	-569.4
(444)	C2H	+ C6H3S	= C8H4		7	-488.2
(445)	C4H2	+ C6H3S	= C2H	+ C8H4	12	81.2
(446)	C4H2	+ C6H3S	= C10H5S		13	-219.0
(447)	C6H2	+ C6H3S	= C6H	+ C6H4	-4	81.2
(448)	C6H2	+ C6H3S	= C4H	+ C8H4	12	81.2
(449)	C4H2	+ C8H3S	= C4H	+ C8H4	-4	81.2
(450)	C6H2	+ C8H3S	= C6H	+ C8H4	-4	81.2
(451)	C2H3	+ C2H4	= H	+ C4H6	16	-46.4
(452)	C2H	+ C2H3	= C4H4		7	-501.9
(453)	C2H3	+ C4H	= C6H4X		7	-501.9
(454)	C2H3	+ C6H	= C8H4		7	-501.9

(455)	C2H3	+ C2H3	= C4H6		7	-506.8
(456)	C4H6	= H	+ C4H5U		-29	460.3
(457)	C4H6	= H	+ C4H5S		-29	426.8
(458)	H	+ C4H6	= H2	+ C4H5U	2	11.6
(459)	C2H2	+ C4H5U	= C2H	+ C4H6	-4	45.6
(460)	C2H2	+ C4H5S	= C2H	+ C4H6	-4	79.1
(461)	C2H	+ C4H5S	= C6H6		7	-468.5
(462)	C2H	+ C6H7U	= C8H8		7	-501.9
(463)	C2H2	+ C6H7U	= H	+ C8H8	11	4.0
(464)	C4H2	+ C4H5U	= C4H	+ C4H6	-4	47.7
(465)	C4H2	+ C4H5U	= C8H7SX		13	-232.7
(466)	C8H7SX	= H	+ A1C2H		20	45.8
(467)	H	+ C8H7SX	= C8H8		29	-426.8
(468)	H2	+ C8H7SX	= H	+ C8H8	-2	21.8
(469)	C2H2	+ C8H7SX	= C2H	+ C8H8	-4	79.1
(470)	H	+ C4H6	= H2	+ C4H5S	2	-21.8
(471)	C2H3	+ C6H2	= C8H5SZ		7	-232.7
(472)	C2H3	+ C6H2	= C2H	+ C6H4X	12	67.5
(473)	C2H3	+ C6H2	= C4H	+ C4H4	12	67.5
(474)	C2H3	+ C6H2	= C2H4	+ C6H	-4	47.7
(475)	C2H3	+ C4H3S	= C6H6		7	-473.3
(476)	C2H3	+ C4H4	= C6H7S		13	-305.0
(477)	C2H3	+ C4H4	= C2H	+ C4H6	14	-4.8
(478)	C2H3	+ C4H4	= H	+ C6H6	16	-46.4
(479)	C2H3	+ C4H4	= C2H4	+ C4H3S	15	-33.5
(480)	C2H3	+ C6H4	= C8H7S		13	-285.2
(481)	C2H3	+ C6H4X	= C8H7S		13	-285.2
(482)	C2H3	+ C8H4	= C4H4	+ C6H3S	11	-13.7
(483)	C2H	+ C4H3S	= C6H4X		7	-488.2
(484)	C4H	+ C4H3S	= C8H4		7	-488.2
(485)	C4H2	+ C4H3S	= C8H5SY		13	-219.0
(486)	C4H2	+ C4H3S	= C2H	+ C6H4X	12	81.2
(487)	C4H3S	+ C6H2	= C4H4	+ C6H	-4	81.2
(488)	C4H3S	+ C6H2	= C4H	+ C6H4X	12	81.2
(489)	C4H3S	+ C4H3S	= C8H6		7	-459.6
(490)	C4H3S	+ C4H4	= C8H7S		13	-271.5
(491)	C4H3S	+ C8H4	= C6H3S	+ C6H4X	12	-0.0
(492)	H	+ C4H4	= C4H5S		5	-258.5
(493)	C2H	+ C2H4	= H	+ C4H4	17	-41.6
(494)	C4H	+ C4H4	= C8H5S		8	-300.2
(495)	C6H7S	= H	+ C6H6		-5	258.5
(496)	H	+ C6H6	= C2H4	+ C4H3S	-16	13.0
(497)	H	+ C6H7S	= C6H8		29	-426.8
(498)	C2H	+ C6H7S	= C8H8		7	-468.5
(499)	C8H8	= C2H3	+ C6H5S		-7	473.3
(500)	H2	+ C6H7S	= H	+ C6H8	-2	21.8
(501)	H	+ C6H8	= C2H3	+ C4H6	-16	46.4
(502)	C2H2	+ C6H7S	= C2H	+ C6H8	-4	79.1
(503)	C2H2	+ C6H7S	= H	+ C8H8	11	37.5
(504)	C4H2	+ C6H7S	= C4H	+ C6H8	-4	81.2
(505)	C4H2	+ C6H7S	= C2H	+ C8H8	12	100.9
(506)	C8H7S	= H	+ C8H6		-5	238.8
(507)	H	+ C8H7S	= C8H8		29	-426.8
(508)	C8H8	= C2H3	+ C6H5U		-7	506.8
(509)	H2	+ C8H7S	= H	+ C8H8	-2	21.8
(510)	C2H2	+ C8H7S	= C2H	+ C8H8	-4	79.1
(511)	C4H2	+ C8H7S	= C4H	+ C8H8	-4	81.2
(512)	C6H5U	= H	+ C6H4X		-5	205.3
(513)	C4H2	+ C6H5S	= C4H	+ C6H6	-4	81.2
(514)	C4H2	+ C6H5S	= C2H	+ C8H6	12	81.2
(515)	C6H2	+ C6H5S	= C6H	+ C6H6	-4	81.2
(516)	C6H2	+ C6H5S	= C4H	+ C8H6	12	81.2
(517)	C8H5SY	= H	+ C8H4		-5	238.8
(518)	C8H5SZ	= H	+ C8H4		-5	238.8
(519)	H	+ C8H5SY	= C8H6		29	-426.8

(520)	H	+ C8H5SZ	= C8H6		29	-426.8
(521)	C2H	+ C8H5S	= C10H6		7	-488.2
(522)	C2H	+ C8H5SY	= C10H6		7	-488.2
(523)	C2H	+ C8H5SZ	= C10H6		7	-488.2
(524)	H2	+ C8H5SY	= H	+ C8H6	-2	21.8
(525)	H2	+ C8H5SZ	= H	+ C8H6	-2	21.8
(526)	C2H2	+ C8H5SY	= C2H	+ C8H6	-4	79.1
(527)	C2H2	+ C8H5SZ	= C2H	+ C8H6	-4	79.1
(528)	C4H2	+ C8H5S	= C4H	+ C8H6	-4	81.2
(529)	C4H2	+ C8H5SY	= C4H	+ C8H6	-4	81.2
(530)	C4H2	+ C8H5SZ	= C4H	+ C8H6	-4	81.2
(531)	C6H2	+ C8H5S	= C6H	+ C8H6	-4	81.2
(532)	C6H2	+ C8H5SY	= C6H	+ C8H6	-4	81.2
(533)	C6H2	+ A1-	= C6H	+ A1	-24	37.2
(534)	C6H2	+ A1-	= C4H	+ A1C2H	26	57.0
(535)	C4H2	+ A1C4H2S	= C4H	+ A1C4H3	-4	81.2
(536)	C4H2	+ A1C4H2S	= C2H	+ A1C6H3	12	81.2
(537)	A1C6H3	= C2H	+ A1C4H2S		-7	488.2
(538)	C6H2	+ A1C4H2S	= C6H	+ A1C4H3	-4	81.2
(539)	C6H2	+ A1C4H2S	= C4H	+ A1C6H3	12	81.2
(540)	A1C8H5	= C2H	+ A1C6H4U		-7	574.2
(541)	C4H2	+ A1C8H4S	= C4H	+ A1C8H5	-4	81.2
(542)	C4H2	+ A1C8H4S	= C2H	+ A1C10H5	12	81.2
(543)	C4H2	+ A1C8H4S	= A1C12H6S		13	-719.0
(544)	C6H2	+ A1C8H4S	= C6H	+ A1C8H5	-4	81.2
(545)	C6H2	+ A1C8H4S	= C4H	+ A1C10H5	12	81.2
(546)	C6H4	+ A1C8H4S	= C6H3S	+ A1C8H5	-15	-0.0
(547)	C4H4	+ A1-	= A1C4H4S		27	-253.9
(548)	A1C4H4S	= H	+ H	+ A2-	18	495.3
(549)	H	+ A1C4H4S	= A1C4H5		29	-426.8
(550)	A1C4H5	= C2H3	+ A1C2H2U		-7	506.8
(551)	H2	+ A1C4H4S	= H	+ A1C4H5	-2	21.8
(552)	C2H2	+ A1C4H4S	= C2H	+ A1C4H5	-4	79.1
(553)	C2H2	+ A1C4H4S	= H	+ A1C6H5	11	37.5
(554)	C4H2	+ A1C4H4S	= C4H	+ A1C4H5	-4	81.2
(555)	C4H2	+ A1C4H4S	= C2H	+ A1C6H5	12	100.9
(556)	C6H4	+ A1-	= C6H3S	+ A1	33	-43.9
(557)	C6H4X	+ A1-	= C4H3S	+ A1C2H	26	-24.2
(558)	C6H4	+ A1-	= A1C6H4SX		27	-234.1
(559)	A1C6H4SX	= H	+ H	+ A2C2H-	18	495.3
(560)	H	+ A1C6H4SX	= A1C6H5		29	-426.8
(561)	A1C6H5	= C2H	+ A1C4H4U		-7	501.9
(562)	A1C6H5	= H	+ H	+ A2C2H	18	451.3
(563)	H2	+ A1C6H4SX	= H	+ A1C6H5	-2	21.8
(564)	C2H2	+ A1C6H4SX	= C2H	+ A1C6H5	-4	79.1
(565)	C2H2	+ A1C6H4SX	= H	+ A1C8H5	11	17.7
(566)	C4H2	+ A1C6H4SX	= C4H	+ A1C6H5	-4	81.2
(567)	C4H2	+ A1C6H4S	= C4H	+ A1C6H5	-4	81.2
(568)	C4H2	+ A1C6H4SX	= C2H	+ A1C8H5	12	81.2
(569)	C4H2	+ A1C6H4S	= C2H	+ A1C8H5	12	81.2
(570)	C6H4	+ A1C6H4S	= C6H3S	+ A1C6H5	-15	-0.0
(571)	C6H4	+ A1C6H4SX	= C6H3S	+ A1C6H5	-15	-0.0
(572)	C6H4	+ A1C6H4SX	= C4H3U	+ A1C8H5	12	33.5
(573)	C6H4	+ A1C6H4S	= C4H3U	+ A1C8H5	12	33.5
(574)	C4H2	+ A1C2H2U	= C4H	+ A1C2H3	-4	47.7
(575)	C2H	+ A1C6H4S	= A1C8H5		7	-488.2
(576)	C2H	+ C8H5U	= C10H6		7	-521.7
(577)	C2H	+ C6H3U	= C8H4		7	-521.7
(578)	C6H3U	= H	+ C6H2		-5	152.8
(579)	C2H	+ A1C2HC2H2U	= A1C2HC4H3		7	-501.9
(580)	C2H2	+ A2-X	= A2R5		27	-375.1
(581)	C10H9S	= H	+ A1C2HC2H3X		20	107.3
(582)	C10H8	= H	+ H	+ A1C2H)2X	18	492.3
(583)	C10H8	= H	+ H	+ A1C2H)2	18	492.3
(584)	C12H9S	= H	+ A1C2HC4H3X		20	127.1

(585) C12H8X	= H	+ H	+ A1C2HC4HX	18	492.3
(586) C12H8X	= H	+ H	+ A1C2H)3	18	512.1
(587) C12H10	= H	+ H	+ A1C2HC4H3X	18	553.9
(588) C10H7S	= H	+ H	+ A1C2H)2-	18	536.3
(589) C14H10	= C6H5U	+ C8H5S		-7	493.1
(590) C14H10	= H	+ H	+ A1C2H)2C4H3	18	573.7
(591) C14H9S	= H	+ A1C2H)2C4H3		20	146.8
(592) C10H7SX	= H	+ A1C2H)2X		20	65.5
(593) C12H7SX	= H	+ A1C2HC4HX		20	65.5
(594) C12H7SY	= H	+ A1C2H)3		20	85.2
(595) C12H7SZ	= H	+ A1C2HC4HX		20	65.5
(596) C14H8X	= H	+ H	+ A1C2H)4	18	531.8
(597) C14H8X	= H	+ H	+ A1C2H)2C4H	18	512.1
(598) C14H7S	= H	+ A1C2H)2C4H		20	85.2
(599) C14H7SX	= H	+ A1C2H)4		20	105.0
(600) C6H2	+ A1-	= A1C6H2S		27	-181.6
(601) C6H2	+ A1C4H2S	= A1C10H4S		13	-219.0
(602) H	+ A1C10H4S	= A1C10H5		29	-426.8
(603) H2	+ A1C10H4S	= H	+ A1C10H5	-2	21.8
(604) C2H2	+ A1C10H4S	= C2H	+ A1C10H5	-4	79.1
(605) C6H4	+ A1C4H2S	= A1C10H6S		13	-271.5
(606) C6H2	+ A1C8H4S	= A1C14H6S		13	-219.0
(607) A1C12H6S	= A1C2H)3	+ A1-		20	80.6
(608) C4H2	+ A1C4H4S	= A1C8H6S		13	-199.2
(609) C6H4	+ A1C4H4S	= A1C10H8S		13	-251.7
(610) C4H2	+ A1C6H4SX	= A1C10H6S		13	-219.0
(611) C6H4	+ A1C6H4SX	= A1C12H8S		13	-271.5
(612) C6H8	= H	+ R6%		18	381.9
(613) C2H3	+ C6H4X	= C4H3S	+ C4H4	12	-13.7
(614) C2H3	+ C6H4	= C4H3U	+ C4H4	12	19.8
(615) C4H2	+ C4H3U	= C2H	+ C6H4	12	47.7
(616) H	+ A2C2H	= H2	+ A2C2H-	23	22.1
(617) C2H	+ A2C2H	= C2H2	+ A2C2H-	24	-35.2
(618) A2C2H	= H	+ A2C2H-		-21	470.8
(619) H	+ A2C2H)2X	= C2H2	+ A2C2H-	25	6.5

chain and non-chain reaction rates. Their mechanism was subsequently extended to higher temperatures and also found to be suitable for describing ethylene pyrolysis[31]. In our work we distinguish between the isomers of the C_4H_3 radical, namely $H-C\equiv C-\dot{C}=CH_2$ and $H-C\equiv C-CH=\dot{C}H$; thus, the product of the reaction $C_2H_2 + C_2H_2 = C_4H_3 + H$ was assumed to be the latter, in line with the theoretical study of Dewar and co-workers[32]. The rest of the mechanism was generated according to physical organic chemistry principles to comprise the likely radical and atom reactions (no migrations of hydrogen atoms or complex isomerizations were included) that could lead eventually to cyclization and growth of aromatics.

The rate coefficients for reactions 1-18 were used exactly as given in Table II of Ref. 24. Rate coefficients for reactions 19, 20 and 21 were chosen to equal those of reactions 5, 9 and 8, respectively. For the purpose of assigning rate coefficient expressions the reactions were grouped into classes as shown in Table IV. The rate coefficient expression chosen for a prototype reaction was assigned to the rest of the class without change. We assume thereby that a decrease in reaction rate due to increasing mass is offset by growing reaction-path degeneracy. To assign rate coefficients for classes where no experimental data are available, the viewpoint was adopted that reasonable upper limits based on collision theory would be preferable to transition state theory estimates based on assumed transition structure properties. The values of the rate coefficients were limited to 2×10^{13} $cm^3 mol\ s^{-1}$ for bimolecular reactions of organic species and to 1×10^{14} $cm^3 mol\ s^{-1}$ if hydrogen atom is a reactant. The principle of detailed balancing was always obeyed.

As our modeling indicated that it is not important to describe some reaction sequences in complete detail, these sequences were simplified to keep the reaction mechanism of manageable size. For example, reaction class 31, the irreversible fragmentation of aromatic radicals, is not a true reaction class. It was used to include ring fragmentation effects for large aromatic radicals after detailed models of ring fragmentation (including e.g. A2- = A1C4H3-) indicated that although ring rupture was an important reaction route for aromatic radicals with one ring, it was not important for aromatic radicals with more than one ring. Even with this overestimate of fragmentation rates for the polycyclic radicals, fragmentation was not a significant reaction route for these species.

Reliable thermodynamic properties were available from the literature for only a few of the species of interest. Group additivity estimation methods[21] were therefore used to obtain a large fraction of necessary thermodynamic data. A detailed discussion of all group values used in this work along with illustrations of their applications to carbon polymerization reactions is reported elsewhere[19].

The main test mixture used in the computer experiments was 1.09% C_2H_2-Ar at $\rho_5 = 3.8 \times 10^{-5}$ mol/cm^3 with T_5 values from 1500 to 2100 K, to simulate Series B of Ref. 24. The pressure range of this series, 5-7 bar, is consistent with the choice of high-pressure limits for unimolecular rate coefficients. The computations were carried out to a reaction time of 2 ms using a constant-pressure model. The computed temperature changes wer at most a few degrees. The computations were done with an IBM 370-3081 computer using the LSODES integrator[36].

3.Results and Discussion

The primary objective of our investigation was to discover the principal route(s) for formation of soot. Other important aspects, e.g. product distributions for various experimental conditions, will be the subject of our future studies. Their omission does not affect the main conclusions of the present work.

a) Formation of the first aromatic ring

Our initial working hypothesis was that a multiplicity of cyclization pathways would account for the overall cyclization rate. Following this hypothesis, a reaction network was composed that included 26 different cyclization reactions of species up to $C_{14}H_x$. These reactions are of two classes, non-radical and radical cyclizations (Table IV). An example of the former is (see Ref. 24)

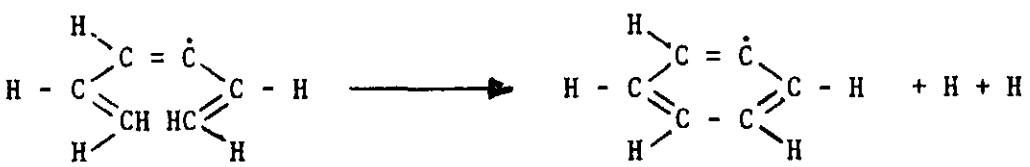

The second cyclization class can be further subdivided into

a) cyclization of more stable radicals, e.g.

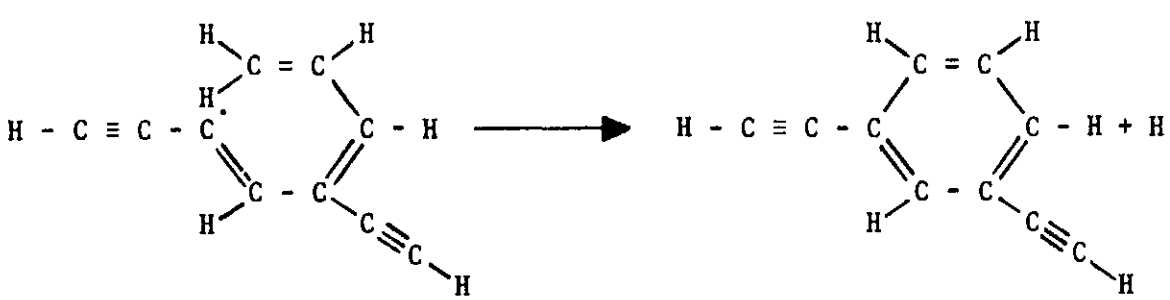

TABLE IV. REACTION CLASSES AND RATE COEFFICIENT EXPRESSIONS.

Number	Reaction Class	Prototype Reaction	Rate Coefficient for Forward Direction	Remarks
1	Ethynyl radicals plus H_2.	$C_2H + H_2 = C_2H_2 + H$	$3.5 \times 10^{12} \exp(-8.8/RT)$	Warnatz[33]
2	H abstractions of olefinic H.	$H + C_2H_4 = C_2H_3 + H_2$	$1.5 \times 10^{14} \exp(-42.7/RT)$	Warnatz[33]
3	Ethynyl abstractions of ethynyl H.	$C_2H + C_4H_2 = C_2H_2 + C_4H$	2×10^{13}	For exothermic direction.
4	Ethynyl abstractions of olefinic H.	$C_2H + C_2H_4 = C_2H_2 + C_2H_3$	2×10^{13}	
5	H additions to triple bonds.	$H + C_2H_2 = C_2H_3$	$5.5 \times 10^{12} \exp(-10/RT)$	Warnatz[33], k_∞
6	H additions to double bonds.	$H + C_2H_4 = C_2H_5$	$1 \times 10^{13} \exp(-6.3/RT)$	Warnatz[33], k_∞
7	Recombinations of organic radicals.	$C_2H + C_2H = C_4H_2$	1×10^{13}	
8	Ethynyl additions to triple bonds.	$C_2H + C_4H_2 = C_6H_3$	1×10^{13}	
9	Polyacetylene formations.	$C_2H + C_2H_2 = C_4H_2 + H$	2×10^{13}	
10	Ethynyl attacks on triple bonds followed by C-C bond rupture.	$C_2H + C_6H_2 = C_4H_2 + C_4H$	1×10^{13}	For exothermic direction.
11	Vinyl attacks on triple bonds, H loss.	$C_2H_3 + C_2H_2 = C_4H_4 + H$	$1.6 \times 10^{13} \exp(-105/RT)$	Kiefer et al.[31]
12	Vinyl attacks on triple bonds followed by C-C bond rupture.	$C_2H_3 + C_4H_2 = C_4H_4 + C_2H$	1×10^{13}	$k_{12} = k_{10}$
13	Vinyl additions to triple bonds.	$C_2H_3 + C_4H_2 = C_6H_5$	1×10^{13}	$k_{13} = k_8$
14	Vinyl attacks on double bonds followed by C-C bond rupture.	$C_2H_3 + C_4H_4 = C_2H + C_4H_6$	1×10^{13}	$k_{14} = k_{10}$
15	Vinyl abstractions of olefinic H.	$C_2H_3 + C_4H_4 = C_2H_4 + C_4H_3$	$1 \times 10^{12} \exp(-68/RT)$	Ebert et al.[34]

Table IV. (continued)

Number	Reaction Class	Prototype Reaction	Rate Coefficient for Forward Direction	Remarks
16	Vinyl attacks on olefinic bonds, H loss.	$C_2H_3 + C_2H_4 = C_4H_6 + H$	1×10^{10} exp(-34/RT)	Ebert et al.[34]
17	Ethynyl attacks on olefinic bonds, H loss.	$C_2H + C_2H_4 = C_4H_4 + H$	6×10^{11} exp(-16/RT)	$(k_9 k_{16})^{\frac{1}{2}}$
18	Irreversible non-radical cyclizations.	$H_2C{=}CH{-}CH{=}\dot{C}{-}CH{=}CH_2 \rightarrow$ phenyl+H+H	1×10^{5}	
19	H additions to aromatics.	H+benzene = benzene-H	1×10^{13} exp(-6.3/RT)	$k_{19} = k_6$
20	Radical cyclizations.	$C_{10}H_7 = Ar(C_2H)_2$+H	1×10^{10}	
21	H recombinations with aryl radicals.	H+phenyl = benzene	1×10^{13}	
22	Aromatic fragmentations.	benzene = products	1×10^{16} exp($-\Delta H^0$/RT)	
23	H abstractions of aryl H.	H+benzene = phenyl + H_2	1×10^{14}	
24	Ethynyl abstractions of H from aromatics.	C_2H+benzene = phenyl+C_2H_2	2×10^{13}	$k_{24} = k_3$
25	H attacks on aryl acetylenes.	H+phenylacetylene = C_2H_2+phenyl	1×10^{14}	
26	Aryl attacks on triple bonds followed by C-C bond rupture.	phenyl+C_4H_2 = phenylacetylene+C_2H	2×10^{13}	$k_{26} = k_9$
27	Aryl additions to triple bonds.	phenyl+C_4H_2 = phenylC_4H_2	1×10^{13}	$k_{27} = k_8$
28	H recombinations with ethynyl.	$H + C_2H = C_2H_2$	2×10^{13}	
29	H recombinations with vinyl	$H + C_2H_3 = C_2H_4$	2×10^{13}	Gardiner and Troe[35]
30	Radical cyclization via triple bond.	$HC{\equiv}C{-}CH{=}CH{-}CH{=}\dot{C}H$ = phenyl	1×10^{10}	$k_{30} = k_{20}$

Table IV. (continued)

Number	Reaction Class	Prototype Reaction	Rate Coefficient for Forward Direction	Remarks
31.	Irreversible fragmentation of aromatic radicals.	$A_2C_2H^* = A_1C_2H^*$	$\frac{\text{(net rate of A2- = A1C4H3-)}}{\text{(concentration of A2-)}}$	reverse rate constant = 0; forward rate
32.	Radical disproportionation.	$H + C_2H_3 = H_2 + C_2H_2$	1×10^{13}	$k_{32} = k_7$
33.	Phenyl abstraction of olefinic H.	$A_1- + C_6H_4 = A_1 + C_6H_3S$	2×10^{13}	$k_{33} = k_4$

The units are cm^3, K, kJ, mol, s. The rate coefficients for the reverse direction are computed via equilibrium constants. When the reverse rate coefficients were limited (see text), the forward rate coefficients were computed via equilibrium constants.

b) cyclization of less stable radicals, e.g.

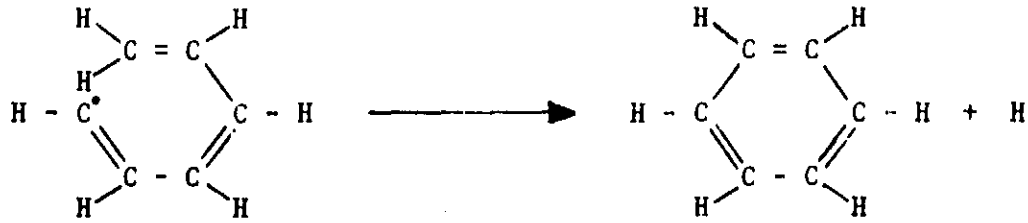

and c) radical cyclization via interaction of an unpaired electron with a triple bond, e.g.

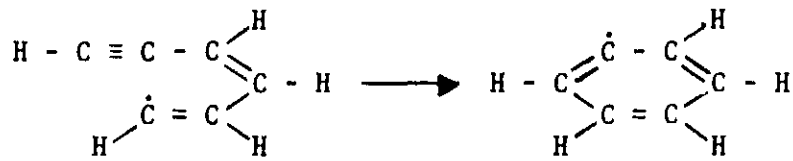

The computational results indicated that for the conditions studied cyclization by the latter reaction has 3, 5 and 8 orders of magnitude more forward flux than the radical, (a) and (b), and non-radical cyclizations, respectively. The dominant reaction pathway for the formation of the first aromatic ring is given in Table V.

A second important reaction of subclass (c)

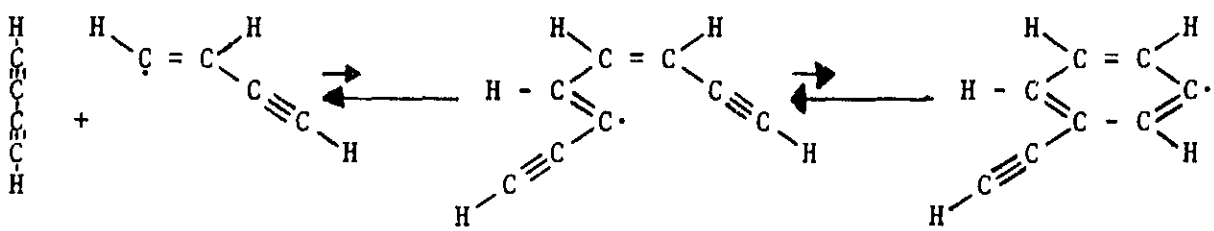

appeared to proceed rapidly but in the reverse direction, being the major fragmentation reaction of the single-ring aromatic hydrocarbons.

b) Formation of two-ring aromatics

About 10 essentially different pathways for the formation of two-ring aromatic species were considered. As in the first-ring cyclization, a single route (Fig. 52) dominated the formation of the

TABLE V. FORMATION OF THE FIRST AROMATIC RING.

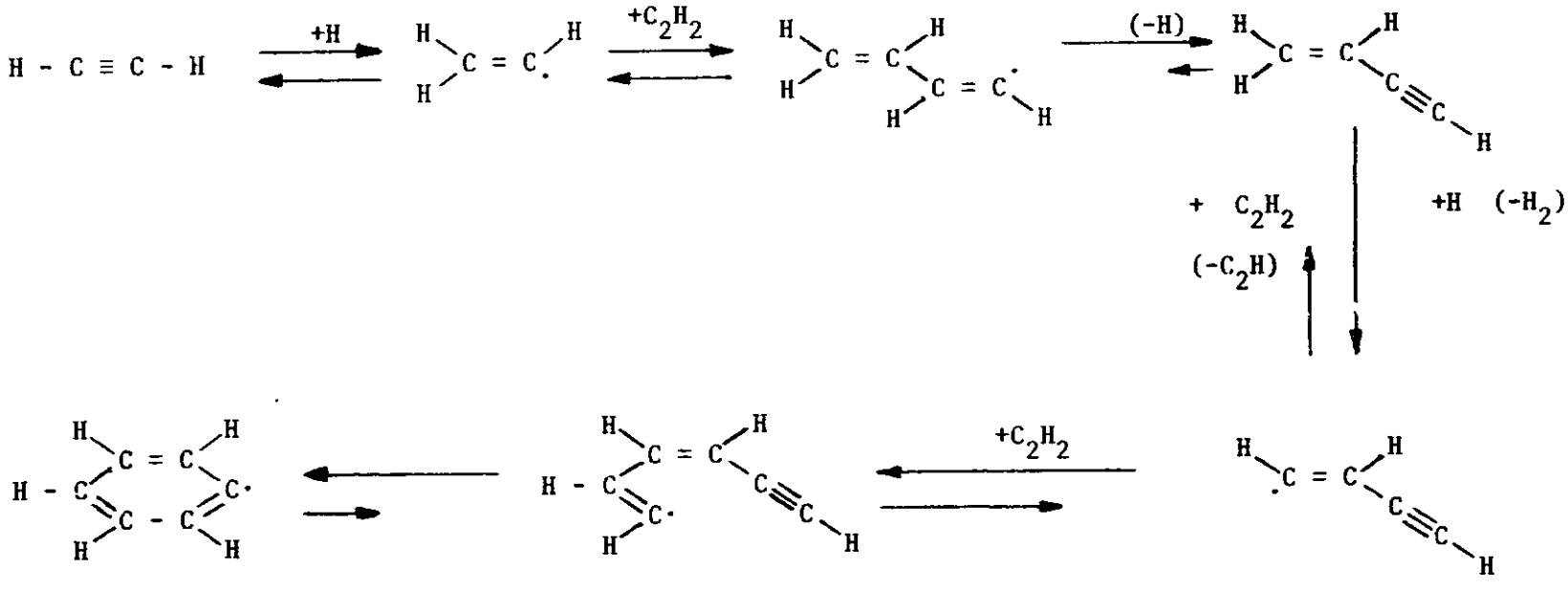

For a given reaction step, the difference in the lengths of the arrows represents the difference in forward and reverse reaction rates as computed for the test case (see text) at T = 1700 K and a reaction time of 0.5 ms. The vertical arrows between C_4H_4 and C_4H_3 represent the net reaction rates: the right arrow for reaction $C_4H_4 + H \rightleftarrows C_4H_3 + H_2$ and the left arrow for reaction $C_4H_4 + C_2H \rightleftarrows C_4H_3 + C_2H_2$.

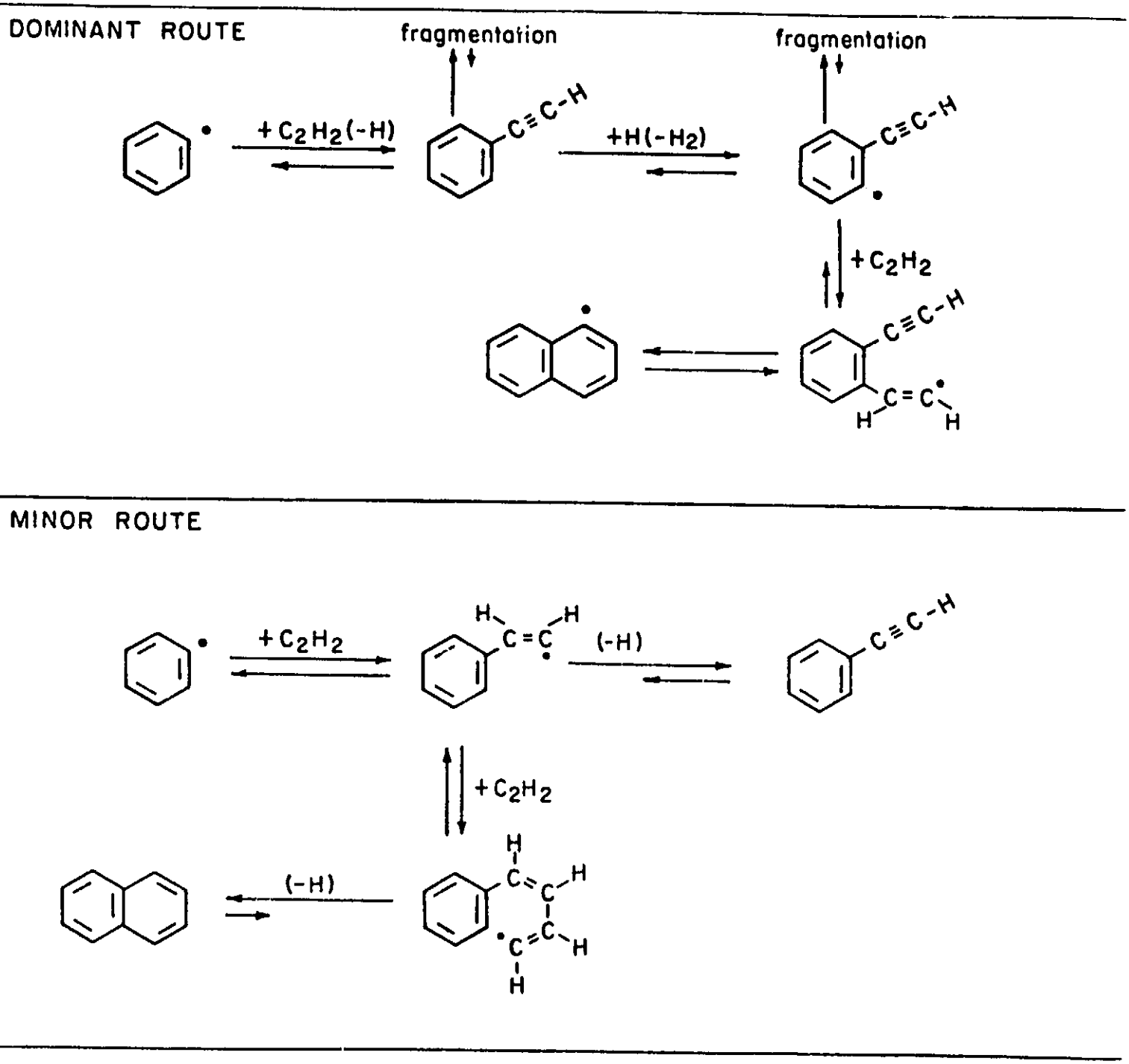

Figure 52. Principal reaction pathways for formation of two-ring aromatics. For a given reaction step, the difference in the lengths of the arrows represents the difference in forward and reverse reaction rates as computed for the test case at T = 1700 K and a reaction time of 0.5 ms.

second ring, for the conditions tested, by at least 3 orders of magnitude. Also shown in Fig. 52 is the next fastest route - a two-step acetylene addition as suggested by Bittner and Howard[12], which appeared to be most important among similar two-step additions such as acetylene addition followed by diacetylene addition, diacetylene addition followed by acetylene addition, two-step diacetylene addition, or similar reactions involving vinyl acetylene[13]. The computational results indicated that the two-step addition mechanism is slow because the first intermediate adduct, such as phenyl-CH=$\dot{C}$H in Fig. 52, is so unstable that stabilization via loss of a hydrogen atom is much faster than the next addition reaction.

An important question is why the dominant route is so much faster than the rest. The reason is that formation of the more stable molecular intermediate phenylacetylene occurs in the dominant route (Fig. 52), whereas in the minor routes the molecular species produced are relatively unreactive side products and all the reactive intermediates are radicals. At first glance one would expect that formation of a stable molecule followed by its reactivation via hydrogen atom abstraction should be slower than radical-reactant interactions, which is true for irreversible kinetics. In the case of consecutive reversible reactions the formation of stable intermediates appears to be the more decisive factor.

Recently, Bockhorn et al.[28] suggested a cyclization mechanism very similar to ours. Their reaction mechanism was developed to explain product distributions obtained in sooting laminar flat flames with a variety of hydrocarbons. The agreement in the cyclization steps suggested independently and from such different viewpoints as product

distribution in flames in their work and a computer experiment in ours is remarkable.

c) Further growth of fused polycyclic aromatics

Based on the computational results for two-ring formation, only the dominant mechanism of cyclization discussed above was considered for the further growth of fused polycyclic aromatics. Two main pathways considered in this study are presented in Fig. 53. Although in the figure they stop at pyrene (and cyclopenta[cd]pyrene), both routes were continued in the computer experiments to benzo[ghi]perylene which was followed by formation of coronene. Route 1 in Fig. 53 generally dominated the carbon mass flux, although both routes proceed with approximately equal rates at the lowest temperatures tested (1500 K). At these temperatures, however, the computed soot yields were extremely low, as discussed in the next section. Thus, for the growth of fused polycyclic aromatics, from coronene to ovalene and further, only Route 1 of Fig. 53 was considered.

Routes 1 and 2 in Fig. 53 are similar in that both proceed through radical as well as molecular intermediates. The molecular intermediates of Route 2 are substituted fused polycyclic aromatics, the unsubstituted fused molecules like acenaphthylene, pyrene and coronene having the role of relatively unreactive side products. On the other hand, these unsubstituted fused aromatics (the cyclopenta group is relatively unstable and must be partially lost, in one way or another, along the reaction pathway; to indicate this on the diagram of Fig. 53, the group is drawn with dashed lines) are included in Route 1 as reactive intermediates. What distinguishes these intermediates is their high thermodynamic stability, increasing from acenaphthylene to pyrene, to

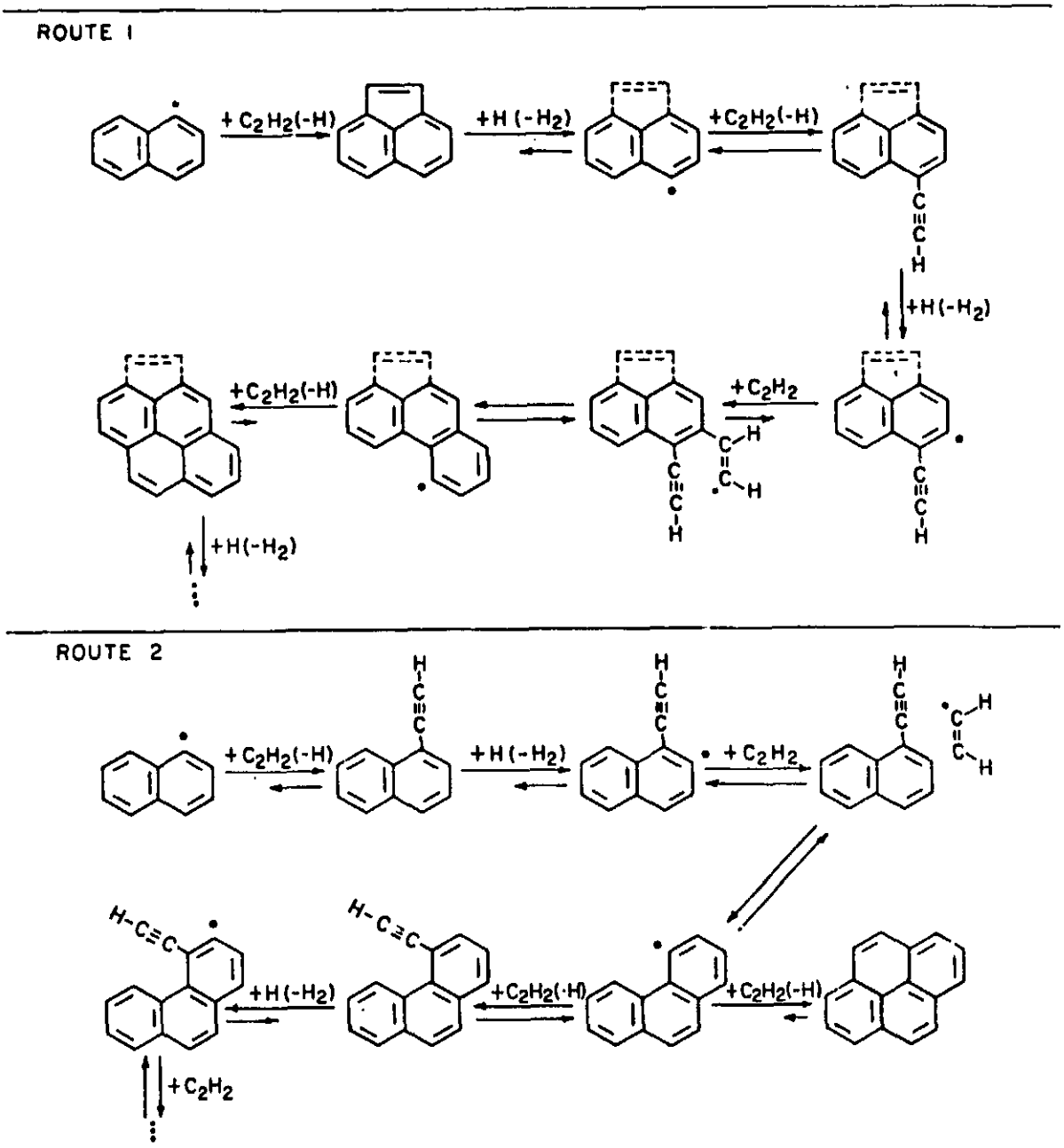

Figure 53. Principal reaction pathways for formation of fused polycyclic aromatics. For a given reaction step, the difference in the lengths of the arrows represents the difference in forward and reverse reaction rates computed for the test case at T = 1700 K and a reaction time of 0.5 ms.

coronene and to ovalene. The computational results indicate that their formation reactions are practically irreversible; this is particularly true for the formation of acenaphthylene, coronene and ovalene. These irreversible reactions have the effect of "pulling" the chain of reversible steps, which is crucial for soot formation.

d) Species concentration profiles

The time development of the concentrations of selected species at a temperature of 1700 K is presented in Figs. 54-58. Figure 54 presents the concentrations of H, H_2 and H_{eq}. H_{eq} is the hypothetical hydrogen atom concentration which would be in equilibrium with the calculated concentrations of H_2; that is, $[H_{eq}] = \sqrt{K_{18}[H_2]}$, where K_{18} is the equilibrium constant of reaction 18 (see Table III). The temperature dependences of the concentrations of the same species at a reaction time of 500 microseconds are shown in Figs. 59-63.

e) Formation of soot

For modeling purposes we defined soot, as in our experimental work, as a collection of species absorbing light of a specific wavelength, or, similarly[7], as a collection of species above a certain size. In the present modeling the list of these species was chosen to begin at coronene. The choice of a larger species would not greatly affect the soot yields at longer reaction times. The computed soot yield was defined, again as in our experimental work, as the number of carbon atoms accumulated in soot divided by the initial number of carbon atoms of acetylene.

To compute soot yields we assumed an infinitely long reaction sequence of Route 1 (Fig. 53), all species of this route beginning with coronene constituting soot. This is, of course, a simplification:

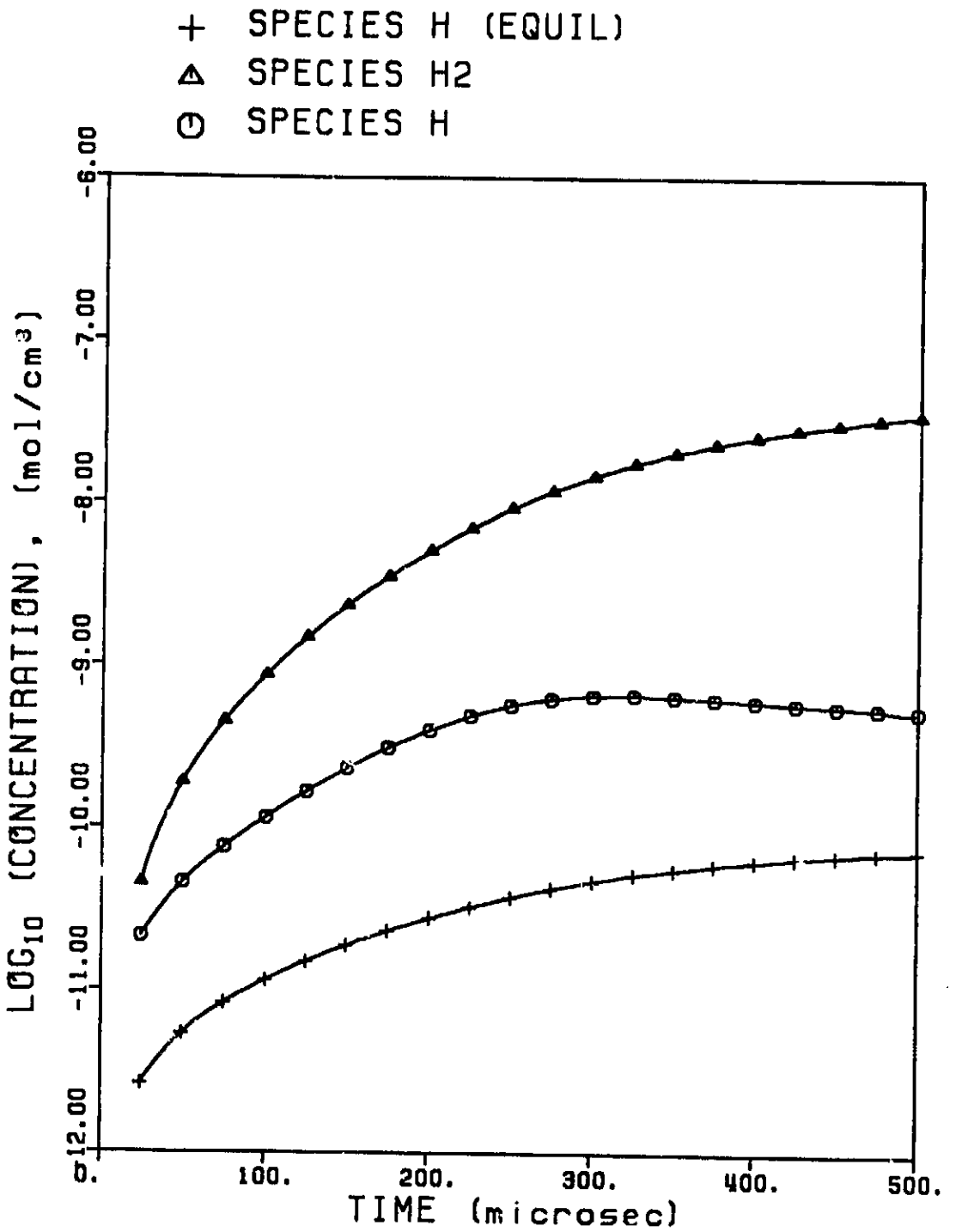

Figure 54. Time dependence of computed concentrations of H, H_2 and H_{eq} for the test case at T = 1700 K. H_{eq} is the hypothetical concentration of hydrogen atoms which would be in equilibrium with the computed concentrations of H_2. The symbols designate computational results, the lines cubic spline fits.

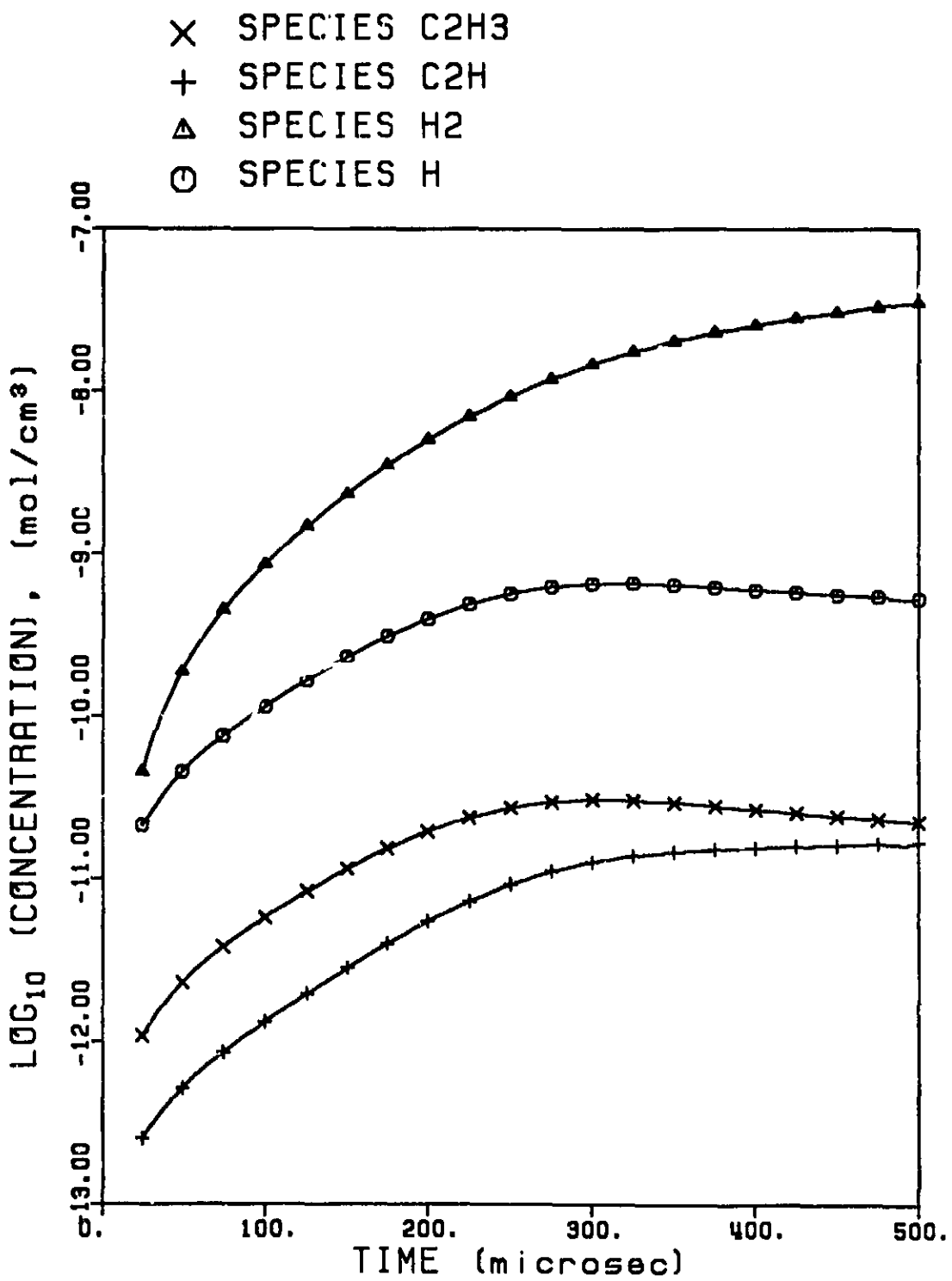

Figure 55. Time dependence of computed concentrations of H, H_2, C_2H and C_2H_3 for the test case at T = 1700 K. The symbols designate computational results, the lines cubic spline fits.

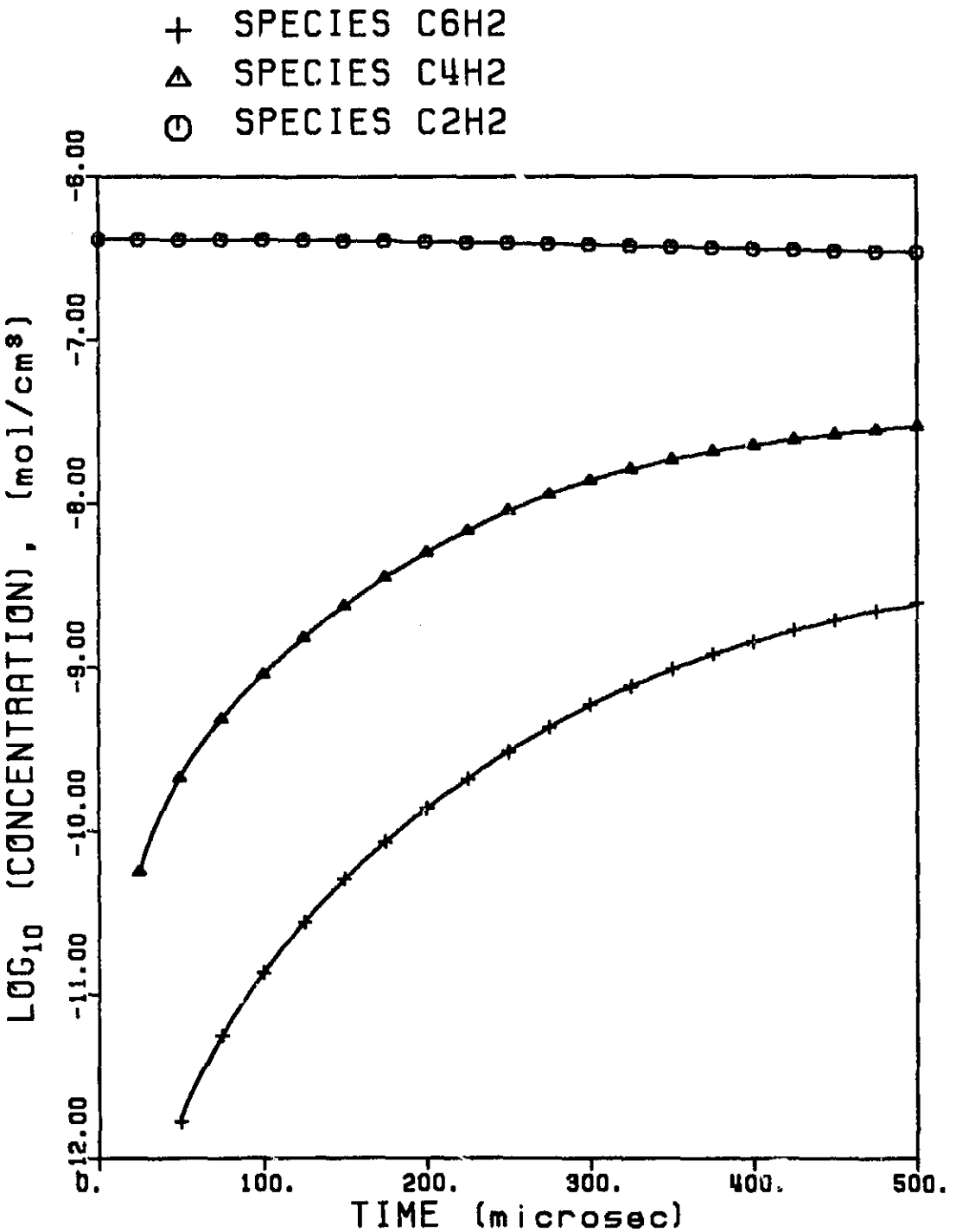

Figure 56. Time dependence of computed concentrations of C_2H_2, C_4H_2 and C_6H_2 for the test case at T = 1700 K. The symbols designate computational results, the lines cubic spline fits.

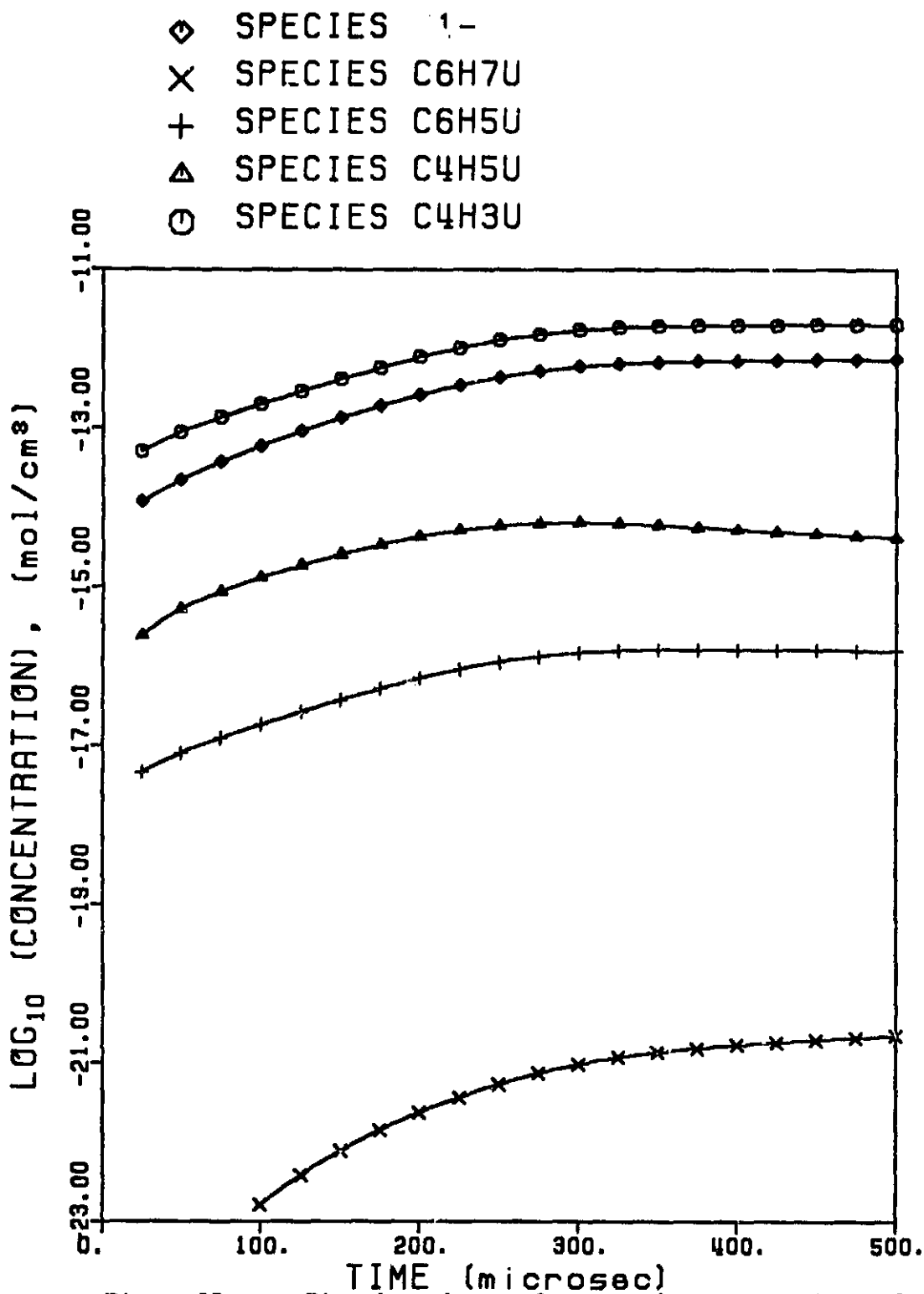

Figure 57. Time dependence of computed concentrations of intermediate-sized radicals for the test case at T = 1700 K. The structure for each species is presented in Table II. The symbols designate computational results, the lines cubic spline fits.

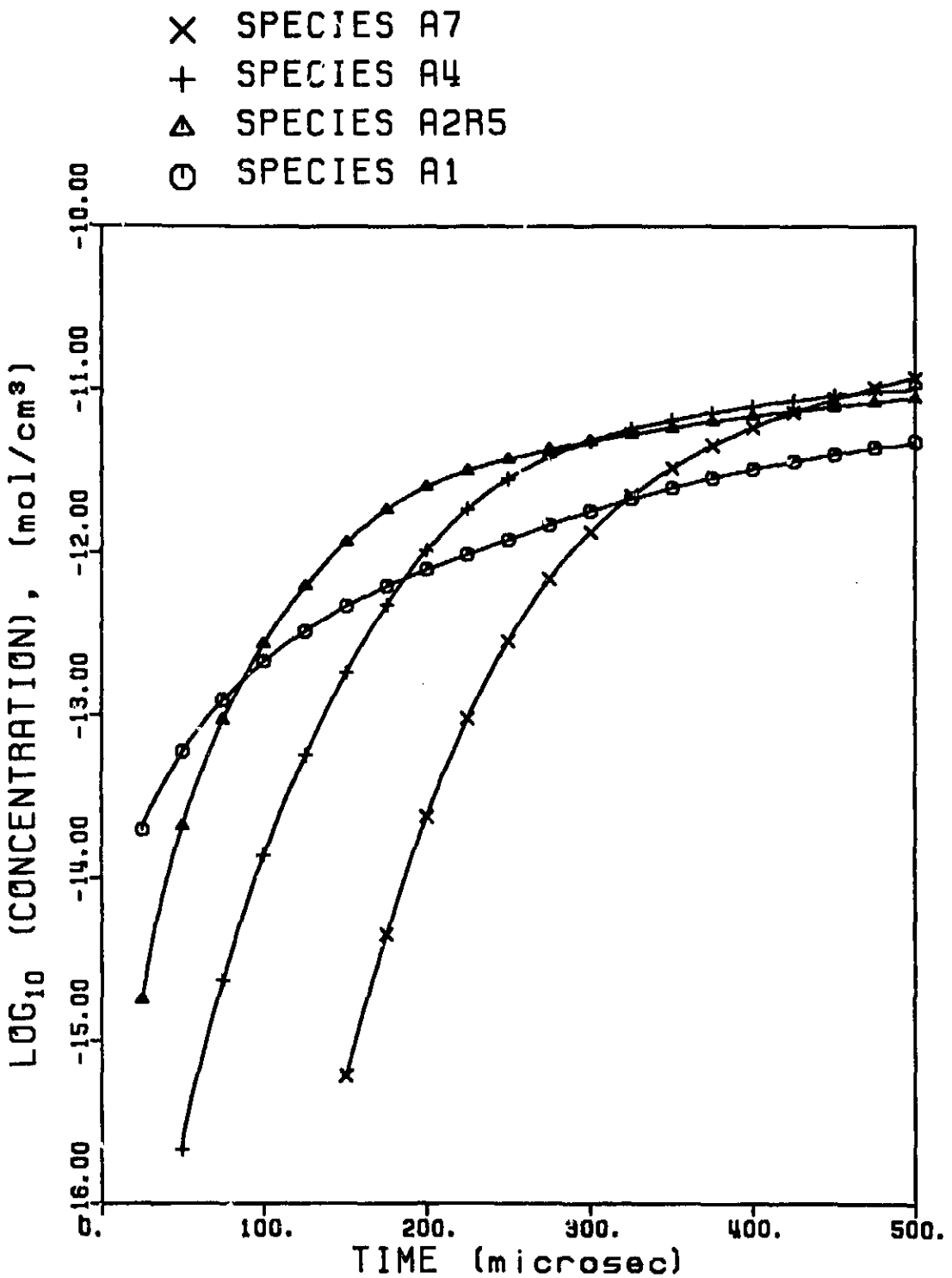

Figure 58. Time dependence of computed concentrations of intermediate- and large-sized aromatic molecules for the test case at T = 1700 K. The structure for each species is presented in Table II. The symbols designate computational results, the lines cubic spline fits.

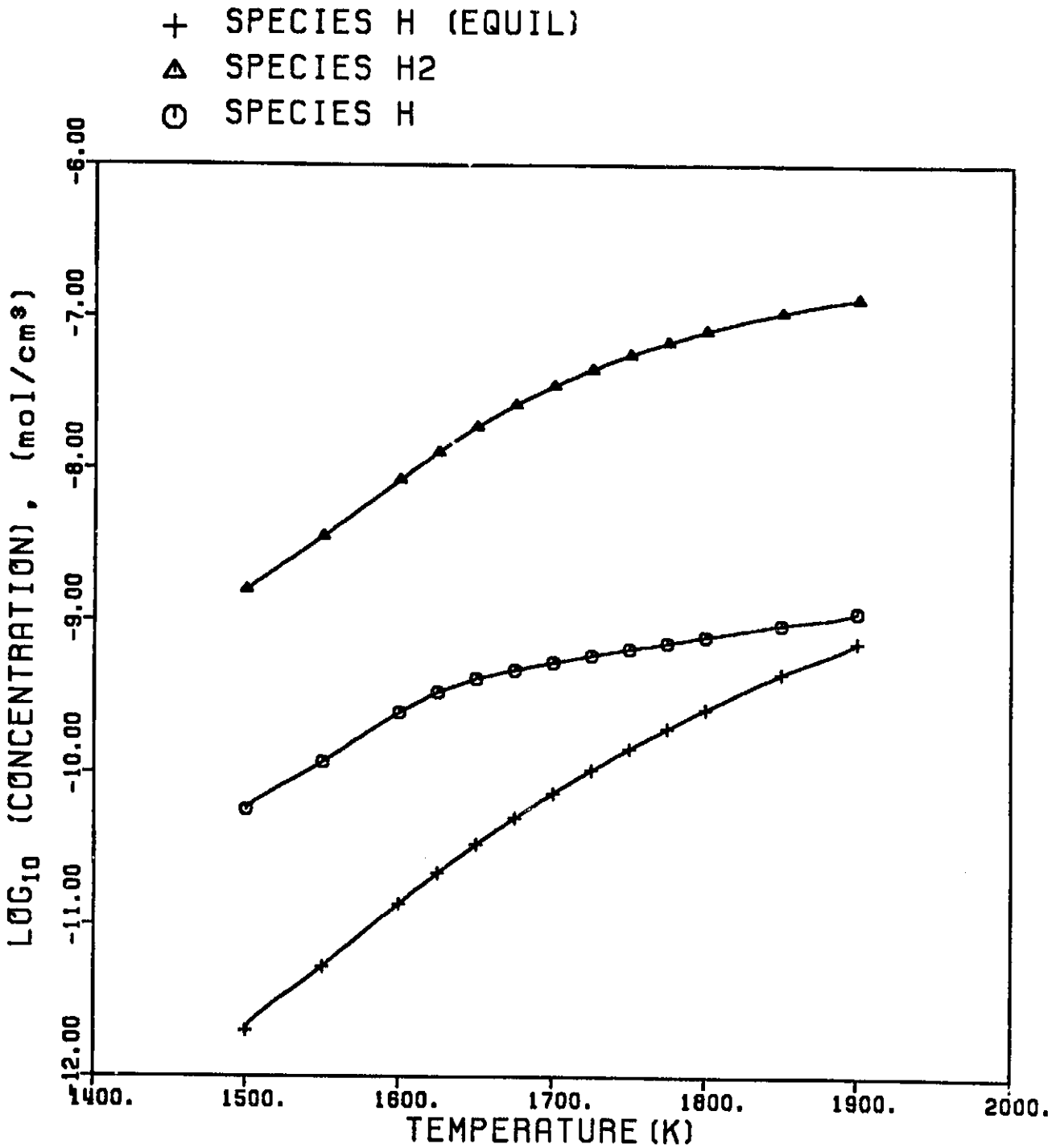

Figure 59. Temperature dependence of computed concentrations of H, H_2 and H_{eq} for the test case at a reaction time of 0.5 ms. H_{eq} is the hypothetical concentration of hydrogen atoms which would be in equilibrium with the computed concentration of H_2. The symbols designate computational results, the lines cubic spline fits.

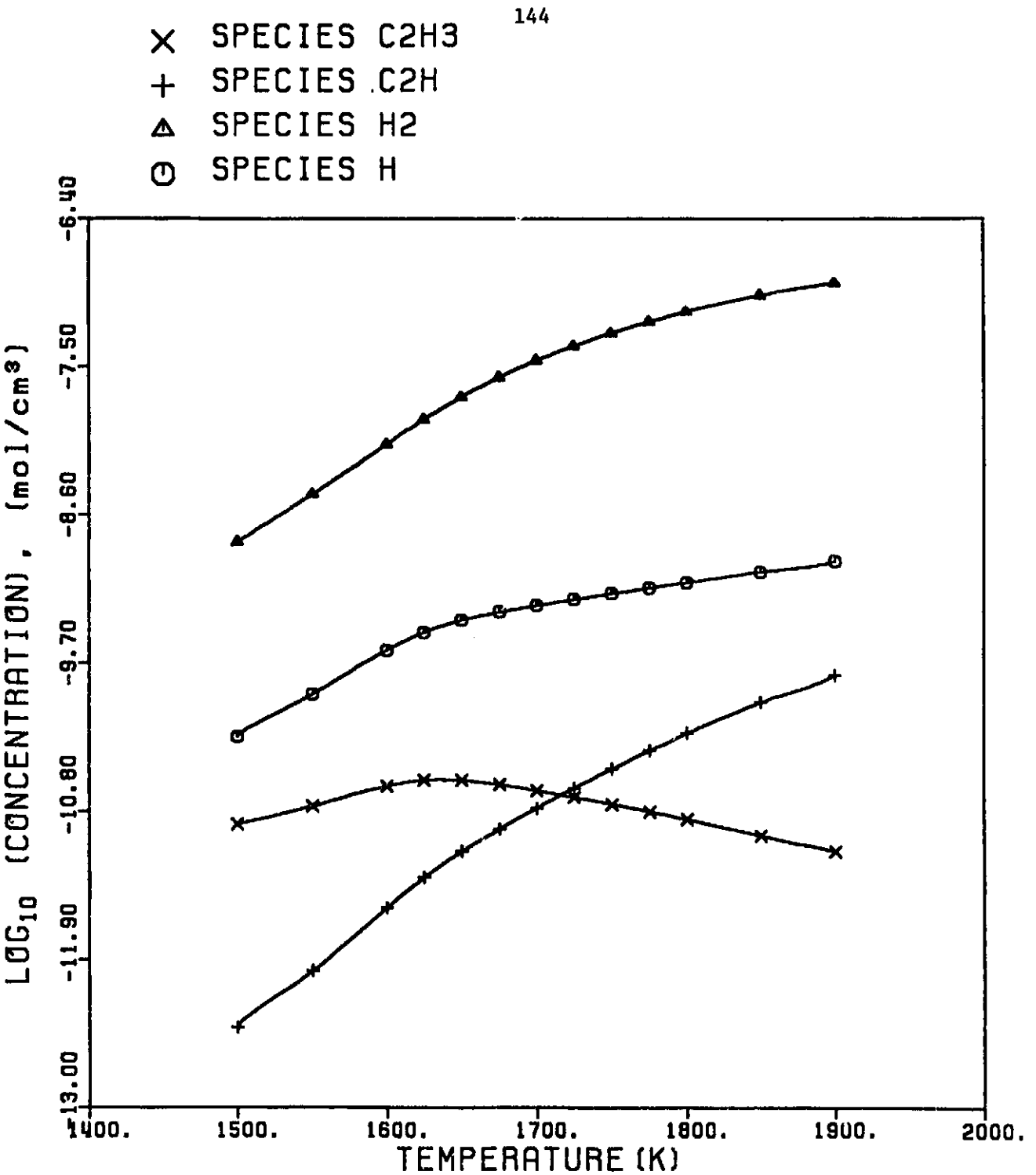

Figure 60. Temperature dependence of computed concentrations of H, H_2, C_2H and C_2H_3 for the test case at a reaction time of 0.5 ms. The symbols designate computational results, the lines cubic spline fits.

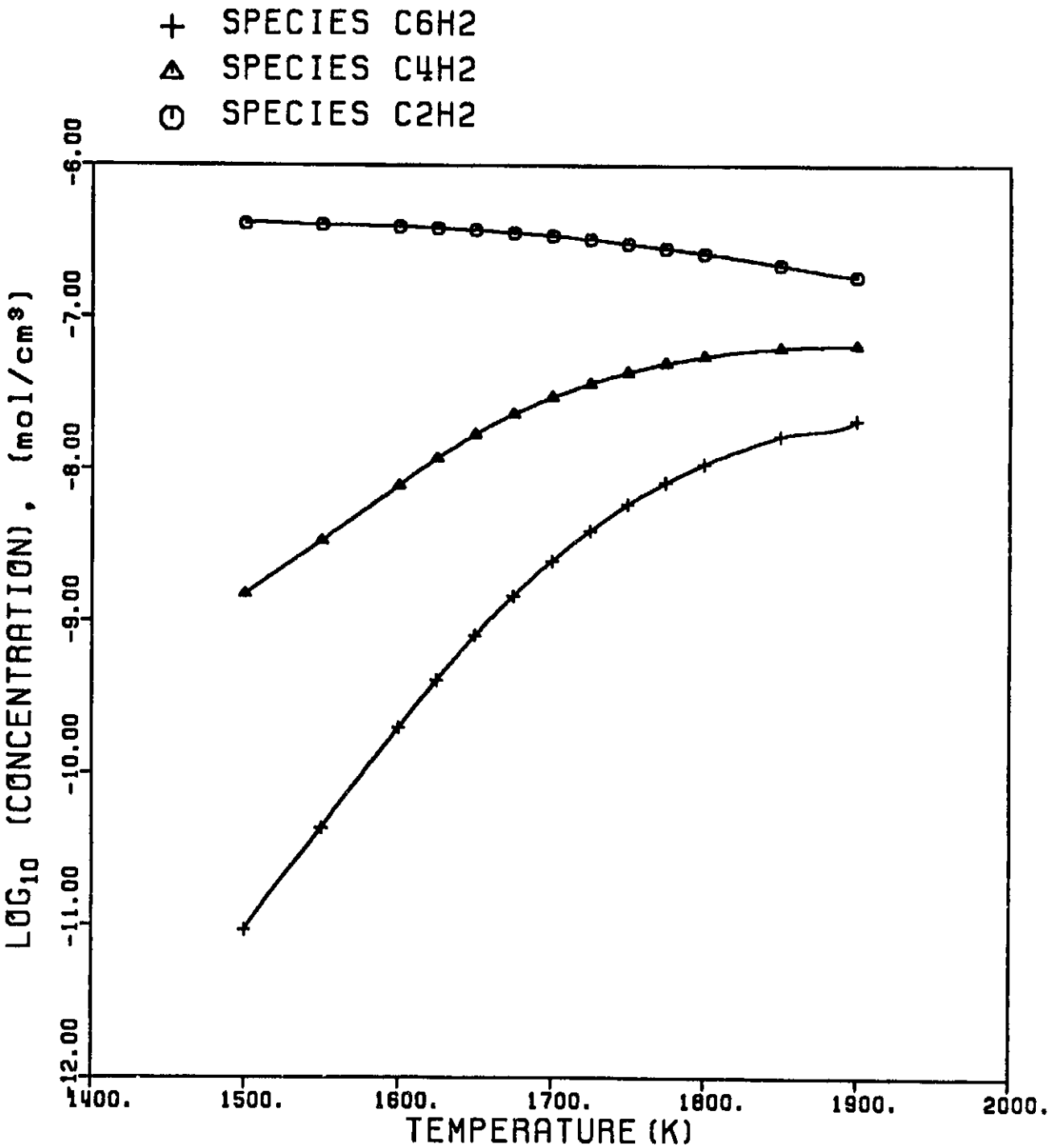

Figure 61. Temperature dependence of computed concentrations of C_2H_2, C_4H_2 and C_6H_2 for the test case at a reaction time of 0.5 ms. The symbols designate computational results, the lines cubic spline fits.

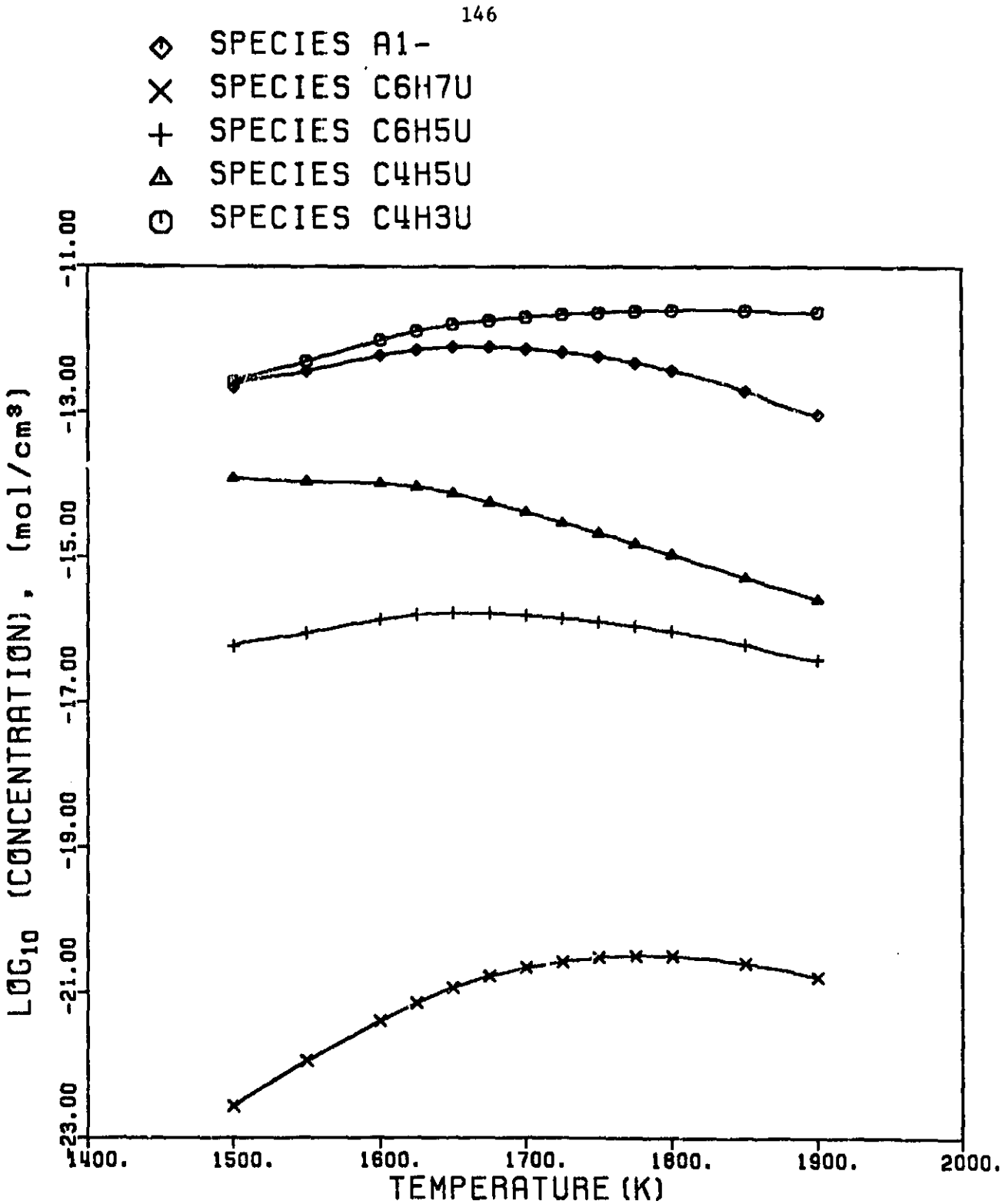

Figure 62. Temperature dependence of computed concentrations of intermediate-sized radicals for the test case for a reaction time of 0.5 ms. The structure for each species is presented in Table II. The symbols designate computational results, the line cubic spline fits.

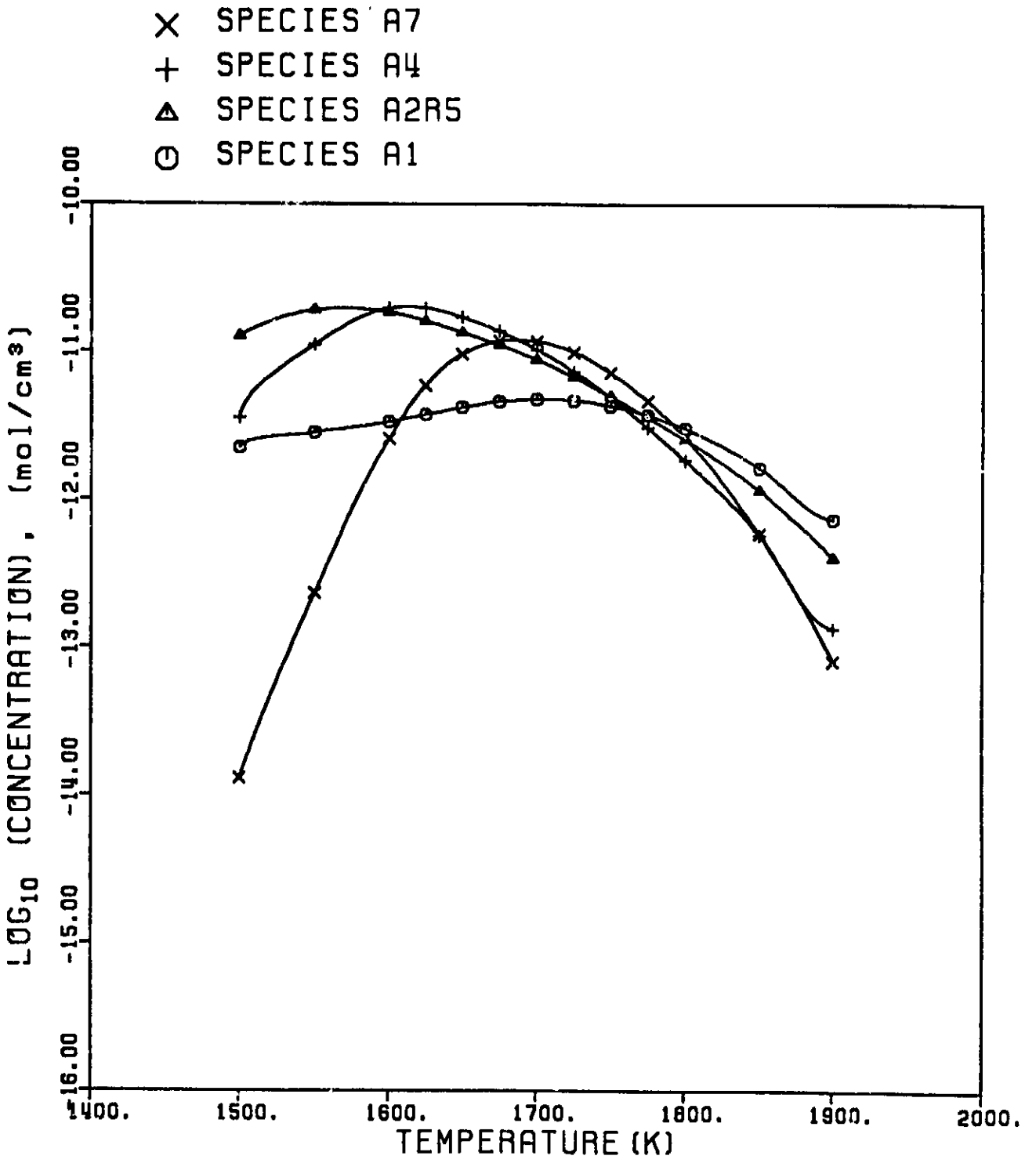

Figure 63. Temperature dependence of computed concentrations of intermediate-and large-sized aromatic molecules for the test case at a reaction time of 0.5 ms. The structure for each species is presented in Table II. The symbols designate computational results, the lines cubic spline fits.

somewhere in the growth process mechanisms such as physical condensation, particle coagulation and surface reactions become more efficient and take over the soot formation process[15,25]. In view of this, the model of an infinitely long reaction sequence provides only a lower-limit estimate of soot yield.

As discussed in the previous section, the fused polycyclic aromatic molecules are formed by practically irreversible reactions. Therefore, Route 1 can be viewed as a sequence of similar strings of reversible reactions, from acenaphthylene to pyrene, from pyrene to coronene, from coronene to ovalene, etc., the strings being connected by irreversible reactions (Fig. 64). Given such a model, the total number of carbon atoms accumulated in soot species can be computed exactly. In this computation we assumed the equilibrium constants of the corresponding reversible reactions in the replicating strings to be unchanged after coronene.

The mathematical formalism of this process can be presented as[37,38]

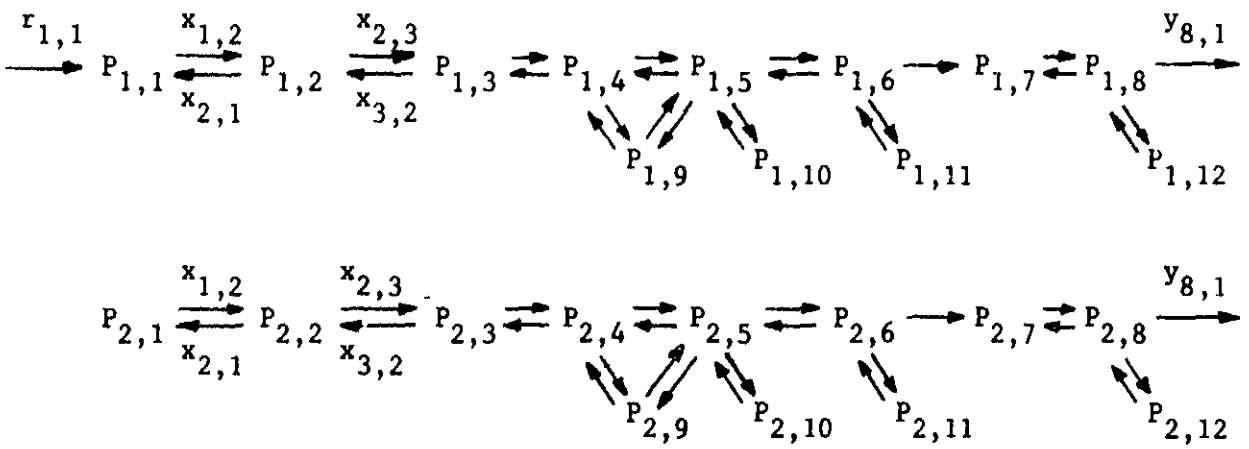

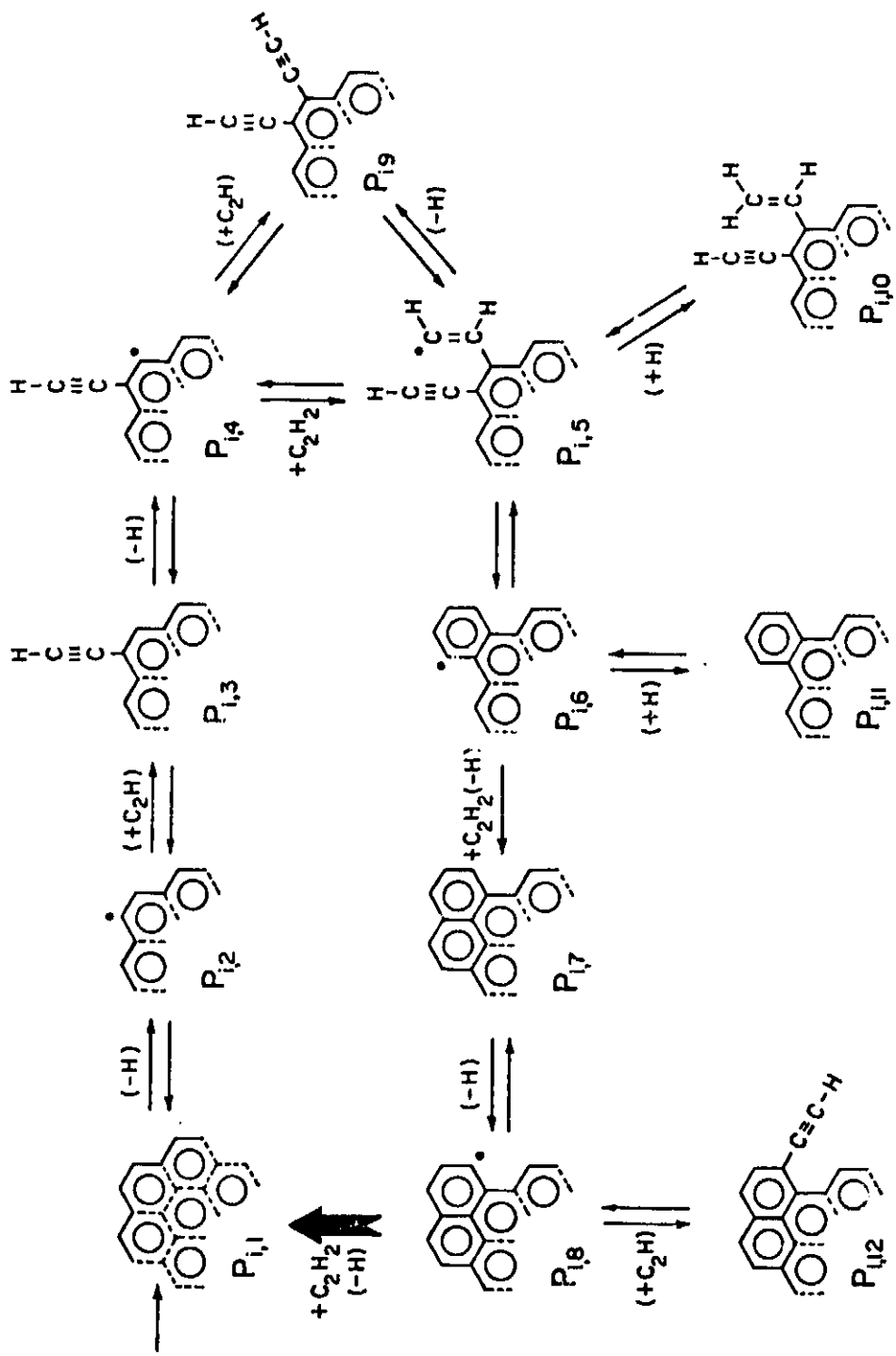

Figure 64. A schematic diagram of the polymerization mechanism for soot formation in acetylene pyrolysis.

where:

P_{ij} is the symbolic representation of species j within string i (Fig. 64);

$P_{1,1}$ is coronene

$r_{1,1}$ is the rate of formation of coronene

$$x_{1,2} = x_{3,4} = x_{7,8} = x_{10,5} = x_{11,6} = k_{23}[H] + k_{-24}[C_2H] + k_{-21}$$

$$x_{2,1} = x_{4,3} = x_{8,7} = x_{5,10} = x_{6,11} = k_{-23}[H_2] + k_{24}[C_2H_2] + k_{21}[H]$$

$$x_{2,3} = x_{4,9} = x_{8,12} = k_{-25}[C_2H_2] + k_7[C_2H]$$

$$x_{3,2} = x_{9,4} = x_{12,8} = k_{25}[H] + k_{-7}$$

$$x_{4,5} = k_{27}[C_2H_2] \qquad x_{5,4} = k_{-27}$$

$$x_{5,6} = k_{30} \qquad x_{6,5} = k_{-30}$$

$$x_{5,9} = k_{-5} \qquad x_{9,5} = k_5[H]$$

$$x_{6,7} = y_{8,1} = k_{-25}[C_2H_2]$$

and k_ℓ and $k_{-\ell}$ are the rate coefficients for the forward and reverse directions, respectively, assigned to reaction class ℓ (Table IV). The differential equations for the sum concentrations in this mechanism are

$$\sum_{i=1}^{\infty} \left\{ \frac{d[P_{i,1}]}{dt} \right\} = r_{1,1} - \sum_{i=1}^{\infty} x_{1,2}[P_{i,1}] + \sum_{i=1}^{\infty} x_{2,1}[P_{i,2}] + \sum_{i=1}^{\infty} y_{8,1}[P_{i,8}]$$

$$\sum_{i=1}^{\infty} \left\{ \frac{d[P_{i,2}]}{dt} \right\} = \sum_{i=1}^{\infty} x_{1,2}[P_{i,1}] - \sum_{i=1}^{\infty} x_{2,1}[P_{i,2}] - \sum_{i=1}^{\infty} x_{2,3}[P_{i,2}]$$

$$+ \sum_{i=1}^{\infty} x_{3,2}[P_{i,3}]$$

. . . . . .

$$\sum_{i=1}^{\infty} \{\frac{d[P_{i,8}]}{dt}\} = \sum_{i=1}^{\infty} x_{7,8}[P_{i,7}] - \{\sum_{i=1}^{\infty} (x_{8,7} + x_{8,12} + y_{8,1})\}[P_{i,8}]$$

$$+ \sum_{i=1}^{\infty} x_{12,8}[P_{i,12}]$$

. . . . . .

$$\sum_{i=1}^{\infty} \{\frac{d[P_{i,12}]}{dt}\} = \sum_{i=1}^{\infty} x_{8,12}[P_{i,8}] - \sum_{i=1}^{\infty} x_{12,8}[P_{i,12}]$$

or

$$\frac{dS_1}{dt} = r_{1,1} - x_{1,2}S_1 + x_{2,1}S_2 + y_{8,1}S_8$$

$$\frac{dS_2}{dt} = x_{1,2}S_1 - (x_{2,1} + x_{2,3})S_2 + x_{3,2}S_3$$

. . . . . .

$$\frac{dS_8}{dt} = x_{7,8}S_7 - (x_{8,7} + x_{8,12} + y_{8,1})S_8 + x_{12,8}S_{12}$$

. . . . . .

$$\frac{dS_{12}}{dt} = x_{8,12}S_8 - x_{12,8}S_{12}$$

where $S_j = \sum_{i=1}^{\infty} [P_{ij}]$, $j = 1, 2, \ldots, n$.

These 12 differential equations were added to the set of differential equations that describes the rates of change in the concentrations of the species which were considered individually. All mass balances were maintained exactly. Integration of the entire set of differential equations for the initial conditions of the test case (including $S_j[t=0]$

= 0, j = 1,2,...,12) generated the profiles of the species concentrations and the concentration sums.

The rate of increase of carbon atoms in species j is

$$\frac{dM_j}{dt} = \sum_{i=1}^{\infty} \Delta m^r_{ij} r_{ij} + \sum_{j'\neq j} \Delta m^x_{j'j} x_{j'j} S_{j'} - \sum_{j'\neq j} \Delta m^x_{jj'} x_{jj'} S_j$$

$$+ \sum_{j'\neq j} \Delta m^y_{j'j} y_{j'j} S_{j'} - \sum_{j'\neq j} \Delta m^y_{jj'} y_{jj'} S_j$$

from which the total amount of soot grows as

$$\frac{dM}{dt} = \sum_{j=1}^{n} \left\{\frac{dM_j}{dt}\right\} = \sum_{j=1}^{n} \sum_{i=1}^{\infty} \Delta m^r_{ij} r_{ij} + \sum_{j=1}^{n} \sum_{j'\neq j} (\Delta m^x_{j'j} x_{j'j} + \Delta m^y_{j'j} y_{j'j}) S_{j'}$$

$$- \sum_{j=1}^{n} \sum_{j'\neq j} (\Delta m^x_{jj'} x_{jj'} + \Delta m^y_{jj'} y_{jj'}) S_j \qquad (5)$$

where: Δm^r_{ij} is the measure of direct mass production from small reactants;

$\Delta m^x_{jj'}$ is the measure of mass production associated with interconversion of species with the same degree of polymerization;

and $\Delta m^y_{jj'}$ is the measure of mass production involving an increase in polymerization.

In our case, one has $\Delta m^x = 0$ for H-atom abstractions and $\Delta m^x = \Delta m^y = 2$ for C_2 additions. The value of $\Delta m^r_{1,1}$ is equal to the number of carbon atoms in $P_{1,1}$, which is 24.

Using the above values of Δm, eq.(5) takes the form

$$\frac{dM}{dt} = 24 r_{1,1} + 2x_{2,3} S_2 - 2x_{3,2} S_3 + (2x_{4,5} + 2x_{4,9}) S_4$$

$$- 2x_{5,4}S_5 + 2x_{6,7}S_6 + (2x_{8,12} + 2y_{8,1})S_8$$

$$- 2x_{9,4}S_9 - 2x_{12,8}S_{12} \qquad (6)$$

where M is the total number of carbon atoms accumulated in species beginning with coronene. Equation (6) with the initial condition M[t=0]=0 was added to the previous set of differential equations of the species concentrations and the concentration sums S_j. The soot yield is defined as in our experimental work[24] as the number of carbon atoms accumulated in soot divided by the initial number of carbon atoms of acetylene; that is, the soot yield equals M divided by twice the initial concentration of acetylene. The soot growth curve using this polymerization model is given in Fig. 65.

As seen in Fig. 65, the model correctly predicts the existence of an induction time for soot appearance as observed experimentally. Closer examination of this figure shows that the rate of soot formation (the slope of the soot-yield curve) decreases after a reaction time of about 1 ms. This deceleration is the result of the "thermodynamic resistance" of the kinetic system. The reaction network is basically of a consecutive type and is composed of reversible reactions. Initially, when the "bottleneck" reactions are far from partial equilibrium, the dynamic development of the system exhibits the exponential growth typical of chain reactions. This is manifested in the existence of the induction period. As the concentrations of intermediate species grow, the rates of reverse reactions increase, bringing the reactions towards a state of partial equilibrium. When this state is attained by the "bottleneck" reactions, the mass flux through them decreases, which accounts for the deceleration in soot formation. This is probably the

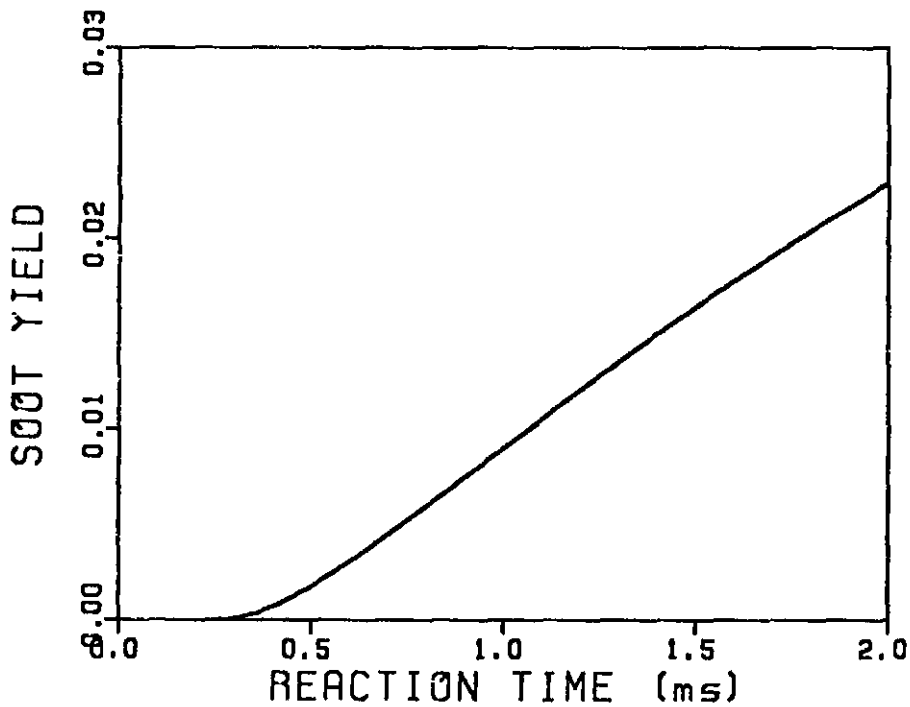

Figure 65. A profile of soot growth for a 1.09% C_2H_2-Ar mixture at ρ_5 = 3.8 x 10^5 mol/cm^3 and a temperature of 1700 K.

point at which coagulation and surface growth would begin to dominate the process.

Soot yields computed in the above manner at various temperatures are given in Fig. 66. Figure 67 presents the corresponding experimental results[24]. Except for the shift in the temperature range (see below), the computed soot yields compare well with the experimental ones (cf. Figs. 66 and 67). The model predicts both the soot bell and its shift to lower temperatures with reaction time. The width of the bell is in good agreement with experiment. The absolute values of the soot yields also agree well if one takes into account that the laser-extinction technique overestimates actual soot yields by a factor of 2 to 3[6,40]. Additional computer experiments showed that computed soot yields are dramatically reduced by decreases in the initial concentration of acetylene or by addition of hydrogen, in accord with experimental observations.

As for the nature of the soot-yield bell, the computational results support our previous conjecture[24] that competition between kinetic and thermodynamic factors is responsible for the phenomenon. At the lower temperature bound of the bell, pyrolysis reactions are rate controlling. As temperature increases, the thermodynamic stability of the intermediates[41], particularly of small aromatic radicals, decreases and eventually limits the soot yield. At high temperatures fragmentation is dominant even at the first-ring level. The shift of the soot-yield maximum to lower temperatures at longer reaction times is due to the fact that the inflection point of soot-yield time dependence (see Fig. 65), which is determined by the attainment of the state of partial equilibrium by the "bottleneck" reactions, is reached sooner at higher temperatures.

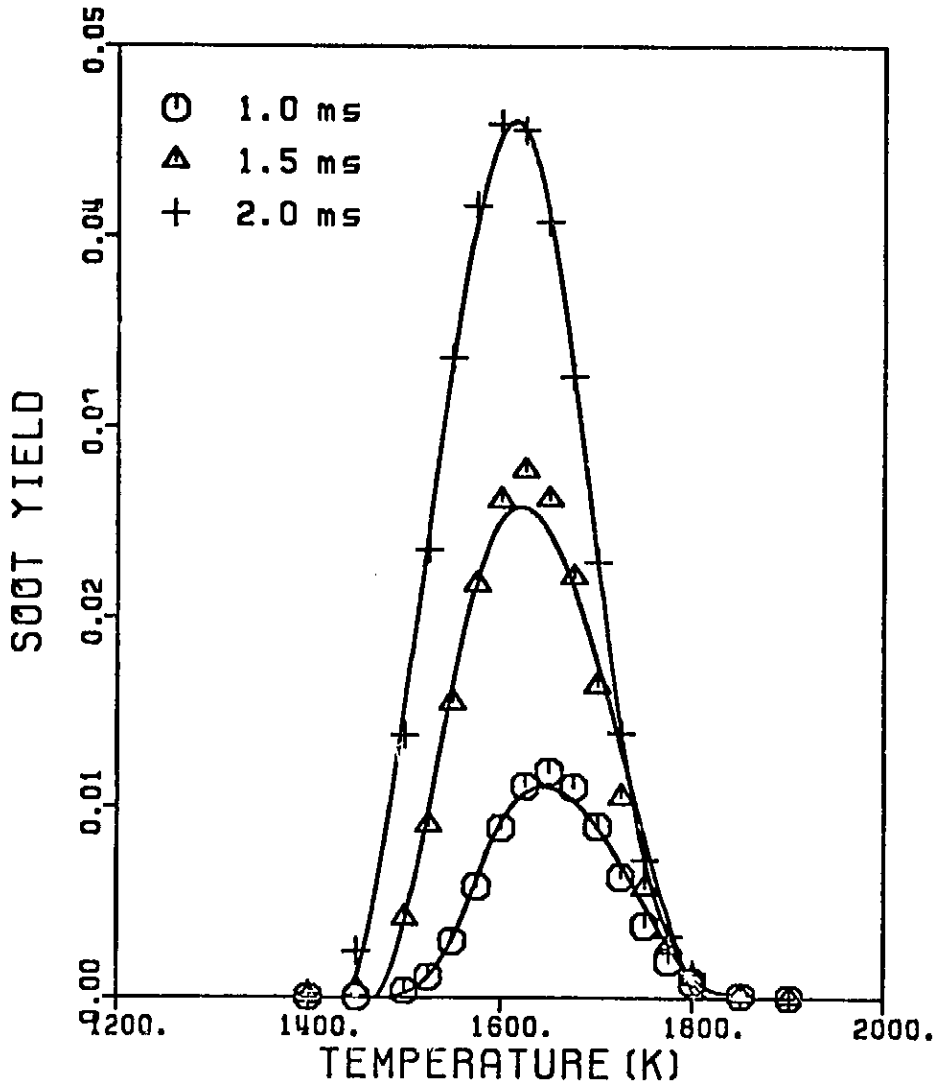

Figure 66. Computed soot yields in a 1.09% C_2H_2-Ar mixture at $\rho_5 = 3.8 \times 10^{-5}$ mol/cm^3. The symbols designate computational results, the lines cubic spline fits.

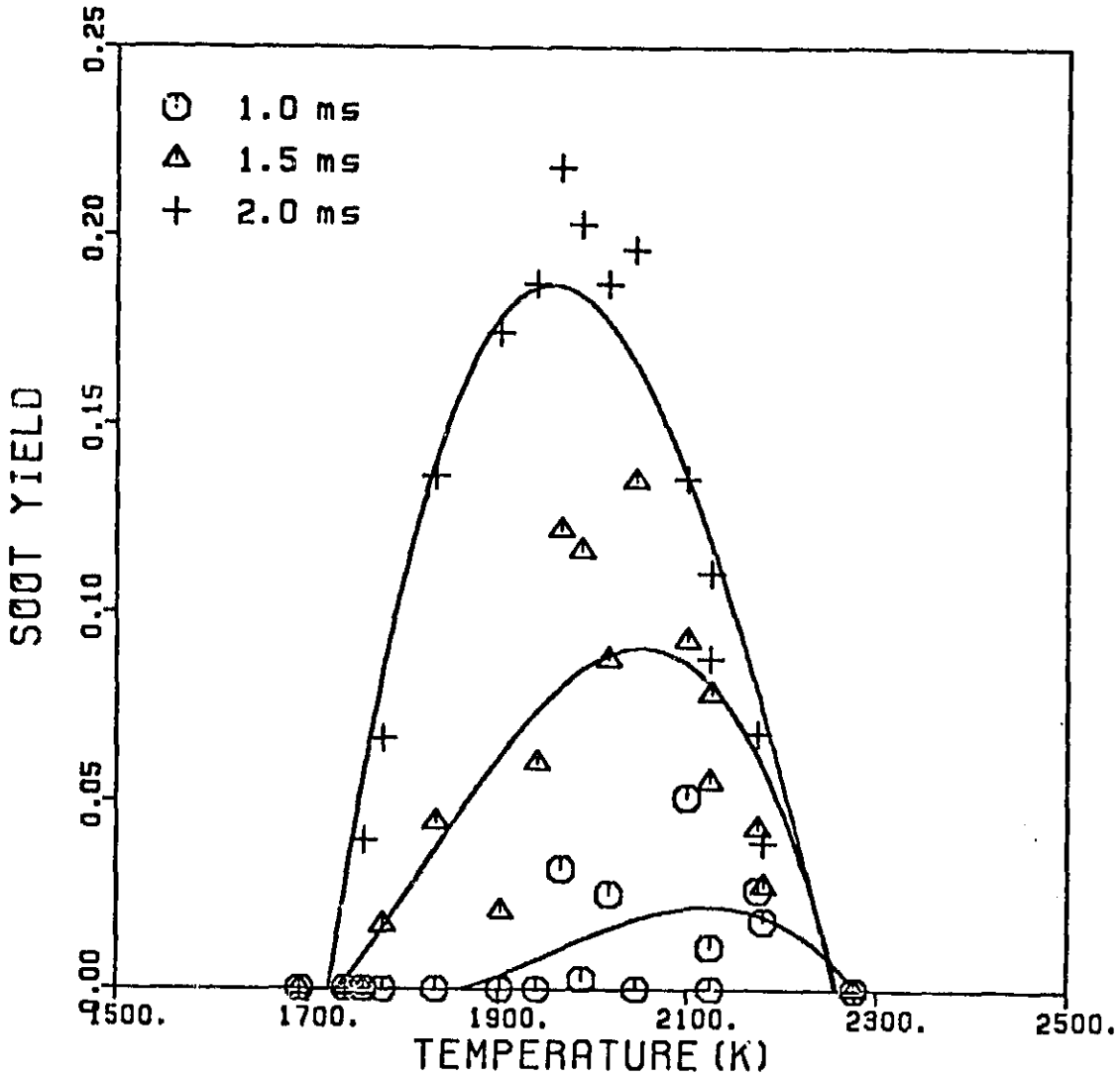

Figure 67: Experimental soot yields in a 1.09% C_2H_2-Ar mixture at ρ_5 = (3.82-3.90) x 10^{-5} mol/cm^3 using laser-extinction at 3.39 μm (series B of Ref. 24). The soot yields are calculated assuming Rayleigh scattering[6] and using the value of Lee and Tien [39] for the complex refractive index at 3.39 μm. The symbols designate experimental points, the lines cubic spline fits.

Table VI presents the results of a sensitivity analysis for the reaction classes of Table IV. Somewhat surprisingly, only a small number of reaction classes, and sometimes only a single reaction within a class, have large sensitivities (Table VI). The strongest kinetic effect, i.e. the largest value of S_k^Y, is caused by the practically irreversible formation of the fused polycyclic aromatics (Class 27) and their reactivation by hydrogen atoms (Class 23). It is interesting to note that the ratio $[H]^2/[H_2]$ is much larger than the corresponding equilibrium value (Figs. 54 and 59). The concentration of hydrogen atoms is controlled, for given initial conditions, primarily by chain reactions 6 and 7 (Table III) and its numerical value is well approximated by assuming a steady-state for these two reactions. Only at high temperatures, when most initial pyrolysis reactions reach a state of partial equilibrium, does the concentration of hydrogen atoms relax to its equilibrium value on the time scale of interest here. These results lead us to conclude that the overshoot by hydrogen atom of its equilibrium concentration is a driving kinetic force for soot formation.

Analysis of the sensitivities with respect to equilibrium constants, S_K^Y, indicates that the thermodynamic bottleneck for the growth in soot yield is at the formation of the first aromatic ring. The largest values of S_K^Y, obtained for Classes 13 and 8 (Table VI), are basically the sensitivities for the reactions

$$C_2H_2 + HC{\equiv}C\text{-}CH{=}\dot{C}H \rightleftarrows HC{\equiv}C\text{-}CH{=}CH\text{-}CH{=}\dot{C}H$$

and $$C_2H_2 + C_2H \rightleftarrows HC{\equiv}C\text{-}CH{=}\dot{C}H,$$

respectively.

TABLE VI. SENSITIVITIES OF SOOT YIELD WITH RESPECT TO RATE COEFFICIENTS AND EQUILIBRIUM CONSTANTS.

Reaction Class	S_k^Y	S_K^Y
1	-0.10	0.10
3	-0.04	-0.20
5	-0.01	0.03
8	-0.02	0.78
13	0.16	0.79
23	2.02	0.12
24	-0.06	0.06
25	0.27	-0.28
27	1.30	0.24
29	-0.03	0.00
30	0.70	0.56

The sensitivities are defined[42] as

$$S_k^Y = \ell n(Y_k/Y_0)/\ell n(1/5) \quad \text{and} \quad S_K^Y = \ell n(Y_K/Y_0)/\ell n5,$$

where Y_0 is the soot yield computed for 1.09% C_2H_2-Ar mixture at ρ_5 = 3.80 x 10^{-5} mol/cm^3, T_5 = 1700K, and reaction time of 0.5 ms; Y_k and Y_K are the soot yields computed for the same conditions but with the rate coefficient reduced by a factor of 5 and with the equilibrium constant increased by a factor of 5, respectively, for a given reaction class.

The reaction classes omitted have absolute sensitivity values less than 0.005.

The results of the sensitivity analysis (Table VI) indicate a strong interaction between rate coefficients and equilibrium constants. This we believe to be the cause for the mismatch in the temperature ranges of the experimental and numerically simulated soot-yield bells. Further study of the thermochemical and rate constant data and the mechanism itself should reveal the cause of this mismatch.

MAIN CONCLUSIONS

1. The presented experimental results futher support our earlier conjecture that the soot formation mechanism is the same for both pyrolysis and oxidation of hydrocarbons.
2. The experimental results performed to investigate the effect of fuel structure on soot formation can be rationalized within the framework of our conceptual models and thus support them. One deviation is the results obtained with vinylacetylene. These results indicate that conjugation by itself is not a sufficient factor for determining the sooting tendency of a molecule - structural reactivity in the context of the chemical kinetics is the dominant factor in soot formation. The latter conclusion is also supported by the results of our detailed kinetic modeling.
3. It was demonstrated that soot formation in shock-tube pyrolysis of acetylene can be explained by a detailed kinetic mechanism composed of conventional hydrocarbon reactions. The main mass growth was found to proceed through a single dominant route in which fused polycyclic aromatics play a particularly important role: their practically irreversible formation reactions have the effect of "pulling" chains of reversible reactions in which H-atoms reactivate aromatic molecules. The main reaction bottleneck appears at the formation of the first aromatic ring. The overshoot by hydrogen atom of its equilibrium concentration is a driving kinetic force for soot formation. The model is in accord with product distributions observed in flames.

FUTURE RESEARCH DIRECTIONS

The ultimate goal of this program is the development of a detailed kinetic model for soot formation in combustion of hydrocarbon fuels. To achieve this goal, and taking into account our present results, we will concentrate on the following objectives:

1. The continuation of the experimental investigation of soot formation in fuel mixtures.
2. Refinement of the developed chemical kinetic model of soot formation in acetylene pyrolysis.
3. Extension of the developed chemical kinetic model of soot formation to other conditions. Of immediate interest are acetylene oxidation and pyrolysis of other representative fuels.

REFERENCES

1. Frenklach, M., "Shock Tube Study of the Fuel Structure Effects on the Chemical Mechanisms Responsible for Soot Formation", NASA Report CR-174661, November 1983.

2. Frenklach, M., Ramachandra, M.K. and Matula, R.A., "Soot Formation in Shock-Tube Oxidation of Hydrocarbons", Twentieth Symposium (International) on Combustion, The Combustion Institute, in press.

3. Frenklach, M., Clary, D.W., Gardiner, W.C. Jr. and Stein, S.E., "Detailed Kinetic Modeling of Soot Formation in Shock-Tube Pyrolysis of Acetylene", Twentieth Symposium (International) on Combustion, in press.

4. Graham, S.C., Homer, J.B. and Rosenfeld, J.L.J., "The Formation and Coagulation of Soot Aerosols Generated by the Pyrolysis of Aromatic Hydrocarbons", Proc. R. Soc. London A344:259 (1975).

5. Frenklach, M., Taki, S. and Matula, R.A., "A Conceptual Model for Soot Formation in Pyrolysis of Aromatic Hydrocarbons", Combust. Flame 49:275 (1983).

6. Frenklach, M., Taki, S., Li Kwok Cheong, C.K. and Matula, R.A., "Soot Particle Size and Soot Yield in Shock Tube Studies", Combust. Flame 51:37 (1983).

7. Bauer, S.H. and Zhang, L.M., "Shock Tube Pyrolysis of Polycyclic Aromatics-Detection of Soot Precursors", 14th International Symposium on Shock Tubes and Waves, p. 654, New South Wales University, Australia, 1983.

8. Rawlins, W.T., Tanzawa, T., Schertzer, S.P. and Krech, R.H., "Synthetic Fuel Combustion: Pollutant Formation. Soot Initiation Mechanisms in Burning Aromatics", Physical Sciences Report TR-361, 1983.

9. Rawlins, W.T., Cowles, L.M. and Krech, R.H., "Spectral Signatures (0.2-5μm) of Soot Initation in the Pyrolysis of Toluene Near 2000 K", Twentieth Symposium (International) on Combustion, The Combustion Institute, in press.

10. Fussey, D.E., Gosling, A.J. and Lampard, D., "A Shock Tube Study of Induction Times in the Formation of Carbon Particles by Pyrolysis of the C_2 Hydrocarbons", Combust. Flame 32:181 (1978).

11. Cundall, R.B., Fussey, D.E., Harrison, A.J. and Lampard, D., "Shock Tube Studies of the High Temperature Pyrolysis of Acetylene and Ethylene", J. Chem. Soc. Faraday I, 74:1403 (1978).

12. Bittner, J.D. and Howard, J.B., "Composition Profiles and Reaction Mechanisms in a Near-Sooting Premixed Benzene/Oxygen/Argon Flame", Eighteenth Symposium (International) on Combustion, p. 1105, The Combustion Institute, 1981.

13. Bittner, J.D., Howard, J.B. and Palmer, H.B., "Chemistry of Intermediate Species in the Rich Combustion of Benzene", in Soot in Combustion Systems and Its Toxic Properties (J. Lahaye and G. Prado, Eds.), p. 95, Plenum, 1983.

14. Bittner, J.D. and Howard, J.B., "Structure of Sooting Flames", in Soot in Combustion Systems and its Toxic Properties (J. Lahaye and G. Prado, Eds.), p. 57, Plenum, 1983.

15. Haynes, B.S. and Wagner, H.Gg., "Soot Formation", Prog. Energy Combust. Sci. 7:229 (1981).

16. Calcote, H.F., "Mechanisms of Soot Nucleation in Flames - A Critical Review", Combust. Flame 42:215 (1981).

17. Glassman, I., "Phenomenological Models of Soot Processes in Combustion Systems", Princeton University Mechanical and Aerospace Engineering Report No. 1450, July 1979.

18. Frenklach, M. and Clary, D., "Aspects of Autocatalytic Reaction Kinetics", Ind. Eng. Chem. Fundam. 22:433 (1983).

19. Stein, S.E., to be published.

20. Stull, D.R., Westrum, E.F., Jr. and Sinke, G.C., The Chemical Thermodynamics of Organic Compounds, p. 532, Wiley, 1969.

21. Benson, S.W., Thermochemical Kinetics, Wiley, 1976.

22. Singh, H.J. and Kern, R.D., "Pyrolysis of Benzene Behind Reflected Shock Waves", Combust. Flame 54:49 (1983).

23. Smith, R.D. and Johnson, A.L., "Mass Spectrometric Study of the High Temperature Chemistry of Benzene", Combust. Flame 51:1 (1983).

24. Frenklach, M., Taki, S., Durgaprasad, M.B. and Matula, R.A., "Soot Formation in Shock-Tube Pyrolysis of Acetylene, Allene and 1,3-Butadiene", Combust. Flame 54:81 (1983).

25. Wagner, H.Gg., "Soot Formation in Combustion", Seventeenth Symposium (International) on Combustion, p. 3, The Combustion Institute, 1979.

26. Particulate Carbon: Formation during Combustion (D.C. Siegla and G.W. Smith, Eds.), Plenum, 1981.

27. Soot in Combustion Systems and Its Toxic Properties (J. Lahaye and G. Prado, Eds.), Plenum, 1983.

28. Bockhorn, H., Fetting, F. and Wenz, H.W., "Investigation of the Formation of High Molecular Hydrocarbons and Soot in Premixed Hydrocarbon-Oxygen Flames", Ber. Bunsenges. Phys. Chem. 87:1067 (1983).

29. Côme, G. M., "The Use of Computers in the Analysis and Simulation of Complex Reactions", Comprehensive Chemical Kinetics (C. H. Bamford and C. F. H. Tipper, Eds.), Vol. 24, Chap. 3, Elsevier, New York, 1983.

30. Tanzawa, T. and Gardiner, W.C., Jr., "Reaction Mechansm of the Homogeneous Thermal Decomposition of Acetylene", J. Phys. Chem. 84:236 (1980).

31. Keifer, J.H., Kapsalis, S.A., Al-Alami, M.Z. and Budach, K.A., "The Very High Temperature Pyrolysis of Ethylene and the Subsequent Reactions of Product Acetylene", Combust. Flame 51:79 (1983).

32. Kollmar, H., Carrion, F., Dewar, M.J.S. and Bingham, R.C., "Ground States of Molecules. 58. The C_4H_4 Potential Surface", J. Am. Chem. Soc. 103:5292 (1981).

33. Warnatz, J., "Rate Coefficients in the C/H/O System", Combustion Chemistry (W.C Gardiner, Jr., Ed.), Ch. 5, Springer-Verlag, 1984.

34. Ebert, K.H., Ederer, H.J. and Isbarn, G., "Thermal Decomposition of n-Hexane", Int. J. Chem. Kinet. 15:475 (1983).

35. Gardiner, W.C., Jr. and Troe, J., "Rate Coefficients of Thermal Dissociation, Isomerization, and Recombination Reactions", Combustion Chemistry (W.C. Gardiner, Jr , Ed.), Ch. 4, Springer-Verlag, 1984.

36. Hindmarsh, A.C., "Toward a Systematized Collection of ODE Solvers", Paper presented at the 10th IMACS World Congress on Systems Simulation and Scientific Computation, Montreal, Canada, August, 1982.

37. Frenklach, M. and Gardiner, W.C., Jr., "Representation of Multi-Stage Mechanisms in Detailed Computer Modeling of Polymerization Kinetics", J. Phys. Chem. 88:6263 (1984).

38. Frenklach, M., "Computer Modeling of Infinite Reaction Sequences: A Chemical Lumping", Chem. Engr. Sci., to appear.

39. Lee, S.C. and Tien, C.L., "Optical Constants of Soot in Hydrocarbon Flames", Eighteenth Symposium (International) on Combustion, p. 1159, The Combustion Institute, 1981.

40. Dyer, T.M.and Flower, W.L., "A Phenomenological Description of Particulate Formation During Constant Volume Combustion", p. 363 in Ref. 26.

41. Stein, S.E., "On the High Temperature Chemical Equilibria of Polycyclic Aromatic Hydrocarbons", J. Phys. Chem. 82:566 (1978).

42. Frenklach, M., "Modeling", Combustion Chemistry (W.C. Gardiner, Jr., Ed.), Ch. 7, Springer-Verlag, 1984.

APPENDIX A - PUBLICATIONS AND PRESENTATIONS

The following list is an update from the previous report[1].

Publications

1. Miller, D. L., Frenklach, M. Y., Laughlin, P. J., and Clary, D. W., "Transferring Data from a Nicolet Digital Oscilloscope to an IBM Mainframe Computer Using an APPLE II+ Microcomputer. Part I", Computer Applications in the Laboratory 3:184 (1984).

2. Miller, D. L., Frenklach, M. Y., Laughlin, P. J., and Clary, D. W., "Transferring Data from a Nicolet Digital Oscilloscope to an IBM Mainframe Computer Using an APPLE II+ Microcomputer. Part II", Computer Applications in the Laboratory 4:260 (1984).

3. Frenklach, M., "Systematic Optimization of a Detailed Kinetic Model Using a Methane Ignition Example", Combust. Flame 58:69 (1984).

4. Frenklach, M. and Gardiner, W. C., Jr., "Representation of Homogeneous Polymerization in Detailed Computer Modeling of Chemical Kinetics", J. Phys. Chem. 88:6263 (1984).

5. Frenklach, M., Clary, D. W., Gardiner, W. C., Jr., and Stein, S., "Detailed Kinetic Modeling of Soot Formation in High-Temperature Pyrolysis of Acetylene", Twentieth Symposium (International) on Combustion, in press.

6. Frenklach, M., Ramachandra, M. K. and Matula, R. A., "Soot Formation in Shock-Tube Oxidation of Hydrocarbons", Twentieth Symposium (International) on Combustion, in press.

7. Frenklach, M., "Computer Modeling of Infinite Reaction Sequences: A Chemical Lumping", Chem. Eng. Sci., in press.

8. Frenklach, M., Clary, D., and Matula, R. A., "Empirical Modeling of Soot Formation in Pyrolysis of Aromatic Hydrocarbons", accepted to the 15th International Symposium on Shock Waves and Shock Tubes, University of California, Berkeley, July 29-August 1, 1985.

9. Frenklach, M., Clary, D. W., Gardiner, W. C., Jr., and Stein, S. E., "Shock-Tube Pyrolysis of Acetylene: Sensitivity Analysis of the Reaction Mechanism for Soot Formation," accepted to the 15th International Symposium on Shock Waves and Shock Tubes, University of California, Berkeley, July 29-August 1, 1985.

Presentations

1. Clary, D., Franklach, M., Gardiner, W. C., Jr., and Stein, S., "Mechanism of Soot Nucleation", the Detroit Meeting of the American Physical Society, March 26-30, 1984 (Bull. Am. Phys. Soc. 29:487 (1984)).

2. Frenklach, M., "Kinetic Modeling of Soot Formation Chemistry in the Shock-Tube Pyrolysis of Acetylene", workshop on "The Mechanism of Soot Formation", AeroChem Research Laboratories, Princeton, N.J., June 15-15, 1984.

3. Miller, D. L., Clary, D. W., a · renklach, M., "Developing an Oscilloscope/Microcomputer/Mainframe C munication System", session entitled "Microcomputers in Government and Education", Joint National Meeting of the Operations Research Society of America and the Institute of Management Sciences, Dallas, Texas, November 26-28, 1984.

4. Frenklach, M., "Computer Modeling of Infinite Series of Reversible Reactions", session entitled "Thermal Reaction Pathway Fundamentals", the 77th Annual AIChE National Meeting, San Francisco, California, November 25-30, 1984.

5. Frenklach, M., "Computer Modeling of Infinite Reaction Sequences: A Chemical Lumping", University of Houston, Department of Chemical Engineering, Houston, Texas, September 14, 1984.

6. Frenklach, M., "Chemistry of Soot Formation", Louisiana State University, Department of Chemistry, Baton Rouge, September 21, 1984.

7. Frenklach, M., "Computer Modeling of Chemical Kinetics", Rice University, Department of Chemical Engineering, Houston, Texas, November 15, 1984.

APPENDIX B - PROFESSIONAL PERSONNEL

Dr. M. Y. Frenklach	-	Principal Investigator
Dr. R. A. Matula	-	Participating Faculty
Dr. M. K. Ramachandra	-	Research Associate
D. Clary	-	Graduate Student
T. Yuan	-	Graduate Student
P. Laughlin	-	Undergraduate Student

1. Report No.	2. Government Accession No.	3. Recipient's Catalog No.
NASA CR-174880		

4. Title and Subtitle

Shock Tube Study of the Fuel Structure Effects on the Chemical Kinetic Mechanisms Responsible for Soot Formation Part II

5. Report Date

May 1985

6. Performing Organization Code

7. Author(s)

M. Frenklach, D.W. Clary, and M.K. Ramachandra

8. Performing Organization Report No.

None

10. Work Unit No.

9. Performing Organization Name and Address

Louisiana State University
Department of Chemical Engineering
Baton Rouge, Louisianna

11. Contract or Grant No.

NAG 3-477

13. Type of Report and Period Covered

Contractor Report

12. Sponsoring Agency Name and Address

National Aeronautics and Space Administration
Washington, D.C. 20546

14. Sponsoring Agency Code

505-31-04

15. Supplementary Notes

Final report. Project Manager, Erwin A. Lezberg, Internal Fluid Mechanics Division, NASA Lewis Research Center, Cleveland, Ohio 44135.

16. Abstract

Soot formation in oxidation of allene, 1,3-butadiene, vinylacetylene and chlorobenzene and in pyrolysis of ethylene, vinylacetylene, 1-butene, chlorobenzene, acetylene-hydrogen, benzene-acetylene, benzene-butadiene and chlorobenzene-acetylene argon-diluted mixtures was studied behind reflected shock waves. The experiments were conducted at temperatures from 1500 to 3000 K, pressures from 1 to 3 bar and carbon atom concentrations of approximately 2 and 5×10^{17} atoms/cm^3. Soot was monitored by measuring the attenuation of a laser beam at 632.8 nm. The obtained experimental results can be rationalized within the framework of our conceptual models. The results show that vinylacetylene is much less sooty than allene, which indicates that conjugation by itself is not a sufficient factor for determining the sooting tendency of a molecule. Structural reactivity in the context of the chemical kinetics is the dominant factor in soot formation. The report also presents the results of detailed chemical kinetic modeling of soot formation in pyrolysis of acetylene. The main mass growth was found to proceed through a single dominant route composed of conventional radical reactions. The practically irreversible formation reactions of the fused polycyclic aromatics nd and the overshoot by hydrogen atom over its equilibrium concentration are the g driving kinetic forces for soot formation.

17. Key Words (Suggested by Author(s))	18. Distribution Statement
Soot formation Combustion kinetics Pyrolysis Chemical kinetic modeling	Unclassified - unlimited STAR Category 25

19. Security Classif. (of this report)	20. Security Classif. (of this page)	21. No. of pages	22. Price*
Unclassified	Unclassified	170	A08

*For sale by the National Technical Information Service, Springfield, Virginia 22161